

# DESORPTION STUDIES IN A PACKED BED OF MOLECULAR SIEVES USING IMBEDDED ELECTRICAL HEATERS

**A THESIS**

*submitted in fulfilment of the  
requirements for the award of the degree*

*of*  
**DOCTOR OF PHILOSOPHY**  
*in*  
**CHEMICAL ENGINEERING**

By

**RAJ KUMAR VYAS**




**DEPARTMENT OF CHEMICAL ENGINEERING  
UNIVERSITY OF ROORKEE  
ROORKEE-247 667, INDIA**

**FEBRUARY, 1996**

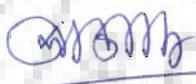
## CANDIDATE'S DECLARATION

I hereby certify that the work which is being presented in the thesis entitled **DESORPTION STUDIES IN A PACKED BED OF MOLECULAR SIEVES USING IMBEDDED ELECTRICAL HEATERS** in the fulfilment for the award of the **Degree of Doctor of Philosophy** and submitted in the Department of Chemical Engineering of the University of Roorkee is an authentic record of my own work carried out during a period from August 1991 to August 1994 as full time and thereafter as part time upto February 1996 under the supervision of **Prof. Surendra Kumar**.

The matter presented in this thesis has not been submitted by me for the award of any other degree of this or any other University.

  
(**Raj Kumar Vyas**)


This is to certify that the above statement made by the candidate is correct to the best of my knowledge.


  
(**Dr. Surendra Kumar**)  
Professor  
Deptt. of Chemical Engg.  
University of Roorkee

Date : February 5, 1996

The Ph.D. viva-voce examination of Shri R. K. Vyas, Research Scholar has been held on 17.7.1996.....

  
Signature of  
Supervisor

  
Signature of  
Head, CHED 17.7.96

  
Signature of  
External Examiner

**Dr. S.C. GUPTA**  
**PROF. & HEAD**  
**DEPTT. OF CHEM. ENGG.**  
**UNIVERSITY OF ROORKEE, ROORKEE.**



DR. S. C. GUPTA  
PROF & HEAD  
DEPTT. OF CHEM. ENGG  
UNIVERSITY OF ROORKEE, ROORKEE

## ABSTRACT

Adsorption-Desorption is a widely used separation process in chemical and other process industries. The advent of zeolite molecular sieves has further enhanced its utility due to their specificity of separation by size. The various desorption processes may be classified as thermal swing, pressure swing, purge gas stripping, and displacement desorption.

Thermal swing desorption process is used in numerous purification systems; its applications are growing at a steady rate for last three and a half decades. Zeolite molecular sieves being capable of retaining its adsorption capacity even at relatively high temperatures make a good combination with this process. This desorption process is facilitated by passing a hot inert carrier gas through the adsorbent bed. In this technique, condensable adsorbates can easily be recovered by passing the effluent from the adsorber through a condenser. However, if the adsorbate is noncondensable, then additional separation unit shall naturally be required to remove the adsorbate from carrier gas. Besides, heating of carrier gas consumes a large amount of energy and only a small fraction of it is utilized in desorption. Therefore, in order to recover contamination free noncondensable adsorbate without any significant loss and also to reduce the energy consumption, it is necessary to heat the bed without carrier gas. Jacketted heating is possible but it loses its applicability to large diameter beds used commercially, because of the relatively poor thermal conductivity of molecular sieves. Thus, the packed bed desorption in which bed is heated by internally imbedded electrical heaters, appears to be a potential alternative. To the best of our knowledge potentials of this technique have not yet been fully explored.

In our Laboratory, preliminary studies on this desorption process have proved its viability [Prasad (1988)]. 13X molecular sieves manufactured indigenously, were used as adsorbent. The bed saturated with water vapour was desorbed using an electrical heater, imbedded in the bed. Main emphasis in this research work was on dry bed conduction studies and so the effective thermal conductivity/diffusivity of bed was determined. It has been reported in the literature that the thermal conductivity of a packed bed depends upon temperature, but the dependence is scarcely estimated. Furthermore, these studies include few experimental runs on desorption. A mathematical model has also been proposed for this desorption process, which assumed desorption to be completely conduction controlled and ignored the intraparticle diffusional effects. Due to this reason, model predictions were quite far from the experimental ones; predicted and experimental desorption times are about 2.5 hour and 8-9 hour respectively. Besides, 13X molecular sieves used were indigenously manufactured, for which no systematic characterization was

available and done by Prasad (1988).

In view of the viability of proposed desorption process, the present research project has been undertaken. In formulating the objectives, it has been kept in mind that the results of this research work may further enhance our knowledge of this desorption process, so that it may be designed and used commercially. In the present study too, water vapour-13X molecular sieves has been considered as adsorbate-adsorbent system. The main objectives of the thesis are confined to three aspects of this desorption process, namely Characterization of 13X molecular sieves, Estimation of  $k(T)$  for the packed bed, and Development of Mathematical model. Accordingly, the conclusions have been summarized below.

Characterization of 13X molecular sieves has been done by determining various properties, e.g. surface area and total micropore volume, by using adsorption measurements. For this purpose various available methods, viz. BET, Langmuir, t-Plot, Dubinin-Radushkevich (DR) equation and Dubinin-Astakhov (DA) equation have been used. Adsorption measurements have been done using two gaseous adsorbates - nitrogen and argon which are having a symmetric molecule and are nonpolar in nature.

Computational algorithm and software have been developed to use adsorption measurement data in DR and DA equations. A software for estimation of two parameters in DA equation has also been developed; one of them, i.e. exponent  $n$ , is of direct use. Besides, statistical analysis of estimated parameters has been carried out by plotting 99.95% confidence limits of predicted values and a contour for 95% joint confidence region. The analysis shows that the estimated parameters are correlated, and their values are correct. Value of exponent,  $n$ , in DA equation has been found to be 1.95 and 1.78 for nitrogen and argon adsorption on 13X molecular sieves, respectively.

Critical analyses of the methods used and the results obtained have been carried out. The analysis indicates that the exponent, 2, used in DR equation can be safely used for the determination of micropore volume and surface area of 13X molecular sieves. This enables one to avoid the use of DA equation which is relatively cumbersome and time consuming as it requires estimation of the value of exponent,  $n$ . Besides, surface area obtained from BET method is approximately 17-25% less than that of Langmuir's method, DR equation, and DA equation with the two adsorbates used in the present study. This observation is also in agreement with the observations made in literature. The values of surface area and micropore volume of 13X molecular sieves have been found to be  $755.8 \text{ m}^2/\text{g}$  and  $0.2686 \text{ cm}^3/\text{g}$  respectively. The results obtained are closely in agreement with the values reported in literature.

In order to obtain transient radial temperature profiles, an experimental unit has been designed and fabricated. It consists mainly of a cylindrical column (I.D. = 94 mm, Height = 600 mm), packed with 13X molecular sieves. An electrical heater imbedded into the bed coaxially, was used to provide a source of thermal energy. The bed was heated under dry conditions using two heater wattages, e.g. 0.1 and 0.13333 kW/m. A PC based on-line data acquisition system has been developed on an existing data logger. A software has been developed in C language to display and store the measured temperatures at desired locations. The software is a 6400 lines code. It is interactive, user friendly, and possesses several advanced features such as context sensitive help and security of data against power failure. The data acquisition software is general in application as it can also be used to acquire three types of other commonly measured variables, viz. DC voltage, AC voltage, and resistance.

Dependency of effective thermal conductivity of a bed of 13X molecular sieves on temperature has been estimated by using transient radial temperature profiles obtained in the dry packed bed. Effective thermal conductivity,  $k$ , has been estimated to vary linearly with temperature  $T$ . The correlation obtained for  $k$  is as follows :

$$k(T) = 8.17635 \times 10^{-5} + 10.915427 \times 10^{-7} (T - T_0)$$

where,  $T_0 = 303$  K

Using the above correlation, effective thermal conductivity of a packed bed of 13X molecular sieves varies from  $8.18 \times 10^{-5}$  to  $22.15 \times 10^{-5}$  kW/m K for a temperature range of 303-431 K. These values are in agreement with the values reported in literature for the catalytic and other similar materials.

Statistical analysis of the estimated parameters of correlation has been carried out by plotting the joint confidence contour for an approximate 95% confidence level. Although, the dependence of  $k$  on  $T$  is linear but its use in the model partial differential equations meant for estimation of parameters results into a nonlinear estimation problem. Therefore, the joint confidence contour plotted is of deflated banana shape in a two parameter space. The elongated shape of the contour indicates that the estimated parameters are highly correlated.

A mathematical model for this thermal desorption process has also been developed in the present research work. This model also includes the transport of adsorbate within the molecular sieve pellet by diffusion. For simplicity, linear isotherm is assumed to govern the equilibrium relationship. This model consists of partial differential equations for bed as well as for the pellet and is to be solved by a suitable numerical method with appropriate initial and boundary conditions. As the solution of this class of differential equations is



complex and requires large computer time, therefore, it is desirable to simplify it without sacrificing accuracy of its predictions. To do so, adsorbed phase concentration profile within the molecular sieves pellet is assumed to be parabolic in shape with respect to its radius throughout the desorption. It is reported in the literature that this assumption, at one hand, is true in almost all the cases and at all the times, significantly simplifies the model and saves the computation time substantially, at the other.

Simplified model equations of the bed have been solved numerically by using control volume finite difference method. This method has the advantage of satisfying the conservation equations in the discretized form even if the discretization grid is coarse. This method forms the basis of the computational algorithm developed in the thesis. The predictions of the model proposed here, adequately match the experimental observations.

It has been found in the present study that the thermal desorption of water vapour from molecular sieves 13X is mainly controlled by intraparticle diffusion of adsorbate, and the effective diffusivity of water vapour in molecular sieves is strongly concentration dependent. Therefore, in order to further improve the predictions of the model, concentration dependence of diffusivity has been investigated. It has been found that a relationship of following type adequately represents the desorption behaviour.

$$D(q) = \frac{D_0}{\left(1 - \alpha_2 \frac{q}{q_s}\right)^2}$$

Where  $\alpha_2 = 0.87753$  and  $D_0 = 1.5 \times 10^{-11} \text{ m}^2/\text{s}$ .

It is our view that the research work carried out in the thesis has a wide scope for applications in industry. The technique of desorption and the proposed model will be useful in the applications where recovery of adsorbate is a must to improve the economics of the process. This type of system is particularly suitable for smaller units which are used for mobile purposes/vehicles.

The developed model can also be used for modelling the desorption from a large size adsorption column used in the process industries. In such a case, multiple heaters imbedded into the bed on a specific pattern, e.g. triangular, shall be used as a source of thermal energy. The computational algorithm developed for a single heater can also be used for this system with little modification, but it may require a large computer time. Fortunately, with the development of fast computing machines, solution of model equations for desorption with diffusional transport considerations for a large grid size is now feasible.

## ACKNOWLEDGEMENTS

In carrying out any creative work such as academic research, persistent inspiration and constant encouragement from various sources, serve as a driving force. It would be apt to convey the feelings of one's heart in acknowledging their encouragement and assistance with kindest regards.

The first is the almighty God (*the parmatma*), and then the *Guru* (the teacher). Traditionally, we have respected our *Gurus* as *Sakshat Parambrahma*. In Sanskrit :

गुरुर्ब्रह्मा गुरुर्विष्णु गुरुर्देवो महेश्वरः ।  
गुरुर् साक्षात् परम् ब्रह्मम् तस्मै श्रीगुरवे नमः ॥

[Teachers are worshipped as Lord Brahma (God of creation), Lord Vishnu (God of protection), and Lord Maheshwara (God of destruction); I bow down to my respected Guide.]

I express my profound sense of gratitude to my revered guide and mentor Dr. Surendra Kumar, Professor of Chemical Engineering, University of Roorkee for his assiduity and deep insight into the subject. In fact, he introduced me to the fascinating field of adsorption - desorption in/from zeolite molecular sieves. I am greatly indebted to him for stimulating input of ideas, erudite guidance, and regular encouragement towards excellence throughout this research work. I consider myself fortunate to have had the opportunity to work under his able guidance and enrich myself from his vast knowledge. He shall always be a constant source of inspiration to me.

I welcome this opportunity to express my sincere regards and thanks to Dr. S.C. Gupta, Prof. & Head, Chemical Engineering Department and my other teachers for providing me the available facilities.

I wish to express my profound sense of gratitude to Dr. (Mrs.) Shashi for her affection, moral support, and constant inspiration during this work.

Almighty has been generous enough to bless me with mature, helpful, and cooperative friends and colleagues. I wish to venerate and thank my friends in Reaction Engineering Research Laboratory Shri Omer Salim Zain and Dr. (Smt.) Surekha Bhanot for



providing me a congenial and stimulating research environment and personal help extended in hour of need. It was a memorable time I had with them.

I am grateful to my newer colleagues, viz. Km. Arti Chamoli, Shri R.P. Singh, and Shri Arinjay Kumar for their cooperation and moral encouragement. I am greatly indebted to Km. Arti, Shri Omer, and Dr.(Mrs.) Shashi for their constructive suggestions, useful discussions, and constant help.

I wish to gratefully acknowledge the help I received from my friend Shri Sanjeev Singh in obtaining experimental measurements and useful data for characterization of molecular sieves. I wish to thank Shri V.S. Kushwaha for his help and assistance in developing the Data Acquisition System. I am greatly indebted to my friend Shri Satish Annigeri for extending all possible help in extracting best from Computer Softwares of general utility. His knowledge in this field is amazing and has been indeed useful to me.

Use of books and monographs form an integral part of the research work. In this regard, I owe special thanks to Km. Mohini Shastry for helping me in getting some critical monographs which have been immensely useful. Services of Librarian of Chemical Engineering Deptt. Shri Balram Singh are greatly appreciated for performing his job with a smile.

Laboratory work is always a critical area in theoretico - experimental studies. In this regard, services rendered by Shri S.S. Mangla and Shri Satya Pal Singh deserves special mention.

A part of the computer work was done at CAD Centre of Chemical Engineering Deptt. I am thankful to Shri Akhilesh K. Sharma and Shri S.C. Sharma for their cooperation and help.

I wish to express my gratefulness to my family friends Ms. Indra Gupta, Shri Vimal Bhanot, Smt. Fatoom Mohlatee, Shri Hemant-Smt. Sheela Choudhary, and Syt. Shriniwas Verma for extending their moral support, help and much needed good wishes. A word of gratitude is due to Prof. M.K. Vasantha for his constant moral boosting.

I cannot enunciate in proper words my heartfelt appreciation for my dear friends Shri Rakesh Kumar (Tyagi) and Shri Dhananjay K. Griyage, for their love and affection.

There is a dearth of proper words to express my feelings for my parents and elder brothers who apart from providing me the best available education have always encouraged me in all my endeavours. I owe much of my academic success to them. I also remember with respect and love my parents Shri S.R. Vyas and Smt. Narvada Devi, and brothers and *bhabhijis*, Shri Umesh Kumar - Smt. Premlata, Shri Arvind Kumar - Smt. Santosh, and Shri Krishna Kumar - Smt. Renu for their blessings and moral support. Words can never express my indebtedness towards them.

I am delighted to recall the special warmth and affection bestowed upon me by my parents-in-law Shri R.R. Harsh and Smt. Indra Harsh and brother- and sister-in-law Shri Sanjeev- Smt. Anju Harsh.

Financial assistance from the University Grants Commission, New Delhi and the Extra Mural Research Division of Council of Scientific and Industrial Research, New Delhi, Govt. of India by awarding me Research Fellowship in Engineering and Technology and Research Associateship respectively, are gratefully acknowledged.

I am grateful to the authors of various text books, monographs, and research papers whose work has been used in this thesis and in improvement of my understanding of the subject to a greater depth. I also wish to thank all those who have contributed directly or indirectly but could not be acknowledged.

Last but not the least, the author acknowledges his indebtedness to his wife Sangeeta for her patience, constant inspiration, and understanding.

**(RAJ KUMAR VYAS)**

# CONTENTS

ABSTRACT	i
ACKNOWLEDGEMENTS	v
CONTENTS	ix
LIST OF FIGURES	xvii
LIST OF TABLES	xxiii
NOMENCLATURE	xxvii
CHAPTER I INTRODUCTION	1
1.1 OBJECTIVES	6
1.2 ORGANISATION OF THESIS	7
CHAPTER II LITERATURE REVIEW	9
2.0 INTRODUCTION	9
2.1 HISTORICAL BACKGROUND	10
2.1.1 Naturally Occurring Zeolites	10
2.2 INDUSTRIAL ADSORPTION SEPARATION PROCESSES	14
2.2.1 Adsorbents and their Uses	14
2.2.2 Synthesis of Zeolites	15
2.3 ADSORPTION PROCESSES	17
2.3.1 Regeneration Process Cycles	19
2.3.1.1 Pressure Swing Process	19
2.3.1.2 Thermal Swing Process	20
2.3.1.3 Purge Gas Stripping Process	20

2.3.1.4	Displacement Desorption Process	20
2.3.1.5	Steam Stripping Process	20
2.3.1.6	Gas Chromatography	21
2.3.1.7	Moving Bed and Simulated Moving Bed Processes	21
2.3.1.8	Parametric Pumping Process	21
2.3.1.9	Cycling Zone Processes	22
2.4	CHARACTERIZATION OF MOLECULAR SIEVES	22
2.5	EFFECTIVE THERMAL CONDUCTIVITY OF ADSORBENT PACKED BED	25
2.5.1	Relationship based on Reynolds No.	30
2.5.2	Static Contributing Factors	30
2.5.2.1	Axial Effective Thermal Conductivity	30
2.6	ADSORPTION/DESORPTION MODELLING STUDIES	31
2.6.1	Mathematical Modelling of Adsorption Kinetics / Diffusion in Biporous Adsorbents	35
2.6.1.1	Resistance to Transfer Processes	36
2.6.1.2	Equilibrium Relationship	37
2.6.1.3	External Fluid Film Control	38
2.6.1.4	Macropore Diffusion Control	39
2.6.1.5	Bed Diffusion	39
2.6.1.6	Micropore Diffusion Control	40
2.7	MOTIVATION FOR THE PRESENT STUDY	41
2.8	CONCLUDING REMARKS	44
<b>CHAPTER III</b>	<b>CHARACTERIZATION OF MOLECULAR SIEVES</b>	<b>45</b>
3.0	INTRODUCTION	45
3.1	SURFACE AREA DETERMINATION METHODS	45
3.1.1	BET Method	46
3.1.2	Langmuir Method	47

3.2	MICROPORE VOLUME AND MICROPORE SURFACE AREA	48
3.2.1	Dubinin - Radushkevich Equation	49
3.2.2	Dubinin - Astakhov Equation	50
3.2.3	t - Plot Method	51
3.2.4	MP - Method	52
3.3	PORE SIZE DISTRIBUTION	53
3.3.1	Horváth - Kawazoe Method	54
3.4	BULK PROPERTIES	54
3.4.1	Bulk Density	55
3.4.1.1	Apparent Bulk Density	55
3.4.1.2	Apparent Unit Density	55
3.4.2	Mechanical Properties	55
3.4.2.1	Crushing Strength	56
3.4.2.2	Attrition Losses	57
3.5	INSTRUMENT USED FOR PHYSISORPTION MEASUREMENTS	58
3.5.1	Results of Characterization by BET, Langmuir, and t-Plot Methods	58
3.5.2	Analysis of Results of BET, Langmuir, and t-Plot Methods	63
3.6	CHARACTERIZATION BY DUBININ - RADUSHKEVICH AND DUBININ - ASTAKHOV EQUATIONS	65
3.6.1	Characterization by Dubinin - Radushkevich Equation	66

3.6.1.1	Stepwise Procedure of Dubinin - Radushkevich Equation	66
3.6.1.2	Results of Dubinin - Radushkevich Equation	67
3.6.2	Characterization by Dubinin - Astakhov Equation	67
3.6.2.1	Stepwise Procedure of Dubinin - Astakhov Equation	67
3.6.2.2	Results of Dubinin - Astakhov Equation	74
3.6.3	Analysis of Results of Dubinin - Radushkevich and Dubinin - Astakhov Curves	77
3.6.3.1	Micropore Surface Area by Dubinin - Radushkevich Equation	80
3.6.3.2	Total Micropore Volume by Dubinin - Radushkevich and Dubinin - Astakhov Equations	81
3.6.3.3	Characteristic Adsorption Energy in Dubinin - Astakhov Equation	81
3.6.3.4	Critical Analysis of Results of Dubinin - Radushkevich and Dubinin - Astakhov Equations	81
3.7	CONFIDENCE INTERVALS	82
3.7.1	Confidence Limits of Predicted Values	82
3.7.2	Individual Confidence Intervals and Joint Confidence Region	84
3.8	CHARACTERIZATION BY OTHER METHODS	84
3.9	DETERMINATION OF BULK DENSITY AND MECHANICAL PROPERTIES	87
3.10	CONCLUDING REMARKS	87



<b>CHAPTER IV</b>	<b>TRANSIENT TEMPERATURE MEASUREMENTS - EXPERIMENTAL</b>	
	<b>SET UP, PROCEDURE AND RESULTS</b>	<b>91</b>
4.0	INTRODUCTION	91
4.1	EXPERIMENTAL SET UP	91
4.1.1	Description of Packed Bed Column	93
4.1.1.1	Components of Packed Bed	97
4.1.1.2	Assembling of Packed Bed Column	98
4.1.2	Power Supply	100
4.1.3	Development of a PC Based Data Acquisition Software	102
4.1.3.1	Software	103
4.1.3.2	Advantages	104
4.2	EXPERIMENTAL PROCEDURE	104
4.3	RESULTS	105
4.4	CONCLUDING REMARKS	110
<b>CHAPTER V</b>	<b>ESTIMATION OF TEMPERATURE-DEPENDENT EFFECTIVE</b>	
	<b>THERMAL CONDUCTIVITY OF ADSORBER/DESORBER BED</b>	<b>111</b>
5.0	INTRODUCTION	111
5.1	EXPERIMENTAL DATA	112
5.2	MODEL EQUATION	112
5.3	ESTIMATION METHOD	115
5.3.1	Numerical Solution	115
5.3.2	Computational Algorithm	120
5.4	RESULTS AND DISCUSSION	121

5.4.1	Average Effective Thermal Conductivity and Thermal Diffusivity	124
5.4.2	Improved Correlation for k	136
5.4.3	Statistical Analysis	137
5.5	CONCLUDING REMARKS	143
<b>CHAPTER VI MATHEMATICAL MODELLING OF THERMAL DESORPTION PROCESS</b>		<b>147</b>
6.0	INTRODUCTION	147
6.1	DEVELOPMENT OF MATHEMATICAL MODEL	147
6.1.1	Model Equations	148
6.1.1.1	Packed Bed	150
6.1.1.2	MS Pellet	152
6.1.1.3	Constitutive Relationships	156
6.1.1.4	Remarks	157
6.1.2	Simplified Model	159
6.1.2.1	Model Equation	162
6.2	NUMERICAL SOLUTION	163
6.3	EXPERIMENTAL DATA ON THERMAL DESORPTION	165
6.4	RESULTS AND DISCUSSION	167
6.4.1	Model Predictions with Constant Diffusivity	171
6.4.1.1	Transient Profiles	176
6.4.2	Model Predictions with Variable Diffusivity	181
6.4.2.1	Comparison of Model Predictions with Experimental Data	182

6.4.2.2	Transient Profiles	186
6.4.2.3	Effect of Increase in Heater Wattage on Desorption	193
6.4.3	Computational Aspects	195
6.5	CONCLUDING REMARKS	196
	CHAPTER VII CONCLUSIONS AND RECOMMENDATIONS	197
7.1	CONCLUSIONS	197
7.1.1	Final Remarks	202
7.2	RECOMMENDATIONS FOR FUTURE WORK	202
	LIST OF RESEARCH PUBLICATIONS	205
	REFERENCES	207
APPENDIX-A	COMPARISON OF EXPERIMENTALLY OBSERVED TEMPERATURES WITH THOSE PREDICTED BY USING $\bar{k}$ AND $k(T)$ CORRELATION	225

## LIST OF FIGURES

*Note : Figures are numbered on the basis of the section where they are referred to.*

3.6-1	Dubinin-Radushkevich Plot for 13X Molecular Sieves, Adsorbate : Nitrogen	68
3.6-2	Dubinin-Radushkevich Plot for 13X Molecular Sieves, Adsorbate : Argon	69
3.6-3	Linear Curve Fitting for Dubinin-Radushkevich Plot for 13X Molecular Sieves in Appropriate Linear Region, Adsorbate : Nitrogen	70
3.6-4	Linear Curve Fitting for Dubinin-Radushkevich Plot for 13X Molecular Sieves in Appropriate Linear Region, Adsorbate : Argon	71
3.6-5	Dubinin-Astakhov Plot for 13X Molecular Sieves with optimized value of n, Adsorbate : Nitrogen	75
3.6-6	Dubinin-Astakhov Plot for 13X Molecular Sieves with optimized value of n, Adsorbate : Argon	76
3.6-7	Linear Curve Fitting for Dubinin-Astakhov Plot for 13X Molecular Sieves in Appropriate Linear Region, Adsorbate : Nitrogen	78
3.6-8	Linear Curve Fitting for Dubinin-Astakhov Plot for 13X Molecular Sieves in Appropriate Linear Region, Adsorbate : Argon	79

3.7-1	99.95% Confidence Limits of Predicted Values and Data of Appropriate Linear Region, Adsorbate : Nitrogen	83
3.7-2	95% Joint Confidence Contour for Dubinin-Astakhov Plot for 13X Molecular Sieves, Adsorbate: Nitrogen	85
4.1-1	Block Diagram showing Packed Bed, PC based Data Acquisition System, and the Power Supply	92
4.1-2	Packed Bed Assembly for Molecular Sieves	94
4.1-3	Thermocouple Locations in Radial and Axial Directions in Packed Bed	95
4.1-4	Circuit Diagram for Experimental Set up	101
4.3-1	Temperature Profiles at distances 6.5, 10, 15, and 25 mm from Centre under Transient Conditions for $Q_L = 0.1$ and $0.13333$ kW/m during Dry Bed Conduction Experiments	108
4.3-2	Temperature Profiles at distances 30, 40, and 45 mm from Centre under Transient Conditions for $Q_L = 0.1$ and $0.13333$ kW/m during Dry Bed Conduction Experiments	109
5.2-1	Cylindrical Shell for Energy Balance in a Packed Bed with Coaxial Heater	113
5.3-1	Control Volume in Two Dimensional Cylindrical Coordinates	117
5.4-1	Comparison of Experimental and Predicted Temperatures at Different Times for $Q_L = 0.1$ kW/m using $k(T)$ Relationship, i.e equation (5.4-1)	122

5.4-2	Comparison of Experimental and Predicted Temperatures at Different Times for $Q_L = 0.13333$ kW/m using $k(T)$ Relationship, i.e, equation (5.4-1)	123
5.4-3	Comparison of Experimental and Predicted Temperatures at Different Times for $Q_L = 0.1$ kW/m using Avg. $k (1.444845 \times 10^{-4}$ kW/m K)	126
5.4-4	Comparison of Experimental and Predicted Temperatures at Different Times for $Q_L = 0.13333$ kW/m using Avg. $k (1.444845 \times 10^{-4}$ kW/m K)	127
5.4-5	Comparison of Predicted Radial Temperature Profiles using $k(T)$ , i.e. equation (5.4-1) and Avg. $k (1.444845 \times 10^{-4}$ kW/m K) with Experimental values at Time = 300 s for $Q_L = 0.1$ kW/m	128
5.4-6	Comparison of Predicted Radial Temperature Profiles using $k(T)$ , i.e. equation (5.4-1) and Avg. $k (1.444845 \times 10^{-4}$ kW/m K) with Experimental values at Time = 600 s for $Q_L = 0.1$ kW/m	129
5.4-7	Comparison of Predicted Radial Temperature Profiles using $k(T)$ , i.e. equation (5.4-1) and Avg. $k (1.444845 \times 10^{-4}$ kW/m K) with Experimental values at Time = 900 s for $Q_L = 0.1$ kW/m	130
5.4-8	Comparison of Predicted Radial Temperature Profiles using $k(T)$ , i.e. equation (5.4-1) and Avg. $k (1.444845 \times 10^{-4}$ kW/m K) with Experimental values at Time = 1200 s for $Q_L = 0.1$ kW/m	131
5.4-9	Comparison of Predicted Radial Temperature Profiles using $k(T)$ , i.e. equation (5.4-1) and Avg. $k (1.444845 \times 10^{-4}$ kW/m K) with Experimental values at Time = 1500 s for $Q_L = 0.1$ kW/m	132



5.4-10	Comparison of Predicted Radial Temperature Profiles using $k(T)$ , i.e. equation (5.4-1) and Avg. $k$ ( $1.444845 \times 10^{-4}$ kW/m K) with Experimental values at Time = 1800 s for $Q_L = 0.1$ kW/m	133
5.4-11	Comparison of Predicted Radial Temperature Profiles using $k(T)$ , i.e. equation (5.4-1) and Avg. $k$ ( $1.444845 \times 10^{-4}$ kW/m K) with Experimental values at Time = 2100 s for $Q_L = 0.1$ kW/m	134
5.4-12	Comparison of Predicted Radial Temperature Profiles using $k(T)$ , i.e. equation (5.4-1) and Avg. $k$ ( $1.444845 \times 10^{-4}$ kW/m K) with Experimental values at Time = 2400 s for $Q_L = 0.1$ kW/m	135
5.4-13	Comparison of Experimental and Predicted Temperatures at Different Times for $Q_L = 0.1$ kW/m using Improved $k(T)$ Relationship, i.e. equation (5.4-4)	138
5.4-14	Comparison of Experimental and Predicted Temperatures at Different Times for $Q_L = 0.13333$ kW/m using Improved $k(T)$ Relationship, i.e. equation (5.4-4)	139
5.4-15	Transient Radial Temperature Profiles for 4 h for $Q_L = 0.1$ kW/m using Improved $k(T)$ Relationship, i.e. equation (5.4-4)	140
5.4.16	Transient Radial Temperature Profiles for 4 h for $Q_L = 0.13333$ kW/m using Improved $k(T)$ Relationship, i.e. equation (5.4-4)	141
5.4-17a	Contour for 95% Joint Confidence Region	142
5.4-17b	Enlarged Portion of Contour for 95% Joint Confidence Region Enclosing Point P	144

6.1-1	Comparison of Predicted Percent Desorption vs. Time using Model without Intraparticle Diffusion with Experiment-A	149
6.1-2	Spherical Shell for Adsorbate Balance in a Molecular Sieve Pellet	154
6.3-1	Schematic Diagram of Experimental Setup for Modified Thermal Desorption Process	166
6.3-2	Experimentally Observed Percent Desorption vs. Time for Experiments A and B	170
6.4-1	Comparison of Predicted Percent Desorption vs. Time using Proposed Model Considering Intraparticle Diffusion (Constant Diffusivity) for Experiment-A	172
6.4-2	Comparison of Predicted Percent Desorption vs. Time using Proposed Model Considering Intraparticle Diffusion (Constant Diffusivity) for Experiment-B	173
6.4-3	Comparison of Model Predictions by Equation (6.1-29) for Different Profiles using Constant Diffusivity for Experiment-A	175
6.4-4	Radial Adsorbate Concentration Profiles Developed in Bed during Desorption [Predicted by Model with $D_e = 3 \times 10^{-11} \text{ m}^2/\text{s}$ for Experiment-A]	177
6.4-5	Radial Temperature Profiles Developed in Bed during Desorption [Predicted by Model with $D_e = 3 \times 10^{-11} \text{ m}^2/\text{s}$ for Experiment-A]	178
6.4-6	Variation of Adsorbate Concentration with Time at Selected Radial Locations during Desorption [Predicted by Model with $D_e = 3 \times 10^{-11} \text{ m}^2/\text{s}$ for Experiment-A]	179

6.4-7	Variation of Temperature with Time at Selected Radial Locations during Desorption [Predicted by Model with $D_e = 3 \times 10^{-11} \text{ m}^2/\text{s}$ for Experiment-A]	180
6.4-8	Variation of Diffusivity with Fractional Uptake for Two Types of Concentration - Dependent Diffusivity Correlations	183
6.4-9	Comparison of Model Predictions with Experimental Results (Experiment-A)	184
6.4-10	Comparison of Model Predictions with Experimental Results (Experiment-B)	185
6.4-11	Comparison of Experimental and Predicted values of Percent Desorption using Diffusivity Correlation for Experiment-A	189
6.4-12	Comparison of Experimental and Predicted values of Percent Desorption using Diffusivity Correlation for Experiment-B	190
6.4-13	Variation of Adsorbate Concentration with Time at Selected Radial Locations during Desorption [Predicted by Model with Diffusivity Correlation for Experiment-A]	191
6.4-14	Variation of Temperature with Time at Selected Radial Locations during Desorption [Predicted by Model with Diffusivity Correlation for Experiment-A]	192
6.4-15	Percent Desorption vs. Time Profiles for Different Heater Wattages (Experiment-A)	194

## LIST OF TABLES

*Note : Tables are numbered on the basis of the section where they are referred to.*

1.0-1	Common Industrial Adsorptive Gas Separation Processes	2
1.0-2	Potential Uses of Zeolites	3
2.1-1	General Adsorbents, their Properties and Uses	11
2.1-2	Chronological History of Adsorption, Zeolite Minerals and Zeolite Molecular Sieves	12
2.1-3	Naturally Occurring Zeolites and year of their Discovery	13
2.2-1	Applications of Zeolite Molecular Sieves	16
2.2-2	Characteristics of Major Synthetic Zeolite Molecular Sieves	18
2.2-3	Type of Synthetic Zeolites Used in Commercial Applications	18
2.3-1	Comparison of commonly used Regeneration Methods	23 - 24
2.4-1	Research Papers on Surface Area Determination by BET and t-plot Methods; Pore Volume by t-plot method and Pore Volume Distribution by other methods	26 - 27

2.4-2	Research Papers on Theory of Volume Filling in Micropores (TVFM)	28
2.4-3	Research Papers on Physical Testing of Pellets	28
2.5-1	Thermal Conductivities of Some Porous Catalysts in Air at 90 °C, Atmospheric Pressure	32
2.5-2	Thermal Conductivities of Selected Porous Materials	33
2.5-3	Thermal Conductivity of nickel-impregnated silica and silica-alumina	34
2.6-1	Modelling Studies on Adsorption/Desorption of Water on Adsorbents	42 - 43
3.5-1	Sample Details of 13X Molecular Sieves used in Physical Adsorption Measurements	59
3.5-2	Physical Adsorption Data of Nitrogen Gas on 13X Molecular Sieves	60
3.5-3	Physical Adsorption Data of Argon Gas on 13X Molecular Sieves	61 - 62
3.5-4	Characterization of 13X Molecular Sieves by BET, Langmuir and t-Plot Methods	64
3.6-1	Characterization of 13X Molecular Sieves by Dubinin-Radushkevich and Dubinin-Astakhov Equations	72
3.9-1	Density and other Properties of 13X Molecular Sieves	88
3.9-2	Mechanical Properties and Pore Diameter of 13X Molecular Sieves as reported by the Manufacturer	88

4.3-1	Experimentally Observed Temperatures along Radial Direction in Packed Bed of 13X Molecular Sieves for $Q_L = 0.1$ kW/m	106
4.3-2	Experimentally Observed Temperatures along Radial Direction in Packed Bed of 13X Molecular Sieves for $Q_L = 0.13333$ kW/m	107
6.1-1	Mathematical Model of Thermal Desorption Process	158
6.1-2	Simplified Mathematical Model of Thermal Desorption Process	164
6.3-1	Operating Conditions of Thermal Desorption Experiments with Imbedded heater	168
6.3-2	Experimentally Observed Percent Desorption for Experiments A and B	169
6.4-1	Comparison of Percent Deviation in Predicted Percent Desorption using proposed Constant and Variable Diffusivities for Experiment-A	187
6.4-2	Comparison of Percent Deviation in Predicted Percent Desorption using proposed Constant and Variable Diffusivities for Experiment-B	188
A.1	Experimentally Observed Temperatures and Temperatures Predicted Using $\bar{k}$ and $k(T)$ relationship alongwith their Percent Deviations for $Q_L=0.1$ kW/m at 300 s	225
A.2	Experimentally Observed Temperatures and Temperatures Predicted Using $\bar{k}$ and $k(T)$ relationship alongwith their Percent Deviations for $Q_L=0.1$ kW/m at 600 s	226



A.3	Experimentally Observed Temperatures and Temperatures Predicted Using $\bar{k}$ and $k(T)$ relationship alongwith their Percent Deviations for $Q_L=0.1$ kW/m at 900 s	227
A.4	Experimentally Observed Temperatures and Temperatures Predicted Using $\bar{k}$ and $k(T)$ relationship alongwith their Percent Deviations for $Q_L=0.1$ kW/m at 1200 s	228
A.5	Experimentally Observed Temperatures and Temperatures Predicted Using $\bar{k}$ and $k(T)$ relationship alongwith their Percent Deviations for $Q_L=0.1$ kW/m at 1500 s	229
A.6	Experimentally Observed Temperatures and Temperatures Predicted Using $\bar{k}$ and $k(T)$ relationship alongwith their Percent Deviations for $Q_L=0.1$ kW/m at 1800 s	230
A.7	Experimentally Observed Temperatures and Temperatures Predicted Using $\bar{k}$ and $k(T)$ relationship alongwith their Percent Deviations for $Q_L=0.1$ kW/m at 2100 s	231
A.8	Experimentally Observed Temperatures and Temperatures Predicted Using $\bar{k}$ and $k(T)$ relationship alongwith their Percent Deviations for $Q_L=0.1$ kW/m at 2400 s	232

---

## NOMENCLATURE

---

*Note : Nomenclature is provided for each Chapter separately because one variable has been used in different contexts in different Chapters.*

### CHAPTER II

$a$	=	specific external surface area ; ( $m^{-1}$ )
$C$	=	adsorbate concentration in fluid phase; ( $kmol/m^3$ )
$C^*$	=	concentration of adsorbate in fluid phase at equilibrium; ( $kmol/m^3$ )
$C_M$	=	adsorbate concentration in vapour phase in macropores; ( $kmol/m^3$ )
$D_c$	=	diffusivity of adsorbate in zeolite crystal; ( $m^2/s$ )
$D_p$	=	pore diffusivity; ( $m^2/s$ )
$K$	=	equilibrium constant for linear isotherm; (-)
$k_{ea}$	=	static contribution due to conduction; ( $kW/m K$ )
$k_{eb}$	=	static contribution due to natural convection; ( $kW/m K$ )
$k_{ec}$	=	static contribution due to radiation; ( $kW/m K$ )
$k_{eff}$	=	total effective thermal conductivity; ( $kW/m K$ )
$k_f$	=	film mass transfer coefficient ; ( $m/s$ )
$l$	=	bed depth; (m)
$q$	=	adsorbate concentration in adsorbent particle; ( $kmol/m^3$ )
$\bar{q}$	=	average adsorbate phase concentration in adsorbent particle; ( $kmol/m^3$ )
$q^*$	=	adsorbate concentration in adsorbent particle at equilibrium; ( $kmol/m^3$ )
$R$	=	radial coordinates for macroparticles; (-)
$Re$	=	Reynolds number; (-)
$r$	=	radial coordinate
$r_c$	=	radius of zeolite crystal; (m)
$r_p$	=	radius of pellet; (m)
$z$	=	coordinate

## Greek symbols

- $\epsilon$  = bed voidage; (-)  
 $\epsilon_p$  = porosity of adsorbent pellet; (-)

## CHAPTER III

- $A$  =  $R T \ln (p_o/p)$ ; (kJ/mol), also used as parameter as described in section 3.7.2
- $A_A$  = constant in Lennard-Jones potential; (J/molecule)
- $A_a$  = constant in Lennard-Jones potential; (J/molecule)
- $a_1$  = constant [used in equation (3.1-2)]
- $a_2$  = constant [used in equation (3.1-2)]
- $a_m$  = surface area occupied by one adsorbate molecule; ( $\text{\AA}^2$ )
- $B$  = parameter as described in section 3.7.2
- $b$  = constant (-)
- $b_1$  = constant [used in equation (3.1-2)]
- $b_2$  = constant [used in equation (3.1-2)]
- $C$  = constant; (-)
- $d$  =  $d_a + d_A$ ; (nm)
- $d_A$  = diameter of an adsorbate molecule; (nm)
- $d_a$  = diameter of an adsorbent atom; (nm)
- $E$  = characteristic adsorption energy; (kJ/mol)
- $F_{1-\alpha}$  ( $m, n-m$ ) =  $(1-\alpha)$  point of the F distribution with  $m$  and  $(n-m)$  degrees of freedom; (-)
- $K$  = Avogadro's number; (molecule/mol), also used as energy to radius conversion factor; (kJ-nm/mol)
- $k$  = constant; (-)
- $l$  = distance between nuclei of two layers of carbon molecules; (nm) ( $l$  should be greater than  $d$ )
- $M$  = molecular weight of the adsorbate; (-)

- $m$  = degree of freedom in equation (3.7-2)
- $N_A$  = average number of molecules of adsorbate per unit surface area; (molecules/cm<sup>2</sup>)
- $N_a$  = average number of molecules of adsorbent per unit surface area; (molecules/cm<sup>2</sup>)
- $N_{Vm}$  = number of molecules in monolayer; (-)
- $n$  = exponent used in D-A equation; (-), also used as number of observations in equation (3.7-1); (-)
- $n_{opt}$  = optimised value of  $n$  in D-A equation; (-)
- $p$  = pressure of adsorbate; (mm Hg), also number of parameters in equation (3.7-1); (-)
- $p_i$  = absolute pressure of adsorbate at step  $i$ ; (mm Hg)
- $p_o$  = saturation pressure of adsorbate; (mm Hg)
- $R$  = gas constant; (kJ/mol K)
- $S$  = specific surface area of adsorbent; (m<sup>2</sup>/g)
- $S_j$  = surface area of  $j$ th group of pores; (m<sup>2</sup>/g)
- $S_{j+1}$  = surface area of  $(j+1)$ th group of pores; (m<sup>2</sup>/g)
- $s(\hat{Y}_i)$  = estimated standard error of predicted value of  $Y_i$ ; (-)
- $T$  = temperature; (K)
- $t$  = statistical thickness of adsorbed layer; (Å)
- $t_1$  = film thickness of adsorbed layer of the narrowest pores; (Å)
- $t_2$  = film thickness of adsorbed layer of the widest pores; (Å)
- $t(n-p, 1-\frac{\alpha}{2}) = (1-\frac{\alpha}{2})$  percentage points of the  $t$  distribution with  $(n-p)$  degrees of freedom; (-)
- $V_a$  = adsorbed volume of the adsorbate; (cc/g STP)
- $V_i$  = volume of adsorbate adsorbed upto step  $i$ ; (cc/g STP)
- $V_o$  = micropore volume; (cc/g STP)
- $V_{o_j}$  = pore volume of  $j$ th group of micropores; (cc/g)
- $V_m$  = volume of monolayer of molecules to cover whole surface of adsorbent; (cc/g STP)

- $V_{sp}$  = specific volume of the adsorbate; (cc/g STP)  
 $W_o$  = limiting or total pore volume; (cc/g)  
 $X$  = adsorbed volume of liquid adsorbate; (cc)  
 $Y$  =  $(3n+1)/3n$ , a parameter used in equation (3.6-7); (-)  
 $Y_i$  = experimentally obtained value of  $\log_{10}(V_i)$ ; (-)  
 $\hat{Y}_i$  = predicted value of  $Y_i$  from least squares; (-)

#### Greek symbols

- $\alpha$  = level of significance; (-)  
 $\beta$  = affinity constant of adsorbate relative to saturation pressure; (-)  
 $\Delta H_1$  = heat of adsorption of the first layer; (kJ/mol)  
 $\Delta H_c$  = heat of condensation of adsorbate; (kJ/mol)  
 $\phi_{min}$  = minimum sum of square of residuals; (-)  
 $\sigma$  = distance between nuclei of an adsorbate-adsorbent atom pair with zero energy of interaction in equation (3.3-1); (nm), also used as cross sectional area of adsorbate molecule in equation (3.6-1); (nm<sup>2</sup>)

#### CHAPTER V

- $a$  = coefficient in discretization equation  
 $b$  = constant term in discretization equation  
 $C_p$  = specific heat of molecular sieves ; (kJ/kg K)  
 $d_p$  = average diameter of pellets ; (m)  
 $k$  = effective thermal conductivity; (kW/m K)  
 $k_o$  = effective thermal conductivity of bed at reference temperature,  $T_o$  ; (kW/m K)  
 $k(T)$  = effective thermal conductivity of bed at temperature  $T$  ; (kW/m K)  
 $\bar{k}$  = average effective thermal conductivity of bed ; (kW/m K)  
 $L$  = length of packed bed ; (m)

$l_p$	= average length of pellets ; (m)
$Q_L$	= rate of heat supplied by imbedded heater per unit length ; (kW/m)
$R$	= inner radius of packed bed ; (m)
$r$	= radial distance ; (m)
$r_o$	= outer radius of imbedded heater ; (m)
$S$	= general source term ; (kJ/m <sup>3</sup> s)
$S_P$	= coefficient of $T_P$ in the linearized source expression ; (-)
$T$	= temperature ; (K)
$t$	= time ; (s)

### Greek symbols

$\alpha$	= thermal diffusivity of bed ; (m <sup>2</sup> /s) and also level of significance in equation (5.4-5) ; (-)
$\beta$	= parameter used in linear model ; (kW/m K <sup>2</sup> )
$\gamma$	= relaxation factor ; (-)
$\Delta r$	= r-direction width of the control volume ; (m)
$\Delta V$	= volume of the control volume ; (m <sup>3</sup> )
$\Delta \theta$	= $\theta$ -direction width of the control volume
$\delta \theta$	= $\theta$ -direction distance between two adjacent grid points
$\partial$	= partial derivative
$\theta$	= coordinate (cylindrical)
$\rho$	= bulk density ; (kg/m <sup>3</sup> )
$\epsilon$	= prespecified tolerance; (-)

### Subscripts

$b$	= bed
$C$	= constant part
$E$	= neighbour in the positive $\theta$ -direction, i.e. on the east side
$e$	= control volume face between P and E
$f$	= final
$h$	= heater surface
$i$	= ith grid point



- N = neighbour in the positive r-direction, i.e. on the north side
- n = no. of grid points used in discretization, and control volume face between P and N
- o = initial
- P = central grid point under consideration
- S = neighbour in the negative r-direction, i.e. on the south side
- s = control volume face between P and S
- W = neighbour in the negative  $\theta$ -direction, i.e. on the west side
- w = control volume face between P and W

### Superscripts

- o = value of parameter at previous time step
- exp = experimentally observed values
- pre = predicted values

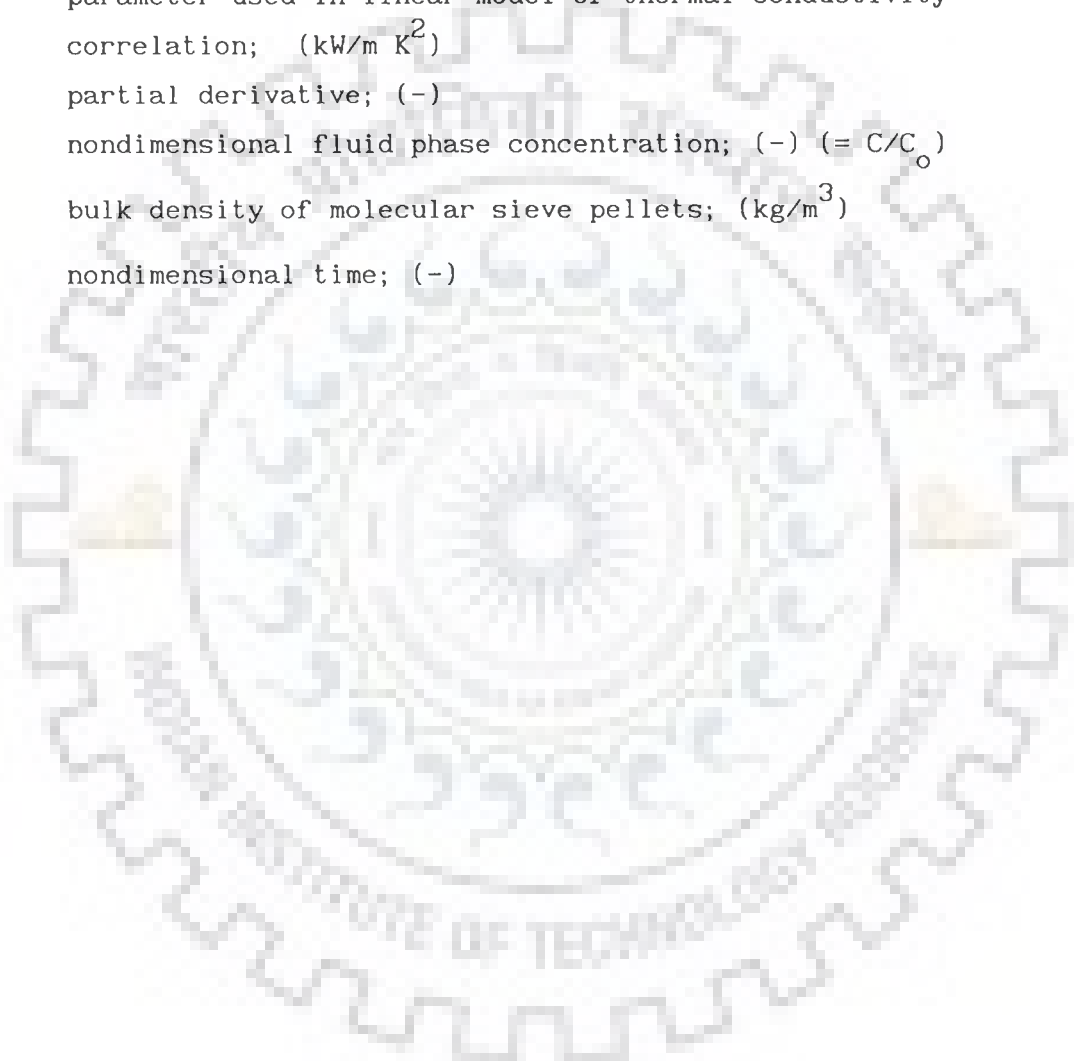
## CHAPTER VI

- A = nondimensional adsorbed phase concentration; (-)
- $\bar{A}$  = average nondimensional adsorbed phase concentration; (-)
- $a_1, a_2$  = coefficients in parabolic concentration profile; (-)
- $a_n$  = coefficient in general concentration profile; (-)
- C = adsorbate concentration in fluid phase; ( $\text{kmol}/\text{m}^3$ )
- $C_p$  = specific heat of adsorbent pellets; ( $\text{kJ}/\text{kg K}$ )
- $D_e$  = effective diffusivity of adsorbate in adsorbent pellets; ( $\text{m}^2/\text{s}$ )
- $D_o$  = Diffusivity at minimum concentration; ( $\text{m}^2/\text{s}$ )
- $D(q)$  = concentration dependent effective diffusivity; ( $\text{m}^2/\text{s}$ )
- $\Delta H$  = heat of desorption; ( $\text{kJ}/\text{kmol}$  of water)
- K = desorption rate equilibrium constant for linear isotherm; (-)

- $k$  = effective thermal conductivity of adsorbent pellets;  
 (kW/m K)
- $K'$  =  $K \frac{C_o}{q_o}$  ; (-)
- $K^o$  = preexponential factor in desorption rate equilibrium constant; (-)
- $L$  = length of adsorbent bed; (m)
- $n$  = exponent of  $x$  in general equation for concentration profile; (-)
- $p$  = total pressure in the packed bed during desorption; (atm)
- $Q$  = rate of heat supplied by the imbedded coaxial heater; (kW)
- $q$  = adsorbed phase concentration; (kmol/m<sup>3</sup>)
- $\bar{q}$  = adsorbed phase concentration averaged over pellet volume; (kmol/m<sup>3</sup>)
- $\bar{q}_b$  = adsorbed phase concentration averaged over adsorbent packed bed; (kmol/m<sup>3</sup>)
- $Q_L$  = rate of heat supplied by the imbedded coaxial heater per unit length; (kW/m)
- $q_o$  = initial average adsorbed phase concentration in packed bed; (kmol/m<sup>3</sup>)
- $q_s$  = adsorbed phase concentration at saturation; (kmol/m<sup>3</sup>)
- $R$  = radius of packed bed; (m)
- $R_g$  = ideal gas constant; (atm m<sup>3</sup>/kmol K)
- $R'_g$  = ideal gas constant; (kJ/kmol K)
- $r$  = radial distance; (m)
- $r_o$  = outer radius of imbedded coaxial heater; (m)
- $r_p$  = radius of molecular sieve pellet; (m)
- $T$  = temperature; (K)
- $t$  = real time; (s)
- $x$  = nondimensional radius; (-)

## Greek symbols

- $\alpha$  = thermal diffusivity of packed bed of molecular sieves;  
( $\text{m}^2/\text{s}$ )
- $\alpha_1$  = a constant; (-)
- $\alpha_2$  = a constant; (-)
- $\beta$  = parameter used in linear model of thermal conductivity correlation; ( $\text{kW}/\text{m K}^2$ )
- $\partial$  = partial derivative; (-)
- $\phi$  = nondimensional fluid phase concentration; (-) ( $= C/C_o$ )
- $\rho_b$  = bulk density of molecular sieve pellets; ( $\text{kg}/\text{m}^3$ )
- $\tau$  = nondimensional time; (-)



---

## INTRODUCTION

---

Adsorption-Desorption as a unit operation for the separation of adsorbable gases or vapours from inert or sparingly adsorbable gases has been in use in Chemical Industry for a long time. Petroleum refineries and natural gas installations use this process maximum in separation of hydrocarbon mixtures. A large number of industries are also employing it for dehydration of gaseous streams. Commonly used adsorptive gas separation processes are summarized in Table 1.0-1 [Yang (1987)].

In adsorption process, selection of the suitable adsorbent depends upon its adsorption capacity and also on its ability to sustain frequent adsorption - desorption cycles. In earlier times, activated alumina, activated carbon, and silica gel were in use. But these adsorbents do not possess a uniform pore size and can be used only for moderate temperature applications. Uniformity of pore size and large scale deposits of mineral zeolites in nature attracted the attention of researchers. Due to pores of uniform size, zeolites separate molecules from a mixture on the basis of their size. Later, synthetic zeolite molecular sieves have become available in different pore sizes. Consequently, the use of zeolites has increased tremendously in last two decades. Table 1.0-2 provides some potential applications of zeolites [Breck (1980)].

In the conventional adsorption separation process, there are generally two beds of adsorbent; first is used to adsorb the adsorbate from a feed stream, while the second one, which is previously saturated during adsorption, undergoes desorption/regeneration. Thus, the separation process is generally carried out in a cycle. The present

Table 1.0-1 Common Industrial Adsorptive Gas Separation Processes

S.No.	Separation*	Adsorbent
<b>1</b>	<b>Gas bulk Separation</b>	
(a)	n-paraffin/iso paraffins, aromatics	Zeolite
(b)	N <sub>2</sub> /O <sub>2</sub>	Zeolite
(c)	O <sub>2</sub> /N <sub>2</sub>	Carbon molecular sieve
(d)	CO, CH <sub>4</sub> , CO <sub>2</sub> , N <sub>2</sub> , NH <sub>3</sub> /H <sub>2</sub>	Zeolite, activated carbon
(e)	Acetone/vent streams	Activated carbon
(f)	C <sub>2</sub> H <sub>4</sub> /vent streams	Activated carbon
<b>2</b>	<b>Gas Purification</b>	
(a)	H <sub>2</sub> O /Olefin containing cracked gas, natural gas, air, synthesis gas, etc.	Silica, alumina, zeolite
(b)	CO <sub>2</sub> /C <sub>2</sub> H <sub>4</sub> , natural gas etc.	Zeolite
(c)	Organics/vent streams	Activated carbon, others
(d)	Sulphur compounds/natural gas, hydrogen, liquified petroleum gas (LPG), etc.	Zeolite
(e)	Solvents/air	Activated carbon
(f)	Odours/air	Activated carbon
(g)	NO <sub>x</sub> /N <sub>2</sub>	Zeolite
(h)	SO <sub>2</sub> /vent streams	Zeolite
(i)	Hg/chlor-alkali cell gas effluent	Zeolite

\* Adsorbates are listed first.

**Table 1.0-2 Potential Uses of Zeolites**

S.No.	Application
1	<p><b>Adsorption</b></p> <ul style="list-style-type: none"> <li>(a) Adsorbents for sieving</li> <li>(b) Hydrophobic adsorbents</li> <li>(c) Gas storage systems</li> <li>(d) Carriers of chemicals</li> </ul>
2	<p><b>Nuclear Industry Applications</b></p> <ul style="list-style-type: none"> <li>(a) Purification of cesium and strontium radio isotopes</li> <li>(b) Enrichment of isotopes</li> </ul>
3	<p><b>Environmental Engineering</b></p> <ul style="list-style-type: none"> <li>(a) Weather modification</li> <li>(b) Solar energy</li> </ul>
4	<p><b>Agriculture</b></p> <ul style="list-style-type: none"> <li>(a) Fertilizer and soils</li> <li>(b) Animal culture</li> </ul>
5	<p><b>Consumer Applications</b></p> <ul style="list-style-type: none"> <li>(a) Beverage carbonation</li> <li>(b) Laundry detergents</li> <li>(c) Flame extinguishers</li> <li>(d) Electrical conductors</li> <li>(e) Ceramics</li> <li>(f) New catalysts</li> </ul>

research work concerns with the desorption/regeneration process in a packed bed of molecular sieves. Two types of regeneration processes, viz. Thermal Swing and Pressure Swing, are mainly used in almost all applications, and are therefore briefly described in the following paragraph. However, these alongwith other processes of regeneration are described in somewhat more detail in the Chapter II on Literature Review.

In the Thermal Swing Adsorption (TSA) process adsorbate is removed from the adsorbent by increasing bed temperature with hot carrier gas, essentially at constant pressure. While, for desorption of adsorbate in the Pressure Swing Adsorption (PSA) process, pressure is lowered, but the temperature is kept constant. Out of these two processes PSA is relatively newer. This process came into being in mid sixties. PSA is quite suitable for weakly adsorbed species and is very popular in bulk separation of  $O_2$  from air and production of  $H_2$ . Other processes are purge gas stripping and displacement desorption.

TSA is the oldest amongst all the regeneration processes and is widely used for purification purposes. This process is suitable for strongly adsorbed species and is very popular for the removal of water vapour from gaseous streams. The thermal swing desorption is facilitated by passing a hot carrier gas through the adsorbent bed. In this technique, condensable adsorbates can easily be recovered by passing the effluent from the adsorber through a condenser. However, if the adsorbates are noncondensable, then these shall naturally be diluted with the inert carrier gas and their removal may require an additional separation unit. Besides, TSA also suffers with following drawbacks as observed in industrial practice.

- It requires storage and handling of carrier gas cylinders which makes it unsuitable for small adsorber units. The threat of explosion hazards is always there due to oxygen enrichment and high pressure gas in the adsorber columns [Schoofs (1992)].
- The process is energy intensive as it needs large amount of thermal energy.

Therefore, in order to recover contamination free noncondensable adsorbate without any significant loss and also to reduce the energy consumption, it is necessary to heat the bed without carrier gas. Jacketted heating is possible but it loses its applicability to large diameter beds used commercially, because of the relatively poor thermal conductivity of adsorbents. Thus, the packed bed desorption in which bed is heated by internally imbedded electrical heater(s), appears to be a potential alternative. To the best of our knowledge, potentials of this technique have not yet been fully explored, though internally heated adsorber columns were earlier in practice for small size units [Weiner (1974)].

In our Chemical Reaction Engg. Laboratory, preliminary studies on this desorption process has proved its viability [Prasad (1988)]. 13X molecular sieves manufactured indigenously, were used as adsorbent. The bed saturated with water vapour was desorbed using an electrical heater, imbedded in the bed. Main emphasis in this research work was on dry bed conduction studies and so the effective thermal conductivity / diffusivity of bed was determined. It has been reported in the literature that the thermal conductivity of a packed bed depends upon temperature, but the dependence is scarcely estimated. Furthermore, few desorption experimental runs were also conducted. A mathematical model has also been proposed for this desorption process, which assumed desorption to be completely conduction controlled and ignored the intraparticle diffusional effects. Due to this reason, model predictions were quite far from the experimental ones; predicted and experimental desorption times are about 2.5 hours and 8-9 hours respectively. Besides, 13X molecular sieves used were indigenously manufactured, for which no systematic characterization was available/or done by Prasad (1988).

In view of the viability of proposed desorption process, the present research project has been undertaken. In formulating the objectives, it has been kept in mind that the results of this research work may further enhance our knowledge of this desorption process, so that it may be designed and used commercially. In the present study



too, water vapour - 13X molecular sieves has been considered as adsorbate-adsorbent system. This is due to the fact that for drying air, 13X molecular sieve adsorbent pellets are more suited because of their high pore volume and highest hydrothermal stability among the commercially available adsorbents. These properties make it suitable for higher regeneration temperature and increased number of adsorption/desorption cycles.

## 1.1 OBJECTIVES

The main objectives of the thesis are as follows :

- (i) **Characterization of 13X molecular sieves**
  - (a) To determine the surface area and micropore volume of molecular sieves by adsorption experiments.
  - (b) To evaluate the results, obtained by using various methods.
- (ii) **Estimation of dependency of effective thermal conductivity of a packed bed of molecular sieves on temperature**
  - (a) To design and fabricate the experimental set up so that the on-line data acquisition may be possible.
  - (b) To determine the correlation for temperature dependence of effective thermal conductivity.
  - (c) To carry out the statistical analysis of estimated correlation for effective thermal conductivity.
- (iii) **Development of a mathematical model for the proposed desorption process**
  - (a) To develop a mathematical model for the desorption which includes the intraparticle diffusional effects.

- (b) To develop a computational algorithm to solve the model numerically.
- (c) To investigate the dependence of intraparticle diffusivity on adsorbate concentration.
- (d) To validate the model with available experimental results.

## 1.2 ORGANISATION OF THESIS

The thesis has been organised into seven chapters. Chapter II describes the history of development of zeolites, adsorptive separation processes, and the literature review related to various aspects of modified thermal swing process. Characterization of 13X molecular sieves is presented in Chapter III. Results obtained by various methods of characterization are critically analysed here to ascertain the accuracy of their predictions. Chapter IV discusses the details of experimental set up, and the procedure for measuring transient radial temperature profiles in the packed bed of molecular sieves. Furthermore, the correlation for dependence of effective thermal conductivity of bed on temperature is an important constitutive relationship, required for modelling. Its estimation using experimental data, obtained in the preceding chapter, is described in Chapter V. An improved mathematical model of packed bed thermal desorption process, using an imbedded electrical heater has been proposed in Chapter VI. Development of a simplified model is also presented alongwith its validation with the available experimental results. Finally, Chapter VII highlights the main conclusions of the thesis and provides the recommendations for future work.

---

## LITERATURE REVIEW

---

### 2.0 INTRODUCTION

This chapter has been written keeping various aspects in mind, and also an attempt has been made to present information relevant to thermal desorption studies on molecular sieves. One of the considerations has been that the chapter be self contained in itself. Therefore, it begins with a historical background of adsorption process. A chronology is also provided for the adsorption process and zeolites. A brief discussion on availability and types of mineral zeolites is given. Brief details of various techniques used for regeneration are also given.

To discuss the available information on water vapour adsorption and desorption, research papers in this area are briefly reviewed. Results pertaining to the characterization of 13X molecular sieves are collected from the relevant papers and research monographs, and are presented in the text. Various approaches which are used for the estimation of thermal conductivity of materials are presented. The available values of thermal conductivity of catalytic and other porous materials are also compiled.

Various mathematical modelling approaches for adsorption / desorption studies on biporous adsorbents under which zeolite molecular sieve pellets are also categorised, are described in brief with relevant mathematical expressions. Different mass and heat transfer resistances are discussed. Besides, the modelling studies, available in literature on water vapour adsorption/desorption in/from various microporous adsorbents, are presented by listing the various modelling parameters. At the end in concluding remarks, brief summary of the chapter is given.

## 2.1 HISTORICAL BACKGROUND

Process of adsorption was discovered as early as 200 years ago when in 1773 C.W. Sheele and in 1777 A.F. Fontana observed adsorption of gases by charcoal. Later in 1785 Lowitz found that organic colouring matter could also be removed by charcoal. Adsorbents of various types are known to us. Each adsorbent has a particular advantage over the other for a specific application. Common adsorbents, their properties, and predominant uses are listed in Table 2.1-1.

One of the common drawbacks of all these adsorbents is that they do not have a uniform pore size. Thus, these are unsuitable for use in the removal of a specie which is mixed with an adsorbate having little difference in its molecular diameter or simply when high specificity of separation is desired. Zeolite molecular sieves are the adsorbents which have uniform pore size. The name zeolite was suggested by a Swedish mineralogist A.F. Cronstedt in 1756 when he found that mineral stilbite gave off steam on heating. Since then, around 40 mineral zeolites are known. The chronological history of adsorption, zeolite minerals and zeolite molecular sieves is given in Table 2.1-2 .

### 2.1.1 Naturally Occurring Zeolites

Zeolites are naturally occurring minerals. Some 37 kinds of naturally occurring zeolite minerals have been discovered [Barrer (1978)]. Fine crystals of zeolites are found in rocks of volcanic origin. Large deposits of zeolites are available in certain sediments and low grade metamorphic rocks. Various available types of mineral zeolites and their years of discovery are given in Table 2.1-3.

Mineral zeolites for industrial use are largely obtained from their deposits in arid alkaline soils where a single specie of zeolite may be found in beds of several kilometres of thickness. A useful Table on frequency and place of availability of mineral zeolites has been given by Hersh (1961). High grade natural zeolites are processed by crushing, drying, powdering, and screening. Beneficiation techniques

Table 2.1-1 General Adsorbents, their Properties and Uses [Ruthven (1984)]

S.No.	Adsorbent	Chemical Constitution	Pore Size Å	Pore Volume cm <sup>3</sup> /g	Uses
1	Silica gel	SiO <sub>2</sub> .nH <sub>2</sub> O	6-50	0.82	Desiccant at low temp.; gas chromatography.
2	Activated alumina	Al <sub>2</sub> O <sub>3</sub>	7-30	0.37	Desiccant at high temp.; gas chromatography.
3	Activated carbon	C	6-10 <sup>4</sup>	0.95	Purification of air, H <sub>2</sub> , and H <sub>2</sub> O; decolourising agent; removal of non-polar organic vapours and gases, odours.
4	Carbon molecular sieves	C	4-9	0.25	Bulk separation of N <sub>2</sub> or O <sub>2</sub> from air, purification of H <sub>2</sub> .

**Table 2.1-2 Chronological History of Adsorption, Zeolite Minerals and Zeolite Molecular Sieves [Breck (1974), Mantell (1951), Davis (1991)]**

S.No.	Year	Event
1	1100 B.C.	Gideon's tests, adsorption of gases and vapours on fleece.
2	2000 years back (approx.)	First practical use of zeolite rocks as building stones.
3	1756 A.D.	A.F. Cronstedt recognised zeolite as a mineral specie and named "Zeolite". ( <i>Zeo</i> - boil, <i>lithos</i> - stone).
4	1773, 1777 A.D.	C.W. Sheele and A.F. Fontana observed adsorption of gases by charcoal.
5	1785 A.D.	Lowitz removed organic colouring matter from solutions using charcoal.
6	1840 A.D.	A. Damour observed that crystals of zeolites could be reversibly dehydrated.
7	1856 A.D.	H. Eichhorn investigated first physico-chemical property of zeolites, i.e. ion exchange (He used Chabazite and Natrolite).
8	1896 A.D.	G. Friedel observed, zeolite can occlude liquids also. He opined that zeolites consisted of open spongy framework.
9	1909 A.D.	F. Grandjean observed adsorption of gases on zeolites like $\text{NH}_3$ , air, $\text{H}_2$ , etc. (Zeolite used was Chabazite).
10	1930 A.D.	W.H. Taylor showed first analysis of crystal structure of mineral zeolite Analcime.
11	1932 A.D.	J.W. McBain named zeolites as molecular sieves and suggested that pore opening of Chabazite was less than 5 Å.
12	1945 A.D.	R.M. Barrer showed the separation of gas mixture by zeolite mineral Chabazite.
13	1948 A.D.	Union Carbide started industrial research on manufacture of zeolite molecular sieves.
14	1954 A.D.	Introduction of synthetic zeolites and their use as molecular sieve adsorbents.
15	-	Today around 40 mineral zeolites are known, and types of synthetic zeolites are well over 150. In all, around 70 zeolite structures are known to us.

**Table 2.1-3 Naturally Occurring Zeolites and year of their Discovery  
[Barrer (1978)]**

S.No.	Zeolite	Year	S.No.	Zeolite	Year
1	Stilbite	1756	20	Mordenite	1864
2	Natrolite	1758	21	Clinoptilolite	1890
3	Chabazite	1772	22	Offretite	1890
4	Harmotome	1775	23	Erionite	1890
5	Analcime	1784	24	Kehoeite	1893
6	Laumontite	1785	25	Gonnardite	1896
7	Thomsonite	1801	26	Dachiardite	1905
8	Scolecite	1801	27	Stellerite	1909
9	Heulandite	1801	28	Ferrierite	1918
10	Gmelinite	1807	29	Viseite	1942
11	Mesolite	1813	30	Yugawaralite	1952
12	Gismondine	1816	31	Wairakite	1955
13	Brewsterite	1822	32	Bikitaite	1957
14	Epistilbite	1823	33	Paulingite	1960
15	Phillipsite	1824	34	Garronite	1962
16	Levynite	1825	35	Mazzite	1972
17	Herschelite	1825	36	Barrerite	1974
18	Edingtonite	1825	37	Merlinoite	1976
19	Faujasite	1842			

are also available but are yet to be applied on commercial scale. Types of mineral zeolites which find use in large amounts in commercial applications are mordenite, chabazite, erionite, and clinoptilolite. The various species of natural zeolites are listed in literature alongwith their chemical structures [Barrer (1978), Breck (1974)].

## 2.2 INDUSTRIAL ADSORPTION SEPARATION PROCESSES

Use of adsorption on commercial scale as a method for separation of components from a mixture have started around 40 years back when synthetic adsorbents were developed. Even at that stage and till recently, distillation has been the process of choice due to cyclic and discontinuous nature of the adsorption process. But shortage of renewable form of energy and its increasing cost forced the technologists to look back to adsorption. Moreover, such adsorbents have been developed which are specific in respect of separation of components, and by their use, product purity is enhanced.

At the industrial scale, adsorption process is now widely used in chemical and other industries. In one of the applications, use of adsorption is a must when the components to be separated from a mixture have a very little difference in their boiling points or their relative volatility is too low making their separation by distillation a tough task.

### 2.2.1 Adsorbents and their Uses

There are many solids that have the capacity for adsorbing gases or liquids. A few of them are naturally occurring and others are commercially manufactured. Generally, an adsorbent which is to be used at commercial scale must possess the following properties.

- Availability in large quantity
- High adsorption capacity
- High selectivity



- Ability to be regenerated and reused
- Physical strength
- Chemical inertness
- Inexpensive

Out of the approximately 70 zeolite structures which are now available, a few widely used synthesized zeolite molecular sieves and their common uses are given in Table 2.2-1.

### 2.2.2 Synthesis of Zeolites

Zeolites are porous crystalline aluminosilicates. The zeolite framework consists of an assemblage of tetrahedra of  $\text{SiO}_4$  and  $\text{AlO}_4$  which are joined together in various types of regular arrangements through shared oxygen atoms to form an open crystal lattice. These contain pores of molecular dimensions into which adsorbate molecule can penetrate. As the micropore structure is determined by the crystal lattice, it is precisely uniform without distribution of pore size. It is this feature which distinguishes zeolites from other microporous adsorbents.

Synthesis of zeolite molecular sieves is done mainly by two processes, viz. (i) hydrogel process and (ii) clay conversion process. In the hydrogel process the reagents are added in soluble form as sodium silicate and sodium aluminate, whereas in clay conversion process alumina is added as a clay mineral. Formation of the desired zeolite depends on maintenance of the correct conditions of pH, temperature and concentration. Seeding may also be done to promote crystallization [Ruthven (1984)].

Size of synthesized zeolite crystals are very small. It can be as small as 1-10  $\mu\text{m}$ . Use of zeolite crystals in packed bed offers large pressure drop across the two ends. Hence, to prepare a practically useful adsorbent, these crystals are to be pelletised. Pellets of suitable dimensions, porosity, and mechanical strength are made by three common pellet forming processes: extrusion to form

Table 2.2-1 Applications of Zeolite Molecular Sieves [Collins (1968), Yang (1987)]

Molecular sieve type *	Molecules adsorbed	Molecules excluded	Typical applications
3A	H <sub>2</sub> O, NH <sub>3</sub> , He (molecules with an effective diameter <3 Å)	CH <sub>4</sub> , CO <sub>2</sub> , C <sub>2</sub> H <sub>2</sub> , H <sub>2</sub> S, O <sub>2</sub> , C <sub>2</sub> H <sub>5</sub> OH (molecules with an effective diameter >3Å)	Drying cracked gas, ethylene, butadiene, and ethanol.
4A	H <sub>2</sub> S, CO <sub>2</sub> , C <sub>2</sub> H <sub>6</sub> , C <sub>3</sub> H <sub>6</sub> C <sub>2</sub> H <sub>5</sub> OH, C <sub>4</sub> H <sub>6</sub> (molecules with an effective diameter <4Å)	C <sub>3</sub> H <sub>8</sub> , compressor oil (molecules with an effective diameter >4Å)	Drying natural gas, liquid paraffins, and solvents, CO <sub>2</sub> removal from natural gas.
5A	n-paraffins, n-olefins, n-C <sub>4</sub> H <sub>9</sub> OH (molecules with an effective diameter <5Å)	iso compounds, all 4 carbon rings (molecules with an effective diameter >5Å)	n-paraffin recovery from naphtha and kerosene.
10X	iso-paraffins, iso-olefins (molecules with an effective diameter <8Å)	di-n-butylamine and larger (molecules with an effective diameter >8Å)	Aromatic separation.
13X	di-n-butylamine (molecules with an effective diameter <10Å)	(C <sub>4</sub> F <sub>9</sub> ) <sub>3</sub> -N (molecules with an effective diameter >10Å)	Desulphurization, general drying, simultaneous H <sub>2</sub> O and O <sub>2</sub> removal.

\* Each type adsorbs listed molecules plus those of preceding type.

cylindrical pellets, granulation to form spherical beads, and combined processes involving extrusion followed by rolling to form spheres. A clay binder is normally added to help convert the crystals together in order to achieve satisfactory physical strength. The proportion of binder commonly amounts to 10-20% in the final product. The commonly used binders consist of mixtures in various proportions of sepiolite, kaolinite, attapulgite and montmorillonite, often added with silica or alumina. Major characteristics of commonly used synthetic zeolite molecular sieves of Linde (Linde Division, Union Carbide Corporation ) and Davison (Davison Chemical Division, W.R. Grace & Co.) are given in Table 2.2-2. These molecular sieves are commercially available in the forms of powder, pellets, and beads.

One of the area of application of zeolites is their use as catalyst supports due to their high surface area and pore volume. This enables the reactant mixtures to come into intimate contact of each other during catalytic reactions. Easy availability, large surface area, chemical inertness and a rigid and regular pore structure make them most preferred catalyst support for petroleum industry. Various types of synthetic zeolites used in commercial applications and their different forms are given in Table 2.2-3.

### 2.3 ADSORPTION PROCESSES

Adsorption process is a surface phenomena and requires adsorbents having high surface area and pore volume. In last thirty years difficult separations have been carried out using molecular sieves as adsorbents. These separations include gases from gases, liquids from liquids, and ion exchange. Separation by adsorption can be divided into two categories: bulk separation and purification. Bulk separation is defined as adsorption of more than 10% of feed stream by weight, whereas in purification, less than 10% by weight of a gas stream is adsorbed [Yang (1987)]. In these two type of applications, different process cycles are used. Drying of air, natural gas, synthesis gas, and other industrial gases; hydrogen purification,

**Table 2.2-2 Characteristics of Major Synthetic Zeolite Molecular Sieves [Yang (1987)]**

S.No.	Molecular Sieve Type	Major Cation	Nominal Pore Size, Å	Bulk density, <sup>*</sup> kg/m <sup>3</sup>	Water Capacity wt.%
1	3A (Linde)	K	3	640.74	20.0
2	3A (Davison)	K	3	736.85	21.0
3	4A (Linde)	Na	4	656.76	22.0
4	4A (Davison)	Na	4	704.81	23.0
5	5A (Linde)	Ca	5	720.83	21.5
6	5A (Davison)	Ca	5	704.81	21.7
7	10X (Linde)	Ca	8	640.74	31.6
8	13X (Linde)	Na	10	608.70	28.5
9	13X (Davison)	Na	10	688.80	28.5

\* Bulk density is of 1/16 inch pellets or beads.

**Table 2.2-3 Types of Synthetic Zeolites Used in Commercial Applications [Breck (1980)]**

S.No.	Zeolite Type	Forms (Cation)
1	A	Na, K, Ca
2	X	Na, Ca, Ba
3	Y	Na, Ca, NH <sub>4</sub> , Rare earth
4	L	K, NH <sub>4</sub>
5	Omega	Na, H
6	Zeolon, Mordenite	H, Na
7	ZSM <sup>*</sup> -5	Various
8	F	K
9	W	K

\* ZSM- Zeolite Sonoy Mobil

sweetening of natural gas, air purification, and solvent removal are categorised under purification. Bulk separation includes production of oxygen and nitrogen from air and separation of n-paraffins from isoparaffins and aromatics.

Adsorptive separation process is a batch process by nature because the adsorbent used is to be regenerated once it is fully saturated with the adsorbate. But to make the process continuous at industrial/commercial scale, dual bed or multibed systems are used in which each bed goes through adsorption and regeneration cycles. Thus, each bed is operated batchwise individually but the system as a whole works in a continuous manner. A number of processes have been developed using different adsorbent regeneration techniques or a combination of the two regenerative methods.

### **2.3.1 Regeneration Process Cycles**

Adsorption units can be regenerated by a number of regeneration methods or a combination of them. Choice of any method is dictated by economic and technical considerations. These are availability of heat at low cost and type of adsorbate and adsorbent used. Brief descriptions of the various regeneration methods are given below.

#### **2.3.1.1 Pressure Swing Process**

In pressure swing adsorption process, regeneration of bed is carried out by reducing the total pressure of the system essentially at a constant temperature. This type of process is used generally for gaseous systems. Time required for regeneration is usually short. The method is mainly used for bulk separations. Since mechanical energy is required for pressure reduction, this process is more expensive. Moreover, this process can be used only in case of weakly held species.

### **2.3.1.2 Thermal Swing Process**

Regeneration of bed is achieved by raising the temperature in thermal swing adsorption process. Conventionally, the bed temperature is increased by purging the bed with a stream of preheated gas (or sometimes with preheated liquids). This is the oldest and a well known technique. Since time requirement of regeneration is usually large (in hours) so it is used mainly for purification purposes where adsorbed amount is less in comparison to feed rate. Hence, large throughput rates can be handled. In this process, heat is lost in the heating of carrier gas and with the exit gas as it comes out from bed at an elevated temperature.

### **2.3.1.3 Purge Gas Stripping Process**

This process also utilizes a carrier gas but without heating. The bed is regenerated essentially at a constant temperature and pressure. Bed is purged with a non adsorbing inert gas. This method is used only in case of weakly held species because in case of strongly held species, quantity of purge gas required is very large which makes the process uneconomical.

### **2.3.1.4 Displacement Desorption Process**

Displacement desorption process is similar to purge gas stripping process. The difference is only in the carrier stream which in this case is more adsorbing than the already adsorbed one, thereby displacing the adsorbed species. Regeneration is accomplished by reduction of partial pressure of adsorbate and the competitive adsorption of the displacing medium. This technique is also used in displacement chromatography.

### **2.3.1.5 Steam Stripping Process**

This process is a combination of thermal swing and displacement desorption process. Use of steam helps in increasing the

temperature of bed and in addition, it also displaces adsorbed species by adsorbing itself to the adsorbing sites.

#### **2.3.1.6 Gas Chromatography**

Gas chromatography is mainly used at laboratory scale separations. Its potential for separation of gas mixtures which are otherwise difficult to separate, has attracted the attention of researchers for scale up to plant level. An industrial scale process has been developed which can separate  $C_4 - C_{10}$  normal and isoparaffins at the rate of 1,00,000 metric ton/year [Yang (1987)].

#### **2.3.1.7 Moving Bed and Simulated Moving Bed Processes**

These processes are carried out in fixed bed where the gas mixture and solid adsorbent are allowed to contact in a countercurrent movement. Thus, the processes work under steady state as the flow rates and compositions of all the streams entering or leaving the bed are constant. Purasiv HR process is an example of combined fluidized/moving bed process [Yang (1987)]. Examples of simulated moving bed processes are Sorbex processes, viz. Molex, Olex, Parex, Ebex, and Sarex. In all these processes, requirement of adsorbent is less and desorbent is used which is as strongly adsorbed as the most strongly adsorbed component in the feed mixture but can be easily separated by distillation from the mixture components. Sorbex processes are preferred in liquid phase separations because of the problem of axial phase dispersions in vapour phase separations.

#### **2.3.1.8 Parametric Pumping Process**

In this process, the mixture to be separated moves up and down cyclically through the column by reciprocating motion of two sets of pistons one each at the two ends of the adsorber column. This cyclic process results in gradual increase in concentration in the top reservoir. Parametric pumping can be divided into two basic categories, viz. thermal and pressure types. Further, thermal parametric pumping

can be subdivided into direct and recuperative modes. This process has vast potential as it is extensively studied by different researchers but it is yet to find large scale commercial/industrial application. A beautiful description of various parametric pumping processes has been given by Yang (1987).

#### 2.3.1.9 Cycling Zone Processes

This process is similar to parametric pumping. The difference in the two processes is that unlike parametric pumping, the flow direction in cycling zone process does not change. This process can also be divided into two types, viz. thermal and pressure cycling zone processes. pH can also be used as one of the variables for cycling. In a thermal process a series of multibeds can be used in a unit where adjacent beds are at  $180^\circ$  in phase in terms of temperature changes. Number of studies carried out on this process are relatively small and it has yet to be used at commercial scale.

Advantages and disadvantages of all the processes discussed here are summarized in Table 2.3-1.

## 2.4 CHARACTERIZATION OF MOLECULAR SIEVES

Comprehensive research work on adsorption/desorption requires proper characterization of the adsorbent used. Complete characteristics of the adsorbent used in the present study, i.e. 13X molecular sieves, are rarely reported in literature. It is a well established fact that properties of various samples vary with the manufacturer and sometimes from batch to batch [Ruthven (1980)]. We have not come across any publication which have reported all/most of the properties at one place. BET surface area of 13X molecular sieves using nitrogen adsorption values are reported to be  $525 \text{ m}^2/\text{g}$  [Danner and Chol (1978), Hyun and Danner (1985), Breck (1974)] and  $527 \text{ m}^2/\text{g}$  [Inui et al. (1988)]. Dubinin (1967) reports limiting adsorption value, i.e. total



**Table 2.3-1 Comparison of commonly used Regeneration Methods [Ruthven (1984)]**

Method	Advantages	Disadvantages
Thermal swing	Good for strongly adsorbed species; small change in temperature gives large change in equilibrium adsorbed concentration. Desorbate may be recovered at high concentration. Applicable to both gaseous and liquid phase systems.	Thermal aging of adsorbent. Heat losses. Unsuitable for rapid cycling - inefficient use of adsorbent. In liquid systems, high latent heat of interstitial liquid must be added.
Pressure swing	Good where weakly adsorbed species are required in high purity. Rapid cycling - efficient use of adsorbent.	Very low pressure may be required. Mechanical energy more expensive than heat. Desorbate recovered at low purity.
Displacement desorption	Good for strongly held species. Avoids risk of cracking reactions during regeneration and no thermal aging.	Product separation and recovery needed (choice of desorbent is crucial).
Purge gas stripping	Good for thermally unstable adsorbates.	Economical only in case of weakly held species. Uneconomical for strongly held species.
Steam stripping	Suitable for solvent recovery systems.	Requires another step for desorption of water.
Gas chromatography	High separation efficiency. Separation of difficult mixtures having low separation factors or low relative volatilities for distillation is possible.	Practical difficulty in achieving low axial dispersion for large beds. Adsorbent is not used efficiently.

Table 2.3-1 (Contd...)

Method	Advantages	Disadvantages
Moving bed and simulated moving bed	High separation efficiency. Adsorbent requirement is low.	Limited only to liquid phase separations.
Thermal Parametric pumping	High separation factor* $> 10^5$ .	Commercial level process yet to be developed. Only limited to liquid phase separations.
Pressure parametric pumping (Molecular gate)	High separation factor* $> 10^5$ . Gas phase separation can be done. Binary gas mixtures can be separated with high purity of both the components.	Product purity increases at the expense of adsorbent productivity.
Thermal cycling zone	High separation factor.	Suitable for liquid phase separations only. Yet to be tried at commercial scale.
Pressure cycling zone	Good separation factor. Suitable for gas phase separation.	Complicated than Pressure swing process. Less degrees of freedom than pressure swing process. Yet to be tried at commercial scale.

\* Separation factor =  $\frac{\text{conc. in top reservoir}}{\text{conc. in bottom reservoir}}$

pore volume to be 9.55 and 10.27 mmol/g using nitrogen and argon adsorption respectively on 13X molecular sieves. These values are 0.2674 and 0.4108 cc/g respectively in terms of volume. Hyun and Danner (1985) reported micropore volume of 13X MS to be 0.24 cm<sup>3</sup>/g. Breck (1974) reports range of total micropore volume of 13X molecular sieves to be 0.25 to 0.36 cc/g using various adsorbates. In these values, total pore volume using nitrogen and argon as adsorbates are 0.35 and 0.30 cc/g respectively. According to Ponec et al. (1974) the volume of large cavities in 13X molecular sieves is about 0.30 cc/g and that of small ones is 0.05 cc/g. This indicates that it is the ability of adsorbate to penetrate into the pores of adsorbent and the final orientation of adsorbate molecule on adsorbent surface which decides the resulting total micropore volume.

For the sake of continuity, readability and understanding we have discussed the methods used for characterization in brief in Chapter III. Some beautifully presented research work covering most of the researches on characterization have been done by Seifert and Emig (1991), Anderson and Pratt (1985), Innes (1968), Broekhoff and Linsen (1970), Broekhoff and van Dongen (1970), Lee (1985), and Breck (1974). However, other useful research papers on characterization of various adsorbents using different methods are summarized in Tables 2.4-1, 2.4-2, and 2.4-3 listing brief details of their work.

## 2.5 EFFECTIVE THERMAL CONDUCTIVITY OF ADSORBENT PACKED BED

Design of adsorbent packed bed column for thermal desorption requires knowledge of thermal transport properties in the direction of heat flux, i.e. in the radial and axial directions. Radial profile of the temperature requires a two dimensional model while one dimensional model is adequate for a uniform radial temperature. Effective property (e.g. effective thermal conductivity) means the property which depends upon individual phases constituting the packed bed. The usefulness of effective properties is that their use makes the description of a mathematical model simple since they are used in place of their basic

**Table 2.4-1 Research Papers on Surface Area Determination by BET and t-plot Methods; Pore Volume by t-plot method and Pore Volume Distribution by other methods**

S.No.	Author(s)	Brief Details
<b>A Surface Area and Pore Volume Determination</b>		
1	Brown & Cadenhead (1979)	Determination of micropore volume by MP and D-R methods; mesopores by WP method, surface area by BET, MP, and WP methods of Activated Carbons.
2	Parfitt et al. (1975)	Microporous surface area determination by BET and t-plot methods.
3	Dubinin (1974)	Analysis of MP method.
4	Bhambhani et al. (1972)	Determination of surface area of silica gel by BET and t-plot methods.
5	Brunauer et al. (1969)	Modified BET equation is proposed.
6	Lamond and Price (1969)	Surface area and pore size determination of Carbon black micropores by t-plot methods.
7	Mikhail et al. (1968b)	Determination of surface area, pore size, and pore volume of silica gels by MP and corrected modelless (WP) method.
8	Mikhail et al. (1968a)	Surface area and pore volume distributions by MP method.
9	De Boer et al. (1965)	Determination of surface area distribution of narrow and wide pores, total pore volume, and pore size calculation using t-plot method.
10	Lippens and De Boer (1965)	Comparison of surface area from t-plot and BET methods.
11	Lippens et al. (1964)	Nitrogen adsorption isotherm measurement apparatus described. Correlation suggested for t-plots.
12	Barrett et al. (1951)	Pore volume and pore size distribution of coarsely porous adsorbents.
13	Brunauer et al. (1940)	Classification of isotherms.
14	Brunauer et al. (1938)	Classical method, i.e. BET method for determination of surface area.

**Table 2.4-1 (Contd...)**

S.No.	Author(s)	Brief Details
<b>B Pore Size Distribution</b>		
1	Horváth & Kawazoe (1983)	Pore size distribution method for fine pores using adsorption isotherm data.
2	Dollimore & Heal (1964)	Pore size distribution method for super micropores and intermediate pores.
<b>C Apparatus on Nitrogen Adsorption by Continuous Flow Method</b>		
1	Cahen & Marechal (1963)	A surface area determination method, using mixture of nitrogen and helium eliminating the possibility of error due to the presence of water, is discussed.
2	Eberly (1961)	Surface area determination by nitrogen adsorption using a carrier gas with continuous flux is discussed.
3	Nelsen & Eggertsen (1958)	Thermal conductivity measurement technique discussed for determination of nitrogen concentration in effluent stream of BET surface area measurement using mixture of nitrogen and helium.

**Table 2.4-2 Research Papers on Theory of Volume Filling in Micropores (TVFM)**

S.No.	Author(s)	Brief Details
1	Dubinin & Stoeckli (1980)	Value of exponent $n$ is suggested, pore volume and characteristic energy calculated for carbon molecular sieves using TVFM.
2	Rand (1976)	Comparison of Dubinin-Radushkevich and Dubinin-Astakhov equations for linearity of plots and importance of exponent $n$ .
3	Dubinin & Astakhov (1971)	A method based on TVFM is proposed for characterization of zeolites, based on adsorption which can be used for determination of micropore volume, surface area etc.
4	Marsh & Rand (1970)	Study of various parameters of Dubinin-Radushkevich equation using adsorption data on microporous carbons.
5	Dubinin (1967)	Comparison of TVFM and adsorption data in different microporous adsorbents.
6	Bering et al. (1966)	Theory of Volume Filling in Micropores (TVFM) alongwith pore size classification has been discussed.

**Table 2.4-3 Research Papers on Physical Testing of Pellets**

S.No.	Author(s)	Brief Details
1	Beaver (1974)	Description of Crush Strength tests for different forms of catalyts.
2	Dart (1974)	Description of mechanical test for attrition losses.
3	Adams et al. (1974)	Standardization of crush strength and attrition losses testing.

properties for a homogeneous medium. Axial conduction of heat theoretically exists but generally it is so small compared to the heat transfer by bulk flow that it can be neglected [Doraiswamy and Sharma (1984)]. If the temperature profile across the cross section of the bed is flat, then the entire resistance to heat transfer can be assumed to be localized at the wall. In such a case thermal conductivity does not come into picture and the entire heat transfer can be described by overall heat transfer coefficient at the wall. In an another situation where radial temperature profile in a packed bed is uniform from the axis of the bed right upto the wall thickness, the entire radial heat transport can be described by a single parameter, i.e. the effective thermal conductivity of the bed and in such a case, incorporation of wall heat transfer coefficient into the model is not required. Thus, the mathematical description of radial transport of heat in a packed bed can be represented by a two dimensional model using one or two heat transfer parameters. Therefore, three types of following approaches can be possible to analyse radial heat transfer process.

- Assume a one-dimensional model and calculate an overall heat transfer coefficient at the wall.
- Assume a two-dimensional model with two parameters, and calculate effective thermal conductivity for the bed and a heat transfer coefficient at the wall.
- Assume a two-dimensional model with one parameter, and calculate effective thermal conductivity for the bed on the basis of a continuously varying temperature from the axis to the wall.

Coberly and Marshall (1951) and Dewasch and Froment (1972) have used radial temperature profile measurements. Further, Tsang et al. (1976) and Michelsen (1979) have used Orthogonal Collocation and modified Orthogonal Collocation to obtain more reliable values from radial temperature measurements.

### 2.5.1 Relationship based on Reynolds Number

---

Relationships have been proposed in past in which effective thermal conductivity has been expressed as a function of Reynolds number [Coberly and Marshall (1951), Satterfield (1979)]. These relationships are straight line relationships and can be expressed in general form as follows:

$$k_{\text{eff}} = A + B \text{ Re} \quad (2.5-1)$$

where

A = intercept

B = slope

### 2.5.2 Static Contributing Factors

---

Total effective thermal conductivity of a packed bed in the direction of heat flux is contributed by three static factors, viz. conduction, natural convection, and radiation. It can be written as

$$k_{\text{eff}} = k_{\text{ea}} + k_{\text{eb}} + k_{\text{ec}} \quad (2.5-2)$$

Out of these factors, heat transfer due to convection is generally negligibly small compared to that due to conduction. Since temperatures in packed bed are not very high during adsorption or desorption process (i.e.  $< 800^\circ\text{C}$ ), contribution due to radiation can also be neglected. Thus, entire static contribution to effective thermal conductivity may be assumed to be due to conduction alone.

#### 2.5.2.1 Axial Effective Thermal Conductivity

Generally, as stated earlier, effect of axial thermal conductivity is neglected in design calculations of adsorbent packed beds. However, procedures have been developed which indicate relative importance of axial thermal conductivity. This is done in order to



justify as to why its effect can be ignored. Notable studies have been made in this regard. Harriot (1975) has reviewed the models for thermal conductivity estimation and has summarized previously published results.

An excellent review on estimation of effective transport properties is given by Doraiswamy and Sharma (1984). Correlations for estimation of effective radial thermal conductivity have been presented alongwith approximate ranges of radial effective thermal conductivities in packed beds. Effective axial thermal conductivity for 5A MS is reported by Kumar and Dissinger (1986) to be  $\approx 13.794 \times 10^{-4}$  kW/m K. Furthermore, the thermal conductivities of porous catalytic materials which are similar to 13X molecular sieves are reported in Tables 2.5-1, 2.5-2, and 2.5-3.

## 2.6 ADSORPTION/DESORPTION MODELLING STUDIES

In the early years of Chemical Engineering, unit operation of fixed bed adsorption did not receive much attention of researchers because of its unsteady state nature. Hougen and Marshall (1947) were among the first to pay attention to this area. Rosen (1952) came out with first mathematical model on solid diffusion considering the adsorbent particles to be spherical. His pioneering approach to solve the model using a combined method of analytical and numerical solution with a digital computer proved to be a boon in design calculations. Later Mass Transfer Zone (MTZ) concept was advanced with an assumption that it moves through the bed. To consider the effect of increase in temperature of adsorbent particles by the heat of adsorption, it was proposed that the Heat Transfer Zone (HTZ) precedes MTZ [Carter(1980)]. MTZ method is simple to understand and has been widely used in design of adsorber columns. This method required minimum number of tests. The length of MTZ is a measure of the rapidity of the adsorption process. The length of MTZ is independent of the bed length. MTZ lengths can be obtained experimentally. Graphical correlations are made and these graphs are used for design purposes. Generally, it is a function of the

**Table 2.5-1 Thermal Conductivities of Some Porous Catalysts in Air at 90 °C, Atmospheric Pressure [Satterfield (1980)]**

S. No.	Catalyst	k ( $\times 10^3$ kW/m K)		Density, kg/m <sup>3</sup>	
		Particle	Powder	Particle	Powder
1	Cobalt-molybdenum dehydrogenation catalysts	0.35	0.21	1.63	1.56
		0.24	0.14	1.54	1.09
2	Chromia-alumina reforming catalyst	0.29	0.18	1.40	1.06
3	Silica-alumina cracking catalyst	0.36	0.18	1.25	0.82
4	Platinum-alumina reforming catalyst	0.22	0.13	1.15	0.88

**Table 2.5-2 Thermal Conductivities of Selected Porous Materials  
[Satterfield (1980)]**

S. No.	Material	Fluid in pores	Temp. (°C)	Pellet Density (kg/m <sup>3</sup> )	Porosity		k (×10 <sup>3</sup> kW/m K)	
					Macro	Micro	100 kPa	Vacuum
1	Alumina(boehmite) pellets	Air	50	1120	0.134	0.409	0.22	0.16
				670	0.450	0.275	0.13	0.07
2	Pellets of Silver powder	Air	34	2960	0.144	0.574	0.71	0.06
				1350	0.61	0.261	0.17	0.09
3	Cu on MgO pellets*	Air	25-170	700-1200*	--	--	0.08-0.17	--
4	Pt on alumina pellets, 0.05 wt%	Air	--	1340	0.35	0.15	0.15	--
5	Pt on alumina pellets	H <sub>2</sub>	68	570	0.56	0.23	0.26	--
6	Bed of stainless steel shot, 71 μm in diameter	Air	42	577 (bed density)	0.264	--	0.26	0.02
7	Bed of glass beads 29, 80, 200 or 470 μm in dia.	Air	42	1500 (bed density)	0.38	--	0.18	0.05

\* Carbon deposits present to various degrees.

Table 2.5-3 Thermal Conductivity of nickel-impregnated silica and silica-alumina [Satterfield (1980)]

S. No.	Composition	Range of macro porosity	Range of thermal conductivity ( $\times 10^3$ kW/m K)
1	Pure silica (particle dia. $\approx$ 2-3 $\mu$ m)	0.16-0.50	0.17-0.13
2	Porous silica - 25% alumina (particle diameter $\approx$ 70 $\mu$ m)	0.12-0.45	0.20-0.13
3	Coprecipitated 62% Ni on silica	0.35-0.43	0.21-0.16
4	62% Ni impregnated on silica	0.20-0.40	0.21-0.13
5	5% Ni impregnated on silica	0.16-0.32	0.18-0.16
6	0.5% Ni impregnated on silica	0.20-0.33	0.17-0.16
7	0.5% Ni impregnated on silica-25% alumina	0.16-0.33	0.24-0.22

following parameters [Hersh (1961)].

- Type of adsorbent
- Adsorbent particle size
- Fluid velocity
- Fluid properties
- Adsorbate concentration in the entering fluid and in the adsorbent bed (before adsorption starts)
- Temperature
- Pressure
- Previous history of the system

Requirement of drying of various industrial gaseous streams, products, and intermediate products drew attention of chemical engineers and thus several research papers came on this aspect using molecular sieves and other desiccants.

Availability of high speed digital computers later enabled the researchers to solve simultaneous heat and mass balances with rate equations by using suitable numerical techniques. Earlier, most of the studies were made on adsorption. In practice, continuous fixed bed adsorption is a cyclic process and depends upon satisfactory performance of the regeneration. Earlier, research papers on regeneration were limited and the semi-empirical heat balance method was used for calculation. Later, researchers have used fixed bed equations to study the effect of favourable isotherms on the shape of isothermal adsorption and desorption curves [Zwiebel et al. (1972), Garg and Ruthven (1973a&b, 1974a&b, 1975a&b)].

### **2.6.1 Mathematical Modelling of Adsorption Kinetics/Diffusion in Biporous Adsorbents**

---

Zeolite molecular sieve pellets possess two types of porosities, namely macro- and microporosity. Microporosity resides in the zeolite crystals, whereas macroporosity is introduced by the clay binder which is used to form the pellets by assembling the crystals

together. Thus, the existence of two porosities make the pellets biporous. Use of the pellets is preferred because it offers reduced pressure drop across the packed bed compared to that of crystals.

Mathematical modelling of adsorption/desorption kinetics can be done by classifying the various possibilities according to the following criteria.

#### 2.6.1.1 Resistance to Transfer Processes

Adsorption process is a rapid process. The overall rate of adsorption or desorption, is therefore, always controlled by mass or heat transfer resistance. There are several distinct resistances to mass and heat transfer. A detailed examination of kinetic data is needed under carefully controlled condition to know as to which resistance is dominant. Both the types of resistances are discussed in detail in the following subsection.

##### (a) Mass Transfer Resistances

Generally, a biporous adsorbent offers four distinct resistances to mass transfer, which are as follows :

- (i) diffusional resistance of laminar fluid film (only in case of binary or multicomponent fluid phase)
- (ii) diffusional resistance of meso and/or macropores
- (iii) external film resistance at the external surface of microparticle
- (iv) diffusional resistance of micropores

These resistances are effective in the order as they are mentioned during adsorption. During the desorption process they come into effect in the reverse order. The relative magnitude of these resistances varies widely, depending upon the particular system and the prevailing conditions.

Analysis of these mass transfer resistances suggests that resistance due to external fluid film is seldom dominant. Relative importance of macropore and micropore resistances can vary over several orders of magnitude and in few cases both of them may be significant.

*(b) Heat Transfer*

Adsorption process is in general an exothermic process. The temperature of the adsorbent may be assumed to be constant only when the rate of heat dissipation by conduction, convection, and radiation is high relative to the adsorption rate. In addition to mass transfer resistance, three distinct resistances to heat transfer may also be considered, if significant. They are conduction through micro and macro particles; and convection from the external surface. Following types of heat transfer rates are generally considered.

- (i) isothermal; rapid heat transfer
- (ii) nonisothermal; slow heat transfer

Since the thermal conductivity of adsorbent particles is generally much higher than that of a gas, the ratio of time constants for internal and external heat transfer,  $\delta$  is greater than unity [Kärger and Ruthven (1992)]. This implies that internal conduction should always be faster than the external heat transfer. Thus, the assumption that the particles are isothermal with all heat transfer resistance concentrated in the external fluid film with the temperature essentially uniform throughout the adsorbent particle is an excellent approximation under most practically important conditions.

#### **2.6.1.2 Equilibrium Relationship**

Equilibrium relationship describes the relationship between fluid and adsorbed phase concentration. This can be obtained by finding out the governing isotherm, which may be linear or nonlinear.

## *Isothermal Linear Equilibrium System*

The various types of mass transfer controlled systems are described in the following subsections with their mathematical expressions alongwith initial and boundary conditions for adsorption. The description is limited to isothermal systems only.

### **2.6.1.3 External Fluid Film Control**

Generally, when adsorbent is nonporous, adsorbate can be adsorbed onto the external surface only; or when the diffusion within the porous adsorbent particles is very rapid, then the rate of adsorption will be controlled by the laminar fluid film surrounding the particle. Under these conditions, the fluid phase concentration at the particle surface and the adsorbed phase concentration throughout the particle will be in equilibrium. Moreover, there is no gradient of concentration within the particle. The rate of adsorption in this case is given by

$$\frac{d\bar{q}}{dt} = k_f a (C - C^*) \quad (2.6-1)$$

For spherical particle,

$$a = \frac{3}{r_p}$$

and for a small change in concentration, linear equilibrium concentration

$$q^* = KC \quad (2.6-2)$$

and if  $C$  is maintained constant, the rate expression can be written as

$$\frac{d\bar{q}}{dt} = \frac{3k_f}{K r_p} (q^* - q) \quad (2.6-3)$$



#### 2.6.1.4 Macropore Diffusion Control [Garg and Ruthven (1974b)]

In the case when micropore diffusion is rapid, the concentration profile within the crystal will be uniform and rate of adsorption or desorption will be controlled by diffusion through the macropores of the pellet. Bed of small adsorbent particles or zeolite crystals also behaves in the same way. If intracrystalline diffusion is rapid, the adsorption rate may be controlled by the diffusion through the interparticle voids just as in the case of macropore diffusion controlled adsorption in pellets. These two types of situations are similar but not identical to the micropore diffusion controlled situation. The difference in the two is that the accumulation of adsorbate generally occurs mainly in the micropores so the rate of adsorption depends upon micropore capacity as well as on the macropore diffusivity.

The mathematical expression for macropore diffusion controlled adsorption rate is

$$\frac{1}{R^2} \frac{\partial}{\partial R} \left[ R^2 D_p \frac{\partial C}{\partial R} \right] = \frac{\partial C}{\partial t} + \left[ \frac{1-\epsilon_p}{\epsilon_p} \right] \frac{\partial \bar{q}}{\partial t} \quad (2.6-4)$$

*Initial and Boundary Conditions*

$$q(r, 0) = C(R, 0) = 0 \quad (2.6-5)$$

$$\frac{\partial C}{\partial R}(0, t) = 0 \quad (2.6-6)$$

$$C(r_p, t) = C(t) \quad (2.6-7)$$

#### 2.6.1.5 Bed Diffusion [Ruthven (1984)]

A packed bed of zeolite crystals behaves as biporous zeolite pellet when diffusion into the bed occurs at a rate comparable with or slower than diffusion into the adsorbent crystals within the bed. The procedure is similar to that of macropore diffusion controlled

adsorption. The mathematical expression in such a case is given by

$$D_p \frac{\partial^2 C}{\partial z^2} = \frac{\partial C}{\partial t} + \left( \frac{1-\epsilon}{\epsilon} \right) \frac{\partial \bar{q}}{\partial t} \quad (2.6-8)$$

*Initial and Boundary Conditions*

$$q(r,0) = KC(z,0) = 0 \quad (2.6-9)$$

$$\frac{\partial C}{\partial z}(0,t) = 0 \quad (2.6-10)$$

$$C(1,t) = C(t) \quad (2.6-11)$$

#### 2.6.1.6 Micropore Diffusion Control [Garg and Ruthven (1973b, 1974a)]

When diffusion through external fluid film and macropores is rapid and the diffusion within the microparticle is rate controlling, the adsorption rate is given by appropriate solution of the transient diffusion equation, which for a spherical adsorbent crystal may be written as

$$\frac{\partial q}{\partial t} = \frac{1}{r^2} \frac{\partial}{\partial r} \left( r^2 D_c \frac{\partial q}{\partial r} \right) \quad (2.6-12)$$

*Initial and Boundary Conditions*

$$q(r,0) = 0 \quad (2.6-13)$$

$$\frac{\partial q}{\partial r}(0,t) = 0 \quad (2.6-14)$$

$$q(r_c, t) = KC(R, t) \quad (2.6-15)$$

Average adsorbed phase concentration in microparticle can be written as

$$\bar{q}(R, t) = \frac{3}{r_c} \int_0^{r_c} q r^2 dr \quad (2.6-16)$$

Some of the notable modelling studies on adsorption / desorption of water vapour in/from various adsorbents is listed in Table 2.6-1 alongwith their modelling parameters.

Some other experimental research work on adsorption / desorption of water vapour on various adsorbents are reported by Marcussen and Vinding (1982), Jury and Horng (1973), Punwani et al. (1968), and Nutter and Burnet (1966).

## 2.7 MOTIVATION FOR THE PRESENT STUDY

As mentioned in the chapter on Introduction, the modified thermal swing process is a useful regeneration/desorption method for packed bed adsorbers. Such a process is also energy efficient, and suitable in situations where the adsorbate is noncondensable and its recovery is important. Earlier research work on this technique in our laboratory has proved its viability for both small and large scale operations [Prasad (1988)]. These studies were mainly confined to dry bed experiments on small and large diameter adsorbers, though few experimental runs on desorption were also taken. Mathematical model of the desorption process, developed in these studies, assumes desorption to be purely conduction controlled, and neglects the intraparticle diffusion of adsorbate within the molecular sieves pellet. Due to this reason, predictions of the model are unrealistic vis-a-vis experimental observations. Besides, effective thermal conductivity of the adsorbent bed is an important parameter which governs the transport of heat in the adsorber. Although, this parameter varies with the temperature [Bird et al. (1960)], but this dependency is rarely estimated.

In view of the above, present studies on this thermal desorption process has been undertaken to achieve the objectives, mentioned in section 1.1.

Table 2.6-1 Modelling Studies on Adsorption/Desorption of Water on Adsorbents

Author(s)	Thermal Condition	Mass Transfer Resistance	Isotherm	Adsorption or Desorption	System studied	Solution Method
Malecky et al. (1991)	Non-isothermal	--	Non-linear (empirical)	Desorption	C <sub>2</sub> H <sub>4</sub> -H <sub>2</sub> O-3A MS Regenerant: CH <sub>4</sub>	Numerical Solution
Hills (1991)	Isothermal	Fluid to particle + internal diffusion	Linear	Adsorption	Theoretical study	Analytical solution
Haefner & Thodos (1986)	Adiabatic	Gas film + intra-particle	Langmuir	Adsorption	Air-Water vapour-13X MS	Numerical solution
Chihara & Suzuki (1983)	Isothermal Non isothermal	Gas film	Freundlich	Adsorption desorption	Air-Water vapour-silica gel	Numerical solution
Friday & Levan (1982)	Adiabatic	--	Non-linear (empirical)	Desorption	Methane-Water vapour - 4A MS	Numerical solution
Marcussen (1982)	Isothermal Non isothermal	Fluid film	Freundlich	Adsorption	Air-Water vapour-Alumina	Numerical solution
Carter & Barrett (1973)	Isothermal	Fluid film + Intra-particle	Linear	Adsorption	Air-Water vapour-Activated Alumina, Silica gel, 4A MS	Numerical solution

Table 2.6-1 (Contd...)

Author(s)	Thermal Condition	Mass Transfer Resistance	Isotherm	Adsorption or Desorption	System studied	Solution Method
Marcussen (1970)	Adiabatic	Film+Intra particle	Freundlich & Langmuir	Adsorption	Air-Water vapour-Alumina	Numerical solution
Carter (1969)	Adiabatic	Surface + Pore diffusion	Non-linear (empirical)	Adsorption	Air-Water vapour-Alumina	Numerical solution
Carter (1968a)	Isothermal Adiabatic	Fluid film +Intraparticle	Linear	Adsorption	Air-Water vapour-Alumina	Numerical solution
Carter (1968b)	Isothermal Adiabatic	Fluid film +Intraparticle	Nonlinear (empirical)	Adsorption	Air-Water vapour-Alumina	Numerical solution
Lee & Cummings (1967)	Isothermal	Gas film	Linear	Adsorption	Air-Water vapour-Silica gel	Analytical solution
Collins (1967)	Isothermal	--	Linear	Adsorption	Nitrogen-Watervapour-4A MS	Numerical solution
Carter (1966)	Adiabatic	Gas film + Intraparticle	Linear	Adsorption	Air-Water vapour-Activated Alumina	Numerical solution

## 2.8 CONCLUDING REMARKS

In this chapter, historical background of adsorption process and zeolites is described alongwith their chronology. General characteristics and industrial uses of various commercial adsorbents are discussed. Synthetic and mineral zeolites are described. A brief discussion of available literature on effective thermal conductivity estimation of adsorbents and their characterization is given. Various modelling approaches applicable to biporous adsorbents are discussed. A number of research papers on water vapour adsorption /desorption are reviewed from the point of view of modelling. Lastly, the motivation for the proposed study has been explained.



---

## CHARACTERIZATION OF MOLECULAR SIEVES

---

### 3.0 INTRODUCTION

Information about the characteristics of the adsorbent used, is an important part of modelling and simulation studies of any separation process. Adsorbent characterization generally consists of the determination of physical, chemical and mechanical properties. In the present study only physical properties have been determined, because chemical composition of 13X molecular sieves is well known and available in literature [Broussard and Shoemaker (1960), Meier and Olson (1971)], and it does not vary appreciably from one manufacturer to another. The various characteristics of 13X molecular sieves which we propose to discuss are total surface area (comprising external and micropore surface areas), micropore volume, bulk density (apparent bulk density and apparent unit density) and mechanical properties, e.g. attrition losses and crushing strength. Some of the physical properties have been computed by various methods known to us; this permits one to compare them and also to comment on the limitation of each of the method.

In this Chapter, methods used to characterize molecular sieves are briefly described and thereafter, the results are analysed. Values of mechanical properties are given as reported by the manufacturer.

### 3.1 SURFACE AREA DETERMINATION METHODS

Surface area is one of the most important parameters of adsorbents. In general, adsorbents are supposed to have higher surface

area than any other nonporous solid. Although there exists two opposing schools of thoughts amongst scientists as to whether the surface area of microporous adsorbents determined through physisorption methods using nitrogen as adsorbate, is accurate or not. Nevertheless, surface area of microporous adsorbents is a good indicator of pore size distribution. The basis of the surface area determination makes use of adsorption of an adsorbate on walls of the voids. The amount of adsorbate under specified controlled conditions is used to determine the surface area. Gases/vapours are generally used as adsorbate. It is assumed that the adsorbate forms layers of its molecules on the surface, one over the other. Thus a multilayer is formed on the walls of the pores. Volume occupied by a monolayer of adsorbate molecules per unit mass at STP is known as monolayer capacity ( $V_m$ ). This can be calculated by multiplying number of molecules by volume of one adsorbate molecule. Number of molecules is obtained by Avogadro's hypothesis. Adsorbate used for this purpose is generally a nonpolar molecule such as rare gas or most commonly nitrogen. Two methods, employed widely for the purpose of surface area determination, are described below.

### 3.1.1 BET Method

Name of this method has been derived from the names of three scientists, viz. Brunauer, Emmett, and Teller, who originally developed it [Brunauer et al. (1938)]. This is the most frequently used method of analysis of multilayer physical adsorption data. Adsorbate used is mostly nitrogen, but now rare gases such as argon are also used. BET method is based on a detailed molecular model which makes it possible to obtain numerical values of the various parameters of adsorption equilibrium. This theory has been widely accepted and also used as a standard for surface area determination of adsorbents. BET equation for adsorption at a free surface is as follows :

$$\frac{V_a}{V_m} = \frac{C p}{(p_0 - p) \{1 + (C - 1)(p / p_0)\}} \quad (3.1-1)$$



where,

constant C determines the shape of isotherm and can be calculated using the following relationship :

$$C = \frac{a_1 b_2}{b_1 a_2} \exp \left[ \frac{\Delta H_1 - \Delta H_c}{R T} \right] \quad (3.1-2)$$

Surface area ( $S_{BET}$ ) of the adsorbent is given by :

$$S_{BET} = a_m N_{Vm} \quad (3.1-3)$$

For many practical purposes, the BET equation is generally fitted to data over a range  $p/p_0 = 0.05$  to  $0.3$  [Anderson and Pratt(1985)]. In case of fine pore adsorbents this range narrows down considerably and shifts into region of lower pressure, i.e.  $p/p_0 = (0.02$  to  $0.04)$  to  $(0.03$  to  $0.15)$  [Dubinin (1974)]. Use of adsorbate molecules which are non-spherical in shape (e.g. carbon dioxide, n-butane) is usually avoided. Temperature during adsorption is to be so adjusted that adsorbed molecules have a high degree of mobility. Thus, nitrogen (b.p. 77.3 K), argon (b.p. 87.3 K) or krypton (b.p. 90.2 K) are the suitable choices. Temperature during adsorption process is to be measured with a vapour pressure thermometer, because temperature of liquid nitrogen depends upon the establishment of equilibrium between the liquid and gaseous nitrogen at a specified pressure.

Prior to the beginning of adsorption process, the sample of adsorbent is to be degassed to an extent that porous volume of adsorbent becomes devoid of any preadsorbed specie. But temperature of degassing must be less than the maximum temperature that the adsorbent is designed to withstand.

### 3.1.2 Langmuir Method

Langmuir's relationship for adsorption isotherm is also used

to calculate surface area. This relationship is as follows :

$$V_a = \frac{V_m b p^{0.5}}{1 + b p^{0.5}} \quad (3.1-4)$$

For the estimation of  $V_m$ ,  $1/V_a$  is plotted against  $1/p^{0.5}$  and the curve obtained is extrapolated to  $1/p^{0.5} = 0$ , so that the intercept on the  $1/V_a$  axis is equal to  $1/V_m$ . This method relies heavily on the accurate data fitting of the Langmuir's equation [Anderson and Pratt (1985)].

### 3.2 MICROPORE VOLUME AND MICROPORE SURFACE AREA

As the adsorbents used are generally porous, therefore, the regularity of the pore size enhances the selectivity of adsorbent for a particular specie. According to the norms of IUPAC, pore sizes are classified under three categories, viz. macropores (pore diameter  $> 500 \text{ \AA}$ ), mesopores (pore diameter = 20 to  $500 \text{ \AA}$ ), and micropores (pore diameter  $< 20 \text{ \AA}$ ) [Satterfield (1980), Seifert and Emig (1991)]. However, Dubinin (1967) has classified the pore sizes somewhat differently into three categories, viz. macropores (effective pore diameter  $> 2000 \text{ \AA}$ ), intermediate pores (effective pore diameter = 30 to  $2000 \text{ \AA}$ ), and micropores (effective pore diameter = 10 to  $28 \text{ \AA}$ ).

Another terminology used in the literature to indicate pore sizes is supermicropores (equivalent pore diameter = 12 to  $32 \text{ \AA}$ ) [Dubinin (1974)], and ultramicropores (effective pore diameter  $< 8 \text{ \AA}$ ) [Brunauer et al. (1973)]. Pore size is also referred to as pore diameter or pore width depending upon whether the shape of pore is considered cylindrical or slit type.

The most widely used methods for measurement of pore size distribution are based on the analysis of hysteresis observed in physical adsorption, and mercury porosimetry. Other methods are small angle X-ray scattering and optical or electron microscopy. Physical adsorption method is the most preferred method among all these methods

[Cahen and Marechal (1963)]. Lower limit of quantitative pore size determination of methods based on physical adsorption is pore diameter = 7 Å [De Boer et al. (1965), Brown and Cadenhead (1979)]. Upper limit of determination of pore size with this method is 200 Å [Anderson and Pratt (1985)]. Range of application of mercury porosimetry is 100 Å to 150 µm. Although, a few scientists believe that the lower limit of quantitative determination of pore size by physisorption method is only upto 16 to 17 Å [Dubinin (1974)]. However, surface area and pore size of adsorbents having less than this size are often reported in literature [De Boer et al. (1965), Brown and Cadenhead (1979), Parfitt et al. (1975)] using nitrogen adsorption data, but it has remained a vital point for discussion amongst Scientists and Engineers. We too believe that a pore diameter less than 7 Å is not possible to be measured by nitrogen adsorption data due to pore filling rather than the multilayer adsorption.

In the determination of pore structure, i.e. pore size and pore volume employing physical adsorption, adsorbate is allowed to be adsorbed at adsorbent surface by increasing the relative pressure in small steps. The pressure is equilibrated at every step with sample. Initially, the sample is maintained at vacuum and absolute pressure of the system is measured continuously upto saturation vapour pressure  $p_0$ . A plot of amount adsorbed in the  $j$ th step vs. corresponding pressure is called adsorption branch of isotherm. The form of adsorption isotherm so obtained depends on the properties of the adsorbent and is usually classified into one of the five types as suggested by Brunauer et al. (1940). In fact the shape of isotherm enables a preliminary conclusion to be drawn regarding the size of majority of pores which make up the adsorbent. Methods based upon physisorption for pore size determination are discussed below.

### **3.2.1 Dubinin - Radushkevich Equation**

Dubinin-Radushkevich suggested an equation [Marsh and Rand (1970), Rand (1976)] for the determination of pore volume of micropores. The Dubinin - Radushkevich (DR) equation in its simplest

form [Dubinin and Stoeckli (1980)] can be written as follows :

$$\ln V_a = \ln V_o - \frac{k R^2 T^2}{\beta^2} \left[ \ln (p_o/p) \right]^2 \quad (3.2-1)$$

Equation (3.2-1) gives a straight line atleast over a limited range of pressures, i.e.  $10^{-4} < p/p_o < 0.1$  for microporous, mesoporous, and microporous-mesoporous materials [Seifert and Emig (1991)]. In latter cases, micropore volume  $V_o$  can be calculated by extrapolating this linear portion of the graph. In zeolites, a second linear region may also appear at relative pressures below  $10^{-5}$ , which after extrapolation, can lead to unrealistically high value of micropore volume [Rand (1976), Brown and Cadenhead (1979)].

### 3.2.2 Dubinin - Astakhov Equation

Dubinin and Astakhov (1971) have proposed a more generalized relationship for the determination of micropore volume. This takes into account the specific interactions between the adsorbate molecules and the intercrystalline cations, if there is any. This relationship is based on the theory of volume filling in micropores (TVFM) [Bering et al. (1966)]. The method is applicable only to micropores in general and to zeolites in particular. The relationship is similar to that of Dubinin and Radushkevich [Rand (1976)], but according to Dubinin and Astakhov, value of the empirical exponent in this case varies from 3 to 6 instead of 2. With this equation, plot of adsorption data for Dubinin- Radushkevich relationship would yield a straight line, even in the range of lowest pressure. Dubinin-Astakhov (DA) equation is given as follows :

$$V_a = V_o \exp \left[ - (A/E)^n \right] \quad (3.2-2)$$

Thus, it requires only three experimentally determined constants; usually obtained from one adsorption isotherm at the average temperature, i.e.  $V_o$ ,  $A (= RT \ln (p_o/p))$ , and  $n$ . According to Dubinin



G10249

and Astakhov  $n$  would be an integer only. The value of exponent  $n$  in the present study for the two adsorbate gases, viz. nitrogen and argon on 13X molecular sieves has been found to be less than 2 and is a real number and not an integer as opined by Dubinin and Astakhov. This is in agreement with the review work on Dubinin-Astakhov equation in literature [Rand(1976)].

### 3.2.3 $t$ - Plot Method

The  $t$ -plot method is based on the multilayer physical adsorption theory. ' $t$ ' is the statistical thickness of adsorbed layer on the surface of the adsorbent. It is assumed that at a free or quasi free surface for a particular adsorbent at a specified temperature and average thickness of the multilayer,  $t$  is a function of only the relative pressure, i.e.

$$t = f(p/p_0) \quad (3.2-3)$$

Another assumption made in the method is that the function  $f(p/p_0)$  is independent of the chemical nature of adsorbent. Hence, by dividing specific volume of the adsorbate (cc adsorbate/g adsorbent at STP) by volume of first monomolecular layer  $V_m$ , the statistical number  $n$ , of multilayer of adsorbate is obtained with respect to standard isotherm. Standard isotherm of an adsorbent is obtained by carrying out adsorption on a nonporous reference material, which should ideally be of the same material as that of the porous material being tested [Lamond and Price (1969), Bhambhani et al. (1972)].

Thus, thickness of the adsorbate layer,  $t$ , at any value of  $p/p_0$  would be given by the following relationship [Lippens et al. (1964)].

$$\begin{aligned} t &= 10^4 (X/S) \\ &= 10^4 M \left[ \frac{V_{sp}}{22414} \right] \left[ \frac{V_a}{S} \right] \end{aligned} \quad (3.2-4)$$

For nitrogen adsorption at 77.3 K, it reduces to the following simplified form :

$$t = 3.54 \left[ \frac{V_a}{V_m} \right] \quad (3.2-5)$$

The above mentioned relationship is based on the assumption that density of the adsorbed film is the same as that of the liquid nitrogen at its boiling point (77.3 K). A plot of  $V_a$  vs.  $t$  is known as Universal  $t$ -plot for all free or quasi free surfaces. To obtain  $t$ -plot, the thickness of 't' layer obtained for reference material at varying  $p/p_0$  values is plotted as abscissa, and amount of adsorbate adsorbed on test material as ordinate at corresponding  $p/p_0$  values. Thus, a relationship  $V = f(t)$  is obtained. This method can be successfully used to calculate surface area and pore volume for a pore width greater than 7 Å [Brown and Cadenhead (1979)]. It has also been used to ascertain the presence of narrow pores of pore width less than 7 Å qualitatively [De Boer et al. (1965)].

One problem associated with the routine application of  $t$ -plot is the need of standard isotherms for the adsorbent being tested. Such isotherms are rarely available. Due to this reason it has been suggested that the reference material should have the same value of certain parameters, e.g. the value of BET C constant should be same as that calculated from the experimental isotherm [Mikhail et al. (1968a, 1968b)].

#### 3.2.4 MP - Method

This method is an extension of the  $t$ -plot method.  $t$ -plot is a straight line as long as multilayer adsorption occurs unhindered. Presence of micropores makes the straight line to deviate downwards resulting into the lowering of slope of the curve. This is because of the fact that due to filling of the narrow pores, a portion of their surface becomes unavailable for adsorption. The curve in the range of downward deviations is used in this method for the determination of

micropore volume, and micropore surface area distribution [Mikhail et al. (1968a)].

Pore volume (cc/g) of a group of micropores is obtained by the following expression :

$$V_{o_j} = 10^4 \left[ S_j - S_{j+1} \right] \left[ 0.5 (t_j + t_{j+1}) \right] \quad (3.2-6)$$

where,

$S_j$  and  $S_{j+1}$  are surface areas ( $m^2/g$ ) obtained from the slopes at points  $j$  and  $j+1$  respectively on the  $t$ -plot, and  $t_j$  and  $t_{j+1}$  are corresponding adsorbed film thicknesses ( $\text{\AA}$ ).

Mikhail et al. (1968a) have propounded through mathematical proof that it hardly makes any difference in value of micropore volume whether the pores are cylindrical or slit shaped. In both the cases MP-method leads to the same value of volume of the micropores. The surface area belonging to a group of pores is obtained by the difference of  $S_j$  and  $S_{j+1}$ .

### 3.3 PORE SIZE DISTRIBUTION

Adsorbents which are used in commercial applications, normally do not have voids of only one pore size except the crystal of zeolites. But the use of these crystals is limited to very small beds only due to very high pressure drop. In order to make use of them in large sized industrial beds, tablets, beads or pellets are formed of crystals using a suitable binder. Use of binders introduces macropores in the molecular sieves. As far as other adsorbents are concerned they already have nonuniform pore size, i.e. there exists a pore size distribution. One of the methods to determine pore size distribution is discussed in the following section.



### 3.3.1 Horváth - Kawazoe Method

This method is useful for the calculation of effective pore size distribution. It requires adsorption isotherm data and envisages the calculation of an average potential function inside the pores, i.e.  $R T \ln \frac{p}{p_0}$ .

Although, the method was originally developed for slit like pores of carbon molecular sieves but can also be used for other microporous adsorbents. The method gives less accurate values for pore width greater than 13.4 Å [Horváth and Kawazoe(1983)]. It is suggested that the pore size distribution of pore widths greater than 13.4 Å may be determined by the method of Dollimore and Heal(1964) as it gives better accuracy for pore widths greater than 15 Å.

Equation (3.3-1) may be used to calculate the value of average potential function in slit type of pores. In its derivation it is assumed that  $p/p_0 \geq p_c/p_0$ . Equation (3.3-1) is stated below.

$$R T \ln \left[ \frac{p}{p_0} \right] = K \frac{N_a A_a + N_A A_A}{\sigma^4 (1-d)} \left[ \frac{\sigma^4}{3(1-d/2)^3} - \frac{\sigma^{10}}{9(1-d/2)^9} - \frac{\sigma^4}{3(d/2)^3} + \frac{\sigma^{10}}{9(d/2)^9} \right] \quad (3.3-1)$$

### 3.4 BULK PROPERTIES

Bulk properties of the adsorbents can be broadly classified into density, mechanical properties, and thermal properties. Few of the properties, viz. crushing strength and attrition losses are application-specific and their values vary with the type of test performed [Anderson and Pratt (1985)]. Therefore, value of these properties are only mentioned as specified by the manufacturer. These properties are briefly described in the following section.



### **3.4.1 Bulk Density**

In practice; bulk density is normally required for process calculations and design of adsorbers. It is further subdivided into apparent bulk density and apparent unit density. With additional information on pore volume, other properties such as void fraction etc. can also be calculated.

#### **3.4.1.1 Apparent Bulk Density**

Apparent bulk density is the mass per unit volume of adsorbent which packs into a specified and relatively large volume. Since the adsorbents are used in larger units in comparison to their actual crystals, the apparent density depends on the efficiency of packing in space and their apparent unit densities. The various forms (i.e. shapes) in which commercial adsorbents are available, are pellets (or extrudates), beads, and tablets. Each one of these is commonly referred to as unit. Thus, the value of bulk density would vary with the size and shape of these units.

#### **3.4.1.2 Apparent Unit Density**

The apparent unit density is the density of individual adsorbent units such as pellet, bead or tablet. This property is calculated by dividing the mass of an individual unit by its volume. If the individual unit is regular in shape and reasonably large, direct measurement of its volume is possible; but in case of irregular shapes and/or very small sizes, mercury displacement method is to be followed [Anderson and Pratt (1985)]. However, while using this method, possible effects of capillarity must be properly taken into account.

### **3.4.2 Mechanical Properties**

The mechanical properties are indicative of resistance of the

units against disintegration due to load or impact during handling. Resistance of adsorbents to mechanical failure such as dusting, cracking, or crushing is an important engineering consideration for packed bed adsorber columns. In many industrial applications, mechanical or physical failure of the adsorbent is the cause of maloperations and unscheduled process shutdowns, which may result into frequent change of adsorbent. The knowledge of mechanical properties is necessary in order to produce more durable adsorbents and also to define optimum process conditions from the standpoint of adsorbent's operating life [Beaver (1974)].

Generally, mechanical strength decreases with the increase in porosity. Other factors affecting the strength are pore size distribution, pore shape, particle size distribution, and nature of binder used. Besides, presence of macroscopic and microscopic internal stresses, generated during pressing and heating in the manufacturing process (e.g. calcination of zeolite molecular sieves) also play a vital role.

Method of measuring the strength-properties are specific to the type of test being carried out. As adsorbent units are generally small in size and used in packed beds, therefore, simple compressive testing is suitable for this purpose. One such property is crushing strength which is discussed below.

#### **3.4.2.1 Crushing Strength**

There are no standard tests for the determination of crushing strength as yet, like BET method for determining surface area. This is because of the fact that the reduction in strength may also occur during service by maloperation of adsorber column such as chemical attack or thermal shock, which is highly specific to the process [Satterfield (1980)]. Bed crushing strength and bulk crushing strength have also been used interchangeably in the commercial practice. Bulk crushing strength is defined as force required per unit area to generate certain quantity of specified fines (in a specified size of

bed). Obviously, a large number of methods are possible and described in literature to test bulk strength properties [Anderson and Pratt (1985)].

Crush tests may also be made in a variety of ways on individual pellets or on beds of adsorbents. One of the widely used procedures is to slowly force a piston down onto a bed of adsorbent pellets of several hundred cubic centimetre volume, and the displacement is measured as a function of applied pressure [Beaver (1974), Dart (1974), Adams et al. (1974)].

#### 3.4.2.2 Attrition Losses

The value of this property indicates the loss in the mass of adsorbent units under the conditions of rubbing, impact or even static loading. The knowledge of this property is important in order to know the ability of the adsorbent units to withstand abrasive wear which occurs during filling and removal of adsorbents from the fixed bed or attrition in the fluidized bed.

Tests of attrition losses are based on methods which are common to pulverizing mill devices and therefore, they are empirical in the sense that the results do not correlate uniquely with the material properties. The results obtained from these tests, only characterize a given material within the specified limits of the test parameters and test method. In general, cylindrical form of adsorbent units have a higher initial degradation rate than the spherical units. Details of these methods are available in the literature [Anderson and Pratt (1985)].

One representative method of test is to place a quantity of pellets in a rotating horizontal cylinder 15 to 30 cm in diameter, equipped with a single flight (baffle) which raises the pellets and drops them, or a quantity may be dropped one at a time from a specified height, e.g. 3 m. As mentioned earlier, attrition resistance of the fine catalyst is of paramount importance for fluidized bed reactors,

and this is usually determined in an air-jet attrition test [Satterfield (1980)].

### 3.5 INSTRUMENT USED FOR PHYSISORPTION MEASUREMENTS

For the determination of surface area and pore volume of molecular sieves, Multipoint Surface Area and Pore Volume Analyser (Model ASAP 2000 M V 3.00) was used. It has been manufactured by Micromeritics Corporation, USA. This instrument is based upon the principle of physical adsorption and has provision to use a few gases, viz. nitrogen, argon, and krypton, as adsorbate on various adsorbent samples.

To generate physical adsorption data for molecular sieves two types of adsorbates have been used, viz. nitrogen and argon. Choice of these two adsorbate gases have been made on the premise that molecules of these two gases are small, simple, symmetrical, and nonpolar in nature. Further, no interaction of these gases is expected with the adsorbent and hence surface spacing of the molecules would not be getting affected with respect to it. Results obtained are described in the following section.

#### 3.5.1 Results of Characterization by BET, Langmuir, and t-Plot Methods

---

Details of samples of 13X molecular sieves used in physical adsorption of nitrogen and argon are given in Table 3.5-1. Molecular sieves 13X manufactured by M/s Indian Petrochemicals Corporation Ltd., CATAD Division, Thane, Maharashtra, India have been used for characterization in the present study. Tables 3.5-2 and 3.5-3 provide the physical adsorption data with the two adsorbates.

The instrument used is on-line controlled by a PC and provided with a software which analyses the physical adsorption data by BET, Langmuir, t-plot, BJH, and Horváth-Kawazoe methods. The instrument manufacturer may supply the software for other methods also. But

**Table 3.5-1 Sample Details of 13X Molecular Sieves used in Physical Adsorption Measurements**

S.No.	Parameter	Adsorbate	
		Nitrogen	Argon
1	Sample Weight, g	0.1928	0.1837
2	Equilibrium Interval, s	10	5
3	Saturation Pressure, mm Hg	740.00	195.00
4	Bath Temperature, K	77.3	87.3

**Table 3.5-2 Physical Adsorption Data of Nitrogen Gas on 13X Molecular Sieves**

S. No.	Absolute Pressure (mm Hg)	Relative Pressure	Volume Adsorbed (cc/g STP)
1	7.499	0.0101	165.2675
2	22.341	0.0302	168.6111
3	45.561	0.0616	170.4325
4	63.454	0.0857	171.1653
5	75.659	0.1022	171.5560
6	90.139	0.1218	171.8806
7	104.154	0.1407	172.1352
8	118.893	0.1607	172.3742
9	133.585	0.1805	172.5586
10	148.422	0.2006	172.7077
11	185.243	0.2503	172.9323
12	222.354	0.3005	173.1165
13	259.351	0.3505	173.2459
14	295.862	0.3998	173.3545
15	333.055	0.4501	173.4482
16	370.021	0.5000	173.4912
17	421.374	0.5694	173.6369
18	443.973	0.6000	173.8035
19	480.846	0.6498	174.1391
20	517.460	0.6993	174.8144
21	547.507	0.7399	175.7199
22	569.641	0.7698	176.8039
23	591.982	0.8000	178.3276
24	607.031	0.8203	179.6120
25	621.304	0.8396	181.3136
26	636.684	0.8604	183.3946
27	647.265	0.8747	185.1990
28	658.384	0.8897	187.6198
29	669.311	0.9045	190.8396
30	677.156	0.9151	193.8624
31	684.189	0.9246	197.6264
32	690.654	0.9333	201.8196
33	695.365	0.9397	205.8743
34	703.427	0.9506	209.7921
35	707.125	0.9556	218.1550
36	710.269	0.9598	229.1947
37	713.202	0.9638	241.5282
38	715.684	0.9671	254.2999
39	718.161	0.9705	267.2182
40	720.183	0.9732	279.4273
41	721.993	0.9757	293.0341
42	723.493	0.9777	305.8801
43	725.355	0.9802	318.4230
44	726.958	0.9824	330.6990
45	728.251	0.9841	342.9822
46	729.544	0.9859	355.5746
47	730.474	0.9871	367.6452
48	731.302	0.9882	379.5225

**Table 3.5-3 Physical Adsorption Data of Argon Gas on 13X Molecular Sieves**

S.No.	Absolute Pressure (mm Hg)	Relative Pressure	Volume Adsorbed (cc/g STP)
1	0.008	0.000040	3.0898
2	0.013	0.000066	6.1716
3	0.016	0.000081	9.2552
4	0.019	0.000094	12.3387
5	0.020	0.000104	15.4225
6	0.022	0.000111	18.5071
7	0.023	0.000118	21.5919
8	0.025	0.000126	24.6763
9	0.026	0.000133	27.7620
10	0.028	0.000140	30.8467
11	0.028	0.000145	33.9319
12	0.030	0.000153	37.0173
13	0.032	0.000163	40.1016
14	0.033	0.000167	43.1875
15	0.034	0.000176	46.2737
16	0.035	0.000181	49.3601
17	0.036	0.000186	52.4462
18	0.037	0.000190	55.5330
19	0.039	0.000198	58.6199
20	0.040	0.000205	61.7065
21	0.042	0.000213	64.7935
22	0.042	0.000217	67.8807
23	0.043	0.000220	70.9688
24	0.046	0.000235	74.0559
25	0.048	0.000244	77.1441
26	0.049	0.000252	80.2328
27	0.049	0.000252	83.3228
28	0.051	0.000263	86.4123
29	0.053	0.000268	89.5018
30	0.055	0.000281	92.5909
31	0.056	0.000287	95.6818
32	0.060	0.000305	98.7710
33	0.063	0.000324	101.8609
34	0.066	0.000337	104.9525
35	0.068	0.000349	108.0443
36	0.069	0.000354	111.1382
37	0.073	0.000374	114.2299
38	0.083	0.000427	117.3191
39	0.084	0.000430	120.4148
40	0.087	0.000446	123.5098
41	0.091	0.000468	126.6048
42	0.097	0.000499	129.6994
43	0.103	0.000530	132.7950
44	0.111	0.000571	135.8905
45	0.122	0.000629	138.9857
46	0.135	0.000693	142.0825
47	0.152	0.000780	145.1792
48	0.172	0.000885	148.2757

**Table 3.5-3 (Contd..)**

S.No.	Absolute Pressure (mm Hg)	Relative Pressure	Volume Adsorbed (cc/g STP)
49	0.202	0.001039	151.3700
50	0.245	0.001259	154.4618
51	0.309	0.001587	157.5481
52	0.402	0.002070	160.6264
53	0.548	0.002821	163.6872
54	0.782	0.004024	166.7160
55	1.162	0.005980	169.6846
56	1.790	0.009210	172.6244
57	2.771	0.014260	175.4019
58	4.276	0.022009	178.0018
59	6.393	0.032905	180.2058
60	9.806	0.050474	182.4210
61	13.116	0.067511	183.8694
62	17.063	0.087500	185.0000
63	24.804	0.127200	186.5300
64	30.674	0.157300	187.3070
65	34.125	0.175000	188.2690
66	40.433	0.207350	189.0384
67	49.561	0.254160	190.5384
68	59.564	0.305454	191.1538
69	68.250	0.350000	191.7692
70	88.195	0.452280	193.2692
71	107.656	0.552100	195.0000
72	127.160	0.652100	196.3636
73	144.749	0.742300	197.8846
74	150.404	0.771300	198.4848
75	160.271	0.821900	199.2307
76	163.703	0.839500	200.0000
77	168.051	0.861800	200.6923
78	170.879	0.876300	200.7692
79	173.765	0.891100	201.4393
80	178.464	0.915200	202.2307
81	180.375	0.925000	202.9230
82	183.242	0.939700	203.6538
83	185.543	0.951500	204.4615
84	187.688	0.962500	205.1538
85	189.638	0.972500	205.9230
86	193.752	0.993600	206.5555



software support for other methods was not available with the instrument as it was not purchased with the instrument by the institute/laboratory housing it.

Results of the data obtained by using the software for three methods, viz. BET, Langmuir, and t-plot are given in Table 3.5-4.

### 3.5.2 Analysis of Results of BET, Langmuir, and t-Plot Methods

---

Surface area obtained by BET and t-plot methods with nitrogen are in reasonable agreement with the values reported in literature [Danner and Chol (1978), Hyun and Danner (1985), Inui et al. (1988)]. Besides, surface area determined by Langmuir method is larger than that obtained by BET and t-plot methods. The reasons may be explained as follows :

- Sodalite cages of zeolites can contain only one molecule of gases such as argon and passage through six membered ring is generally slow. So except at very high temperatures, transitions between cages occur only infrequently. Therefore, at moderate temperatures the isotherms for such systems conform closely to the ideal Langmuir model as the basic assumptions of the model are accurately fulfilled [Ruthven (1984)]. However, cages of 13X zeolite molecular sieves are larger and can accommodate several molecules. The rate of interchange of molecules between cages of the 13X zeolites may be rapid but as a first approximation it is still reasonable to assume the cages as independent subsystems. Moreover, it is well known that the results obtained from Langmuir model depends on the goodness of fit, as this method depends heavily on the method of curve fitting. Correlation coefficient for Langmuir plot obtained in our results are quite close to unity and this shows that the fitting of data is very good. Therefore, Langmuir's prediction of surface area may be assumed to be accurate.

**Table 3.5-4 Characterization of 13X Molecular Sieves by BET, Langmuir and t-Plot Methods**

S.No.	Parameter	Value obtained for different adsorbates	
		Nitrogen	Argon
1	<b>BET Method</b>		
(a)	Surface area, $m^2/g$	558.2321	596.7568
(b)	Monolayer capacity, $cm^3/g$ STP	128.2349	156.3924
(c)	Correlation coefficient for BET plot	0.9969	0.9987
2	<b>Langmuir's Method</b>		
(a)	Surface area, $m^2/g$	755.7985	769.2091
(b)	Monolayer capacity, $cm^3/g$ STP	173.6191	188.4835
(c)	Correlation coefficient for Langmuir's plot	0.9999	0.9999
3	<b>t-Plot Method</b>		
(a)	Micropore surface area, $m^2/g$	533.9147	551.3114
(b)	Micropore Volume, $cm^3/g$	0.2564	0.2219

- Ruthven (1984) suggests on the basis of experimental results of Brunauer et al. (1938) that the absolute surface area may be determined by BET method to within about 20-25% error. But still this method serves as a standard to check surface area obtained by other methods.

Surface area obtained by BET with both the adsorbates are approximately 17-25% less than that obtained by Langmuir's method. This also supports the correctness of surface area determined by Langmuir's method.

- Seifert and Emig (1991), and Dubinin (1974) state that the t-plot method needs particularly to be appraised critically, whenever a micropore distribution is to be determined quantitatively. According to Seifert and Emig (1991), t-plot method gives qualitative results at best in the case of micropore distribution determination. Therefore, as a consequence it is very likely that it may affect in the same way the values of other parameters, viz. total micropore volume and surface area. Micropore surface area computed from this method are even less than those computed by BET method with both the adsorbates. Therefore, these values may be viewed only qualitatively.

On the basis of above discussion, it can be said that the surface area computed by Langmuir's method may be assumed to be the correct surface area of 13X molecular sieves.

### **3.6 CHARACTERIZATION BY DUBININ - RADUSHKEVICH AND DUBININ - ASTAKHOV EQUATIONS**

This section describes the methodology to obtain parameters, viz. monolayer capacity, total micropore volume, micropore surface area, and micropore volume mean pore diameter by DR and DA equations. Besides, it provides the results and their critical analysis.

### 3.6.1 Characterization by Dubinin - Radushkevich Equation

Details of this equation has already been provided in section 3.2.1. Stepwise procedure used to calculate monolayer capacity, total micropore volume and micropore surface area is given below.

#### 3.6.1.1 Stepwise Procedure of Dubinin - Radushkevich Equation

1. Read the adsorption data, i.e. volume adsorbed, absolute pressure, and saturation pressure.
2. Calculate  $\log_{10}(V_i)$  and  $[\log_{10}(p_o/p_i)]^2$  for all values of  $i = 1$  to  $n_{data}$ , where  $n_{data}$  is total number of data points.
3. Plot  $\log_{10}(V_i)$  vs.  $[\log_{10}(p_o/p_i)]^2$ .
4. Select the adsorption data from the appropriate linear portion of the curve. Appropriate region of the curve is the one which yields reasonable value of micropore volume when extrapolated to y-axis.
5. Calculate the slope and intercept of the linear model by method of least squares using assorted data which are selected in step 4. Check the goodness of fit.
6. Calculate monolayer capacity,  $V_o$  using the intercept of linear model on y-axis, i.e.  $\log_{10}(V_o)$ .
7. Calculate total micropore volume by multiplying  $V_o$  by the density conversion factor (value of density conversion factor for nitrogen and argon are 0.001546 and 0.00128  $\text{cm}^3$  liquid/ $\text{cm}^3$  STP respectively).
8. Compute micropore surface area (MSA) from monolayer capacity using cross sectional area of adsorbate molecule ( $\sigma$ ) by following expression.

$$\text{MSA} = \frac{\sigma \times V_o \times \text{Avogadro's number}}{\text{volume of one g mol at STP}} \quad (3.6-1)$$

### 3.6.1.2 Results of Dubinin - Radushkevich Equation

Figures 3.6-1 and 3.6-2 depict the Dubinin-Radushkevich plots for two adsorbates. Selected appropriate linear portion has also been marked in each figure. Using the assorted data, linearly fitted models are as follows:

*For nitrogen*

$$\log_{10}(V_i) = 2.23984 - 0.00549847 [\log_{10}(p_o/p_i)]^2 \quad (3.6-2)$$

*For argon*

$$\log_{10}(V_i) = 2.28283 - 0.0110678 [\log_{10}(p_o/p_i)]^2 \quad (3.6-3)$$

These linearly fitted curves have been shown in Figures 3.6-3 and 3.6-4. Further, parameters have been estimated according to the stepwise procedure discussed in section 3.6.1.1 and are reported in Table 3.6-1.

It may be noted that the parameters estimated for the two adsorbates are reasonably close to each other and the variation may be attributed to the slight difference in the molecule size of nitrogen and argon. Further, discussion of these results are given in conjunction with the results obtained by using DA equation.

### 3.6.2 Characterization by Dubinin - Astakhov Equation

The theory associated with this method and the resulting mathematical expression has been given in section 3.2.2. Stepwise procedure to calculate optimised value of exponent  $n$ , total micropore volume, micropore volume mean pore diameter, and micropore surface area, is given below.

#### 3.6.2.1 Stepwise Procedure of Dubinin - Astakhov Equation

1. Read the adsorption data, i.e. volume adsorbed, absolute pressure

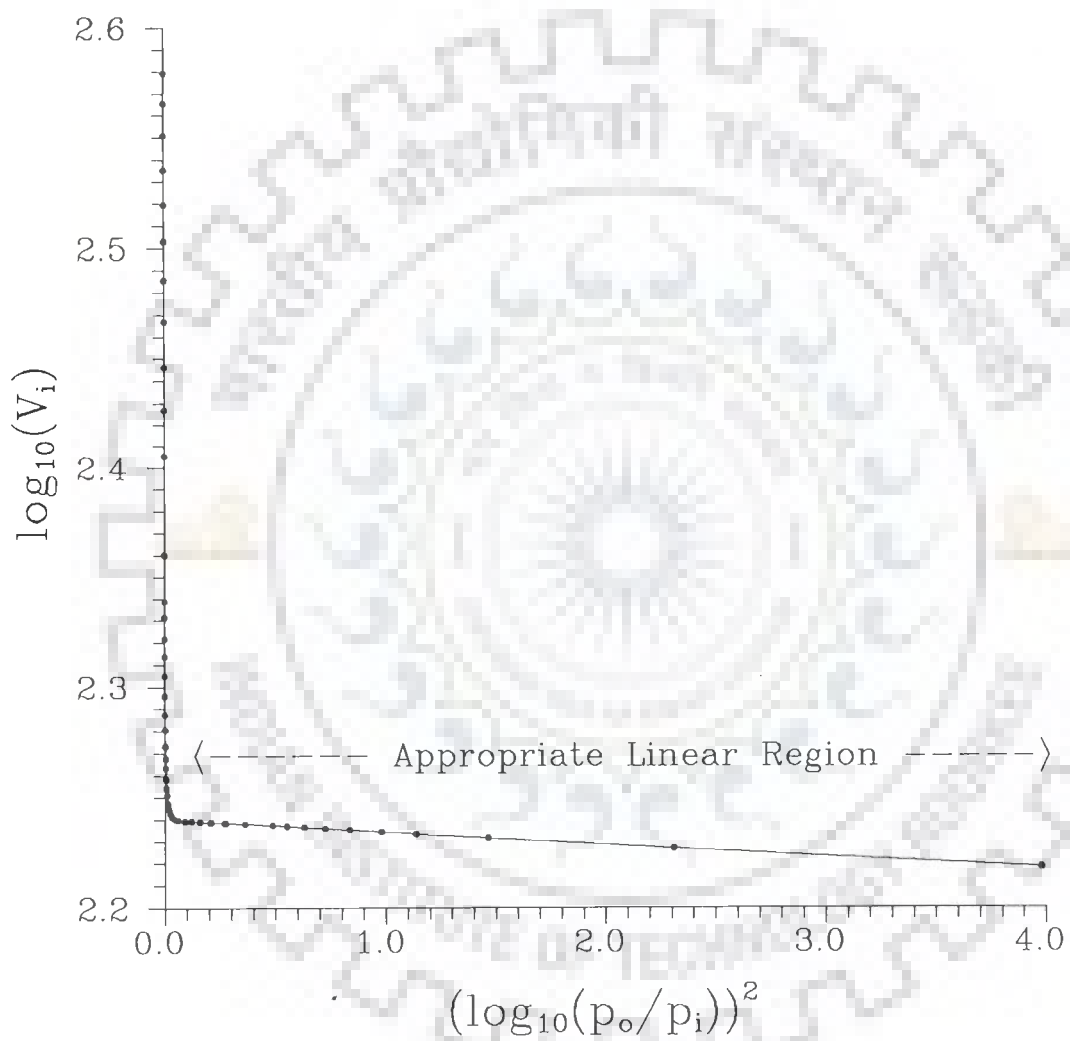


Figure 3.6-1 Dubinin-Radushkevich Plot for 13X Molecular Sieves, Adsorbate: Nitrogen

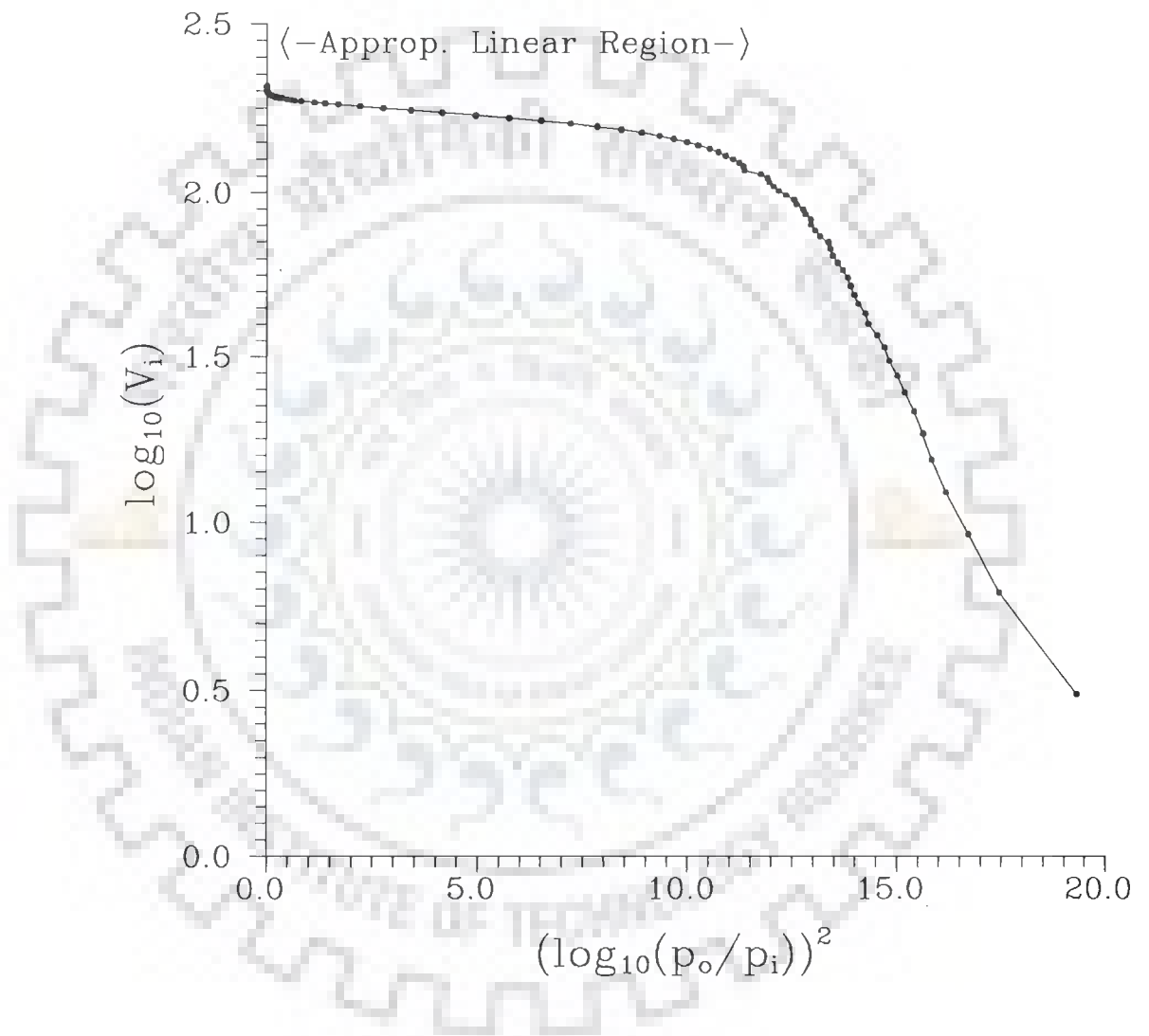


Figure 3.6-2 Dubinin-Radushkevich Plot for 13X Molecular Sieves, Adsorbate: Argon

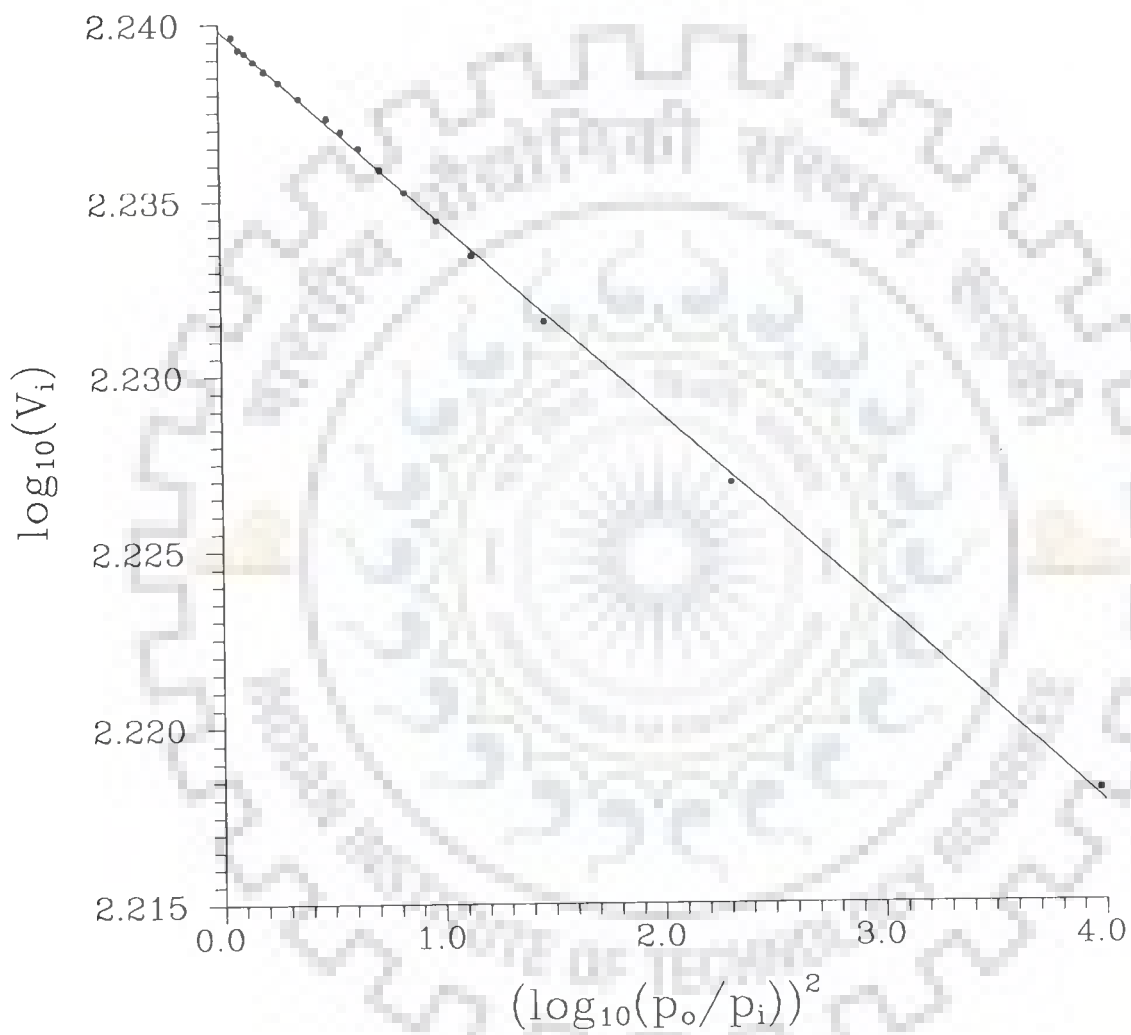


Figure 3.6-3 Linear Curve Fitting for Dubinin-Radushkevich Plot for 13X Molecular Sieves in Appropriate Linear Region, Adsorbate : Nitrogen



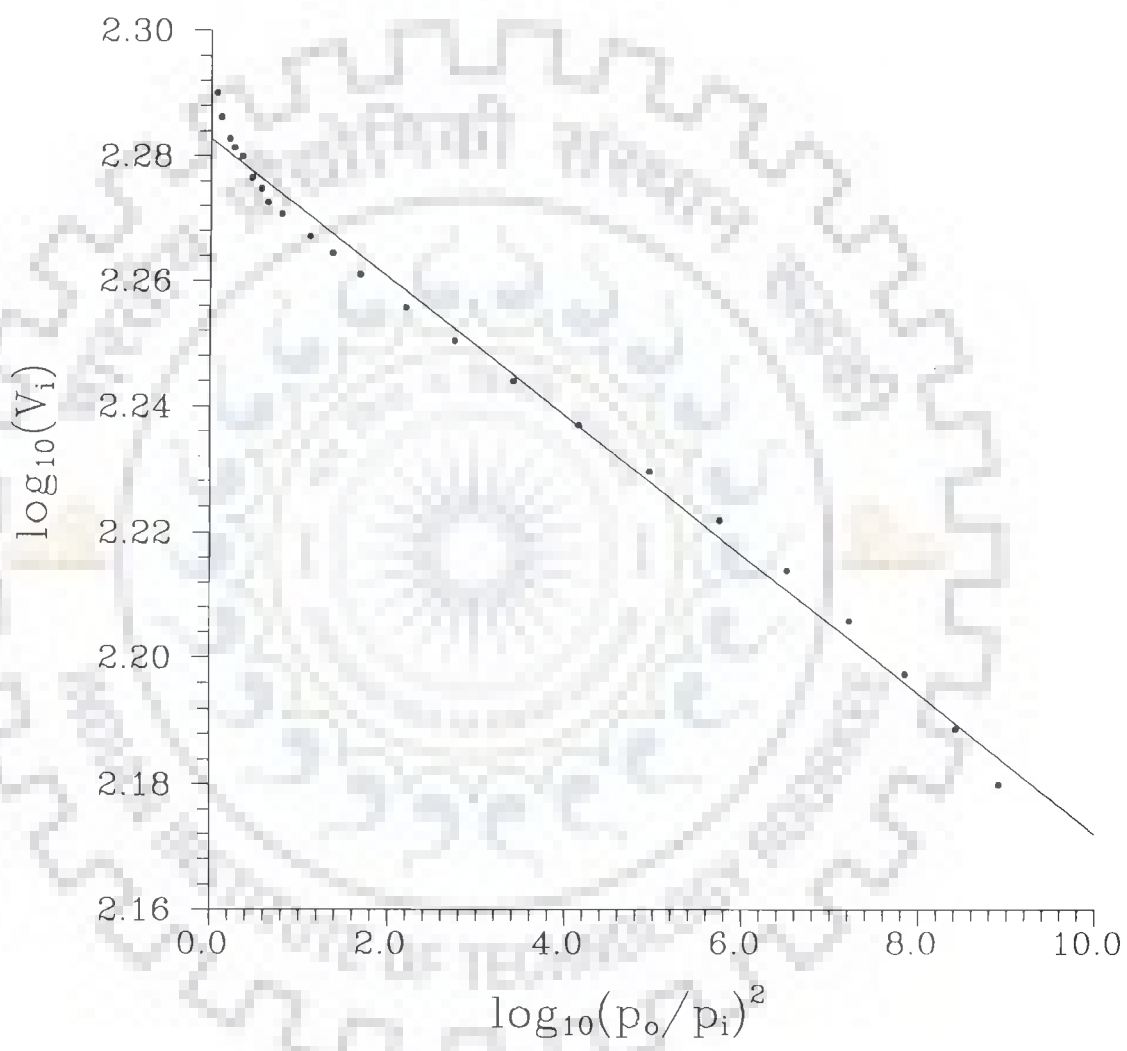


Figure 3.6-4 Linear Curve Fitting for Dubinin-Radushkevich Plot for 13X Molecular Sieves in Appropriate Linear Region, Adsorbate : Argon

**Table 3.6-1 Characterization of 13X Molecular Sieves by Dubinin-Radushkevich and Dubinin-Astakhov Equations**

S.No.	Parameter	Value obtained for different adsorbates	
		Nitrogen	Argon
<b>1</b>	<b>Dubinin-Radushkevich Equation</b>		
(a)	Monolayer capacity, cm <sup>3</sup> /g STP	173.7161	191.7918
(b)	Total micropore volume, cm <sup>3</sup> /g	0.2686	0.2455
(c)	Micropore surface area, m <sup>2</sup> /g	756.2206	752.4478
<b>2</b>	<b>Dubinin-Astakhov Equation</b>		
(a)	Optimized value of Dubinin - Astakhov Exponent, n	1.95	1.78
(b)	Total micropore volume, cm <sup>3</sup> /g	0.2686	0.2469
(c)	Micropore volume mean pore diameter, Å	11.5294	8.6889
(d)	Micropore surface area, m <sup>2</sup> /g	755.5349	751.4132

at each step of equilibrium adsorption and saturation pressure.

2. Calculate  $\log_{10}(V_i)$  and  $\log_{10}(p_o/p_i)$  for all values of  $i = 1$  to  $n_{data}$ , where  $n_{data}$  is total number of data points.
3. Plot  $\log_{10}(V_i)$  vs.  $\log_{10}(p_o/p_i)$ .
4. Select the adsorption data from the appropriate linear region of the curve. Appropriate linear region of the curve is the one which yields reasonable value of the micropore volume when extrapolated to y-axis.
5. Compute  $\log_{10}(V_i)$  and  $[\log_{10}(p_o/p_i)]^n$  for  $n = 1$  to 15 and for all values of  $i = 1$  to  $k$ , where,  $k$  is no. of assorted data points (which lie on the appropriate linear region).
6. Calculate the slope and intercept of the linear model by method of least squares using assorted data selected in step 4, for all the data sets of  $n = 1$  to 15.
7. Compute sum of squares of errors (SEQ) for all data sets of  $n = 1$  to 15 using the following expression.

$$SEQ = \sum_{i=1}^k [Y_i - \hat{Y}_i]^2, \text{ for } n = 1 \text{ to } 15 \quad (3.6-4)$$

8. Select  $n$  which has the least value of SEQ.
9. Make a fine search of value of  $n$  (upto second decimal digit) for minimum value of SEQ same as that described above in steps 6, 7, and 8. This gives optimised value of  $n$ , i.e.  $n_{opt}$ .
10. Plot  $\log_{10}(V_i)$  vs.  $[\log_{10}(p_o/p_i)]^{n_{opt}}$ .
11. Compute slope and intercept of the linear model by the method of least squares for the plot obtained in step 10.

12. Calculate monolayer capacity,  $V_o$  using the intercept from the linear model (obtained in step 11) on y-axis, i.e.  $\log_{10}(V_o)$ .
13. Calculate total micropore volume by multiplying  $V_o$  with density conversion factor.
14. Calculate Characteristic Adsorption Energy using the following relationship

$$E = \frac{2.303 \times R \times T}{(2.303 \times S)^{1/n}} \quad (3.6-5)$$

15. Calculate  $\Gamma(Y)$  by the following relationship [Micromeritics (1993)].

$$\Gamma(Y) = 0.580249 Y^2 - 1.659726 Y + 2.074423 \quad (3.6-6)$$

$$\text{where } Y = \frac{3n + 1}{3n} \quad (3.6-7)$$

16. Calculate micropore surface area (MSA) using the following relationship.

$$\text{MSA} = 10,000 \times 2 \times W_o \left[ \frac{E}{K \times 10^3} \right] \Gamma \left[ \frac{3n + 1}{3n} \right] \quad (3.6-8)$$

### 3.6.2.2 Results of Dubinin - Astakhov Equation

Dubinin-Astakhov plots for two adsorbates with optimized values of  $n$  are shown in Figures 3.6-5 and 3.6-6. Values of  $n$  for nitrogen and argon are 1.95 and 1.78 respectively. Appropriate linear regions of the curves are also marked in these figures. Linearly fitted models with optimized value of  $n$  utilising assorted data are given in the following lines.

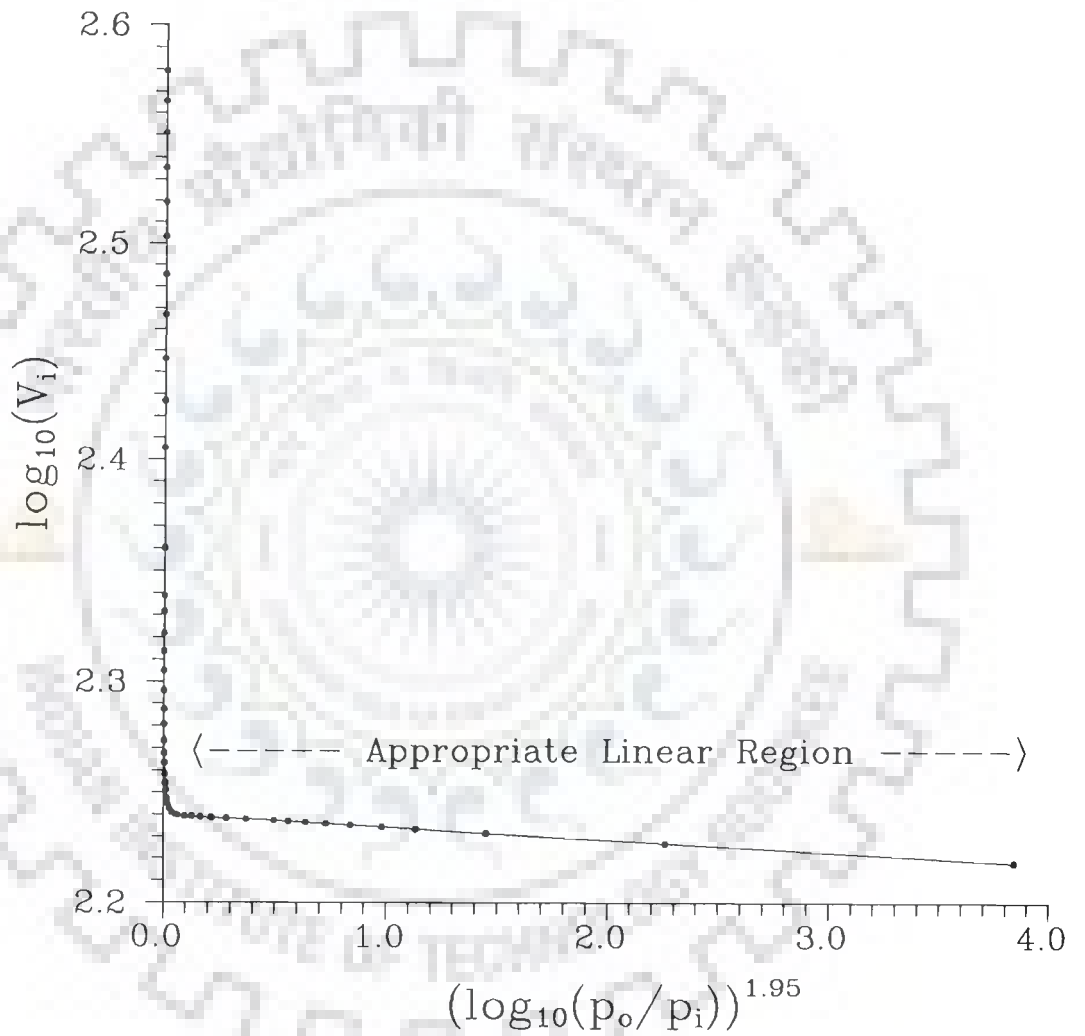


Figure 3.6-5 Dubinin-Astakhov Plot for 13X Molecular Sieves with Optimized Value of  $n$ , Adsorbate : Nitrogen

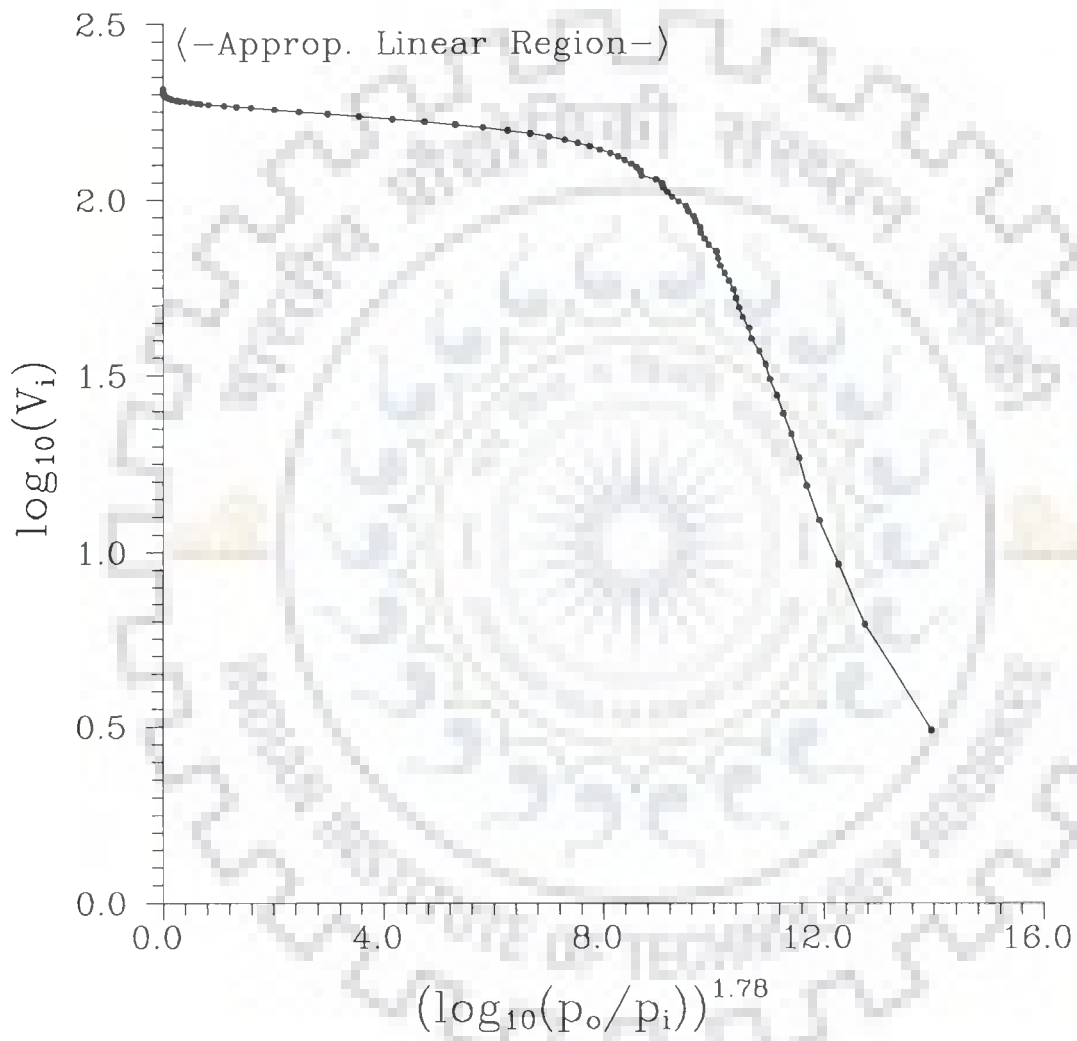


Figure 3.6-6 Dubinin-Astakhov Plot for 13X Molecular Sieves with Optimized Value of n, Adsorbate : Argon

For nitrogen

$$\log_{10}(V_i) = 2.23996 - 0.00569312 \left[ \log_{10}(p_o/p_i) \right]^{1.95} \quad (3.6-9)$$

Sum of squares of errors, SEQ =  $2.001 \times 10^{-7}$

For argon

$$\log_{10}(V_i) = 2.2854 - 0.0141521 \left[ \log_{10}(p_o/p_i) \right]^{1.78} \quad (3.6-10)$$

Sum of squares of errors, SEQ =  $1.7703 \times 10^{-4}$

These curves of linear fitting have been depicted in Figures 3.6-7 and 3.6-8.

The characterization parameters as described in section 3.6.2.1 are given in Table 3.6-1. It can be seen from Table 3.6-1 that the parameters computed here are in close agreement with the results of DR equation and the value of surface area is also in reasonable agreement with the results obtained by Langmuir's method.

### **3.6.3 Analysis of Results of Dubinin - Radushkevich and Dubinin - Astakhov Curves**

It can be seen from the plot of  $\log_{10}(V_i)$  vs.  $[\log_{10}(p_o/p_i)]^n$  that in the case of nitrogen, bulk of adsorption takes place at higher equilibrium pressure. Consequently, a vertical line is obtained at y-axis near the origin. While for argon, adsorption mostly takes place in lower region of equilibrium pressures. It is also observed that the saturation pressure for argon (195 mm Hg) is much less than that of nitrogen (740 mm Hg). Reason for this appears to be the larger molecule size of nitrogen, which requires higher pressure for its entry into the micropores of 13X molecular sieves.

Further, the existence of two linear regions is one of the

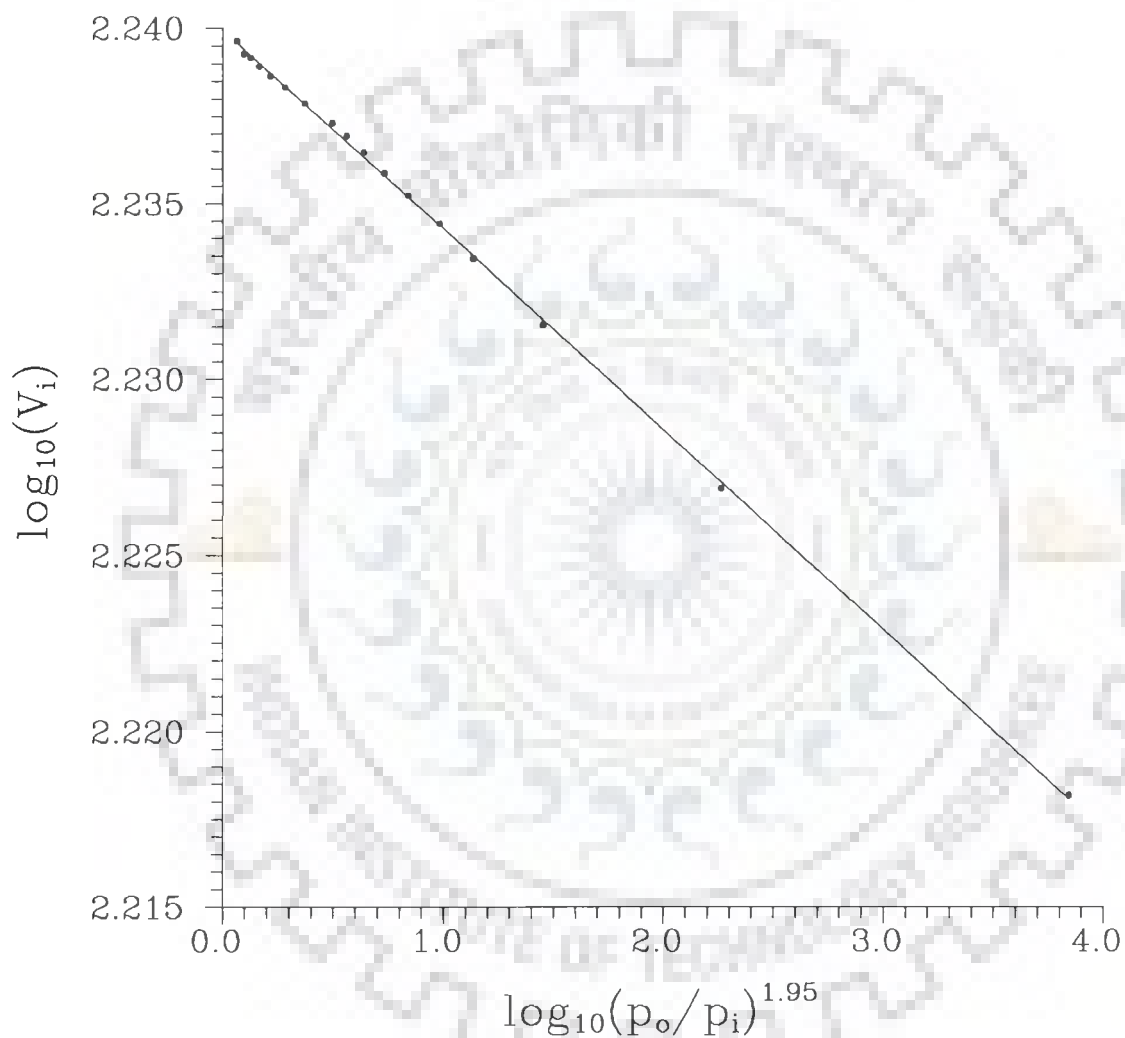


Figure 3.6-7 Linear Curve Fitting for Dubinin-Astakhov Plot for 13X Molecular Sieves in Appropriate Linear Region, Adsorbate : Nitrogen



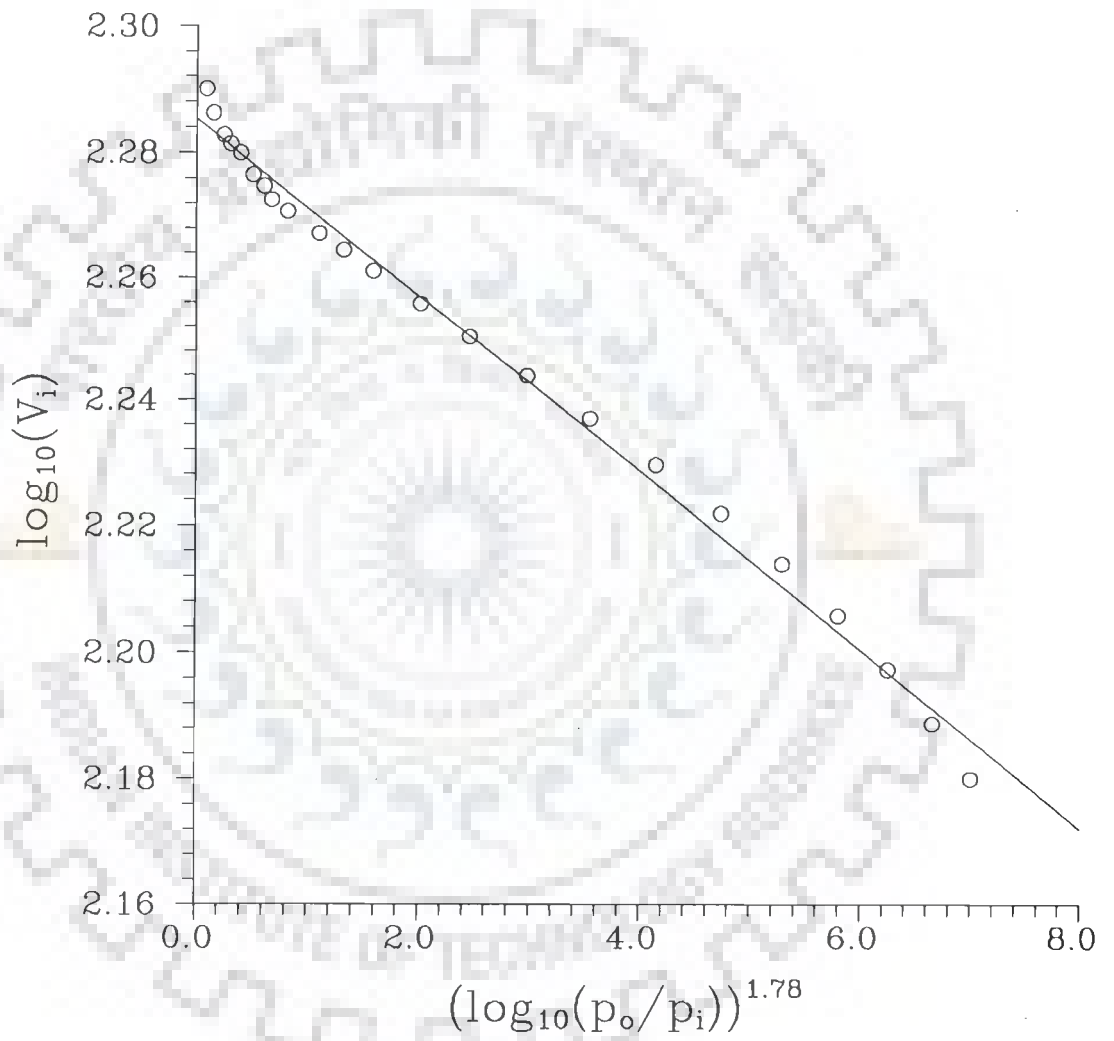


Figure 3.6-8 Linear Curve Fitting for Dubinin-Astakhov Plot for 13X Molecular Sieves in Appropriate Linear Region, Adsorbate : Argon

problems faced in the calculation of micropore volume from the adsorption data on adsorbent. Therefore, it requires judicious selection of the data points to be used for its calculation.

### 3.6.3.1 Micropore Surface Area by Dubinin - Radushkevich Equation

Surface area calculated by DR equation depends on the value of molecular cross-sectional area of adsorbate used. It is directly proportional to the value of molecular cross-sectional area selected. In literature the reported molecular cross-sectional area of nitrogen varies from 0.145 to 0.19 nm<sup>2</sup>/molecule on different substrates. Values on different substrates differ largely because of the difference in orientation, packing patterns, and adsorbate to substrate interaction effects.

We have used the value of area occupied by one nitrogen molecule = 0.162 nm<sup>2</sup>, which is most widely used; it is also used by Emmett [Innes (1968)]. Cross-sectional area of argon has been taken as 0.146 nm<sup>2</sup> as estimated by Livingstone [Innes (1968)].

Micropore surface area of 13X MS computed by DR and DA equations (Table 3.6-1) are in close agreement with each other. Values calculated by using argon are slightly lower than that of nitrogen. Satterfield (1980) reports value of surface area of zeolites to be 500-800 m<sup>2</sup>/g. Vermuelen (1978) reports the value to be in the range of 600-700 m<sup>2</sup>/g. The value of total surface area calculated by us using Langmuir's method [Anderson and Pratt (1985)] was 755.8 and 769.2 m<sup>2</sup>/g with nitrogen and argon respectively. Since the values of total surface area and microporous surface area are same in case of molecular sieves, all these data presented from literature here support the correctness of the surface area value calculated in the present study.

Though, DA equation offers flexibility in the selection of exponent n, which depends upon the interaction between adsorbate and adsorbent. Nevertheless, values calculated by DR equation are

acceptable within the reasonable limits of accuracy. Moreover, DR equation is comparatively simple in application to that of DA equation which entails a cumbersome process of optimizing the value of exponent 'n'.

### **3.6.3.2 Total Micropore Volume by Dubinin - Radushkevich and Dubinin - Astakhov Equations**

It can be observed from Table 3.6-1 that the computed values of total micropore volume of 13X MS using DR and DA equations are almost same by both the adsorbates. These values are comparable to the values reported in the literature [Dubinin (1967), Hyun and Danner (1985)]. Micropore volume computed by using argon in the present study is less than that of nitrogen. This trend is also in agreement with the values reported by Breck (1974). Thus, total micropore volume computed by DA equation using nitrogen, i.e. 0.2686 cc/g as also by DR equation, is the correct value.

### **3.6.3.3 Characteristic Adsorption Energy in Dubinin-Astakhov Equation**

Characteristic Adsorption Energy calculated for Argon adsorption on 13X MS comes to be 11.441 kJ/mol and for nitrogen it is 13.638 kJ/mol, which are in the range of its values for other adsorbates; e.g. for propane having a molecule size between 4.0-4.9 Å, E varies from 17.3636 to 17.53096 kJ/mol for a temperature range of 253 to 369 K [Dubinin and Astakhov (1971), Yang (1987), Barrer (1978)].

### **3.6.3.4 Critical Analysis of Results of Dubinin - Radushkevich and Dubinin - Astakhov Equations**

During characterization of 13X MS, we have found by optimization that exact values of n are 1.95 and 1.78 for nitrogen and argon respectively. This was based on minimization of the sum of squares of errors of the experimental data. Thus, the present analysis also indicates that the exponent, 2, used in Dubinin-Radushkevich equation, can be safely used for the estimation of micropore volume of

13X molecular sieves for convenience in calculation with a little sacrifice in its accuracy. The value thus calculated will be lower than that of actual micropore volume.

### 3.7 CONFIDENCE INTERVALS

In the estimation of parameters by optimization, determination of confidence intervals and joint confidence contour is an imperative exercise. This ensures the reliability of estimation of parameter values. Details of confidence intervals obtained and their determination are given below.

#### 3.7.1 Confidence Limits of Predicted Values

The physical adsorption data were used in Dubinin-Astakhov equation to plot  $\log_{10}(V_i)$  vs.  $\left[\log_{10}(p_o/p_i)\right]^{n_{opt}}$ . Appropriate linear data were fitted to a straight line model. The 99.95% confidence limits have been plotted for the predicted values. It can be seen in Figure 3.7-1 that while line of the data of appropriate linear region is straight, the loci of confidence limits are curved. The curvature of the limits is not very much marked as the confidence region is very small, which presents a hyperbola. Narrow width of confidence interval even at a very high value of confidence coefficient, i.e. 99.95% implies that the fitting of data is very good. This analysis also indicates that the estimation of value of  $n$  is correct. Such an analysis has also been done in the case of argon as adsorbate. Confidence Limits of Predicted value (CLP) are drawn by using following expression [Draper and Smith (1966), Himmelblau (1970)].

$$CLP = \hat{Y}_i \pm t(n - p, 1 - \frac{\alpha}{2}) s(\hat{Y}_i) \quad (3.7-1)$$

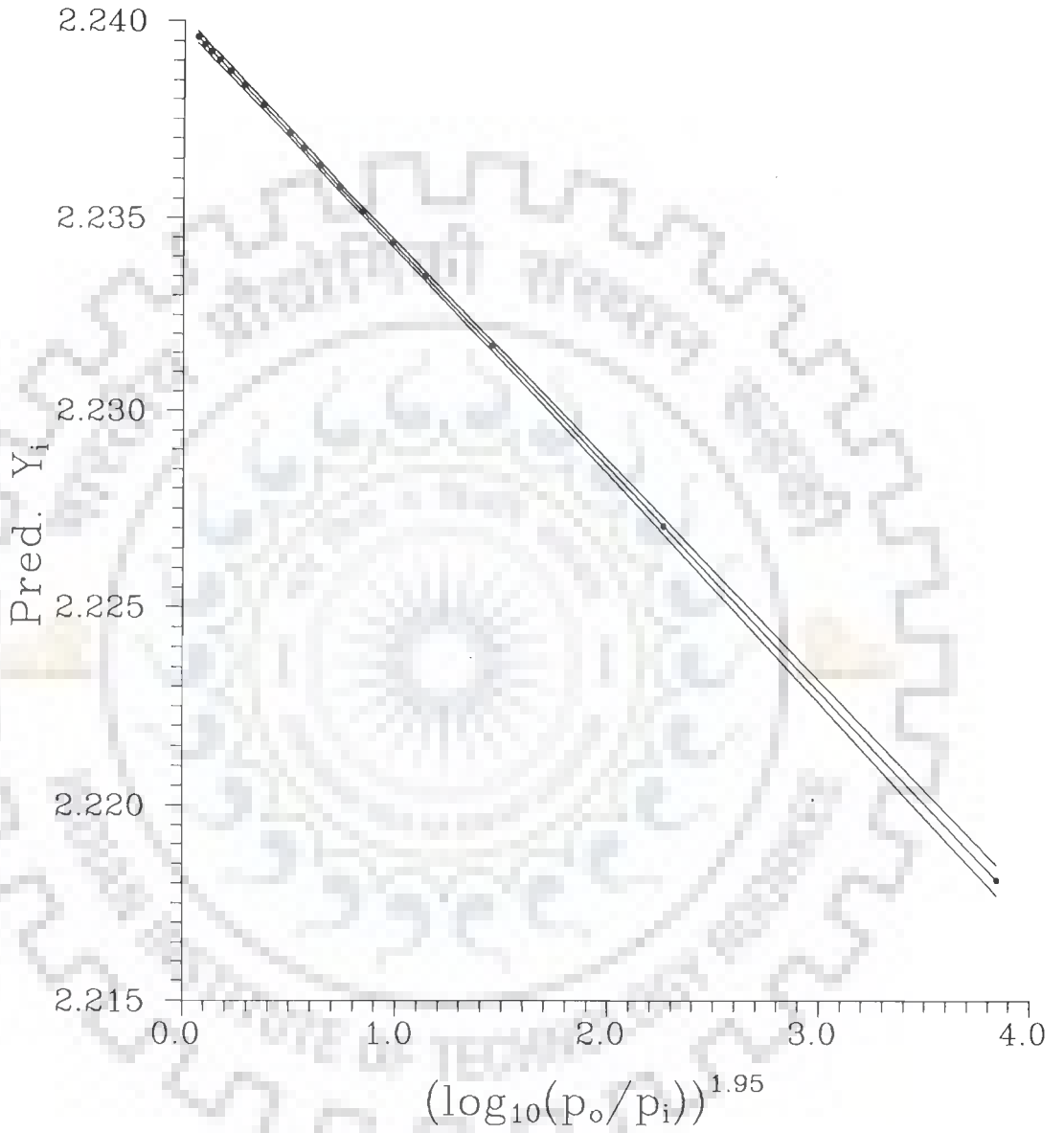


Figure 3.7-1 99.95% Confidence Limits of Predicted Values and Data of Appropriate Linear Region, Adsorbate : Nitrogen

### 3.7.2 Individual Confidence Intervals and Joint Confidence Region

---

In the Dubinin-Astakhov equation, two parameters of straight line, i.e. intercept on y-axis and slope, have been estimated. The joint confidence region (JCR) for these parameters has also been computed. Contour for the joint confidence region has been calculated using following expression [Draper and Smith (1966), Himmelblau (1970)] :

$$\phi_{1-\alpha} = \phi_{\min} \left[ 1 + \frac{m}{n-m} F_{1-\alpha} (m, n-m) \right] \quad (3.7-2)$$

Since we have used a two parameter linear relationship the contour is an ellipse. Using equation (3.7-2), joint confidence contour for 95% confidence level has been drawn, which is shown in Figure 3.7-2. This figure shows that the contour encloses the point  $(a_0, b_0)$ . The principal axes of the ellipse are at an angle to the coordinate axes A and B, because the estimates  $a_0$  and  $b_0$  are correlated. Figure 3.7-2 also shows individual confidence intervals (ICI's) for parameters A and B. Individual confidence intervals are shown by straight dotted lines forming a rectangle. It may also be seen in Figure 3.7-2 that joint confidence contour is enclosed by rectangle of individual confidence intervals. It is now obvious that joint confidence region is more important than individual confidence intervals, because JCR takes into account both the slope and intercept simultaneously, whereas ICI of A is concerned only with the interval that includes the intercept for equations with same slope and likewise, ICI for B is concerned with the interval that includes the slope for equations with same intercept only. The rectangular region outlined by the two estimated ICI's and the ellipse defining the jointly estimated confidence region may contain quite different values of A and B [Himmelblau (1970)].

### 3.8 CHARACTERIZATION BY OTHER METHODS

Determination of micropore distribution was also done by the available software with BJH method [Barret et al. (1951)]. But the

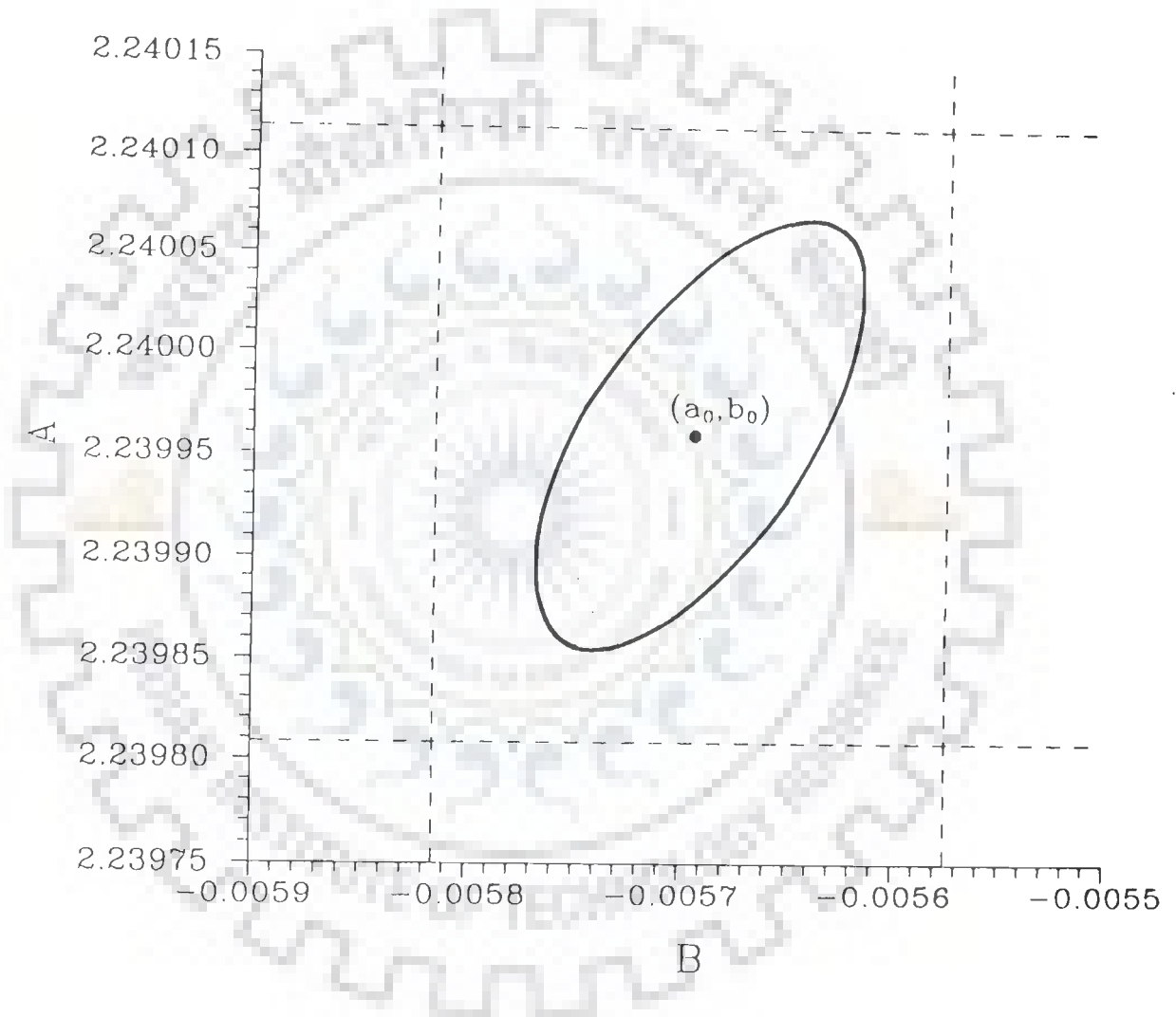


Figure 3.7-2 95% Joint Confidence Contour for Dubinin-Astakhov Plot for 13X Molecular Sieves, Adsorbate: Nitrogen

distribution so obtained was not a true representative of 13X molecular sieves. The discrepancy in the results by this method are probably due to the emphasis of the authors for the arbitrary selection of the value of parameter C. Although authors have suggested the range of the value of parameter C but have also advised that the correctness of the results should also be checked by comparing the surface area results with BET value. It is our opinion that this method is suitable only for the porous solids which have relatively large sized pores and a larger range of pore size distribution. Hence, it is not suitable for 13X molecular sieves. Due to this reason, the results obtained with this method are not being presented here.

MP-method has also been tested to determine micropore volume and micropore surface area. With Halsey parameter, it yields a surface area value ( $604 \text{ m}^2/\text{g}$ ), which is 20% lower than Langmuir value ( $755 \text{ m}^2/\text{g}$ ). While with Harkins and Jura parameters [Harkins and Jura (1944)], it gives 27% less value ( $555 \text{ m}^2/\text{g}$ ) of total surface area. For total micropore volume it gives higher value. Since this method is also based on t-plot method, so it does not give reliable quantitative estimation of micropore volume distribution.

Horváth-Kawazoe method has also been applied for the characterization. Total micropore volume determined by this method using argon is in agreement with the values calculated by D-R and D-A equations. Median pore diameter calculated with this method is approximately equal to the micropore volume mean pore diameter calculated using argon. But the drawback of this method is that it requires a large number of physical data about adsorbate and adsorbent molecules. Extensive use of these data makes the final expression relatively complicated. Besides, this method is applicable to type IV isotherm of BDDT classification of isotherms [Brunauer et al. (1940)], i.e. a mixed microporous-mesoporous material [Seifert and Emig (1991)], and 13X molecular sieves do not come under this category.



### 3.9 DETERMINATION OF BULK DENSITY AND MECHANICAL PROPERTIES

Properties related to density, viz. apparent bulk density and apparent unit density, have been determined and are given in Table 3.9-1. The average dimensions of the cylindrical pellets have also been determined using microscope, and are given in the same table. Mechanical properties of the pellets are generally empirical in nature and their values depend on the type of test being performed. Values of mechanical properties, viz. crushing strength and attrition losses, are presented in Table 3.9-2 as have been reported by the manufacturers. Nominal pore diameter of 13X molecular sieves is 10 Å, which is also reported.

### 3.10 CONCLUDING REMARKS

Characterization of 13X molecular sieves has been done in this chapter using various methods, viz. BET, Langmuir, t-plot, Dubinin-Radushkevich, and Dubinin-Astakhov methods. Some of the results have been obtained directly by the use of purchased software supplied with the physical adsorption measurement instrument, while remaining have been obtained by making appropriate computations with the developed programs.

Nitrogen has been widely used in BET and other methods to characterize microporous adsorbents [Baksh and Yang (1991), Saito and Foley (1991), Hong et al. (1995)] despite the criticism by some of the researchers on its use in physisorption measurements for characterization of microporous solids such as zeolites [Dubinin (1967, 1974)]. This is due to the fact that BET method over a period of time has become a standard method for the determination of surface area using nitrogen as adsorbate. This also serves as a benchmark to test many other methods for surface area determination. Hence, nitrogen has also been used as one of the adsorbates to characterize molecular sieves using physisorption measurements.

**Table 3.9-1 Density and other Properties of 13X Molecular Sieves**

S.No.	Parameter	Value
1	Apparent Bulk density, kg/m <sup>3</sup>	640.0
2	Apparent Unit density, kg/m <sup>3</sup>	890.0
3	Average pellet diameter,* mm	3.0
4	Average pellet length, mm	4.0

\* Shape of pellets : cylindrical

**Table 3.9-2 Mechanical Properties and Pore Diameter of 13X Molecular Sieves as reported by the Manufacturer**

S.No.	Parameter	Value
1	Crushing strength, kg	9-10
2	Loss on attrition, %	< 0.5
3	Nominal pore diameter, Å	10

Individual confidence intervals and joint confidence contour have been drawn to test the reliability of results obtained by Dubinin-Astakhov method with the optimised value of exponent  $n$ . Value of  $n$  for nitrogen as adsorbate is 1.95 and that of argon it is 1.78. Critical analysis of methods and results, obtained by them, has been carried out.

Properties related to dimensions and density of molecular sieve pellets have also been determined. Mechanical properties, being empirical in nature and specific to the applied tests, have therefore been presented as reported by the manufacturer.



---

## TRANSIENT TEMPERATURE MEASUREMENTS - EXPERIMENTAL SET UP, PROCEDURE AND RESULTS

---

### 4.0 INTRODUCTION

Research work involving simulation/modelling has a greater authenticity in respect of degree of confidence when it is supported by experimental observations necessary for simulation. At times, desired physical data to be used in simulation studies are not available in the literature. Thus, it becomes imperative to estimate these data with the experimental observations. Besides, experimental work plays an important role in providing insight into the behaviour of the process. If experimental set up is designed and operated properly, it also generates newer ideas for research in the field.

The aim here is to determine the effective thermal conductivity (in radial direction) of a bed of molecular sieves. Accordingly, transient temperature measurements in the bed are required. The experimental set up, designed for the purpose, is described in the present chapter alongwith the procedure for conducting the experiment. Further, the development of a PC based data acquisition software is also discussed, which has been used to record temperatures at various locations in the bed.

### 4.1 EXPERIMENTAL SET UP

Experimental set up possesses three main constituents - packed bed, data acquisition system, and the power supply. These are depicted in Figure 4.1-1 in the form of a block diagram. The heart of the whole experimental set up is the packed bed of molecular sieves

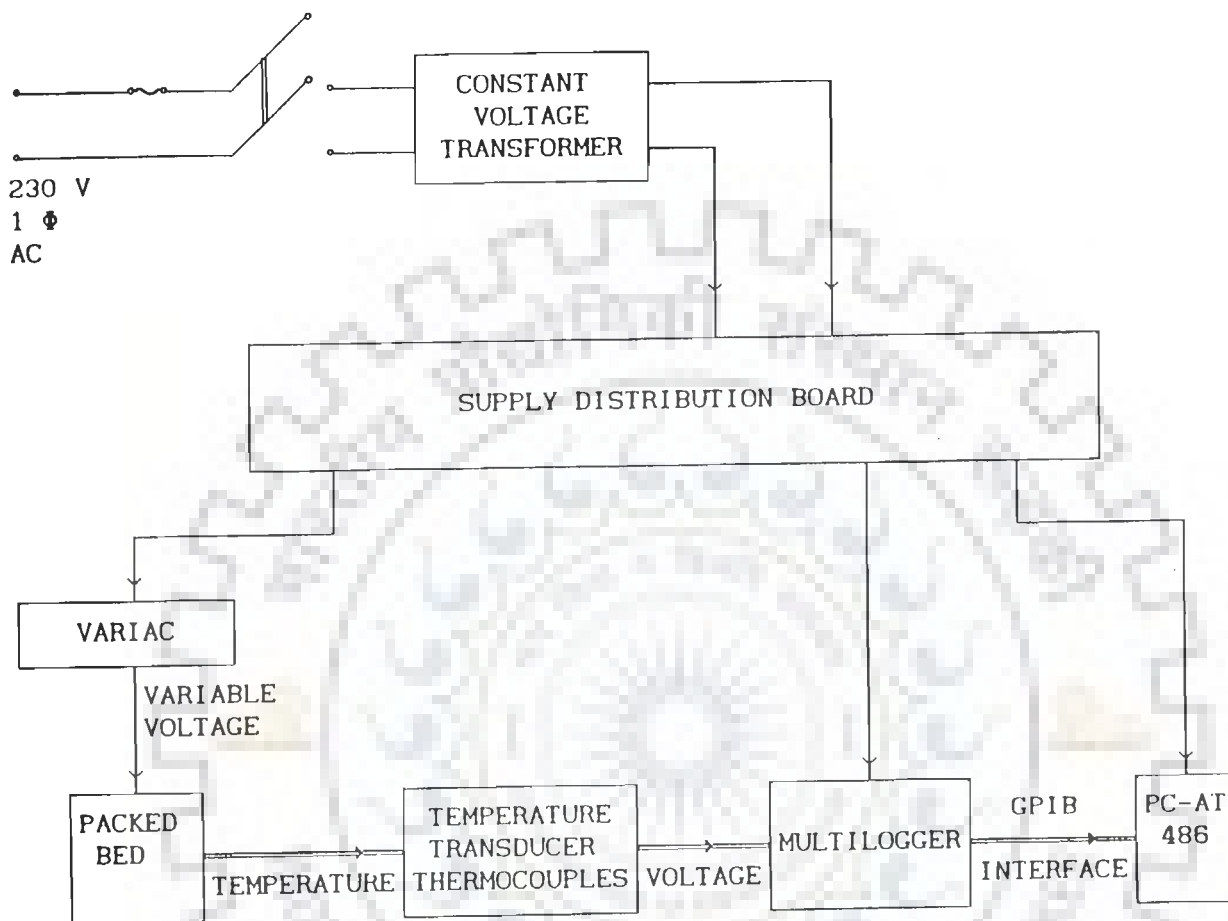


Figure 4.1-1 Block Diagram showing Packed Bed, PC based Data Acquisition System, and the Power Supply

housed in a stainless steel cylinder. The packed bed has been fabricated in the same way as done by Prasad (1988). It is shown in Figure 4.1-2. Outlet of this section can either be connected to vent or to vacuum as per the objective of the experimentation. Pressure in the system is measured by a mercury manometer.

The packed bed column can be further divided into three portions, viz. bottom portion, middle portion and top portion. Bottom and top portions are joined to the middle portion through flanged joints. Thermocouple sensors at various radial and axial locations are placed in the middle portion to measure the temperatures. Number of thermocouple sensors in radial and axial directions are six and three respectively. Larger number of thermocouples are placed in the radial direction as variation in the temperature would be predominant in this direction, since no gas is passed through the bed. Thermocouples are mounted on brass bridges and secured by screws. Figure 4.1-3 shows the thermocouple locations.

A coaxial heater is placed along the central axis of the column for heating the bed. It is placed inside an stainless steel sheath. Remaining space in the middle portion is filled with molecular sieve pellets.

#### 4.1.1 Description of Packed Bed Column

Top and bottom portions of the packed bed column are flanged heads. They are connected to the middle portion and secured by nuts and bolts. Two circular stainless steel plates are sandwiched at the flanged joints, which have a hole at the centre for securing the coaxial heater with nuts. They are used to hold the heater firmly at its two ends. Heater hold plates have two other holes of 25 mm diameter. These holes are used for taking out thermocouple wires through upper plate as well as for taking out molecular sieve pellets during emptying of column. A number of smaller holes of 3 mm diameter are also provided in plates to facilitate passage of entrapped air or gas, if any.

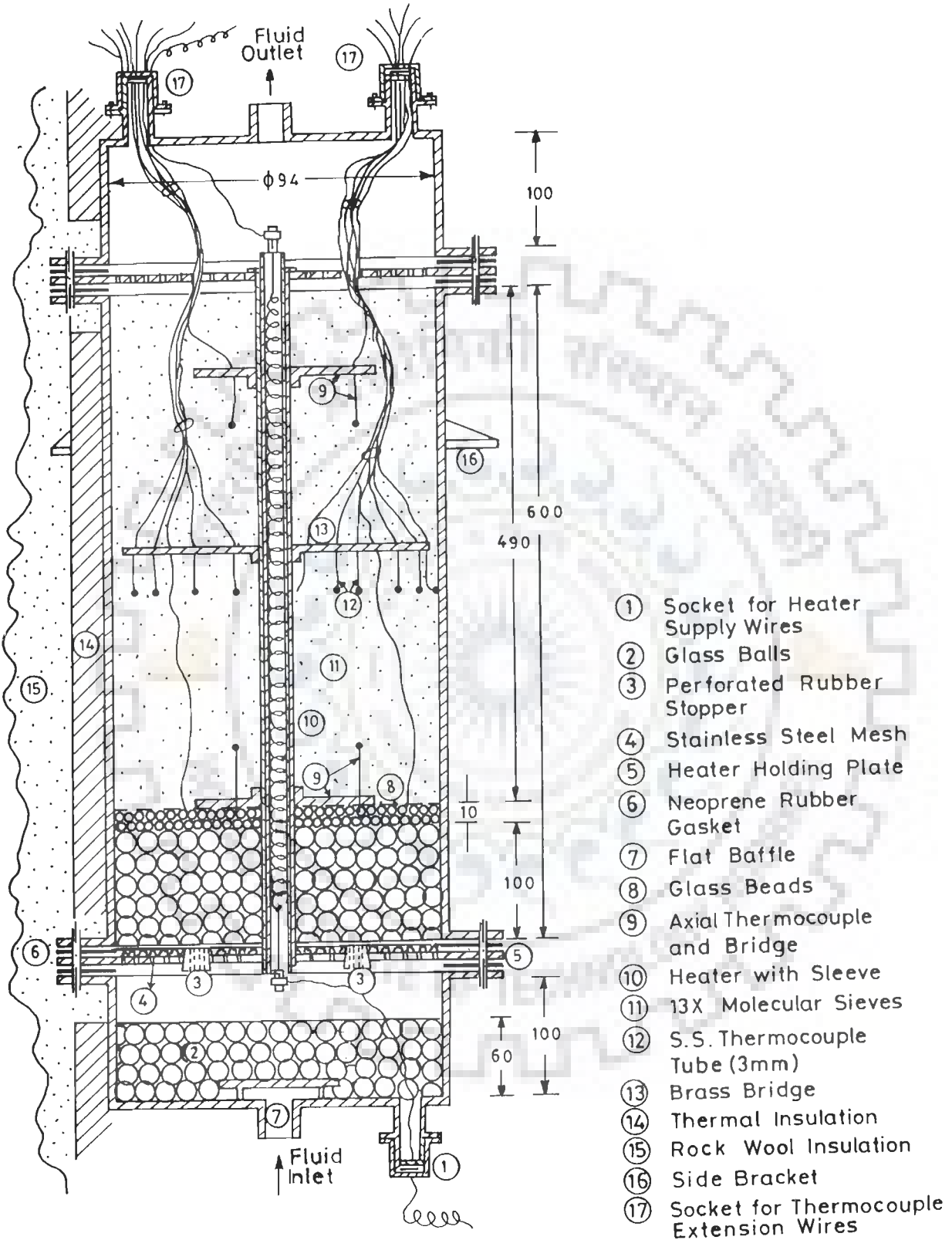
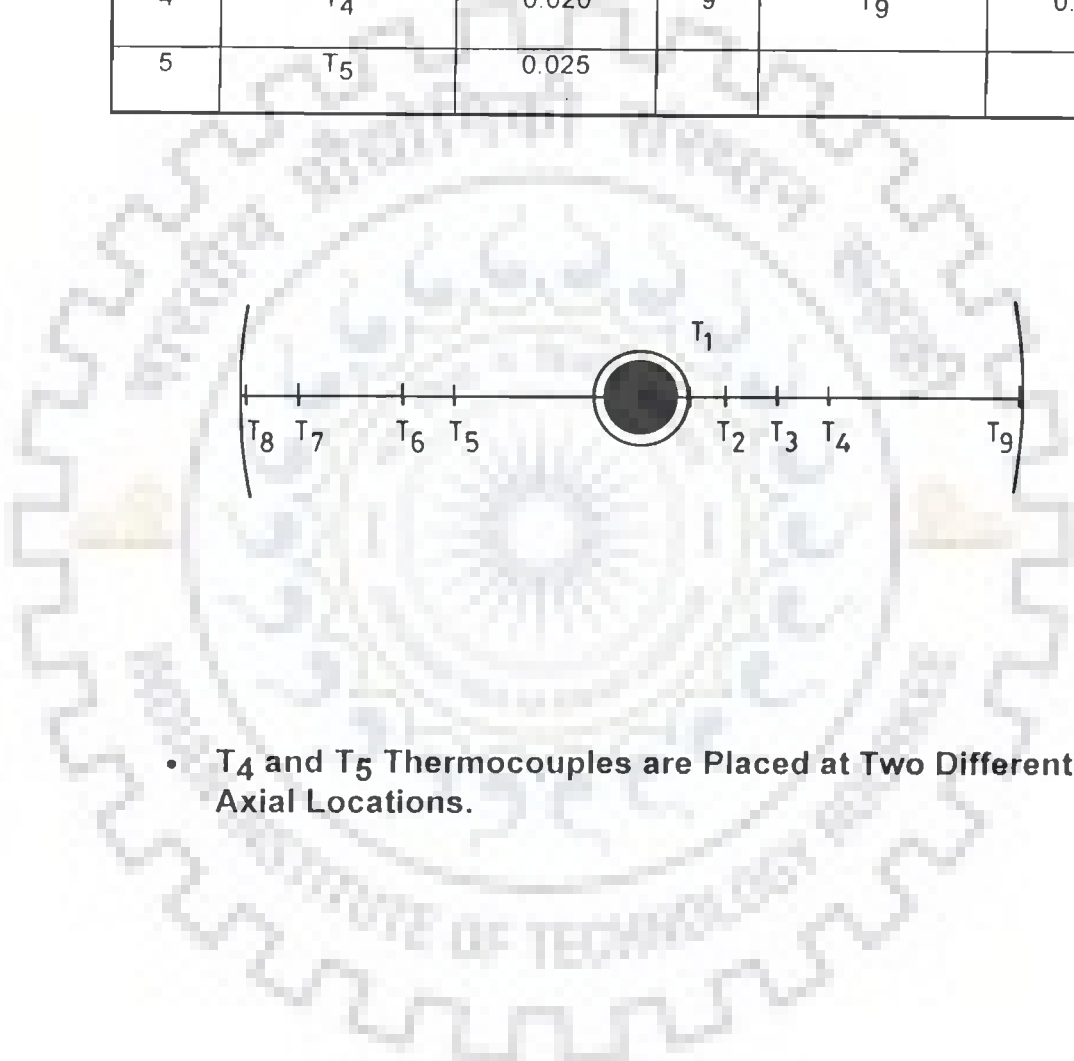


Figure 4-1-2 Packed Bed Assembly for Molecular Sieves

S.No.	Thermocouple No.	Distance from centre (m)	S.No.	Thermocouple No.	Distance from centre (m)
1	T <sub>1</sub>	0.0065	6	T <sub>6</sub>	0.030
2	T <sub>2</sub>	0.010	7	T <sub>7</sub>	0.040
3	T <sub>3</sub>	0.015	8	T <sub>8</sub>	0.045
4	T <sub>4</sub>	0.020	9	T <sub>9</sub>	0.047
5	T <sub>5</sub>	0.025			



- T<sub>4</sub> and T<sub>5</sub> Thermocouples are Placed at Two Different Axial Locations.

Figure 4.1-3 Thermocouple Locations in Radial and Axial Directions in Packed Bed



Lower plate is covered with a fine stainless steel wire mesh to support molecular sieve pellets except at the two large holes, meant for removing sieves at the time of their replacement. These holes are plugged with perforated rubber stoppers after filling adsorbent pellets in the column.

Top cover has four number of openings. One central opening is for venting gas/vapour. And three other openings are provided for different purposes; one of these openings is used for taking out extension wire of the coaxial heater while the remaining two are employed for thermocouple extension wires.

In the bottom cover, only two openings are provided. Central opening is meant for pressurising the bed by nitrogen gas while the other is for heater cable. Openings for supply cable and extension wires are flanged openings. A flat baffle is provided just inside the inlet for better distribution of nitrogen gas across the whole cross-section of the column. Stainless steel needle valves are provided at the inlet and outlet of the column for isolating it from the atmosphere as and when required. At outlet two needle valves are provided in parallel, one is meant for connecting the column to vacuum while the other is for venting the gases into atmosphere. These two sets of valves are required to be operated during the drying of bed and transient radial temperature measurements.

In order to eliminate heat losses, thermal insulation is provided outside the column. A thick layer of asbestos, magnesia and plaster of paris in the ratio 6:2:1 is provided for this purpose. Column is finally covered with insulation pad of glasswool mixed with fine dry mixture of insulation earth material, namely Fuller's earth. Two brackets are provided at the periphery of middle part of the packed bed column, which are used to mount it on a mild steel angle iron frame.

#### 4.1.1.1 Components of Packed Bed

The specifications of molecular sieves used in the present study have already been discussed and determined in Chapter III. Other key components of packed bed, namely coaxial heater and thermocouples are discussed in the following subsections.

##### (i) Coaxial Heater

Coaxial heater is a straight immersion heater. Heating element of the heater is encapsulated in a stainless steel tube. It has threaded brass ends welded at coil ends. These are used as electrical terminals. A stainless steel sheath is provided outside the heater so that it can be removed easily in case of failure of heating element without disturbing other components of the packed bed. Threads have also been provided on the sheath for fixing the coaxial heater on heater hold plates.

Insulating material provided for the separation of tube wall and heating element is the mixture of sodium silicate, alumina and silica powder applied in the form of a coating. Heating coil is of Kanthal wire having a size of 26 SWG and resistance per unit length of 0.045 ohm/cm. The length of coil is 600 mm. Outer coil diameter is 3 mm.

Fabrication of heater has been done by inserting the coil into the tube and properly sealing one end with moisture proof sealant. Fine dry sand at hot temperature was filled in the tube so that the moisture could not enter. Other end is also sealed, just after filling the sand. Heater assembly is dried for 24 hours at 473 K. Thereafter, this heater assembly is available for use.

##### (ii) Thermocouples

Thermocouples used for the measurement of temperatures at

various points in packed bed were copper-constantan type (T-type). Thermocouple wire has been insulated with glass fibre fabric. Hence, it can safely be used at elevated temperatures. To eliminate the chances of leakage through permeable glass fibre fabric insulation, a leak proof coating is also impregnated into it. 26 SWG wires have also been used in thermocouples. Calibration of thermocouples have been done before their use.

#### 4.1.1.2 Assembling of Packed Bed Column

Packed bed column is assembled in three steps. First of all, coaxial heater is fixed on lower heater hold plates followed by fixing of thermocouples on brass bridges at requisite radial and axial distances. Bottom cover is fastened with middle portion sandwiching the lower heater hold plate. Finally, the top cover is joined with middle portion putting the upper heater hold plate in between. Both the flanged joints are provided with neoprene rubber gaskets to eliminate the chances of leakage. Details of assembling of packed bed is described in the next subsection.

##### *Assembling of Packed Bed*

Assembling of the packed bed is commenced with fixing of heater on lower heater hold plate and thermocouples on brass bridges outside the column. Lower threaded end of stainless steel sheath of heater is fixed on the central hole of lower heater hold plate. Thermocouples are fixed on various radial locations at brass bridges. Two brass bridges on lowest position have one thermocouple each, fixed at 490 mm from upper heater hold plate. Brass bridge is fixed on heater sheath through a collared clamp which is secured by three small screws. These screws are positioned at  $120^\circ$  from each other. The hot junctions of thermocouples are placed 50 mm apart from the respective brass bridges in order to avoid the influence of high thermal conductivity of brass on temperatures measured by the thermocouples. Two brass bridges are fixed approximately at the mid height of heater. These brass bridges hold 9 thermocouples to measure temperatures at different

radial locations. Two of them are fixed at extremities - one on the heater sheath and other at the column wall. Two more brass bridges are fixed at 50 mm from the upper heater hold plate. Thus, there are three axial locations.

This whole heater and thermocouple assembly is lowered in the middle portion of the column. Two large holes of lower heater hold plate are plugged by perforated rubber stoppers so that entrapped gases/moisture can pass through the perforations. Remaining portion of lower heater hold plate is supported by a fine stainless steel wire mesh.

Now, bottom cover filled with 8 mm diameter glass beads upto a height of 60 mm, is brought near the lower end of middle portion and supply cable of heater is taken out through the opening in the bottom cover. Two neoprene gaskets, one below and one above the bottom heater hold plate is aligned with the bolt holes, and flanged joint bolts are tightened so that the heater hold plate is sandwiched properly.

Middle portion of the column is filled with layers of 8 mm diameter glass balls, 3 mm diameter glass beads and molecular sieve pellets in that order from bottom; height of layers of these materials are 100, 10, and 490 mm respectively. Filling of the column is done through a conical funnel having a rubber tube connected to its stem. Care is taken that free fall of these materials does not occur to avoid their breakage but at the same time column is also packed thoroughly. Layers of glass beads are provided for proper distribution of gas in the entire cross-section of bed.

Assembling of top cover is started by placing upper heater hold plate at the upper end of middle portion. Extension wires of thermocouples are taken out through two large diameter holes in upper heater hold plate. These wires and heater supply cable are then passed through two openings in top cover. Finally, flanged joint is fastened through nuts and bolts. Neoprene rubber gaskets are used in this joint also to avoid the chances of leakage of air/moisture from outside.

The brackets provided outside of the middle portion of the column for mounting the packed bed column on mild steel angle iron frame, is fixed through nuts and bolts. This whole assembly is checked for leakage by applying vacuum through vacuum pump. If leakage persists, bolts at all joints are checked and tightened once again. Even after this, if leakage continues in the system, araldite adhesive is applied at tube joints and openings in bottom and top cover. After this check, outer wall of the whole column is insulated with insulation, namely mixed paste of magnesia, plaster of paris and asbestos rope.

Flanged sockets at the openings in bottom and top covers are provided for thermocouple extension wires and heater supply cable. Care has been taken so that short circuiting of extension wire may be prevented. Nine holes of 3 mm dia. have been provided for extension wires in the socket cover. Height and outer diameter of socket are 80 mm and 18 mm respectively. A neoprene rubber gasket is provided at the flanged joint which is fastened by nuts and bolts. Araldite adhesive is also applied around the joint to avoid leakage.

Finally, electrical connections of column are made. Extension wires of thermocouples are connected to multilogger.

#### **4.1.2 Power Supply**

Power supply to the experimental set up has been provided through a voltage stabilizer. Circuit diagram of power supply is shown in Figure 4.1-4. Input voltage and current has been monitored by voltmeter and ammeter respectively. Wattage to coaxial heater has been regulated by a variable transformer, and monitored by a wattmeter. It has been kept constant during one set of experiment. Provision is also made to control the maximum temperature of heater surface by placing sensor element of a temperature controller (thermostat with temperature indicator). Besides, manual control of temperature as an alternative/standby arrangement is also possible in the experimental set-up by switching on/off the heater.

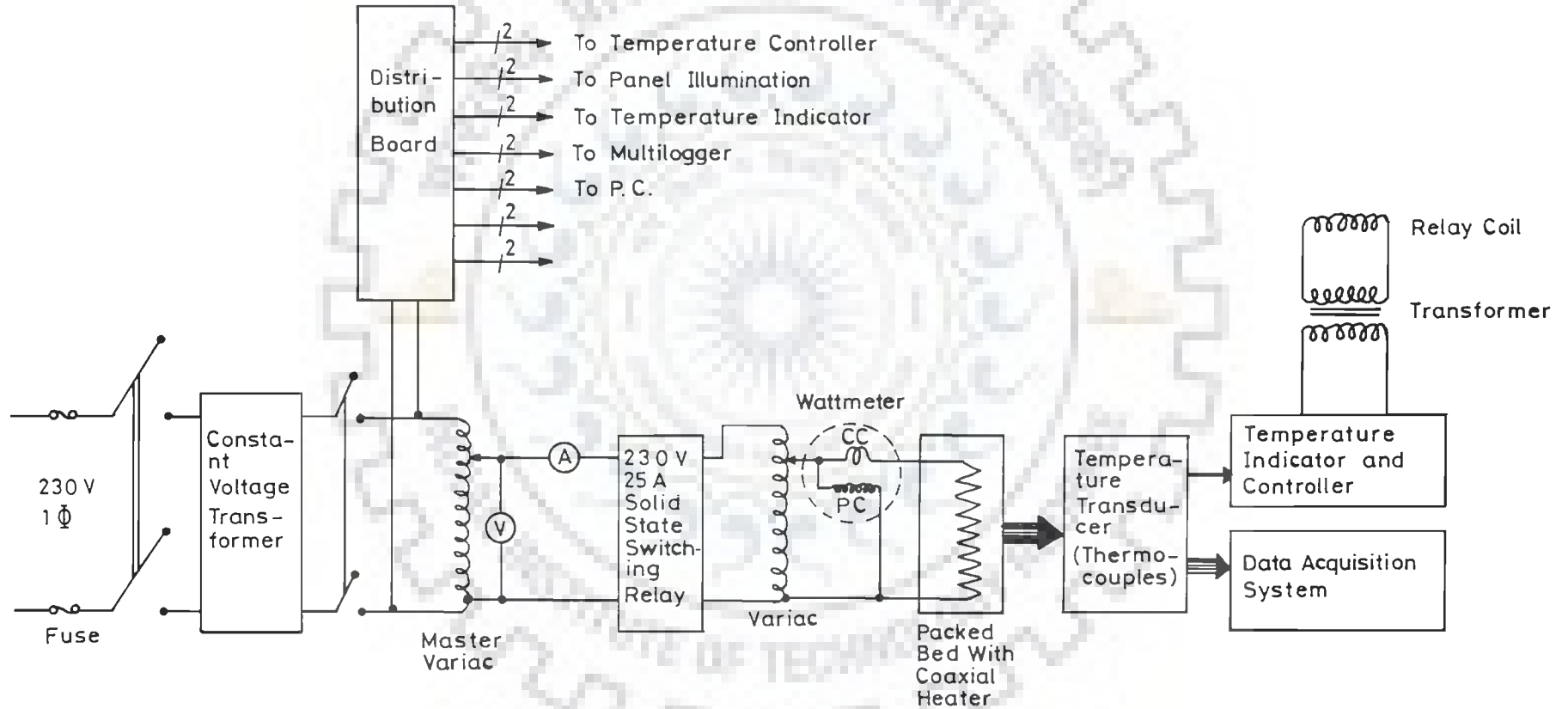


Figure 4-1-4 Circuit Diagram for Experimental Set up

### 4.1.3 Development of a PC Based Data Acquisition Software

---

A PC based data acquisition system has been employed to acquire and record the temperatures. It uses a multilogger model SC-7501, manufactured by M/S Iwatsu Electric Company Ltd., Tokyo, Japan. This multilogger is portable and has a facility to measure temperature. Additionally, it also has provision to measure DC and AC voltages and resistance. It can display and print the measured values by a small in-built printer on thermally sensitive paper roll as well. But this multilogger does not have the facility to store measured values. Thus, it required development of a PC based Data Acquisition Software.

Multilogger has been provided with GPIB (General Purpose Interface Bus) interface. Which is also known as IEEE-488. The GPIB interface enables multilogger to perform its functions under remote control by an external equipment (e.g. PC) and data transfer to the equipment. All the channels (30 nos.) can be scanned with minimum sampling interval of 1 s. The multilogger with PC as master controller can be used to measure the four variables. The details of channels and measurement range of these variables are given below.

#### *Temperature*

No. of Channels : 24 (CH7 to CH30)

Range : -200 °C to 1370 °C

Thermocouple Types : R, K, T, J, E

#### *DC Voltage*

No. of Channels : 30 (CH1 to CH30)

Range : 1  $\mu$ V to 270 V

#### *AC Voltage*

No. of Channels : 6 (CH1 to CH6)

Range : 1  $\mu$ V to 270 V

*Resistance*

No. of Channels : 6 (CH1 to CH6)

Range : 1 m $\Omega$  to 20 M $\Omega$

#### 4.1.3.1 Software

A menu driven, user friendly and interactive software has been developed to control the multilogger using PC-AT 486 through GPIB interface.

The software has been written in C language and it contains about 6400 lines code. It utilizes Turbo C compiler. The software can be used to program multilogger in different modes. The software enables the data acquisition at different sampling rates. A hard copy of data in desired format can be obtained. Graphs showing trend of data can be plotted and printed on a dot matrix printer. The software includes following advanced features.

- \* Context sensitive help at all level of software is included.
- \* The data entered is first checked for its validity, and then it is accepted.
- \* In case of power failure while data acquisition is in progress, data file would not be corrupted in any case; a provision has been made to guard off such a situation.
- \* Auto ranging facility has been incorporated for the measurement of all variables. This makes the data acquisition system suitable for measuring unknown temperature, voltage, or resistance.
- \* Dynamic memory allocation has been used in program to optimize the available system memory.



- \* Programmable Interrupt Controller of the PC has been used to generate interrupt at every 0.1 s for sampling the data. This interrupt driven sampling enables us to do other jobs like printing, plotting, analysis, and display etc. while data acquisition is in progress.

#### 4.1.3.2 Advantages

The control of multilogger using PC makes the multilogger suitable for process control too (On-line and Off-line both) which is not possible if the multilogger is independently used. It also enhances the functions of multilogger in following manner.

- The control of multilogger becomes more user friendly and interactive.
- The data acquired can be analysed on-line and appropriate action can be taken in case of process control.
- The data acquired are saved in a data file for further analysis.

## 4.2 EXPERIMENTAL PROCEDURE

In order to estimate the dry bed effective thermal conductivity, the bed was dried before conducting the experiment for the measurement of radial temperatures under transient conditions. This has been accomplished by heating the bed upto a temperature more than 373 K everywhere in the bed for over 2 hours thereby expelling the moisture, if any.

The bed has also been pressurised with nitrogen gas after drying. Pressure within the bed was maintained slightly higher than atmospheric pressure, i.e. 770-780 mm Hg. This eliminates the possibility of leakage of atmospheric moisture into the bed. The bed

has been allowed to cool thereafter. It takes around 24 hours for the bed to come to normal temperature because it has been thermally insulated from outside.

Prior to conducting the experiments, nitrogen pressure has been released and top portion outlet of bed was connected to vacuum pump. Once the bed is under vacuum, the coaxial heater can be switched on. Radial temperature measurements have been done using thermocouples and recorded on-line with the help of data acquisition system.

Further, maximum allowable temperature for 13X molecular sieves is 523 K. Beyond this temperature, if molecular sieves are kept for long time they lose their adsorption capacity permanently. Under these circumstances, uniform microporous pore structure of molecular sieves collapses. Therefore, to avoid this to happen, heater surface temperature was not allowed to go beyond 523 K. This is done by switching off the heater as soon as the heater surface temperature crosses this limit. Heater is again switched on when the heater surface goes down. This process (switching on and switching off) is continued until the radial temperature measurements are over.

During the transient heating, radial temperatures were recorded upto 40 min at an interval of 5 min.

### 4.3 RESULTS

Radial temperatures in the bed, recorded under transient conditions during experiments, are given in Tables 4.3-1 and 4.3-2 for heater wattages  $Q_L$  of 0.1 and 0.13333 kW/m respectively. In order to have a better view of heating pattern in the bed of molecular sieves, temperatures have also been plotted as a function of time for different radial locations for both the cases. These profiles are given in Figures 4.3-1 and 4.3-2.

It may be noted that the profiles for both the heater

**Table 4.3-1 Experimentally Observed Temperatures along Radial Direction in Packed Bed of 13X Molecular Sieves for  $Q_L = 0.1 \text{ kW/m}$**

S. No.	Time (s) <sub>↓</sub>	Temperature at radial distance (m) from centre, K								
		Dist., m <sub>→</sub> 0.0065	0.010	0.015	0.020	0.025	0.030	0.040	0.045	0.047
1.	00	303.0	303.0	303.0	303.0	303.0	303.0	303.0	303.0	303.0
2.	300	327.2	313.8	308.1	305.8	304.9	304.7	304.5	304.2	304.2
3.	600	348.6	329.0	318.7	313.5	310.2	309.5	308.9	307.1	307.1
4.	900	363.1	340.6	328.0	321.4	316.3	313.6	313.1	309.7	309.7
5.	1200	373.5	349.6	335.5	328.0	322.1	318.9	317.2	312.0	312.0
6.	1500	382.1	357.1	341.9	333.6	327.1	323.9	321.0	314.2	314.2
7.	1800	389.7	363.7	347.6	338.5	331.6	328.6	324.5	316.4	316.3
8.	2100	396.2	369.5	352.7	342.8	335.4	332.9	327.6	318.4	318.2
9.	2400	401.7	374.6	357.3	346.8	339.0	336.5	330.8	320.5	320.3

**Table 4.3-2 Experimentally Observed Temperatures along Radial Direction in Packed Bed of 13X Molecular Sieves for  $Q_L = 0.13333$  kW/m**

S. No.	Time (s) ↓	Temperature at radial distance (m) from centre, K									
		Dist., m →	0.0065	0.010	0.015	0.020	0.025	0.030	0.040	0.045	0.047
1.	00	304.0	304.0	304.0	304.0	304.0	304.0	304.0	304.0	304.0	304.0
2.	300	340.0	320.9	312.0	308.4	306.7	306.5	306.4	305.8	305.7	
3.	600	366.0	340.5	326.0	318.8	313.6	312.3	311.9	309.1	309.1	
4.	900	383.8	354.9	337.0	328.5	321.5	318.8	317.7	312.1	312.1	
5.	1200	397.1	365.1	344.3	336.0	327.4	324.3	322.8	313.9	313.9	
6.	1500	407.7	374.1	352.1	342.8	333.1	329.6	327.7	316.3	316.3	
7.	1800	416.3	382.0	359.2	348.7	338.3	334.4	332.0	319.0	318.9	
8.	2100	423.9	388.9	365.3	354.0	342.9	338.6	335.8	321.5	321.2	
9.	2400	430.3	394.9	370.8	358.7	346.9	342.2	339.1	323.6	323.1	

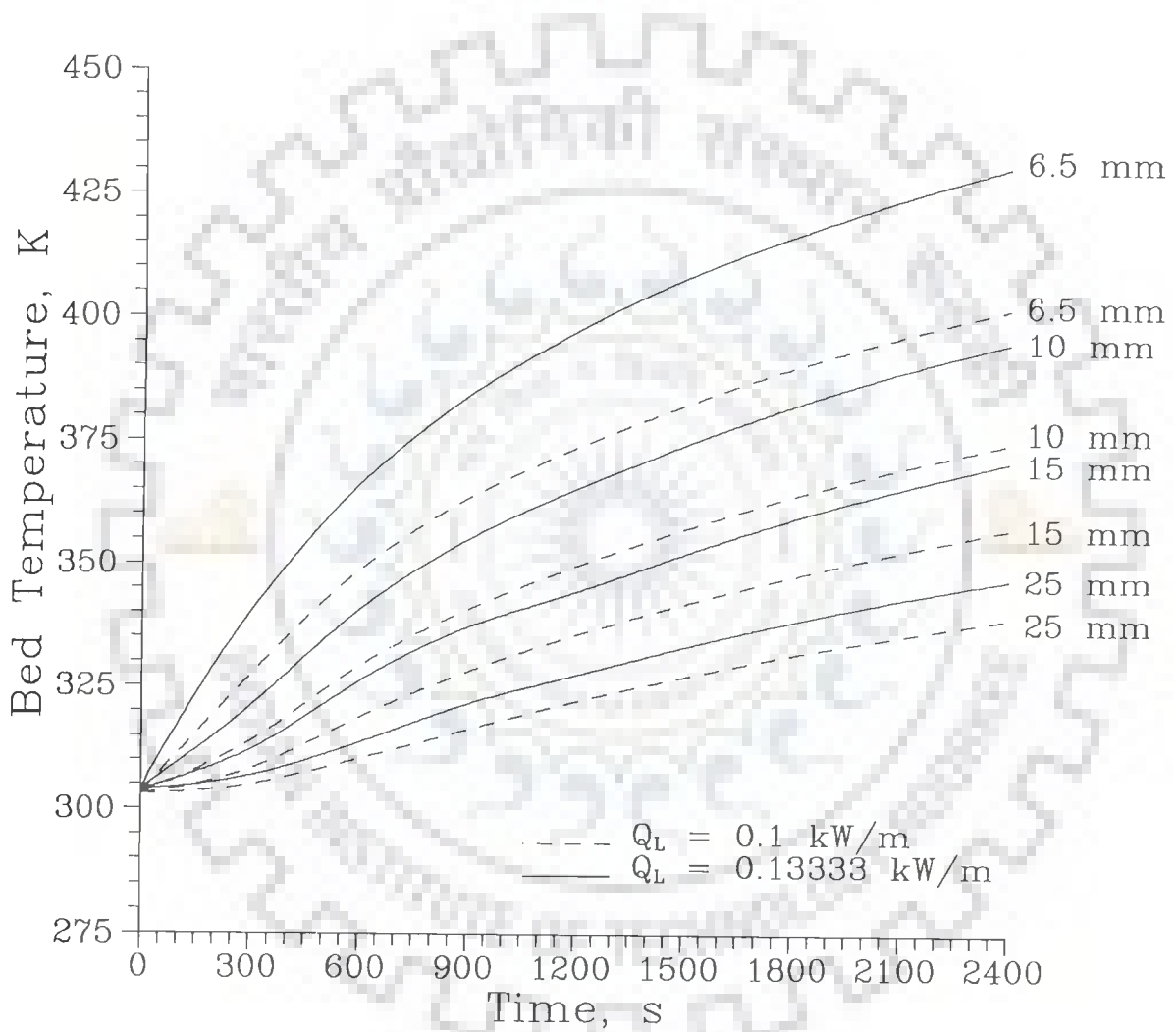


Figure 4.3-1 Temperature Profiles at Distances 6.5, 10, 15, and 25 mm from Centre under Transient Conditions for  $Q_L = 0.1$  and  $0.13333 \text{ kW/m}$  during Dry Bed Conduction Experiments

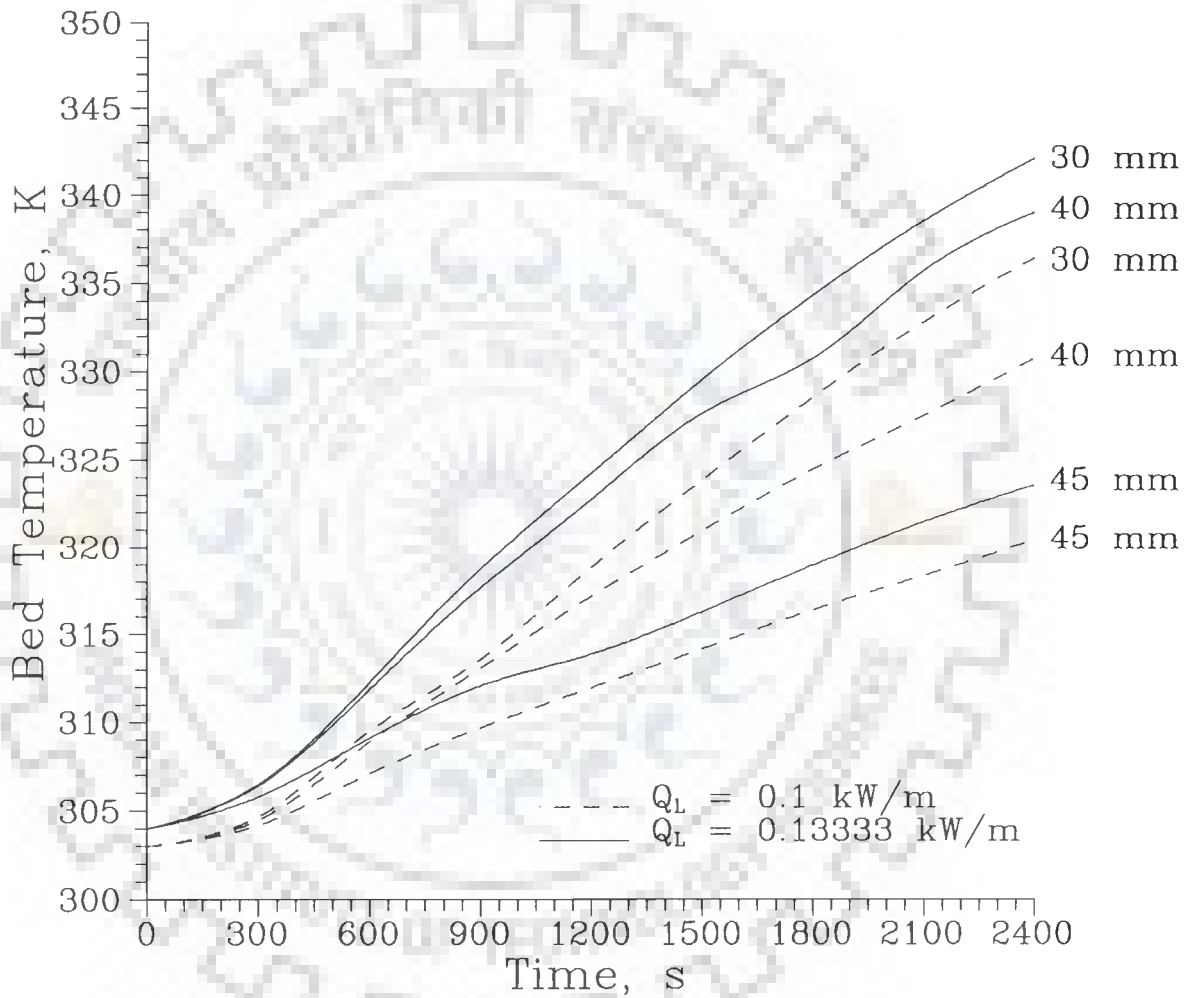


Figure 4.3-2 Temperature Profiles at Distances 30, 40, and 45 mm from Centre under Transient Conditions for  $Q_L = 0.1$  and  $0.13333$  kW/m during Dry Bed Conduction Experiments

wattages are given in the same Figures and that too for selected locations. This has been done to observe the effect of increase in heater wattage on radial temperatures. It may be observed that the rate of heating the bed with 0.13333 kW/m heater is more in comparison to the heating by first heater of lower heater wattage. These results are expected and provide a qualitative check on the correctness of experimental setup, procedure, and associated accessories.

Besides, thermal inertia of the heater also reduces the rate of heating during the initial period of experimentation. This aspect has been discussed in detail in Chapter V on "Estimation of Temperature - Dependent Effective Thermal Conductivity of Adsorber/Desorber Bed".

#### 4.4 CONCLUDING REMARKS

In this chapter, experimental setup and procedure have been described to measure the radial temperatures in the packed bed of molecular sieves under transient conditions. Every possible effort was made to ensure the correctness and reproducibility of measured data.

A data acquisition software has been developed in 'C' language to record and store the measured temperatures at desired locations, in a Personal Computer. The software is interactive, user friendly, and possesses several advanced features as described. If desired, it may be obtained from the author. Although many softwares for specific data acquisition system are available in the market, but no software was available for the multilogger existing in our laboratory. Therefore, the efforts in this direction were considered worthwhile in order to acquire the data in PC by using multilogger. This experience in a related branch has been quite exciting and rewarding in the area of PC based instrumentation.

Transient radial temperature profiles in the bed for two heater wattages 0.1 and 0.13333 kW/m have been obtained. These shall be used in Chapter V for estimating the correlation for effective thermal conductivity of a bed of molecular sieves.

---

## ESTIMATION OF TEMPERATURE-DEPENDENT EFFECTIVE THERMAL CONDUCTIVITY OF ADSORBER/DESORBER BED

---

### 5.0 INTRODUCTION

Analysis, design, and modelling of thermal regeneration process require sufficiently accurate knowledge of thermal transport properties. In the present study, desorber is packed with 13X molecular sieves and the energy required for desorption is supplied by an electrical heater, imbedded coaxially into the bed. In order to predict the rate of desorption by using a mathematical model, one requires the value of effective thermal conductivity of bed,  $k$ . As per the extensive literature survey carried out by us, the values of  $k$  for a packed bed of molecular sieves are rarely reported.

Effective thermal conductivity of a material depends on many factors. For molecular sieves, thermal conductivity is strongly dependent on the void fraction, pore size and fluid contained in the pores. Crystallite size and type of binder used are also important. However, one established fact is that the thermal conductivity of nonmetals like molecular sieves increases with temperature [Bird et al. (1960)]. Furthermore, packed bed of molecular sieves differs from conventional packed bed (containing nonporous material) in the sense that it possesses bed porosity due to interpellet voids as well as intraparticle porosity. Thus, total bed voidage would also contribute to the effective thermal conductivity of the bed. Generally, it has been considered constant over a wide range of temperatures in earlier studies. This is due to the fact that the solution of model equations may be obtained easily.



In this chapter, dependence of  $k$  on temperature has been estimated for the adsorber/desorber. Model chosen for dependence of  $k$  on temperature is linear [Aziz(1988)].

## 5.1 EXPERIMENTAL DATA

In the preceding chapter, dry bed conduction experiments were conducted in a bed of 13X molecular sieves pellets; dimensions of the pellet and bed voidage are given below.

---

average length of pellets, $l_p$	= 0.004 m
average diameter of pellets, $d_p$	= 0.003 m
shape of pellets	= cylindrical
total bed voidage	= 0.42

---

During transient heating, temperatures were recorded upto 40 min at an interval of 5 min using thermocouples at different radial locations as depicted in Figure 4.1-3 (Chapter IV). Tables 4.3-1 and 4.3-2 (Chapter IV) provide the temperatures recorded for two heater wattages of 0.1 and 0.13333 kW/m respectively, used in the experimentation. These experimental data have been used for the estimation of temperature dependency of  $k$ .

## 5.2 MODEL EQUATION

Figure 5.2-1 depicts a cross-sectional view of an elementary cylindrical shell within an adsorber/desorber bed alongwith the imbedded coaxial heater. Following equation describes the transient

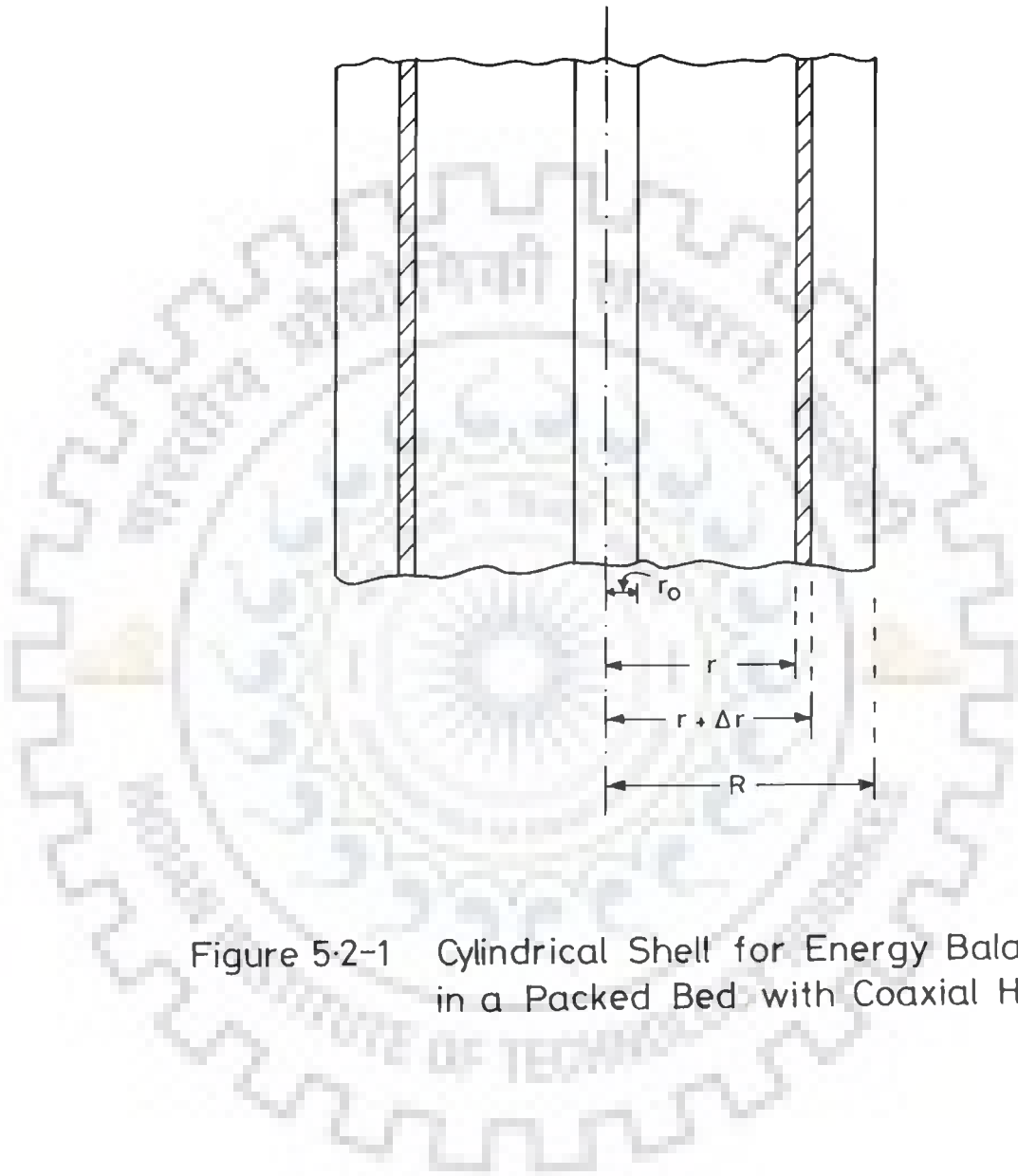


Figure 5-2-1 Cylindrical Shell for Energy Balance in a Packed Bed with Coaxial Heater

thermal conduction in such a system [Carslaw and Jaeger (1959), Bird et al. (1960)].

$$\frac{\partial T}{\partial t} = \frac{1}{\rho_b C_p} \frac{1}{r} \frac{\partial}{\partial r} \left[ k(T) r \frac{\partial T}{\partial r} \right] \quad (5.2-1a)$$

Further, it is assumed that  $k$  varies linearly with temperature ( $T$ ) as given below [Aziz (1988), Özisik (1981), Holman (1976)].

$$k(T) = k_o + \beta (T - T_o) \quad (5.2-1b)$$

Above model is based upon following assumptions [Bird et al. (1960)] :

- (a) Ends of bed are perfectly insulated, i.e. there is no axial temperature gradient.
- (b) Initially, bed is at a uniform temperature.
- (c) Walls of bed are perfectly insulated, i.e. no flux across the bed wall.
- (d) Heater wattage per unit length is constant.

Initial and boundary conditions for the model equation are given below.

#### *Initial Condition*

$$T(r,0) = T_o ; \quad r_o \leq r \leq R \quad (5.2-2a)$$

## Boundary Conditions

$$\left. \frac{\partial T}{\partial r} \right|_{(R, t)} = 0 \quad (5.2-2b)$$

$$\left. \frac{\partial T}{\partial r} \right|_{(r_o, t)} = - \frac{Q_L}{2\pi r_o k} \quad (5.2-2c)$$

### 5.3 ESTIMATION METHOD

An estimation method normally requires the definition of objective function, a numerical method for solving model equation, and a suitable optimization technique. Following objective function is used in the present work.

$$\Phi = \sum_{i=1}^m \sum_{j=1}^n \left[ \frac{T_{i,j}^{\text{exp}} - T_{i,j}^{\text{pre}}}{T_o} \right]^2 \quad (5.3-1)$$

$\Phi$  is simply proportional to the sum of square of errors.

In order to estimate  $k_o$  and  $\beta$ , Nelder-Mead search technique has been employed to minimize  $\Phi$ . Details of this technique are available in standard texts such as Himmelblau (1972) and Rao (1978).

#### 5.3.1 Numerical Solution

Control volume finite difference method [Patankar (1980)] has been used to solve the model equation. Main advantage of this method is that the conservation equations are always satisfied irrespective of grid size and the convergence of method is almost assured. It is purely a matter of our preference as we are adept in using it. However, any

suitable and efficient method for the solution of unsteady state conduction equation may be used [Michelsen (1979), Villadsen and Michelsen (1978), Finlayson (1972)].

It is pertinent to describe here the discretization of a two dimensional diffusion equation in cylindrical coordinate system using control volume finite difference method. Let us consider the following equation :

$$\rho_b C_p \frac{\partial T}{\partial t} = \frac{1}{r} \frac{\partial}{\partial r} \left[ r k \frac{\partial T}{\partial r} \right] + \frac{1}{r} \frac{\partial}{\partial \theta} \left[ \frac{k}{r} \frac{\partial T}{\partial \theta} \right] + S \quad (5.3-2)$$

A two dimensional control volume in cylindrical coordinate is shown in Figure 5.3-1. For grid point P, points E and W are its  $\theta$ -direction neighbours while N and S are the r-direction neighbours. The control volume around P is shown by dashed lines. z-direction thickness of the control volume is assumed to be unity. To obtain discretization equation we multiply equation (5.3-2) by r and integrate with respect to r and  $\theta$  over the control volume.

Discretization equation for equation (5.3-2) at point P after many simplifications can be written as follows [Patankar (1980)] :

$$a_P T_P = a_E T_E + a_W T_W + a_N T_N + a_S T_S + b \quad (5.3-3)$$

where,

$$a_E = \frac{k_e \Delta r}{r_e (\delta\theta)_e} \quad (5.3-4a)$$

$$a_W = \frac{k_w \Delta r}{r_w (\delta\theta)_w} \quad (5.3-4b)$$

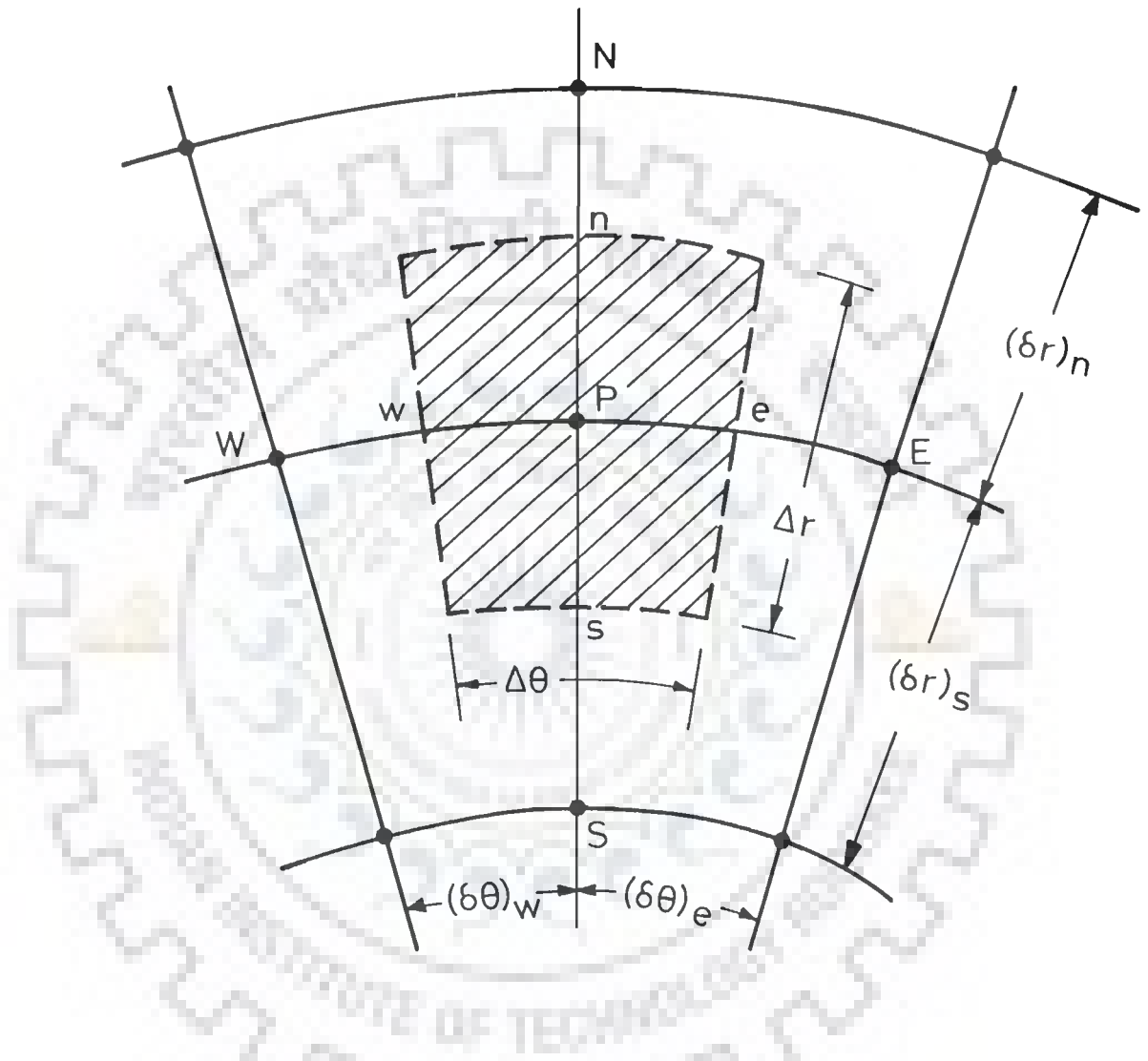


Figure 5-3-1 Control Volume in Two Dimensional Cylindrical Coordinates

$$a_N = \frac{k_n r_n \Delta\theta}{(\delta r)_n} \quad (5.3-4c)$$

$$a_S = \frac{k_s r_s \Delta\theta}{(\delta r)_s} \quad (5.3-4d)$$

$$a_P^o = \frac{\rho_b C_p \Delta V}{\Delta t} \quad (5.3-4e)$$

$$b = S_C \Delta V + a_P^o T_P^o \quad (5.3-4f)$$

$$a_P = a_E + a_W + a_N + a_S + a_P^o - S_P \Delta V \quad (5.3-4g)$$

$$\Delta V = 0.5 (r_n + r_s) \Delta\theta \Delta r \quad (5.3-4h)$$

Here, superscript 'o' signifies the parameter values at previous time step.  $S_C$  and  $S_P$  are constant and coefficient part of the linearized source term obtained by its linearization using Taylor's series. Thus,

$$S = S_C + S_P T_P \quad (5.3-4i)$$

$$S_C = S^* - \left[ \frac{dS}{dT} \right]^* T_P^* \quad (5.3-4j)$$

$$S_P = \left[ \frac{dS}{dT} \right]^* \quad (5.3-4k)$$

where, superscript '\*' denotes the parameter values about which the linearization has been done.

Discretization equation (5.3-3) has been converted into one dimension by assuming unit thickness in the  $\theta$ -direction. Further, discretization equation for the point P is applied to all the grid points which results into the following set of linear equations.

$$\underline{G} \underline{f} = \underline{d} \quad (5.3-5)$$

Where

$$\underline{G} = \begin{bmatrix} B_1 & C_1 & & & & \\ & A_2 & B_2 & C_2 & & \\ & & A_3 & B_3 & C_3 & \\ & & & & & \dots & \\ & & & & & & A_{n-2} & B_{n-2} & C_{n-2} \\ & & & & & & & A_{n-1} & B_{n-1} \end{bmatrix} \quad (5.3-6a)$$

$$\underline{f}^T = [T_1, T_2, \dots, T_{n-2}, T_{n-1}] \quad (5.3-6b)$$

$$\underline{d}^T = [D_1, D_2, \dots, D_{n-2}, D_{n-1}] \quad (5.3-6c)$$

As the coefficient matrix  $\underline{G}$  is tridiagonal in structure, the set of equations (5.3-5) may be easily solved by Thomas algorithm or by the algorithm developed by Kumar et al. (1993). Elements of  $\underline{G}$ ,  $\underline{f}$  and  $\underline{d}$  are described below :

$$A_i = -k_i \frac{r_{i-1}}{\Delta r}, \quad i = 2 \text{ to } n-1 \quad (5.3-7)$$

$$B_i = -C_i + a_{p_i}^o, \quad i = 1 \quad (5.3-8)$$

$$B_i = -(A_i + C_i) + a_{p_i}^o, \quad i = 2 \text{ to } n-2 \quad (5.3-9)$$

$$B_i = -A_i + a_{p_i}^o, \quad i = n-1 \quad (5.3-10)$$

$$a_{p_i}^o = \frac{\rho_b C_p 0.5 \Delta r}{\Delta t} (r_{i-1} + r_{i+1}), \quad i = 1 \text{ to } n-1 \quad (5.3-11)$$

$$C_i = -\frac{k_{i+1} r_{i+1}}{\Delta r}, \quad i = 1 \text{ to } n-2 \quad (5.3-12)$$



$$D_i = a_{p_i}^o T_i^o + \frac{Q_L}{2\pi}, \quad i = 1 \quad (5.3-13)$$

$$D_i = a_{p_i}^o T_i^o, \quad i = 2 \text{ to } n-1 \quad (5.3-14)$$

### 5.3.2 Computational Algorithm

An algorithm for the solution of model equation has been developed, which utilizes the discretization as given by equations (5.3-7) to (5.3-14). This algorithm is described below.

(1) Read input data including the values of  $k_o$  and  $\beta$ .

(2) Calculate FAC1 using following equation.

$$\text{FAC1} = \frac{Q_L \Delta r}{2\pi r_o}$$

(3) Calculate  $a_{p_i}^o$  using equation (5.3-11) for  $i = 1$  to  $n - 1$ .

(4) Set  $T_h = 0$ ,  $J = 0$ , and  $T_{o_i} = T_o$  for all  $i$ .

(5) Set  $J = J + 1$ .

If  $J \leq J_{\max}$ , proceed, otherwise go to step (13).

(6) Calculate Time =  $(J - 1) \Delta t$ .

(7) Set  $T_{old_i} = T_i$  for  $i = 1$  to  $n-1$ .

(8) Calculate  $k_i$  using equation (5.2-1b) for  $i = 1$  to  $n - 1$ .

(9) Calculate  $T_h = T_i + \text{FAC1} \times k_i$  for  $i = 1$ .

(10) Calculate elements of tridiagonal matrix  $\underline{G}$  and vector  $\underline{d}$  using equations (5.3-7) to (5.3-14).

(11) Solve equation (5.3-5) by Thomas algorithm to obtain  $\underline{f}$  which has  $T_{new_i}$  for all  $i$  as its elements.

(12) Check  $\left| (T_{new_i} - T_i) \right| \leq \epsilon$  for  $i = 1$  to  $n - 1$ .

If yes, go to step (5), otherwise calculate  $T_i$  as given below.

$T_i = \gamma T_i + (1 - \gamma) T_{new_i}$  for  $i = 1$  to  $n - 1$  and go to step (8).

(13) Print Results.

#### 5.4 RESULTS AND DISCUSSION

As stated earlier, Experimental data reported in Tables 4.3-1 and 4.3-2 have been used to estimate the effective thermal conductivity of the packed bed of molecular sieves. Values of  $k_o$  and  $\beta$  have been estimated for both the data sets according to the procedure discussed in section 5.3. Equation (5.2-1b) incorporating these values is given below :

$$k = 8.1722 \times 10^{-5} + 9.80664 \times 10^{-7} (T - T_o) \quad (5.4-1)$$

For both the data sets, experimentally observed temperatures and the temperatures predicted by the model using equation (5.4-1) are within  $\pm 10\%$  variation. Figures 5.4-1 and 5.4-2 depict experimental and predicted temperatures for heater wattages of 0.1 and 0.13333 kW/m respectively.

These Figures show that the simulated temperatures are slightly higher as compared to the experimentally observed values at the locations in the vicinity of heater surface. This is because of the fact that the model used here assumes emission of heat right from the instant the heater is switched on, but actually emission of heat starts only after a time lag due to the thermal inertia of heater coil, sand filling, and the sheathing of stainless steel around it.

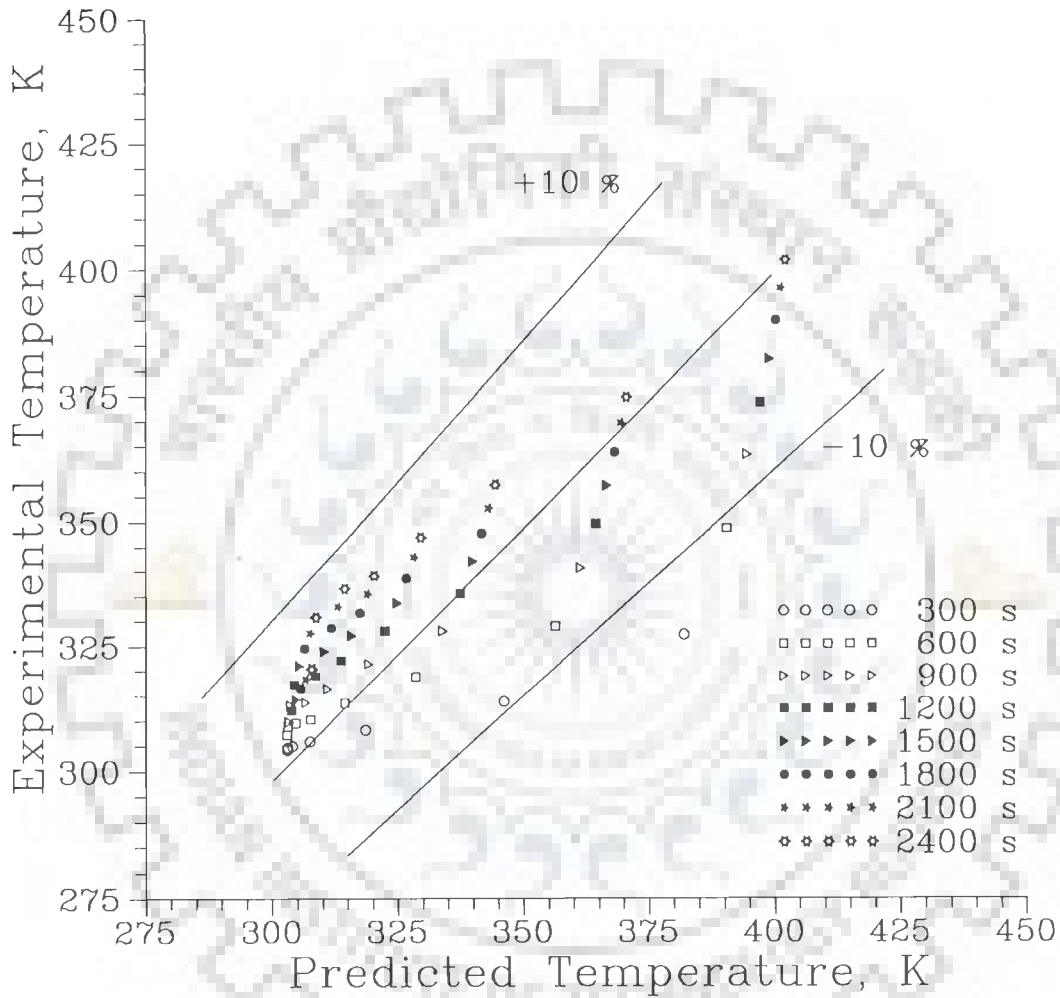


Figure 5.4-1 Comparison of Experimental and Predicted Temperatures at Different Times for  $Q_L = 0.1 \text{ kW/m}$  using  $k(T)$  Relationship, i.e. equation (5.4-1)

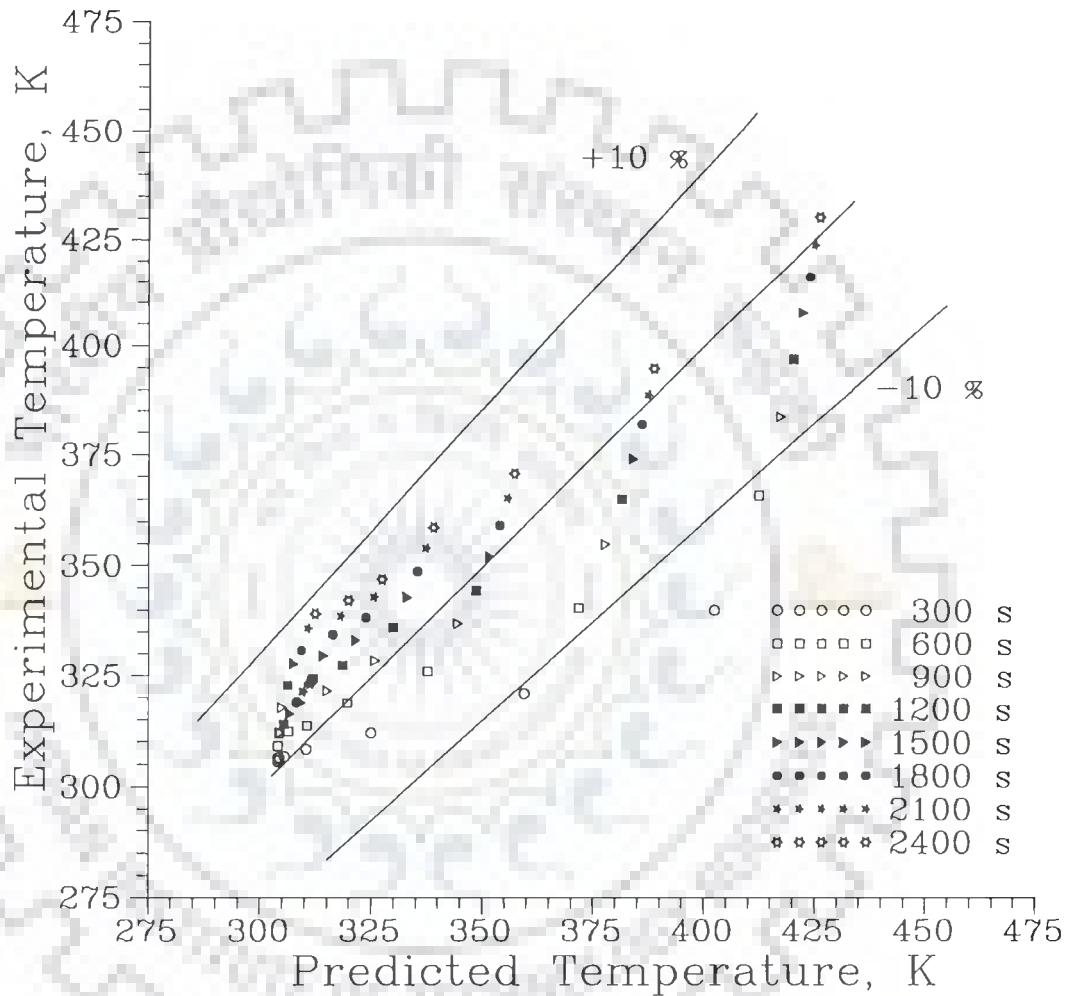


Figure 5.4-2 Comparison of Experimental and Predicted Temperatures at Different Times for  $Q_L = 0.13333 \text{ kW/m}$  using  $k(T)$  Relationship, i.e. equation (5.4-1)

Besides, the magnitude of the value of  $k$  computed in the present work is comparable to the value of effective thermal conductivity reported in the literature for molecular sieves [Kumar and Dissinger (1986)], catalytic and other materials (Tables 2.5-1, 2.5-2, and 2.5-3 ) [Satterfield (1980), Li and Finlayson (1977)].

Chemically, 13X molecular sieves are sodium aluminosilicate. Therefore, silica-alumina cracking catalyst, alumina (boehmite) pellets, pure silica, and porous silica-alumina pellets etc. have been selected for making comparison of estimated values of  $k$ . Thermal conductivity of these materials would naturally be less than that of pellets due to interparticle voidage. This supports the correctness of estimated values of  $k$  of the bed, i.e.  $0.82 \times 10^{-4}$  to  $2.072 \times 10^{-4}$  kW/m K.

#### 5.4.1 Average Effective Thermal Conductivity and Thermal Diffusivity

In order to study the extent of dependence of effective thermal conductivity on temperature, average effective thermal conductivity of the bed has also been computed for the range of experimentally observed temperatures. It has been calculated using following expression.

$$\bar{k} = \frac{\int_{T_o}^{T_f} k(T) dT}{(T_f - T_o)} \quad (5.4-2a)$$

or

$$\bar{k} = k_o - \beta T_o + \frac{\beta}{2} (T_f + T_o) \quad (5.4-2b)$$

Using  $\bar{k}$ , thermal diffusivity of the packed bed under study, is also calculated as given below.

$$\alpha = \frac{\bar{k}}{\rho_b C_p} \quad (5.4-3)$$

values of  $\bar{k}$  and  $\alpha$  calculated from these expressions in the temperature range 303-431 K are as follows :

$$\bar{k} = 1.444845 \times 10^{-4} \text{ kW/m K}$$

$$\alpha = 2.508411 \times 10^{-7} \text{ m}^2/\text{s}$$

Transient radial temperatures are predicted using average effective thermal conductivity. These values are plotted against experimentally observed temperatures and shown in Figures 5.4-3 and 5.4-4 for the two data sets.

In order to get clear picture, radial temperature profiles have also been prepared at different times by using equation (5.4-1) and  $\bar{k}$ . Percent deviation between experimental and predicted temperatures are also given in Tables A.1 to A.8 [Appendix-A] for all measurements for  $Q_L = 0.1 \text{ kW/m}$ . It may be observed from these Tables and Figures 5.4-5 to 5.4-12 that both the two predicted temperatures are higher than the experimental temperature at 2 and 3 locations near the heater surface upto a period of 900 s. As explained earlier, this effect is introduced due to the thermal inertia of the heater. Thereafter, experimental temperatures are quite close to either of the two predicted temperatures. So we may assume that from this instant onwards heater starts emitting heat at its full strength.

Furthermore, following observation is also made from these Figures and Tables.

Temperatures predicted by using equation (5.4-1) are more close to experimental ones in higher temperature range; experimental temperature is more than 320 K and when the heater is operating at its full strength. While predictions by using value of  $\bar{k}$  are nearer to experimental values in lower temperature range. However, the difference in two predicted temperatures is small and acceptable.

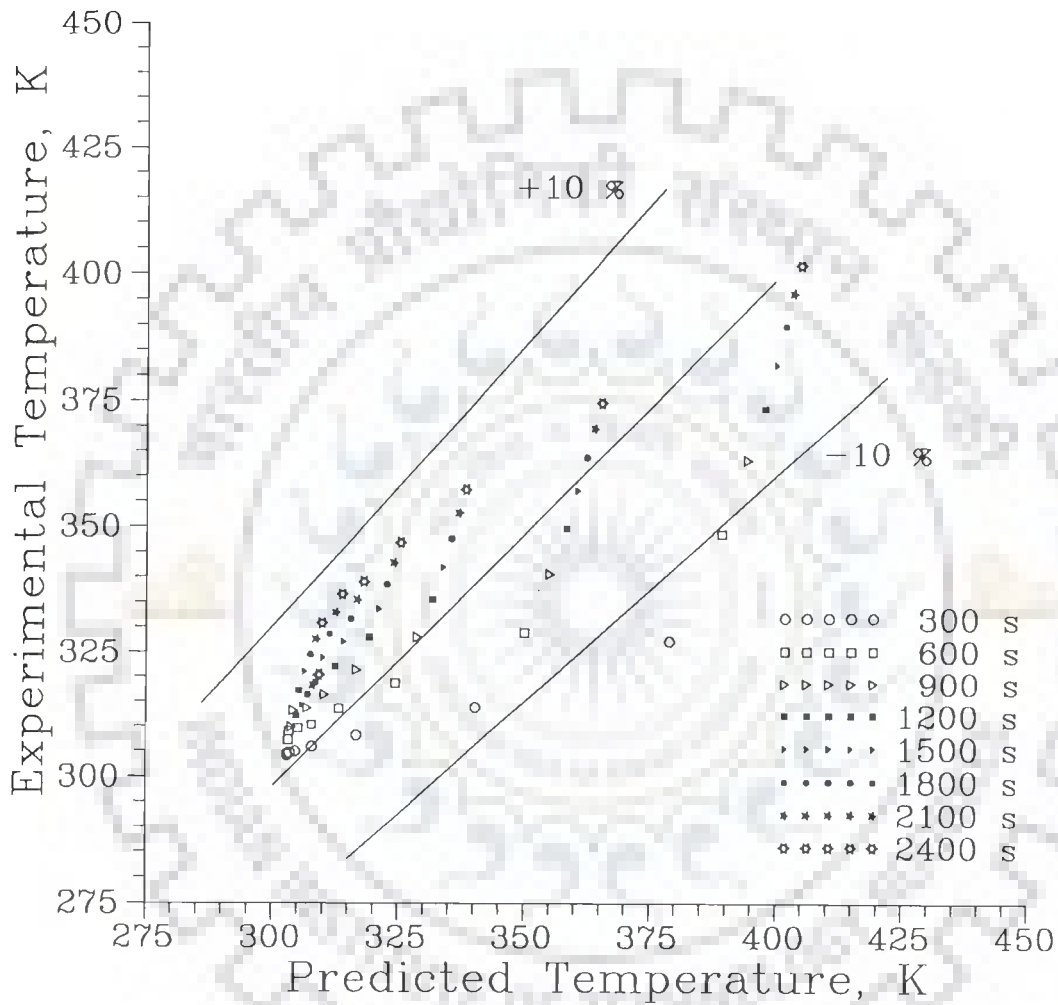


Figure 5.4-3 Comparison of Experimental and Predicted Temperatures at Different Times for  $Q_L = 0.1 \text{ kW/m}$  using Avg.  $k (1.444845 \times 10^{-4} \text{ kW/m K})$

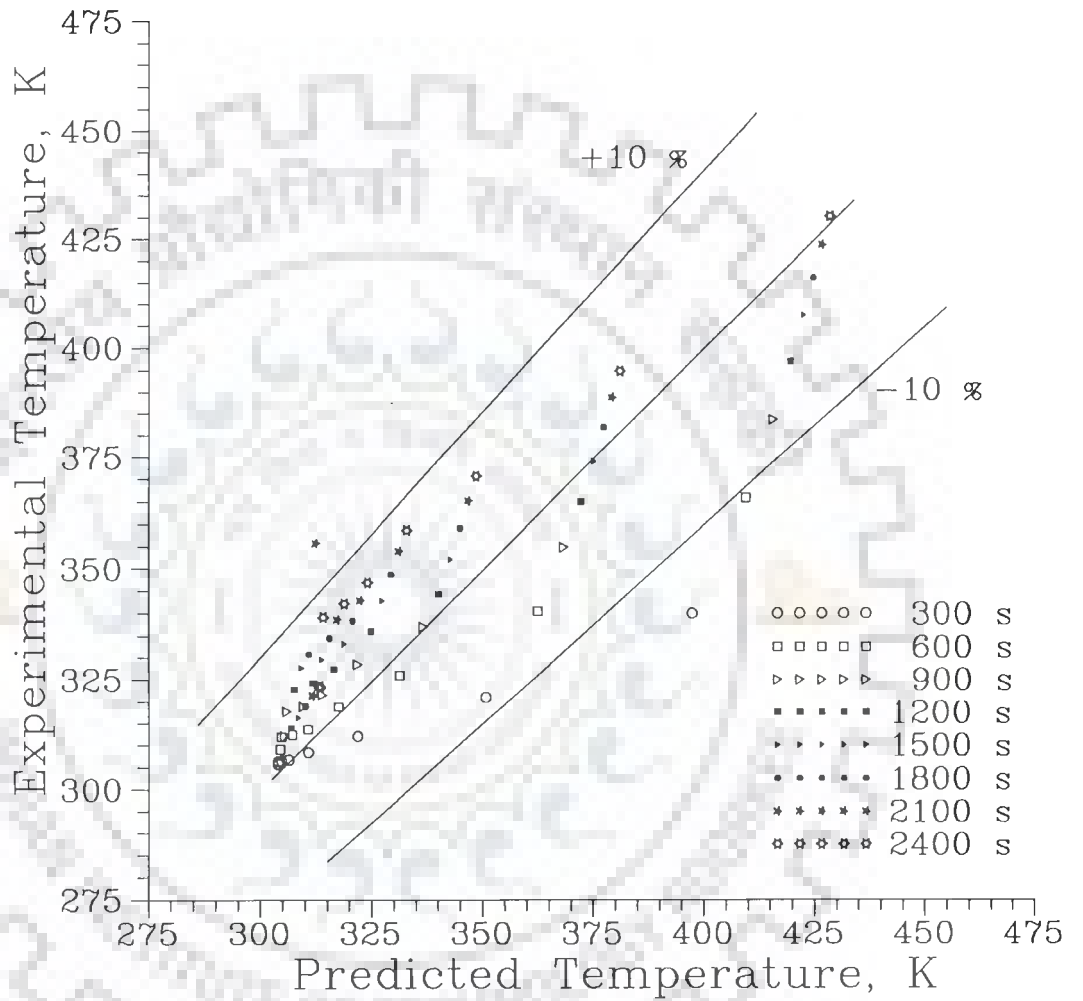


Figure 5.4-4 Comparison of Experimental and Predicted Temperatures at Different Times for  $Q_L = 0.13333$  kW/m using Avg.  $k (1.444845 \times 10^{-4}$  kW/m K)



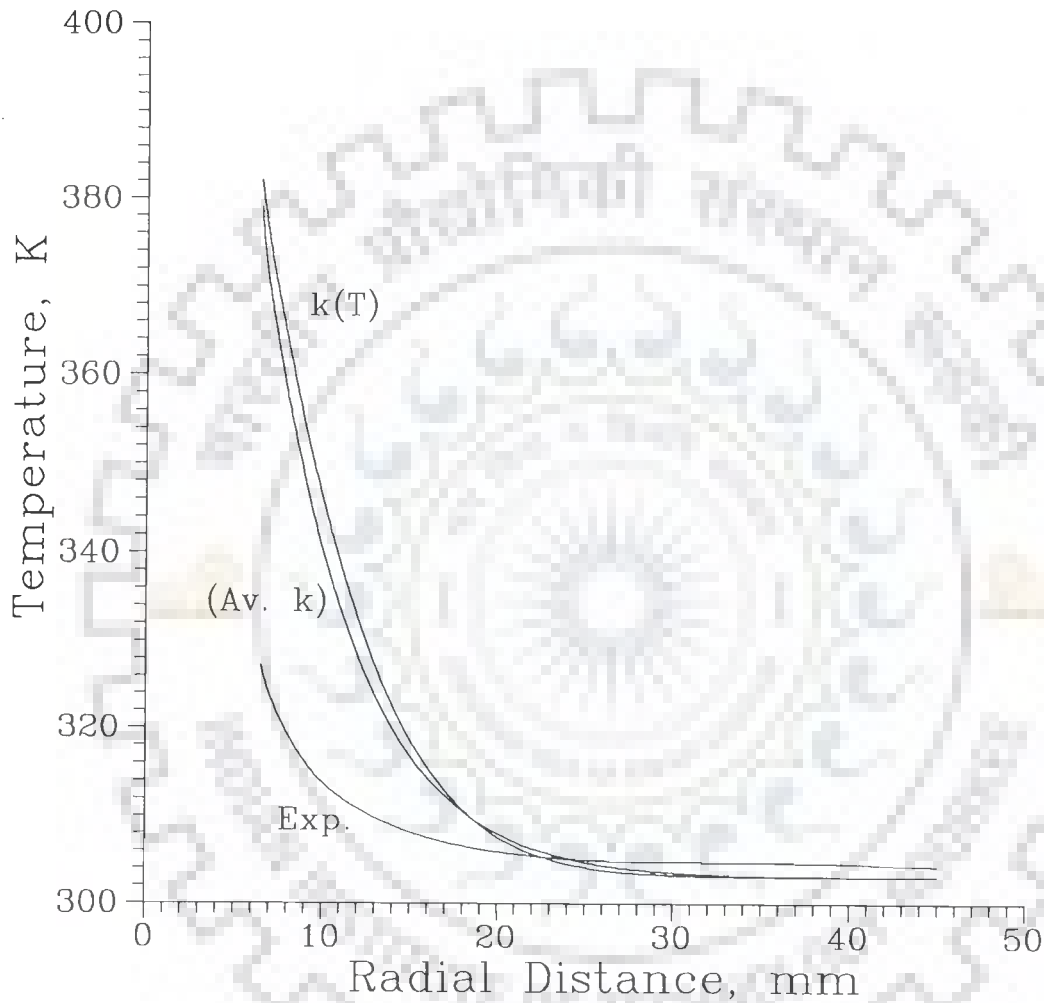


Figure 5.4-5 Comparison of Predicted Radial Temperature Profiles using  $k(T)$ , i.e. equation (5.4-1) and Avg.  $k$  ( $1.444845 \times 10^{-4}$  kW/m K) with Experimental Values at Time = 300 s for  $Q_L = 0.1$  kW/m

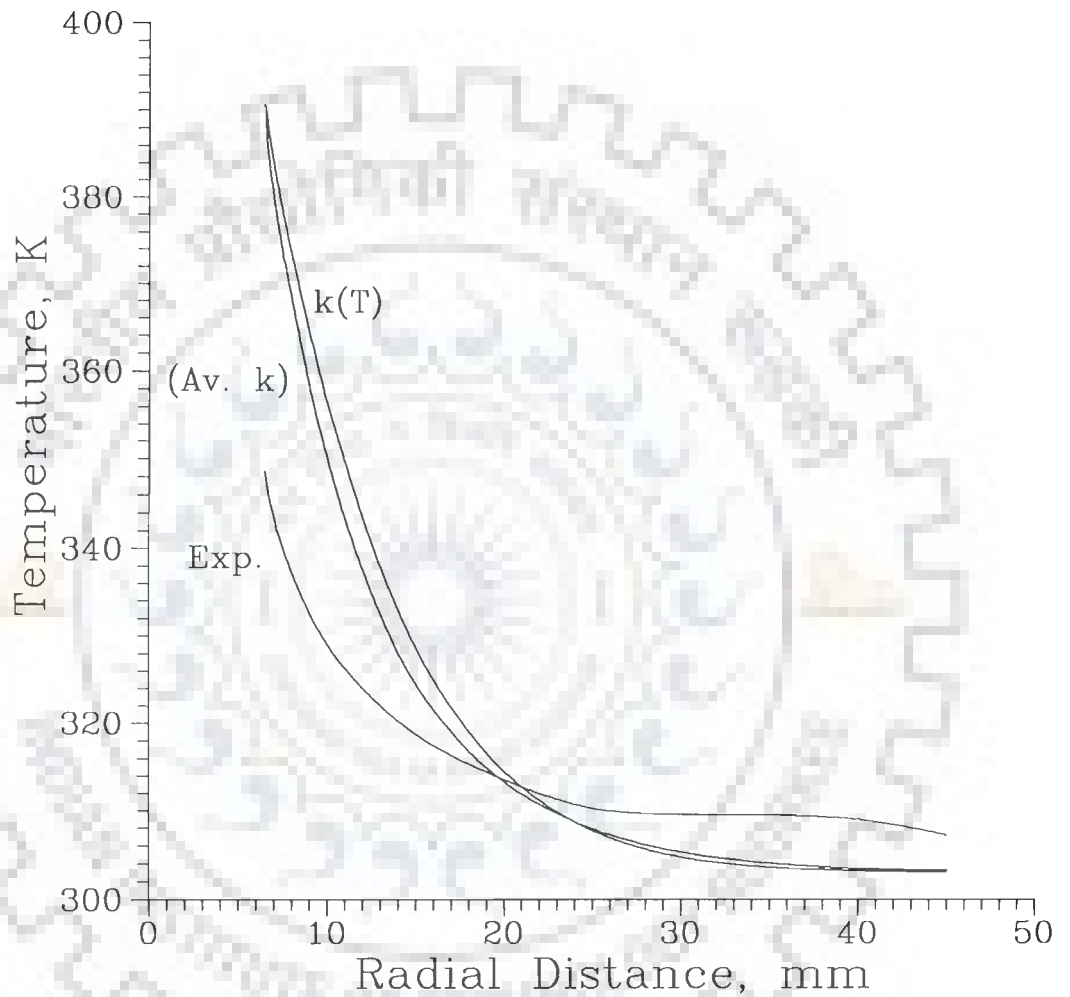


Figure 5.4-6 Comparison of Predicted Radial Temperature Profiles using  $k(T)$ , i.e. equation (5.4-1) and Avg.  $k$  ( $1.444845 \times 10^{-4}$  kW/m K) with Experimental Values at Time = 600 s for  $Q_L = 0.1$  kW/m

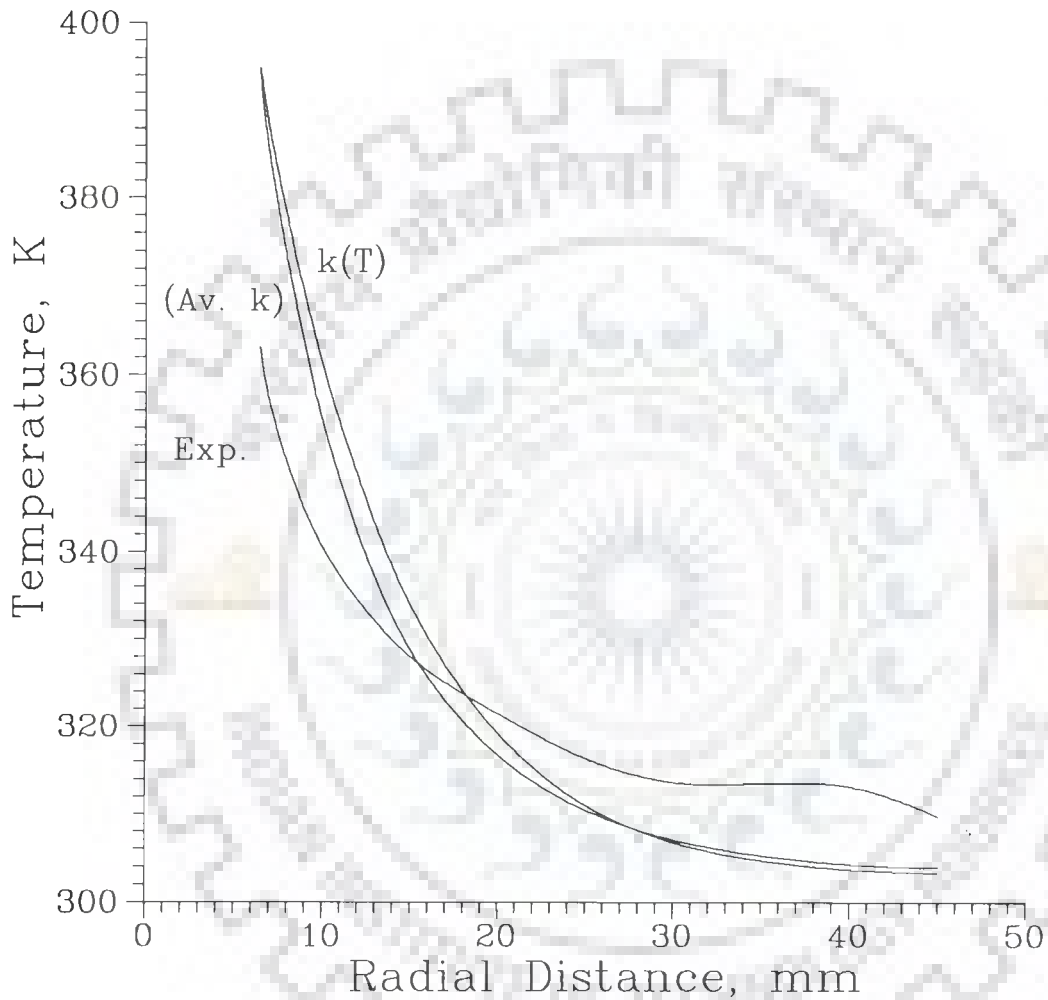


Figure 5.4-7 Comparison of Predicted Radial Temperature Profiles using  $k(T)$ , i.e. equation (5.4-1) and Avg.  $k$  ( $1.444845 \times 10^{-4}$  kW/m K) with Experimental Values at Time = 900 s for  $Q_L = 0.1$  kW/m

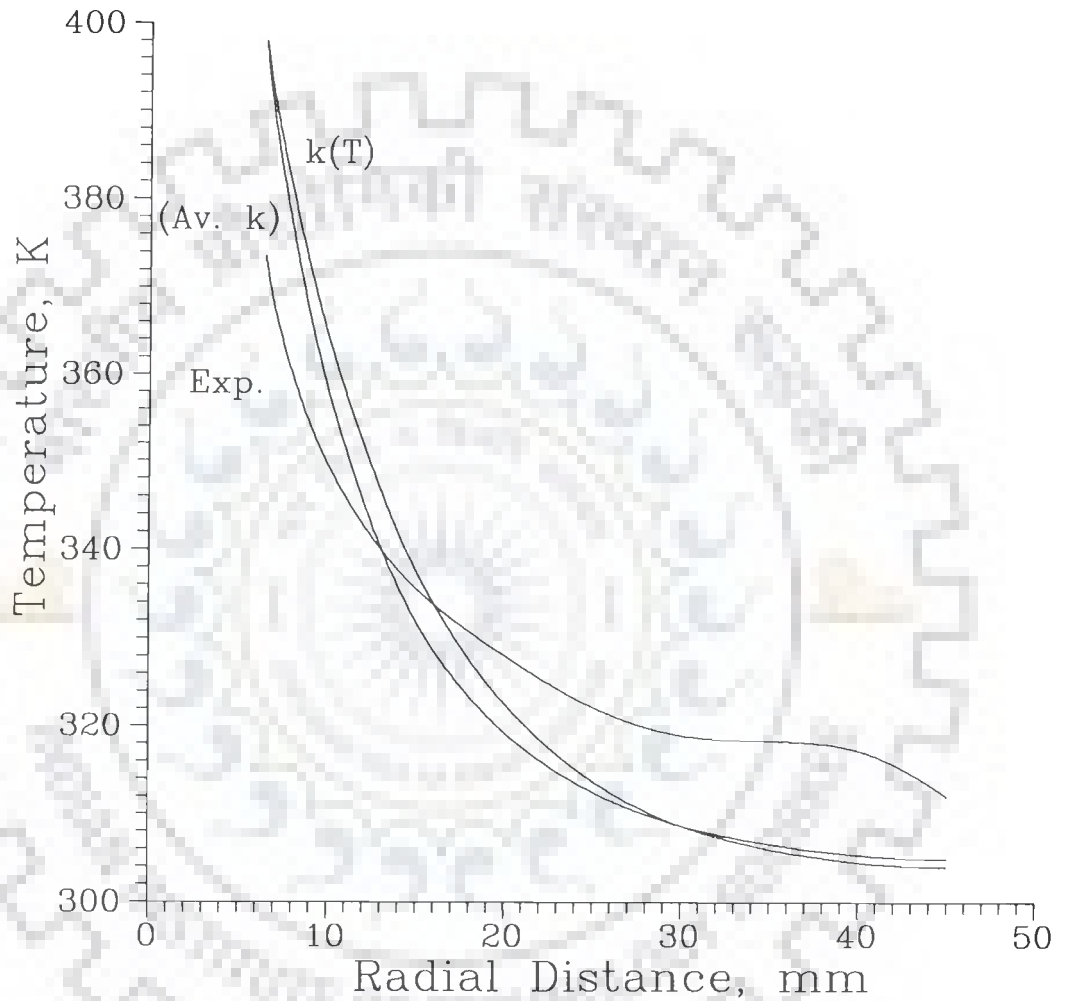


Figure 5.4-8 Comparison of Predicted Radial Temperature Profiles using  $k(T)$ , i.e. equation (5.4-1) and Avg.  $k$  ( $1.444845 \times 10^{-4}$  kW/m K) with Experimental Values at Time = 1200 s for  $Q_L = 0.1$  kW/m

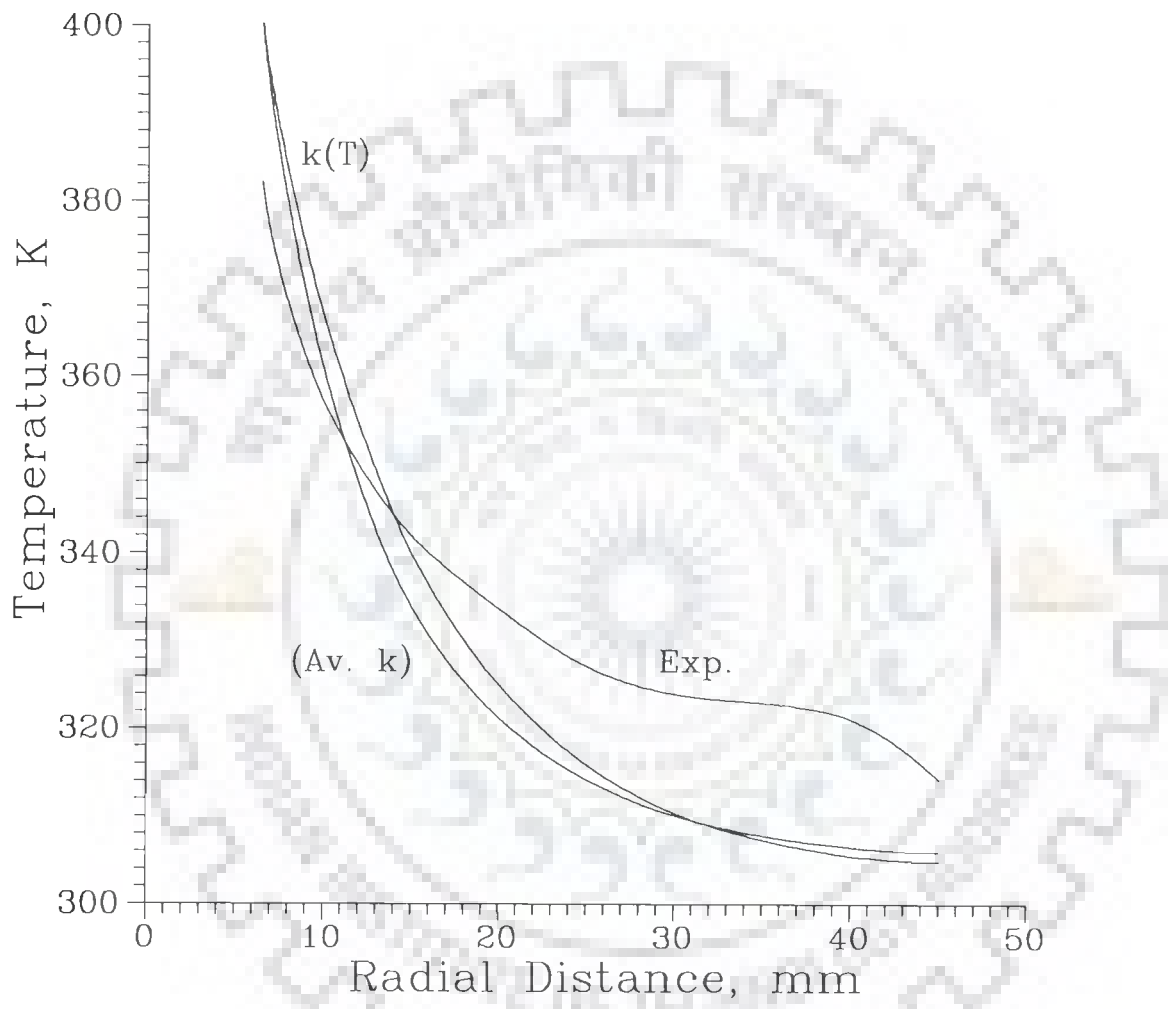


Figure 5.4-9 Comparison of Predicted Radial Temperature Profiles using  $k(T)$ , i.e. equation (5.4-1) and Avg.  $k$  ( $1.444845 \times 10^{-4}$  kW/m K) with Experimental Values at Time = 1500 s for  $Q_L = 0.1$  kW/m

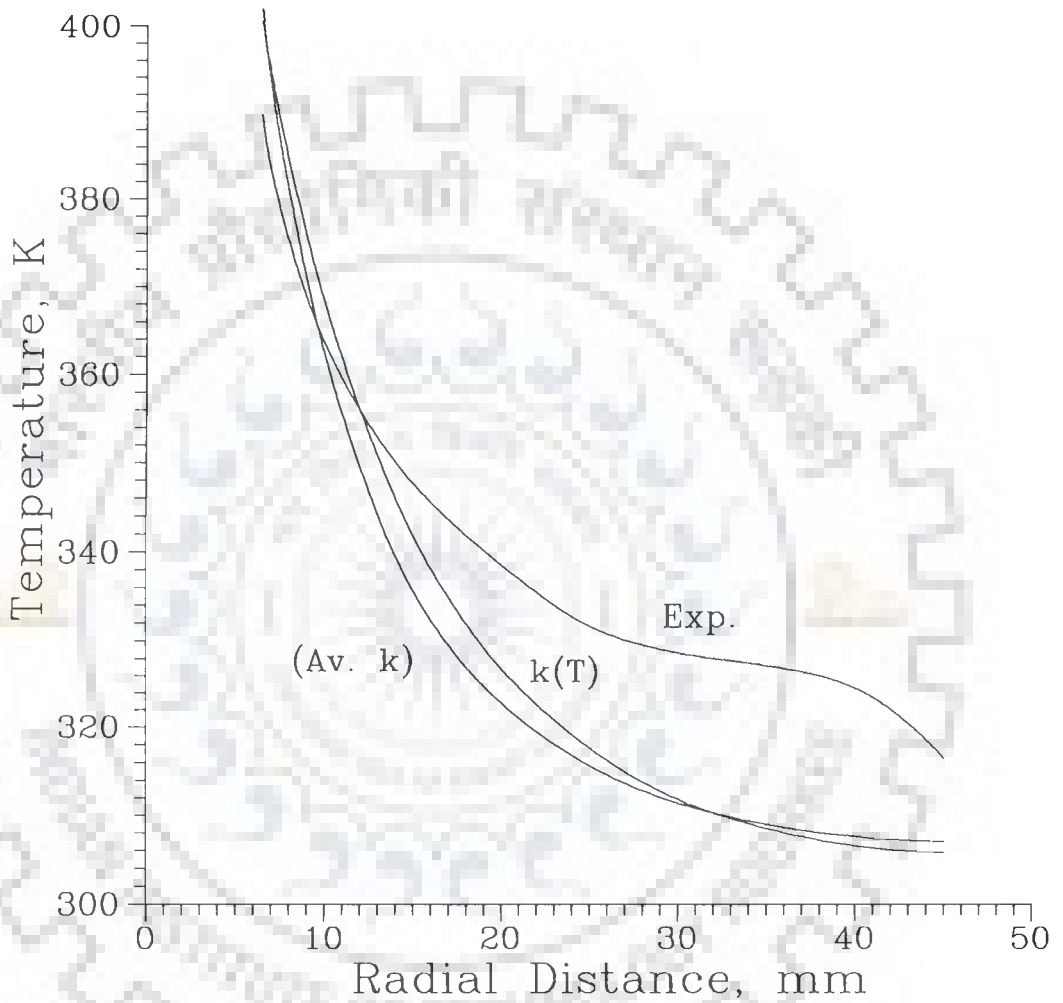


Figure 5.4-10 Comparison of Predicted Radial Temperature Profiles using  $k(T)$ , i.e. equation (5.4-1) and Avg.  $k$  ( $1.444845 \times 10^{-4}$  kW/m K) with Experimental Values at Time = 1800 s for  $Q_L = 0.1$  kW/m

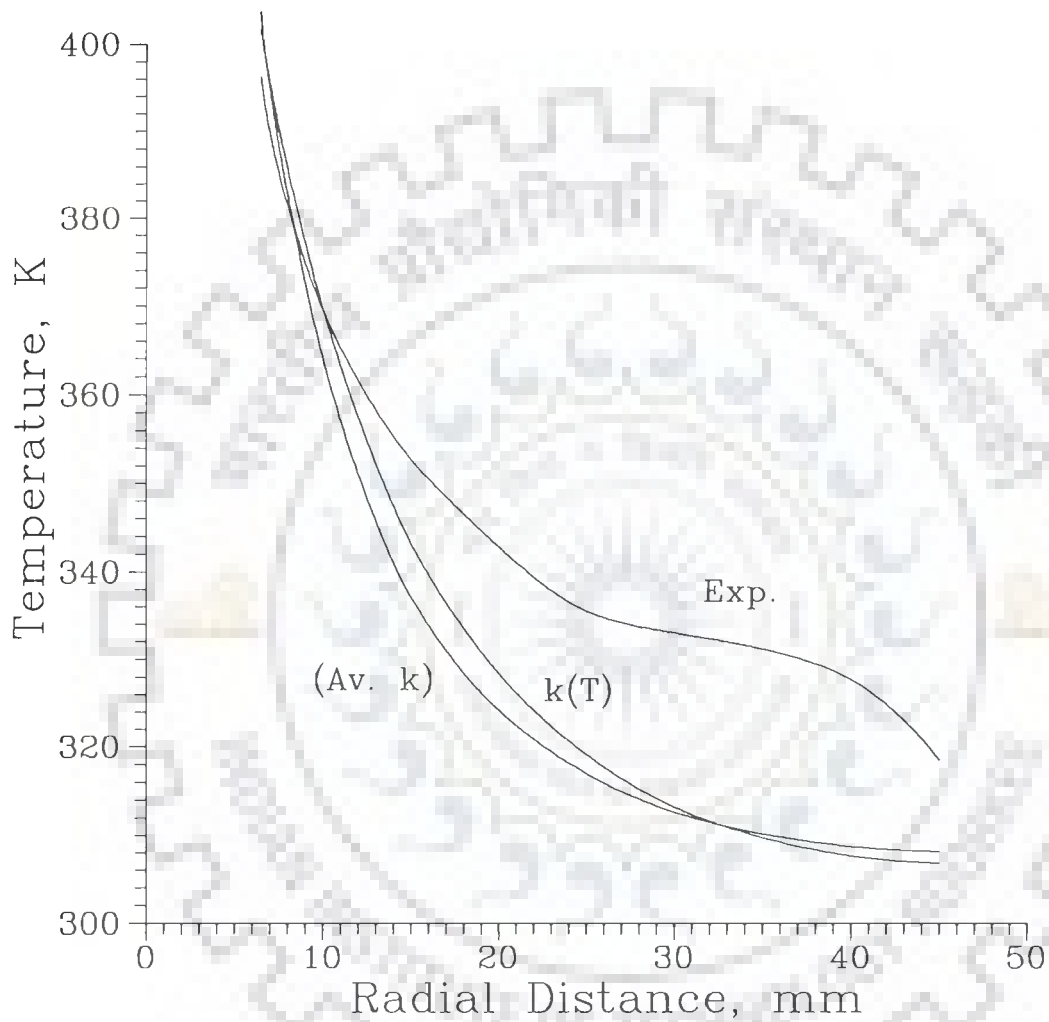


Figure 5.4-11 Comparison of Predicted Radial Temperature Profiles using  $k(T)$ , i.e. equation (5.4-1) and Avg.  $k$  ( $1.444845 \times 10^{-4}$  kW/m K) with Experimental Values at Time = 2100 s for  $Q_L = 0.1$  kW/m

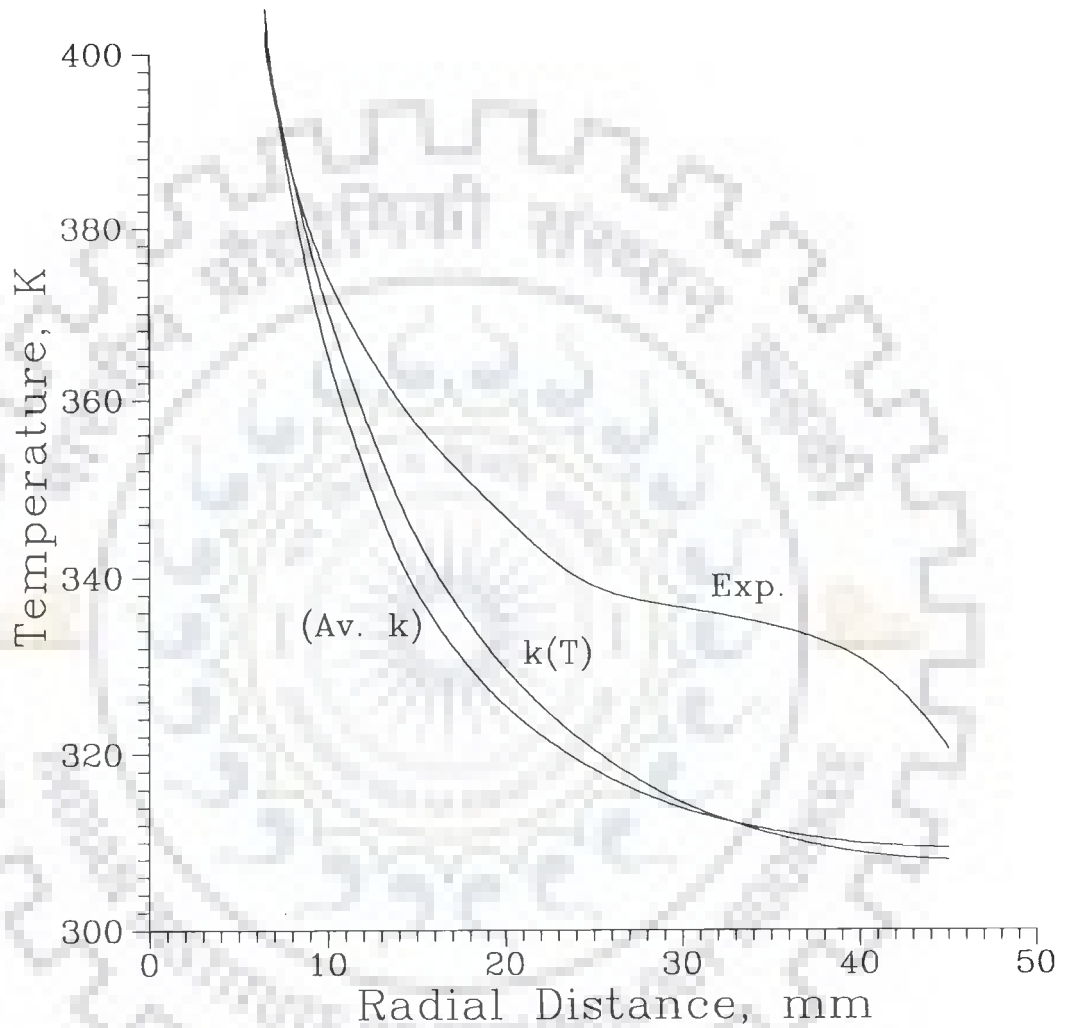


Figure 5.4-12 Comparison of Predicted Radial Temperature Profiles using  $k(T)$ , i.e. equation (5.4-1) and Avg.  $k$  ( $1.444845 \times 10^{-4}$  kW/m K) with Experimental Values at Time = 2400 s for  $Q_L = 0.1$  kW/m



The above observation may be attributed to the fact that  $\bar{k}$  has been obtained by using equation (5.4-1). Obviously, it would underestimate  $k$  in higher temperature range and overestimate  $k$  in lower temperature range.

#### 5.4.2 Improved Correlation for $k$

It has been observed that the thermal inertia of heater affects the radial temperatures appreciably during the initial period of heating the bed. Therefore, it was decided to eliminate this effect from the predictions of  $k_0$  and  $\beta$ . In order to achieve it, experimental data for the period from 1200 to 2400 s were used for the estimation. Initial temperature profile in the bed, required for the solution of model equation was obtained by using experimentally measured temperatures at 1200 s. And values of temperature at intermediate grid points were computed with the help of Lagrange's interpolation formula [Mathews (1994)]. Correlation of  $k$  with the estimated values is given below.

$$k = 8.17635 \times 10^{-5} + 10.915427 \times 10^{-7} (T - T_0) \quad (5.4-4)$$

Values of  $k_0$  and  $\beta$ , estimated now, are higher than the previous ones [equation (5.4-1)]. Consequently, the values of  $\bar{k}$  and  $\alpha$  are also on higher side [ $\bar{k} = 1.516222 \times 10^{-4}$  kW/m K,  $\alpha = 2.63233 \times 10^{-7}$  m<sup>2</sup>/s] for the temperature range of 303-431 K. Values of  $\bar{k}$  and  $\alpha$  computed here are in agreement with the values reported in the literature [Kumar and Dissinger (1986), Prasad (1988)].

Use of improved correlation [equation (5.4-4)] predicts temperatures which are free from the effect of heater inertia. The temperatures predicted from this relationship for the entire period of the experimental data are within acceptable variation. However, the two points which are in immediate vicinity of heater surface, were showing slightly larger variation earlier in Figures 5.4-3 and 5.4-4. This proves that the effect of inertia of heater material was there.

Figures 5.4-13 and 5.4-14 show the comparison of temperatures obtained experimentally, and predicted by using equation (5.4-4). It is clear that all the data points lie within  $\pm 5$  percent error. So the correlation for  $k$  [equation (5.4-4)] is better than the earlier one and should be used in modelling and simulation.

Besides, transient radial profiles have been computed by solving the model equation with equation (5.4-4) for 4 hours as shown in Figures 5.4-15 and 5.4-16. These profiles show that a packed bed of molecular sieves with poor thermal conductivity can be heated uniformly in a reasonable period of two hour by more than  $100^\circ\text{C}$  using an imbedded heater of moderate wattage.

### 5.4.3 Statistical Analysis

In estimation problems it is always desirable to carry out statistical analysis of the estimated parameters. Therefore, it was decided to obtain the joint confidence contour for an approximate 95% confidence level, though its computation is a time consuming process as also observed by other workers [Lerou and Froment (1978)]. The joint confidence contour encloses the values of  $k_o$  and  $\beta$ . Contour is given by the following formula [Draper and Smith (1966), Himmelblau (1970)] :

$$\Phi_{1-\alpha} = \Phi_{\min} \left[ 1 + \frac{m}{n-m} F_{1-\alpha} (m, n - m) \right] \quad (5.4-5)$$

where  $\Phi_{\min}$  is the minimum sum of square of residuals and  $F_{1-\alpha} (m, n-m)$  is the  $(1-\alpha)$  point of the F distribution with  $m$  and  $n$  degrees of freedom,  $\alpha$  being the level of significance. For a two parameter linear model the contour is an ellipse. While for a nonlinear model a banana shape curve is more likely but in such a case confidence level is approximate because parameter distribution is not known.

Using equation (5.4-5), joint confidence contour for an approximate 95% confidence level has been drawn, which has been shown in Figure 5.4-17a. An enlarged portion of curve is also depicted in

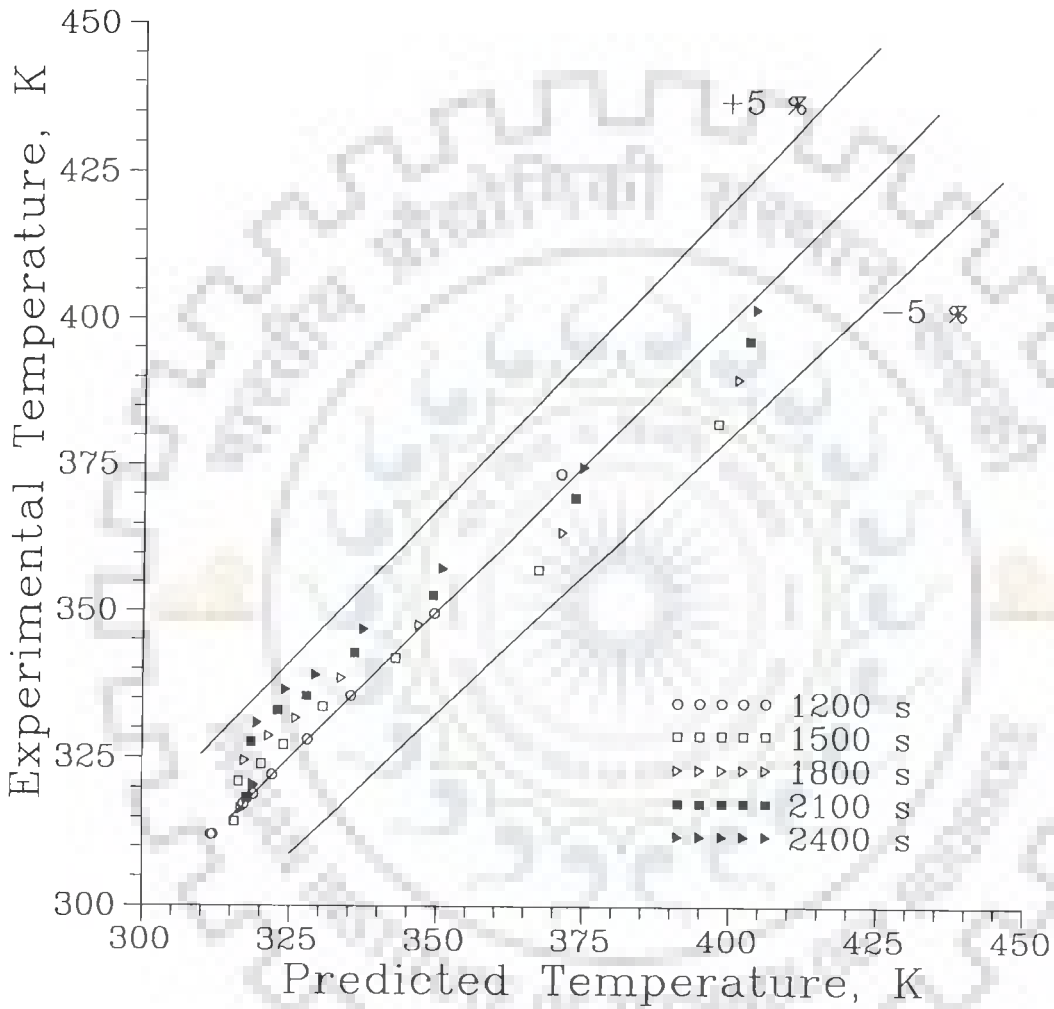


Figure 5.4-13 Comparison of Experimental and Predicted Temperatures at Different Times for  $Q_L = 0.1 \text{ kW/m}$  using Improved  $k(T)$  Relationship, i.e. equation (5.4-4)

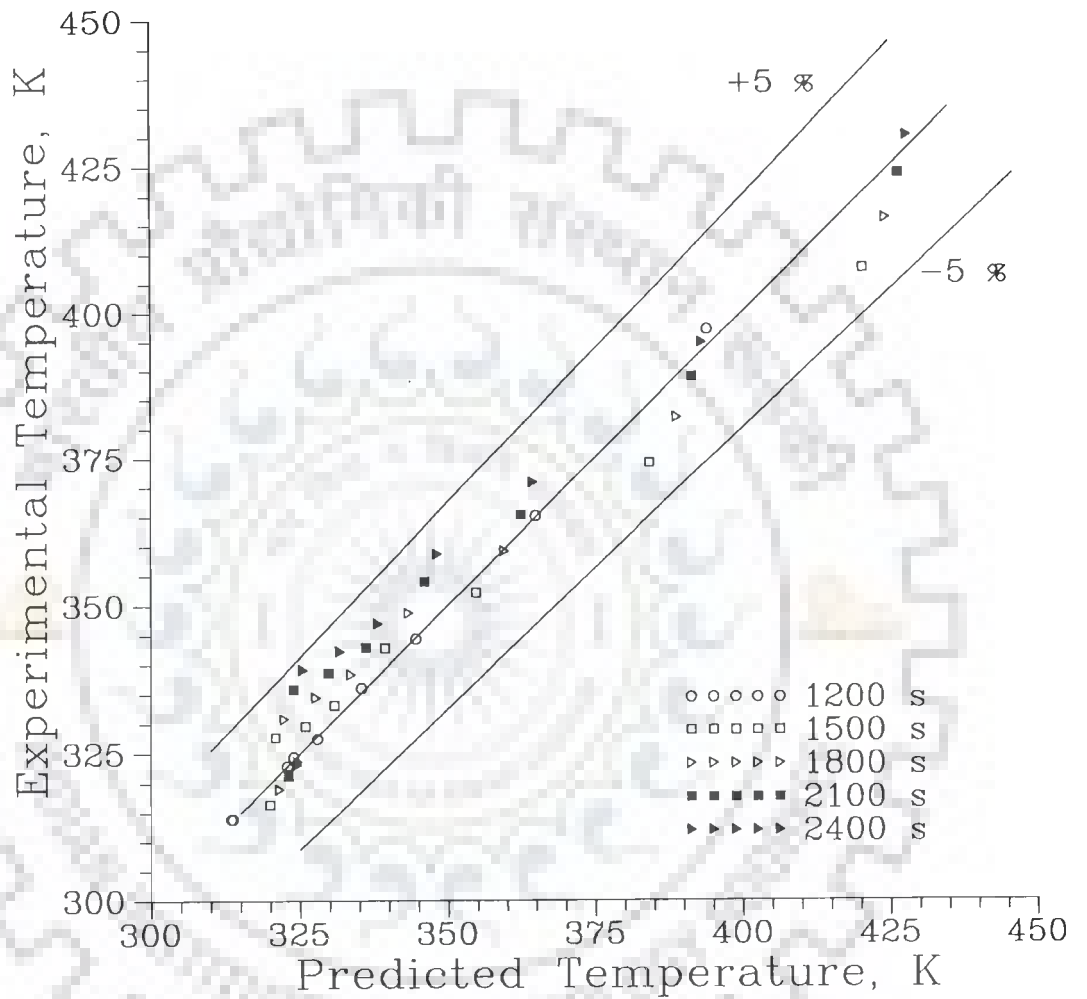


Figure 5.4-14 Comparison of Experimental and Predicted Temperatures at Different Times for  $Q_L = 0.13333 \text{ kW/m}$  using Improved  $k(T)$  Relationship, i.e. equation (5.4-4)

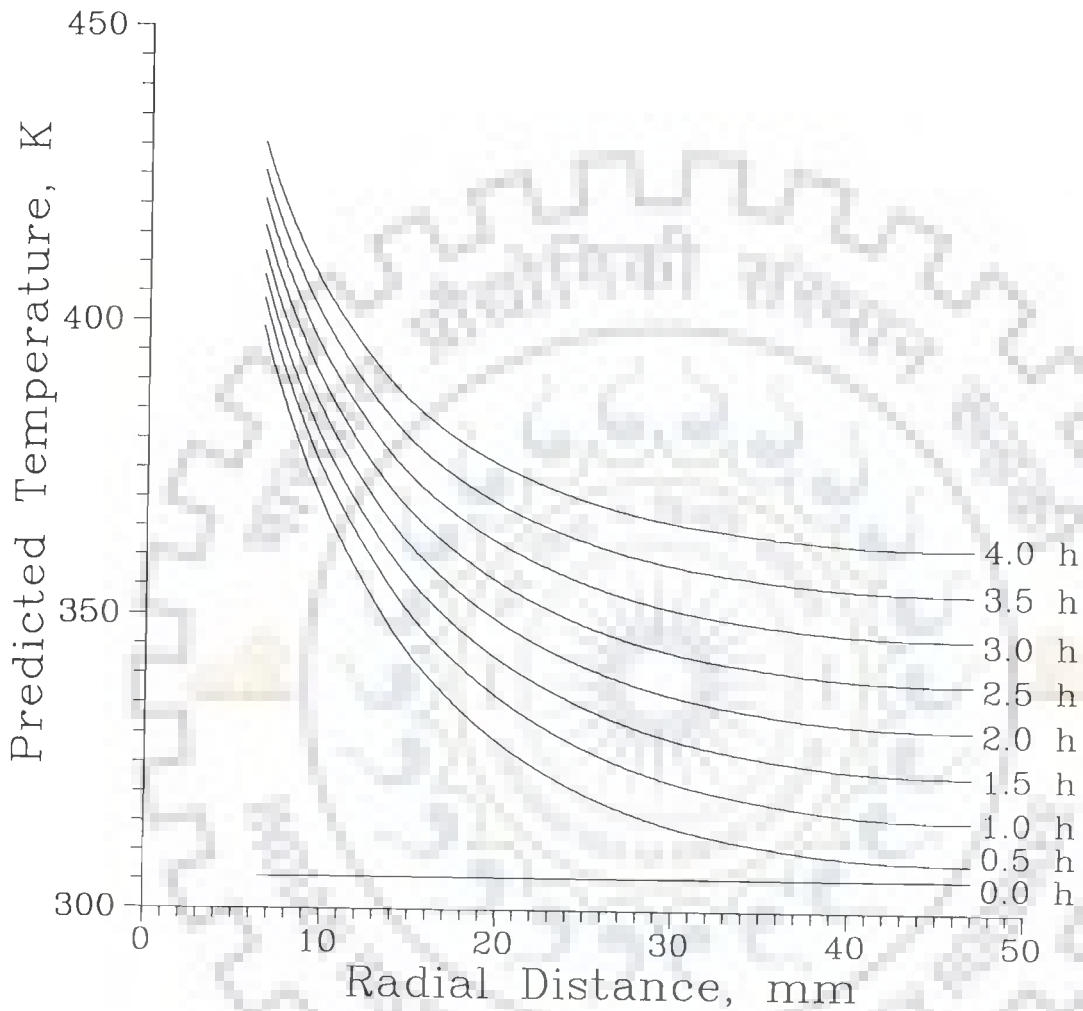


Figure 5.4-15 Transient Radial Temperature Profiles for 4 h for  $Q_L = 0.1 \text{ kW/m}$  using Improved  $k(T)$  Relationship, i.e. equation (5.4-4)

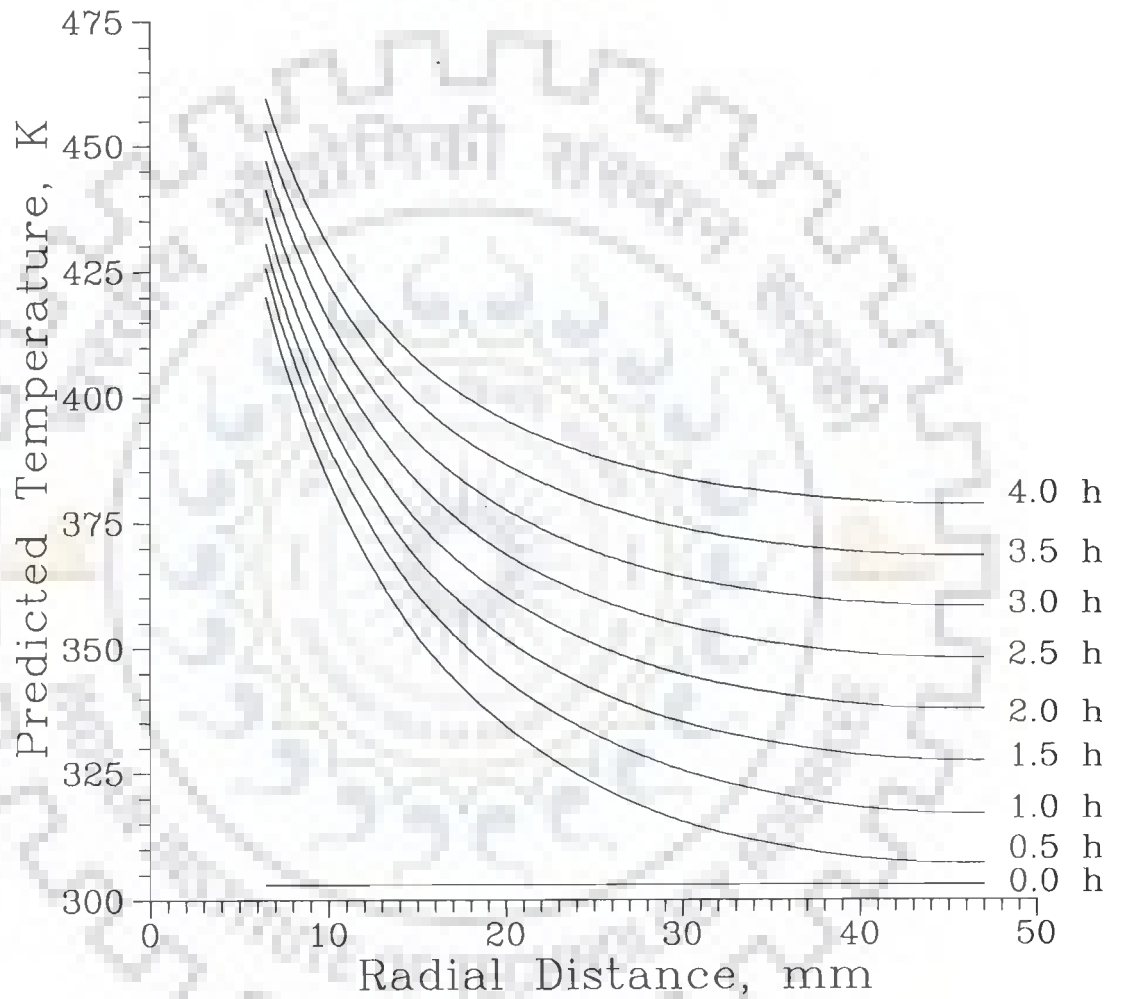


Figure 5.4-16 Transient Radial Temperature Profiles for 4 h for  $Q_L = 0.13333 \text{ kW/m}$  using Improved  $k(T)$  Relationship, i.e. equation (5.4-4)

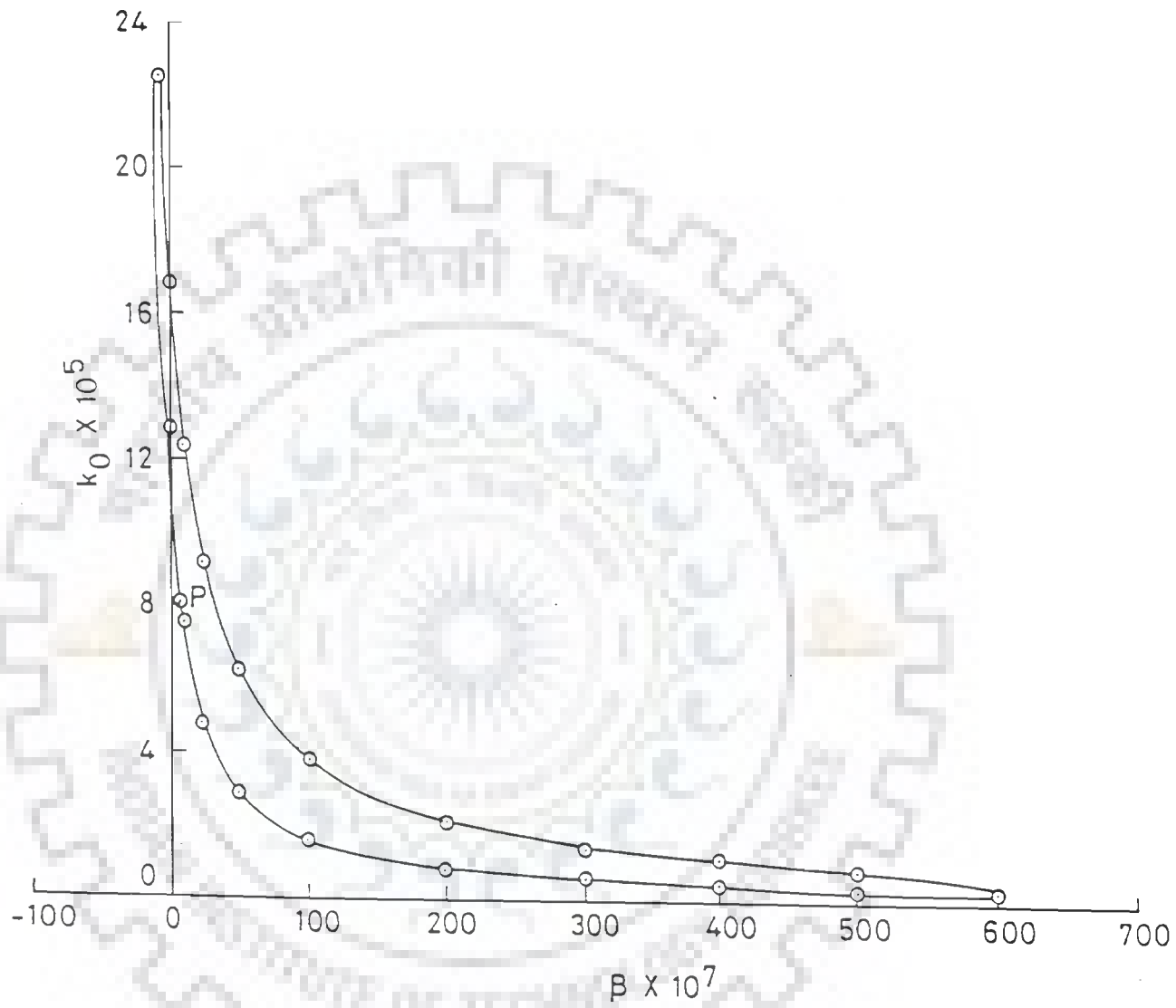


Figure 5.4-17a Contour for 95% Joint Confidence Region

Figure 5.4-17b. This clearly shows point P and excursion of curve to negative side of x-axis. Figure 5.4-17a shows a deflated banana shape curve in parameter space for joint confidence contour. This is understandable because the solution of model equation with linear dependence of  $k$  on  $T$  yields nonlinear equation in parameters  $k_0$  and  $\beta$ . Further, the figure indicates that both the parameters  $k_0$  and  $\beta$  are highly correlated. A small portion of the joint confidence region extends towards the negative side of x-axis. This corresponds to negative values of  $\beta$  and quite high values of  $k_0$ . This indicates that the higher values of  $k_0$  is reduced by the value of term containing  $\beta$  so that the effective thermal conductivity remains in its correct range. It is also noted that the point P of estimated values of the parameters lies within the confidence region [Figure 5.4-17b].

## 5.5 CONCLUDING REMARKS

In the present chapter dependency of effective thermal conductivity of a bed of 13X molecular sieves on temperature has been estimated by using transient radial temperature profiles.  $k$  has been assumed to vary linearly with  $T$ . Statistical analysis of estimated parameters has also been carried out, which ascertains the correctness of estimated model for an approximate 95% confidence level. Further, values of average effective thermal conductivity ( $\bar{k}$ ) and thermal diffusivity ( $\alpha$ ) of the bed have also been calculated by using the proposed relationship [equation (5.4-4)]. The computed values of  $\bar{k}$  and  $\bar{\alpha}$  are comparable to those reported in literature.

The important conclusion which may be drawn from the above study is that the effective thermal conductivity of bed of molecular sieves depends upon temperature. And this dependency should be properly accounted in numerical modelling and simulation studies.

During estimation, temperatures are to be predicted by solving the model equation numerically. A computational algorithm has



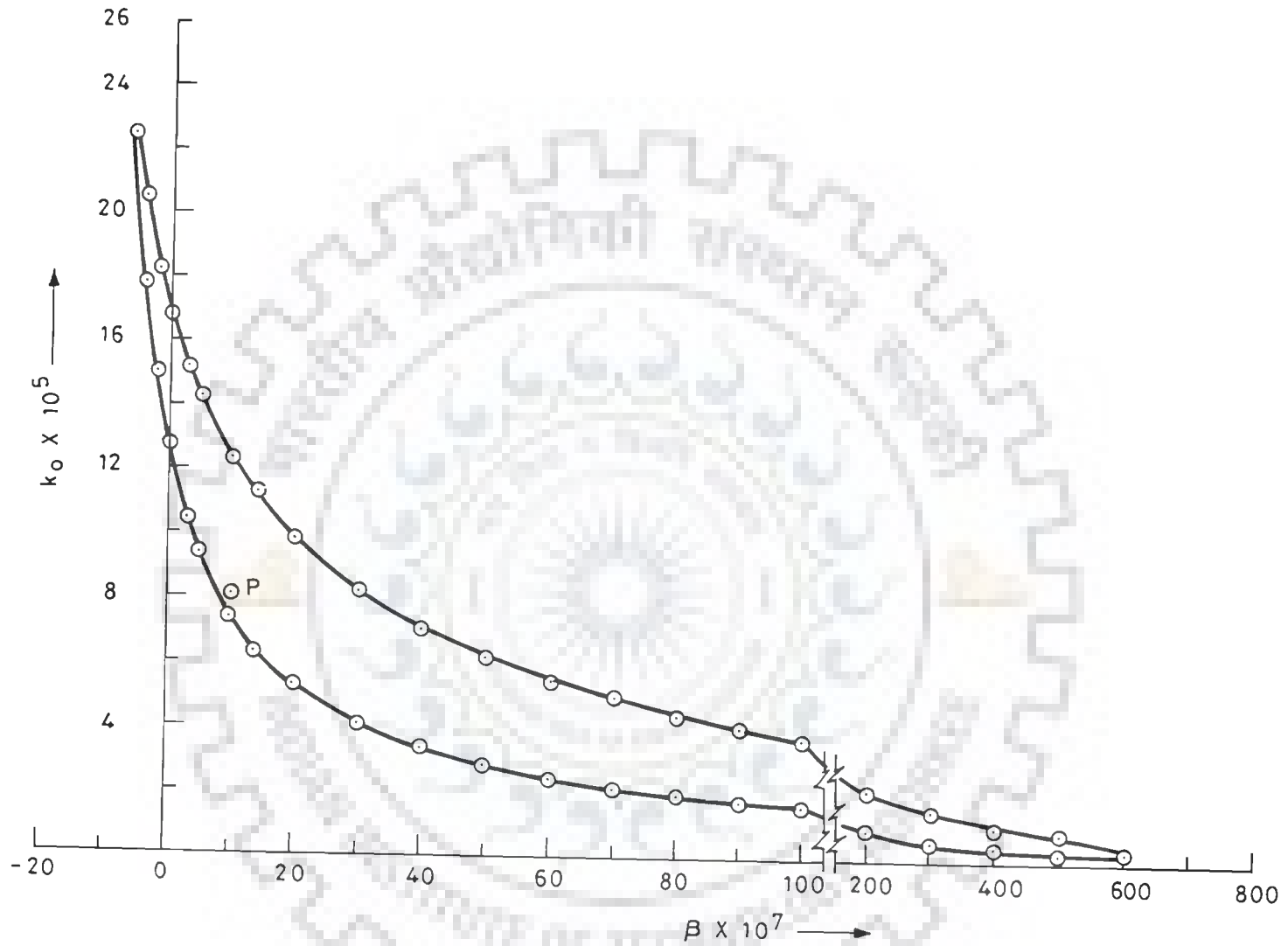


Figure 5-4-17b Enlarged Portion of Contour for 95% Joint Confidence Region Enclosing Point P.

been developed for solving the model equation, which utilizes the control volume finite difference method. This algorithm is applicable to linear as well as nonlinear dependence of  $k$  on temperature.



---

## MATHEMATICAL MODELLING OF THERMAL DESORPTION PROCESS

---

### 6.0 INTRODUCTION

The use of packed bed of molecular sieves for separating and purifying gas mixtures is a growing unit operation in the chemical and other process industries. Design of such separation units is not generally universal due to the complex nature of the adsorption - desorption processes. Suitable mathematical models are needed to design these units, and also to simulate their performance.

The present chapter is devoted to the development of a mathematical model for the modified thermal desorption process - an important step in the adsorption - desorption operations. As stated earlier, this desorption process utilizes the electrical heater(s) imbedded in the bed, to desorb the adsorbate. Developed model equations have been solved numerically; for this purpose control volume finite difference method has been employed. The model predictions have also been validated with available experimental results, obtained on a bed of 13X molecular sieves.

### 6.1 DEVELOPMENT OF MATHEMATICAL MODEL

Adsorber/desorber unit is considered to be a packed bed of molecular sieves. In the modified thermal desorption process, energy required for the desorption of adsorbate is provided by an electrical heater, which is fitted coaxially into the bed. Whereas in conventional thermal swing process, hot carrier gas is used for desorption. In the proposed desorption process, bed of molecular sieves is thus heated through the conduction of heat, emitted by the heater. During

desorption, heat is consumed and the adsorbate diffuses out of the micro- and macro-pores of molecular sieves pellet, to constitute the effluent of unit.

As is evident from the above description, the rate controlling steps in this desorption are as follows :

- Conduction of heat through packed bed of MS pellets
- Diffusion of adsorbate through the MS pellet

In earlier studies in our laboratory [Prasad (1988)], desorption was assumed to be purely conduction controlled, but the model predictions were not at all close to the experimental observations. For example, Figure 6.1-1 depicts percent recovery of adsorbate vs. time for a typical experimental run and also by the computations using the model. It is obvious from the figure that the time required for 89% desorption calculated by the model is 1 1/2 hour, while experimental run takes about 9 hours. This comparison indicates that the diffusion of adsorbate through the MS pellet should not be neglected in a realistic model of the process. In the present research work, efforts have been made to develop a mathematical model for this process which would include effect of both the rate controlling steps. For numerical solution of model and its validation, water vapour - 13X MS is taken as adsorbate - adsorbent system.

### 6.1.1 Model Equations

In view of the discussion in preceding section, model equations would naturally comprise conservation equations for both the packed bed and MS pellet. Therefore, each one of them is considered separately.

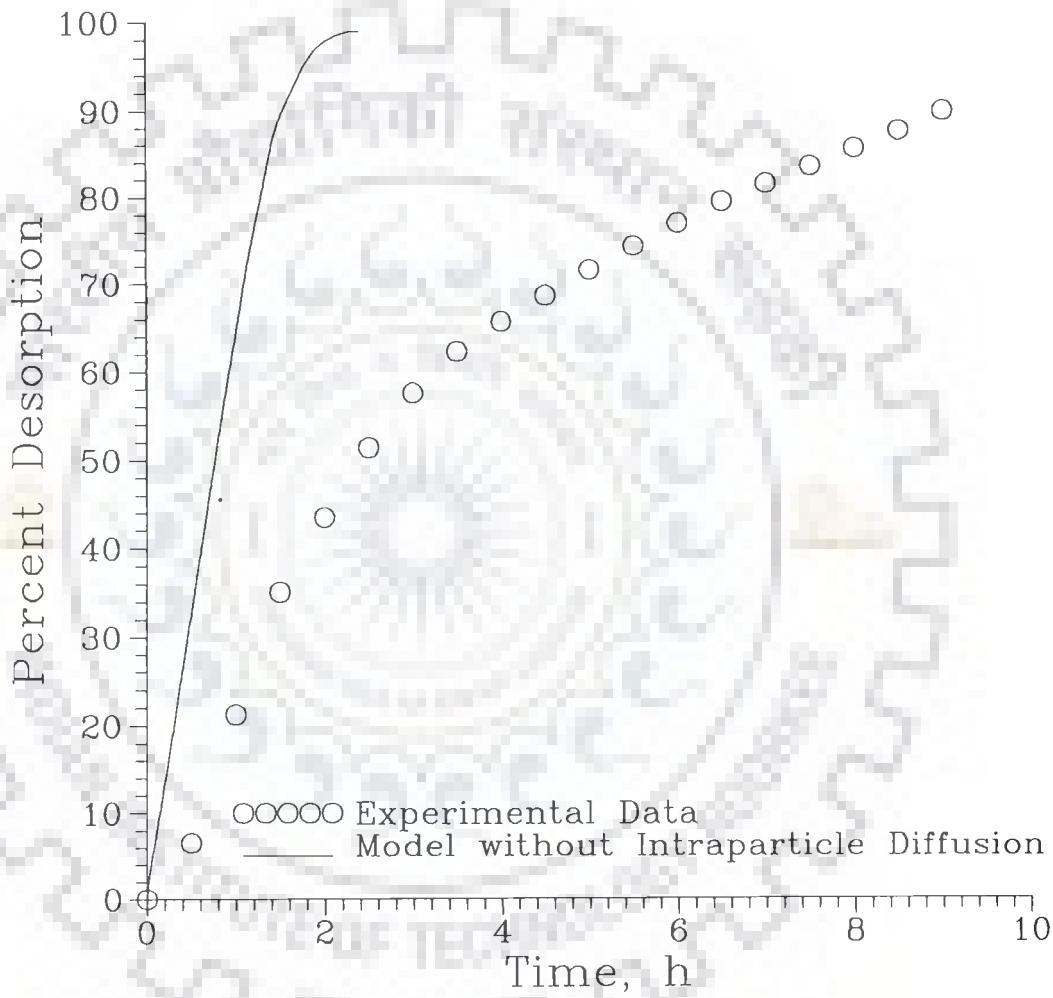


Figure 6.1-1 Comparison of Predicted Percent Desorption vs. Time using Model without Intraparticle Diffusion with Experiment-A

### 6.1.1.1 Packed Bed

Consider a packed bed of molecular sieves as shown in Figure 5.2-1. An electrical heater is imbedded into the bed coaxially. Outer wall of the cylinder containing MS pellets, as well as both the ends of bed are provided with proper and adequate thermal insulation. Besides, following assumptions have been made in deriving the model equations.

#### *Assumptions*

- (i) There is no axial temperature gradient in the bed.  
During dry bed conduction studies [Chapter IV], temperatures measured at two axial locations but at the same radial distance are found to be equal. Also the length of the bed may justifiably be considered to be infinite. Accordingly, it may be assumed that the heat emitted by heater, conducts in radial direction only.
- (ii) There is no heat flux across the wall of the packed bed.
- (iii) Heater wattage per unit length is constant.
- (iv) Initially, packed bed is at a uniform temperature throughout; the desorption process is started only when the bed is fully saturated.
- (v) Thermal equilibrium between molecular sieves and adsorbate vapour always exists.
- (vi) Temperature of the MS pellets remains constant, i.e. decrease in its temperature during desorption over a small differential time step is negligibly small. Thus, isothermal conditions are always maintained within the pellet. This is because of the fact that the rate of diffusion of adsorbate out of pellet is much slower than the rate of conduction of heat in the bed. For example diffusivity of water vapour in 13X MS varies from

$1 \times 10^{-9}$  to  $1.5 \times 10^{-11}$   $\text{m}^2/\text{s}$  depending upon its concentration, while thermal diffusivity of a packed bed of 13X MS is  $2.63233 \times 10^{-7}$   $\text{m}^2/\text{s}$ .

- (vii) Heat of desorption is constant.
- (viii) Heat capacity of molecular sieves and water vapour remains constant during desorption.
- (ix) Thermal conductivity of MS with adsorbate, i.e. water, is considered to be equal to that of dry molecular sieves.
- (x) Effective thermal conductivity of the packed bed of molecular sieves varies linearly with temperature.
- (xi) Adsorbate vapour behaves as an ideal gas.
- (xii) Pressure in the packed bed is maintained constant during desorption. It may be kept equal to the partial pressure of adsorbate in feed mixture in order to avoid pressure swing desorption.

Based upon the above premises, model equation for the packed bed of MS pellets may be obtained by taking energy balance across an elemental volume. Therefore, we consider an elementary cylindrical shell of thickness  $\Delta r$ , located at a radial distance  $r$  from the axis of bed (Figure 5.2-1). Energy balance across this shell yields

$$\left[ \begin{array}{l} \text{rate of accumulation} \\ \text{of energy in the} \\ \text{shell} \end{array} \right] = \left[ \begin{array}{l} \text{rate of input} \\ \text{of energy into} \\ \text{the shell} \end{array} \right] - \left[ \begin{array}{l} \text{rate of energy} \\ \text{output from} \\ \text{the shell} \end{array} \right] + \left[ \begin{array}{l} \text{rate of energy} \\ \text{generation in} \\ \text{the shell} \end{array} \right] - \left[ \begin{array}{l} \text{rate of energy} \\ \text{consumption in} \\ \text{the shell} \end{array} \right] \quad (6.1-1)$$

In the present case, there is no energy generation within the shell,

therefore, the corresponding term may be set equal to zero in the above equation. While the energy shall naturally be consumed during desorption, as it is an endothermic process.

Substitution of individual terms and the application of the limits result into energy balance equation for the packed bed, as given below :

$$\rho_b C_p \frac{\partial T}{\partial t} = \frac{1}{r} \frac{\partial}{\partial r} (k r \frac{\partial T}{\partial r}) - \Delta H \frac{\partial \bar{q}}{\partial t} \quad (6.1-2)$$

Appropriate initial and boundary conditions are as follows :

Initial Condition

$$T|_{(r,0)} = T_o \quad ; \quad r_o \leq r \leq R \quad (6.1-3)$$

Boundary Conditions

$$\left. \frac{\partial T}{\partial r} \right|_{(R,t)} = 0 \quad (6.1-4)$$

$$\left. \frac{\partial T}{\partial r} \right|_{(r_o,t)} = - \frac{Q_L}{2\pi r_o k} \quad (6.1-5)$$

For the meaning of variables, one may refer to the nomenclature.

#### 6.1.1.2 MS Pellet

Molecular sieves are characterized by bidispersed pore structure. Commercially available MS pellets are manufactured by pelletizing zeolite crystals, generally of size 1-10  $\mu\text{m}$  diameter [Garg and Ruthven (1973a), Ruthven (1984)], using a clay binder. Kinetics of desorption in these adsorbents are governed by following diffusional steps in the given order.



- (i) Micropore diffusion, i.e. diffusion of adsorbate from inside of the zeolite crystal to its surface.
- (ii) Macropore diffusion, i.e. diffusion of adsorbate from the surface of zeolite crystal to the surface of pellet through extracrystalline pores formed by the clay binder.
- (iii) Film diffusion, i.e. diffusion of adsorbate from the pellet surface to the bulk phase through a thin fluid film surrounding the pellet.

It has been found that in the process of desorption of adsorbate (water) from the molecular sieves, the micropore diffusion is the rate controlling step because it is slowest amongst all the mass transfer steps [Antonson and Dranoff (1967), Yang (1987)]. This is particularly true because the adsorption of adsorbate vapours in the commercial MS pellet occurs almost entirely within the zeolite crystals [Kärger and Ruthven (1992)]. Macro-porous clay used to bind the crystals contributes negligibly in terms of adsorption step and at the same time it does not offer any significant resistance to the mass transport of smaller molecules such as water (van der Waals Diameter  $\cong 2.8 \text{ \AA}$ ) [Barrer (1971)]. Hence, it is only the micropore or intracrystalline diffusion which plays an important role in desorption. Due to this reason, micropore diffusion of adsorbate shall only be considered in deriving the model equation for the pellet.

For the simplicity of analysis, the adsorbent pellet has been approximated by a spherical pellet of equal surface area [Huang and Fair (1988)]. Accordingly, we consider an elementary spherical shell of thickness  $\Delta r$  at a radius  $r$  within the molecular sieve pellet as shown in Figure 6.1-2. Assumptions used in the formulation of model equation are given below.

#### *Assumptions*

- (i) Initial adsorbed phase concentration in the pellet is uniform as

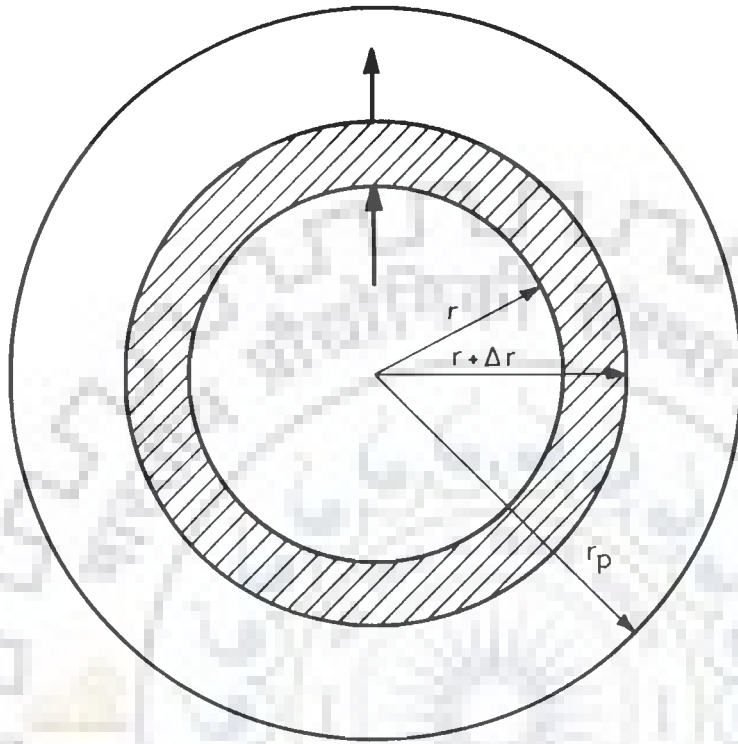


Figure 6-1-2 Spherical Shell for Adsorbate Balance in a Molecular Sieve Pellet

the molecular sieves are of uniform pore size and pore volume.

- (ii) Concentration of adsorbate at the pellet surface is in equilibrium with bulk phase concentration.

Unsteady state adsorbate mass balance across the spherical shell yields

$$\left[ \begin{array}{l} \text{Rate of accumulation} \\ \text{of adsorbate in the} \\ \text{shell} \end{array} \right] = \left[ \begin{array}{l} \text{Rate of flow of} \\ \text{adsorbate into the} \\ \text{shell by diffusion} \end{array} \right] - \left[ \begin{array}{l} \text{Rate of flow of} \\ \text{adsorbate out of} \\ \text{shell by diffusion} \end{array} \right] \quad (6.1-6)$$

Equation (6.1-6) results into the following micropore diffusion equation

$$\frac{\partial q}{\partial t} = \frac{1}{r^2} \frac{\partial}{\partial r} \left( D_e r^2 \frac{\partial q}{\partial r} \right), \quad (6.1-7)$$

where  $D_e$  is effective diffusivity of adsorbate within zeolite crystal. For constant  $D_e$ , the equation assumes the following form

$$\frac{\partial q}{\partial t} = \frac{D_e}{r^2} \frac{\partial}{\partial r} \left( r^2 \frac{\partial q}{\partial r} \right) \quad (6.1-8)$$

On the basis of assumptions, appropriate initial and boundary conditions are as follows :

Initial condition

$$q|_{(r,0)} = q_0 \quad (6.1-9a)$$

Boundary conditions

$$\left. \frac{\partial q}{\partial r} \right|_{(0,t)} = 0 \quad (6.1-9b)$$

$$q|_{(r_p, t)} = f(C) \quad (6.1-9c)$$

Where C is adsorbate concentration in bulk phase and can be obtained by using ideal gas law.

$$C = \frac{p}{R_g T} \quad (6.1-9d)$$

Volume averaged adsorbate concentration in a spherical pellet is given by the following equation.

$$\bar{q} = \frac{3}{r_p} \int_0^{r_p} q r^2 dr \quad (6.1-10)$$

### 6.1.1.3 Constitutive Relationships

In the present research work, water vapour - 13X MS has been considered as adsorbate - adsorbent system. For solving model equations, we require relationships for adsorption isotherm and dependency of effective thermal conductivity of bed of 13X MS pellets (k) on temperature. Values of other parameters have been either determined or taken from the literature.

#### (a) Adsorption Isotherm

Equation (6.1-9c) is in fact adsorption isotherm, which may be assumed to be linear for water vapour - 13X MS system. This is reasonable assumption because the time required in completely saturating the bed by adsorption is almost equal to that required for regeneration of bed by desorption [Prasad (1988)]. This isotherm has been obtained experimentally by Prasad (1988) and is given below.

$$q = KC \quad (6.1-11a)$$

Using Van't Hoff's relationship  $K$  can be calculated as follows :

$$K = K^\circ \exp \left[ - \frac{\Delta H}{R'_g T} \right], \quad (6.1-11b)$$

where  $K^\circ = 4.8587392 \times 10^{-3}$ ,  $\Delta H = 37912.08354$  kJ/kmol of  $H_2O$ , and  $R'_g = 8.3143$  kJ/kmol K .

This linear isotherm has been found to be valid for temperatures between 310 and 333 K [Prasad (1988)], but it has been assumed to be applicable during the entire period of desorption, in which higher temperatures ( $< 523$  K) are experienced. This also enables us in simplifying the model equations as demonstrated in the later section.

(b) *Correlation for  $k$*

In Chapter V, correlation for  $k$  has been determined by conducting dry bed conduction experiments on a bed of 13X MS pellets, which is given below.

$$k = 8.17635 \times 10^{-5} + 10.915427 \times 10^{-7} (T - T_o) \quad (5.4-4)$$

6.1.1.4 Remarks

Model equations for thermal desorption process are summarized in Table 6.1-1. During desorption, prediction of percent recovery of adsorbate with time requires the simultaneous solution of model equations of packed bed and the MS pellet, which may be carried out by using a suitable numerical method. As the concentration of adsorbate in the bed would vary with radial location during desorption, therefore, the average adsorbate concentration in the bed at a given time instant may be calculated by the following equation.

$$\bar{q}_b = \frac{2 \int_{r_o}^R \bar{q} r dr}{(R^2 - r_o^2)} \quad (6.1-12a)$$

Table 6.1-1 Mathematical Model of Thermal Desorption Process

**A. Packed Bed Energy Balance**

$$\rho_b C_p \frac{\partial T}{\partial t} = \frac{1}{r} \frac{\partial}{\partial r} \left( k r \frac{\partial T}{\partial r} \right) - \Delta H \frac{\partial \bar{q}}{\partial t}$$

**Initial Condition**

$$T|_{(r,0)} = T_o$$

Initially bed is at a uniform temperature.

**Boundary Conditions**

$$\left. \frac{\partial T}{\partial r} \right|_{(R,t)} = 0$$

No heat flux at the wall of desorber.

$$\left. \frac{\partial T}{\partial r} \right|_{(r_o,t)} = -\frac{Q_L}{2\pi r_o k}$$

Electrical heater emits constant heat flux from its surface.

**B. Micropore Diffusion of Adsorbate within Zeolite Crystal**

$$\frac{\partial q}{\partial t} = \frac{1}{r^2} \frac{\partial}{\partial r} \left( r^2 D_e \frac{\partial q}{\partial r} \right)$$

**Initial Condition**

$$q|_{(r,0)} = q_o$$

Initially adsorbate concentration is uniform throughout the bed.

**Boundary Conditions**

$$\left. \frac{\partial q}{\partial r} \right|_{(0,t)} = 0$$

$$q|_{(r_p, t)} = f(C)$$

Adsorbate concentration at the pellet surface is in equilibrium with bulk concentration.

Average adsorbate concentration in pellet

$$\bar{q} = \frac{3}{r_p^3} \int_0^{r_p} q r^2 dr$$

**C. Constitutive Relationships**

(i) Adsorption Isotherm

Linear

$$q = f(C) = KC ; K = K^o \exp \left( -\frac{\Delta H}{R_g T} \right)$$

Adsorbate vapour follows ideal gas law.

$$C = \frac{p}{R_g T}$$

(ii) Effective Thermal Conductivity of Packed Bed

k varies linearly with temperature.

$$k = k_o + \beta(T - T_o)$$

Hence,

$$\text{Percent recovery of adsorbate} = \frac{q_o - \bar{q}_b}{q_o} \times 100 \quad (6.1-12b)$$

In principle, numerical solution of model equations may be obtained, but it requires enormous computer time. This is because of the fact that the micropore diffusion equation is to be solved at each grid point during the iterative solution of energy balance equation for packed bed; besides solution of micropore diffusion equation is in itself iterative in nature for several isotherms. In order to utilize the developed model profitably, it is imperative to simplify the model equations without sacrificing the accuracy of solution. Such an effort has been made in the following section.

### 6.1.2 Simplified Model

The model equations (Table 6.1-1) can be considerably simplified if the micropore diffusion equation is eliminated. In order to do this, it is necessary to know a priori the adsorbate concentration profile within the zeolite crystal. Liaw et al. (1979) and Rice (1982) used the parabolic concentration profile in the modelling studies of gas separation by Pressure Swing and Thermal Swing Adsorption processes. This is a reasonable assumption as the profile obtained by exact solution is almost parabolic in shape [Towler and Rice (1974), Yang and Doong (1985), Yang (1987)]. Accordingly, in the present study, parabolic concentration profile within the zeolite crystal is assumed. Furthermore, diffusivity of adsorbate in the zeolite crystal is also considered to be constant.

For simplification, we define non-dimensional variables as follows :

$$A = \frac{q}{q_o}, \quad \tau = \frac{D_e t}{r_p^2}, \quad x = \frac{r}{r_p} \quad (6.1-13)$$

By using these variables, micropore diffusion equation (6.1-8) and the

associated initial and boundary conditions [equations (6.1-9a) to (6.1-9c)] can be converted into the following form.

$$\frac{\partial A}{\partial \tau} = \frac{1}{x^2} \frac{\partial}{\partial x} \left[ x^2 \frac{\partial A}{\partial x} \right] \quad (6.1-14)$$

and

Initial condition

$$A|_{(x,0)} = 1 \quad (6.1-15a)$$

Boundary conditions

$$\left. \frac{\partial A}{\partial x} \right|_{(0,\tau)} = 0 \quad (6.1-15b)$$

$$A|_{(1,\tau)} = K' \Phi \quad (6.1-15c)$$

where

$$K' = K \frac{C_o}{q_o} \quad (6.1-15d)$$

$$\Phi = \frac{C}{C_o} \quad (6.1-15e)$$

Equation of parabolic concentration profile is

$$A = a_o + a_2 x^2 \quad (6.1-16)$$

Therefore, at  $x = 1$  we have

$$A|_{x=1} = a_o + a_2 \quad (6.1-17)$$

which together with equation (6.1-15c) gives

$$a_o + a_2 = K' \Phi \quad (6.1-18)$$

Now, by differentiating equation (6.1-16) with respect to  $x$ , we obtain



$$\frac{\partial A}{\partial x} = 2a_2 x$$

At  $x = 1$ , we have

$$\left. \frac{\partial A}{\partial x} \right|_{x=1} = 2a_2 \quad (6.1-19)$$

In the dimensionless form, the volume averaged adsorbate concentration in the pellet can be expressed as given below.

$$\bar{A} = \int_0^1 3x^2 A dx \quad (6.1-20)$$

By solving the above equation with equation (6.1-16), we obtain

$$\bar{A} = a_0 + \frac{3}{5} a_2 \quad (6.1-21)$$

$a_2$  can be obtained by solving equations (6.1-18 and 6.1-21) and is given below.

$$a_2 = \frac{5}{2} (K' \Phi - \bar{A}) \quad (6.1-22)$$

Now, multiplying both sides of equation (6.1-14) by  $3x^2 dx$ , we get

$$\frac{\partial A}{\partial \tau} 3x^2 dx = 3x^2 dx \frac{1}{2} \frac{\partial}{\partial x} \left[ x^2 \frac{\partial A}{\partial x} \right]$$

Its integration results into the following equation.

$$\frac{\partial}{\partial \tau} \int_0^1 A 3x^2 dx = 3 \int_0^1 \left[ \frac{\partial}{\partial x} \left[ x^2 \frac{\partial A}{\partial x} \right] \right] dx$$

$$\text{or } \frac{\partial \bar{A}}{\partial \tau} = 3 \left[ x^2 \frac{\partial A}{\partial x} \right]_0^1 \quad (6.1-23)$$

Evaluating the limits and using the equations (6.1-19 and 6.1-22), we finally obtain

$$\frac{\partial \bar{A}}{\partial \tau} = 15 (K' \Phi - \bar{A}) \quad (6.1-24)$$

By using equation (6.1-13), we obtain the above equation in dimensional variables as follows :

$$\frac{\partial \bar{q}}{\partial t} = 15 \frac{D_e}{r_p^2} (KC - \bar{q}) \quad (6.1-25)$$

Equation (6.1-25) has the form of Gluekauf's widely used linear driving force approximation for the mass transfer rate [Yang (1987)].

Some of the researchers [Do and Mayfield (1987), Xiu and Wakao (1993)] have used the following general profile for the adsorbate concentration within the zeolite crystal

$$A = a_0 + a_n x^n, \quad (6.1-26)$$

and estimated value of  $n$  using the experimental data. By proceeding in the same way with this profile, we obtain

$$\frac{\partial \bar{q}}{\partial t} = 3(n + 3) \frac{D_e}{r_p^2} (KC - \bar{q}) \quad (6.1-27)$$

It may be easily seen that for  $n = 2$ , above equation reduces to the equation (6.1-25).

#### 6.1.2.1 Model Equation

Equation (6.1.25) is now used to simplify the mathematical model of the thermal desorption process (Table 6.1-1). By substituting  $\frac{\partial \bar{q}}{\partial t}$  from the equation (6.1-25) into equation (6.1-2), we obtain

$$\rho_b C_p \frac{\partial T}{\partial t} = \frac{1}{r} \frac{\partial}{\partial r} \left( k r \frac{\partial T}{\partial r} \right) + \Delta H 15 \frac{D_e}{r_p^2} (KC - \bar{q}) \quad (6.1-28)$$

One may note that '-' sign before  $\Delta H$  in the equation (6.1-2) has been replaced by '+' sign at the time of making the substitution. This is because of the fact that  $\frac{\partial \bar{q}}{\partial t}$  is always negative during desorption. Besides, '-' sign in equation (6.1-2) has been written to indicate the consumption of energy during desorption without considering the sign of  $\frac{\partial \bar{q}}{\partial t}$ . Thus, in order to be consistent with the physics of process, only implicit '-' sign of the term for  $\frac{\partial \bar{q}}{\partial t}$  has been kept in the equation (6.1-28).

Similarly, for the general profile for adsorbate concentration within the zeolite crystal [equation (6.1-26)], one gets

$$\rho_b C_p \frac{\partial T}{\partial t} = \frac{1}{r} \frac{\partial}{\partial r} \left( k r \frac{\partial T}{\partial r} \right) + \Delta H n(n+3) \frac{D_e}{r_p^2} (KC - \bar{q}) \quad (6.1-29)$$

Equation (6.1-28) alongwith initial and boundary conditions, given by equations (6.1-3 to 6.1-5) constitute the simplified model. This is also summarized in the Table 6.1-2.

## 6.2 NUMERICAL SOLUTION

Simplified model can be easily solved by the control volume finite difference method. Algorithm developed in Chapter V for solving the equation (5.2-1a) may also be utilized for this purpose with little modification. The difference between equations (5.2-1a) and (6.1-28) is that the latter contains source term. At the start of iteration for a time step, it may be considered to be constant, and evaluated at previous values of temperatures. So, for the linearization of source term [equation (5.3-4i)], we have

$$S_C = \Delta H 15 \frac{D_e}{r_p^2} (KC - \bar{q}), \quad (6.2-1a)$$

$$S_P = 0 \quad (6.2-1b)$$

Table 6.1-2 Simplified Mathematical Model of Thermal Desorption Process

**A. Model Equation**

$$\rho_b C_p \frac{\partial T}{\partial t} = \frac{1}{r} \frac{\partial}{\partial r} \left( k r \frac{\partial T}{\partial r} \right) + \Delta H \frac{D_e}{r_p^2} (KC - \bar{q})$$

**Initial Condition**

$$T|_{(r,0)} = T_o, \quad \bar{q}|_{(r,0)} = q_o$$

Initially bed is at a uniform temperature and adsorbate concentration.

**Boundary Conditions**

$$\left. \frac{\partial T}{\partial r} \right|_{(R,t)} = 0$$

No heat flux at the wall of desorber.

$$\left. \frac{\partial T}{\partial r} \right|_{(r_o,t)} = -\frac{Q_L}{2\pi r_o k}$$

Electrical heater emits constant heat flux from its surface.

**B. Constitutive Relationships**

**(i) Adsorption Isotherm**

Linear

$$q = KC; \quad K = K^o \exp \left( -\frac{\Delta H}{R'_g T} \right)$$

Adsorbate vapour follows ideal gas law.

$$C = \frac{P}{R_g T}$$

**(ii) Effective Thermal Conductivity of Packed Bed**

k varies linearly with temperature.

$$k = k_o + \beta(T - T_o)$$

In the algorithm for solving equation (5.2-1a), both  $S_C$  and  $S_P$  have been taken to be equal to zero. Consequently, the expression for  $S_C$  shall modify the elements of  $\underline{d}$  [equation (5.3-5)] in accordance with the equation (5.3-4f). With these modifications, computational algorithm described in the section 5.3.2 has been used to solve the simplified model numerically on a PC-AT 486 Computer.

During the desorption, it is desired to compute percent desorption. Consequently adsorbed phase concentration in the desorber is calculated at various times by using equations (6.1-12a and b). As there exists adsorbed phase concentration profile in radial direction, therefore, integral in the equation (6.1-12a) has been evaluated numerically by using Weddle's rule [Sastry (1990), James et al. (1977)].

### 6.3 EXPERIMENTAL DATA ON THERMAL DESORPTION

In the present study, experimental data of Prasad (1988) for thermal desorption with the heating of bed by imbedded electrical heater have been used for the validation of the developed mathematical model. Figure 6.3-1 depicts the schematic diagram of the experimental setup. Adsorbate - adsorbent system studied was water vapour - 13X MS.

In each experimental run, the bed was first allowed to saturate completely by adsorbing the water vapour. To achieve this, a feed consisting of air and water vapour, of known humidity and temperature, was continuously passed through a previously regenerated bed. During adsorption in the bed, humidity and temperature of feed was maintained constant for each experimental run. Adsorption being an exothermic process, results into the increase in bed temperature, which gradually attains a maximum value and then starts decreasing as the bed tends to saturate completely with the water vapour. Although, the bed becomes saturated earlier, but the flow of feed is continued till the bed temperature reduces to the feed temperature and becomes uniform throughout.

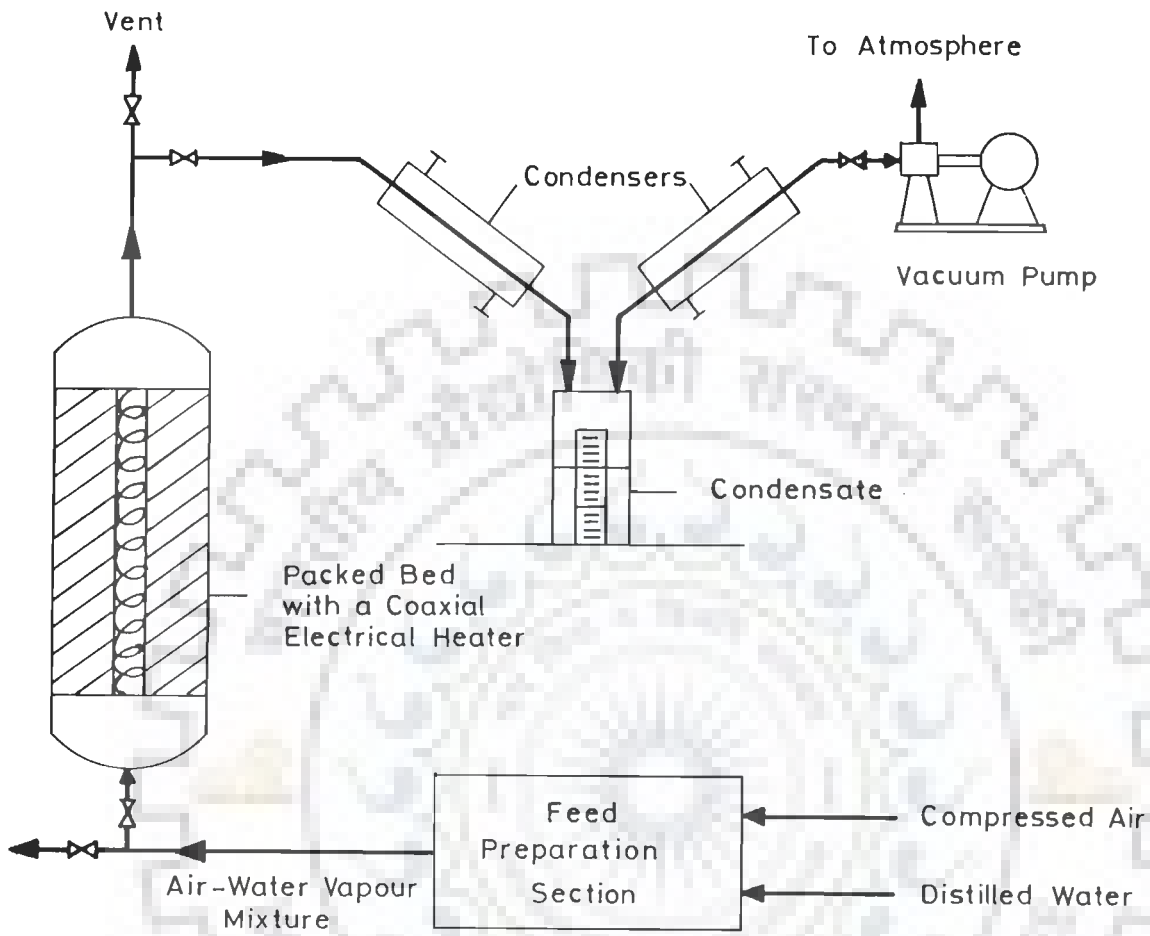


Figure 6-3-1 Schematic Diagram of Experimental Setup for Modified Thermal Desorption Process

Desorption experiment was started as soon as the bed became completely saturated. For this, feed inlet valve was closed, and the vacuum, equivalent to the partial pressure of water vapour in the feed, was applied to the bed. This has been done in order to avoid pressure swing effect or recondensation of desorbed water vapour in the colder portion of the bed like top cover. Imbedded coaxial heater was also switched on simultaneously at the predetermined heater wattage. Desorbed water vapour was allowed to condense in a series of two chilled - water - cooled condensers, and the condensate was collected in a graduated cylinder. This provided a record of percent desorption of adsorbate with time. Further, the desorption experiment was carried out till the recovery of adsorbate vapour from the packed bed became insignificant.

Table 6.3-1 provides the operating conditions of two experimental runs of desorption. While the Table 6.3-2 gives the percent desorption with time for two experiments A and B, respectively. These results are plotted in the Figure 6.3-2.

#### 6.4 RESULTS AND DISCUSSION

Numerical solution of developed model requires the value of diffusivity of adsorbate within zeolite crystal. According to the literature, the values of effective diffusivity for zeolites differ upto an astounding range of five orders of magnitude for the same type of zeolite, obtained from different sources [Weisz (1995)]. The values of diffusivity for water in different type of zeolite molecular sieves vary widely, but a value in the range  $1 \times 10^{-9}$  to  $1 \times 10^{-10}$   $\text{m}^2/\text{s}$  [Antonson and Dranoff (1967), Shibuya and Kawazoe (1978)] appears to be reasonable. However, these values may further differ by an order of magnitude depending upon the source of molecular sieves, initial concentration of adsorbate, etc. In view of foregoing discussion, a value of diffusivity between  $1 \times 10^{-11}$  and  $1 \times 10^{-9}$   $\text{m}^2/\text{s}$  for water in the 13X zeolite molecular sieves, used in present study, may be assumed for solving the model equations.

**Table 6.3-1 Operating Conditions of Thermal Desorption Experiments with Imbedded heater**

S. No.	Operating Parameters		Experiment	
			A	B
1	Feed Quality used for Bed Saturation	% Relative Humidity	50	42
		Measured at Temperature (K)	304	303
2	Feed Mixture Temperature (K)		312	303
3	Concentration of Adsorbate in feed (kmol H <sub>2</sub> O/m <sup>3</sup> of feed)		$8.329 \times 10^{-4}$	$7.251 \times 10^{-4}$
4	Heater Wattage (kW/m)		0.2667	0.2667
5	Maximum Heater Surface Temperature (K)		523	523
6	Duration of Desorption (min)		565	510
7	Operating Pressure in Bed during Desorption (mm Hg)		734.6	722.4
8	Amount of Adsorbate in Packed Bed (ml)	Experimentally recovered	198.3	169.2
		Calculated by Equilibrium relationship	220.7	174.2



**Table 6.3-2 Experimentally Observed Percent Desorption for Experiments A and B**

S.No.	Time (h)	Percent Desorption	
		Experiment-A	Experiment-B
1	0.5	6.57	7.00
2	1.0	21.29	28.01
3	1.5	35.12	43.98
4	2.0	43.50	53.78
5	2.5	51.43	60.78
6	3.0	57.54	67.79
7	3.5	62.30	73.11
8	4.0	65.70	77.59
9	4.5	68.65	80.95
10	5.0	71.59	84.03
11	5.5	74.36	86.55
12	6.0	77.03	89.08
13	6.5	79.52	91.59
14	7.0	81.56	93.56
15	7.5	83.60	95.40
16	8.0	85.64	96.60
17	8.5	87.68	98.00
18	9.0	89.94	-

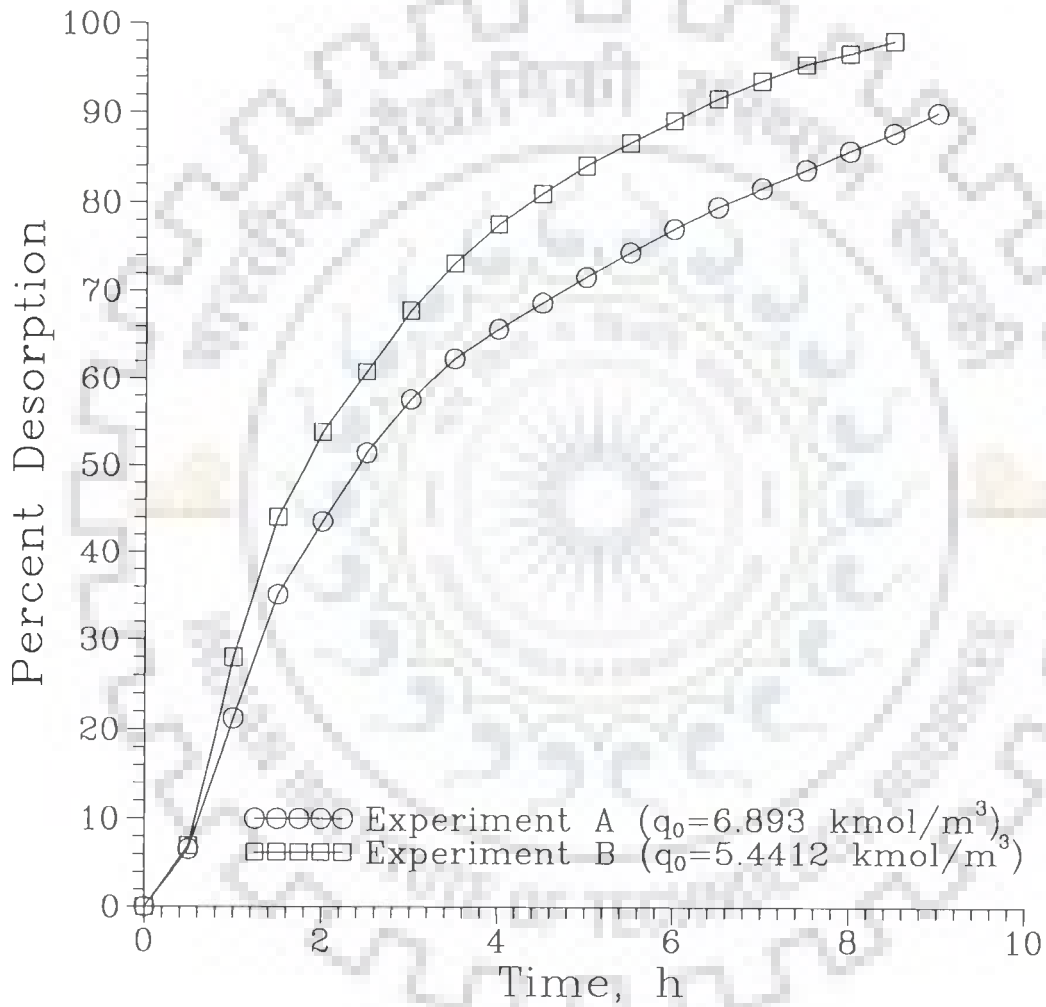


Figure 6.3-2 Experimentally Observed Percent Desorption vs. Time for Experiments A and B

#### 6.4.1 Model Predictions with Constant Diffusivity

---

Predictions of percent desorption versus time for the conditions of experiments A and B have been done by using the model for few values of diffusivity, i.e.  $2 \times 10^{-11}$  to  $6 \times 10^{-11}$   $\text{m}^2/\text{s}$ . The computed results are plotted in Figures 6.4-1 and 6.4-2 for the two experiments respectively.

Figure 6.4-1 contains four plots corresponding to few values of diffusivity,  $2 \times 10^{-11}$ ,  $3 \times 10^{-11}$ ,  $4 \times 10^{-11}$  and  $5 \times 10^{-11}$   $\text{m}^2/\text{s}$ , along with experimental data obtained in the experiment-A. It is obvious that the predictions of percent desorption for  $D_e = 3 \times 10^{-11}$   $\text{m}^2/\text{s}$  are close to those obtained experimentally during the later period of desorption, i.e. after six hours, in comparison to other values of diffusivity. Besides, the model provides a realistic estimate of desorption time with this value of diffusivity. Therefore, it appears justified to choose  $D_e = 3 \times 10^{-11}$   $\text{m}^2/\text{s}$  for the experiment-A.

Figure 6.4-1 also displays the prediction of percent desorption by an earlier model [Prasad (1988)], which assumes desorption to be purely conduction controlled and neglects the intraparticle diffusion. These predictions are far away from the experimental results, and thus, the earlier model cannot be used for simulation at all. On the other hand, it is beyond doubt that the present model is a better and appropriate representation of the thermal desorption process.

Similar observations may be made from the Figure 6.4-2. For the conditions of experiment-B, proper value of  $D_e$  is  $6 \times 10^{-11}$   $\text{m}^2/\text{s}$ . One notes further that both these estimated values of  $D_e$  are in agreement with those reported in literature.

During the first half period of desorption, the predictions from the present model are less than those observed experimentally.

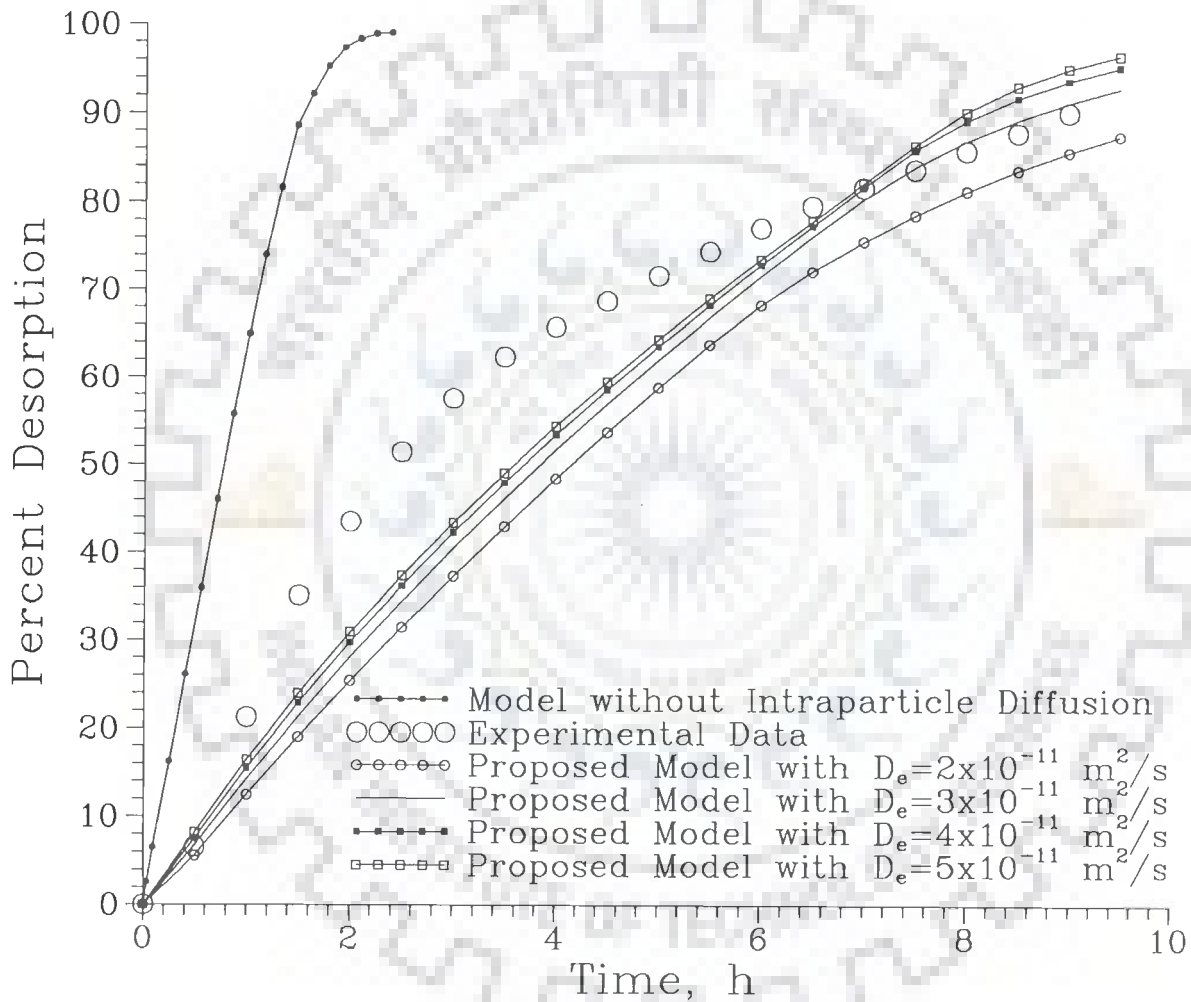


Figure 6.4-1 Comparison of Predicted Percent Desorption vs. Time using Proposed Model Considering Intraparticle Diffusion (Constant Diffusivity) for Experiment-A

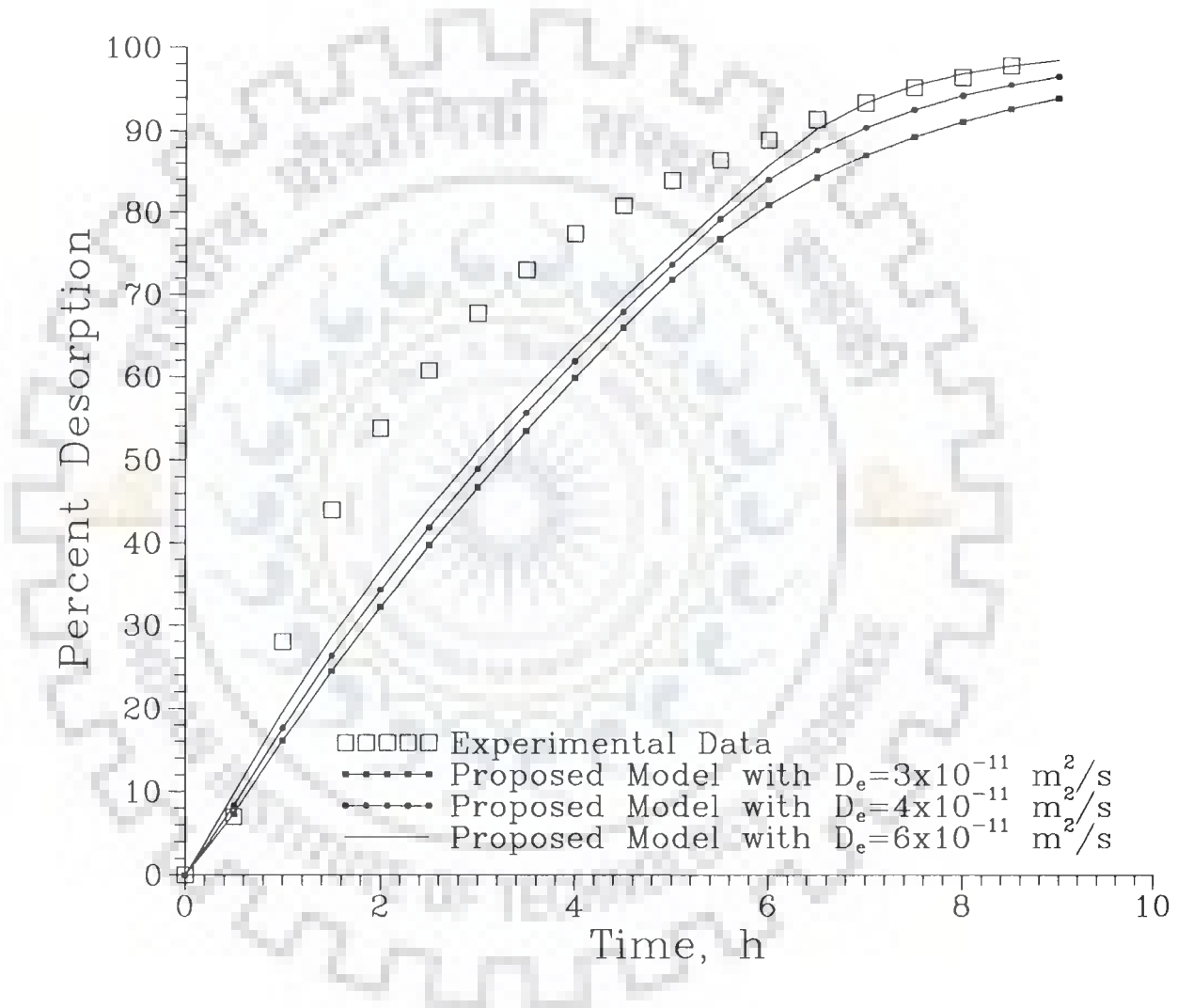


Figure 6.4-2 Comparison of Predicted Percent Desorption vs. Time using Proposed Model Considering Intraparticle Diffusion (Constant Diffusivity) for Experiment-B

This is true for both the experiments [Figures 6.4-1 and 6.4-2]. This deviation may be attributed to the following reasons.

*First, a linear adsorption isotherm has been used in the present model for the entire period of desorption, during which temperature varies from 300 to 523 K. Linear isotherm is only applicable in a limited temperature range (310-333 K). Also isotherm relationship for air-water vapour - zeolite system is in general nonlinear.*

*Secondly, the diffusivities in zeolite molecular sieves are strongly concentration dependent in nature [Garg and Ruthven (1972), Ruthven and Loughlin (1971), Yang (1987)]. While the diffusivity has been taken to be constant (independent of concentration) in the proposed model.*

Linearity of isotherm and the constancy of diffusivity were necessary in order to simplify the mathematical model of the thermal desorption process. Due to this reason, it could be solved within a reasonable computer time. Relaxation of both these assumptions leads to the amazingly high requirement of computer time in solving the model, which would probably prohibit its use. This aspect shall be discussed in somewhat more detail in a later section.

Further, it is assumed in simplifying the mathematical model that the adsorbate phase concentration profile in zeolite crystal is parabolic in shape. In order to verify the validity of this assumption, computations have also been carried out with the model of general profile [equation (6.1-29)] for both  $n = 3$  and  $4$ . The results are presented in the Figure 6.4-3 for experiment-A. The three curves for percent desorption are close to each other during most of the period of desorption, but after about 7 hour time deviation in predictions for  $n = 3$  and  $4$  with respect to  $n = 2$  is comparatively more. This deviation may be minimized by suitably adjusting the value of diffusivity. However, upto 7 hour period, predictions for  $n = 3$  and  $4$  do not result into any significant improvement over those for  $n = 2$ , vis-a-vis

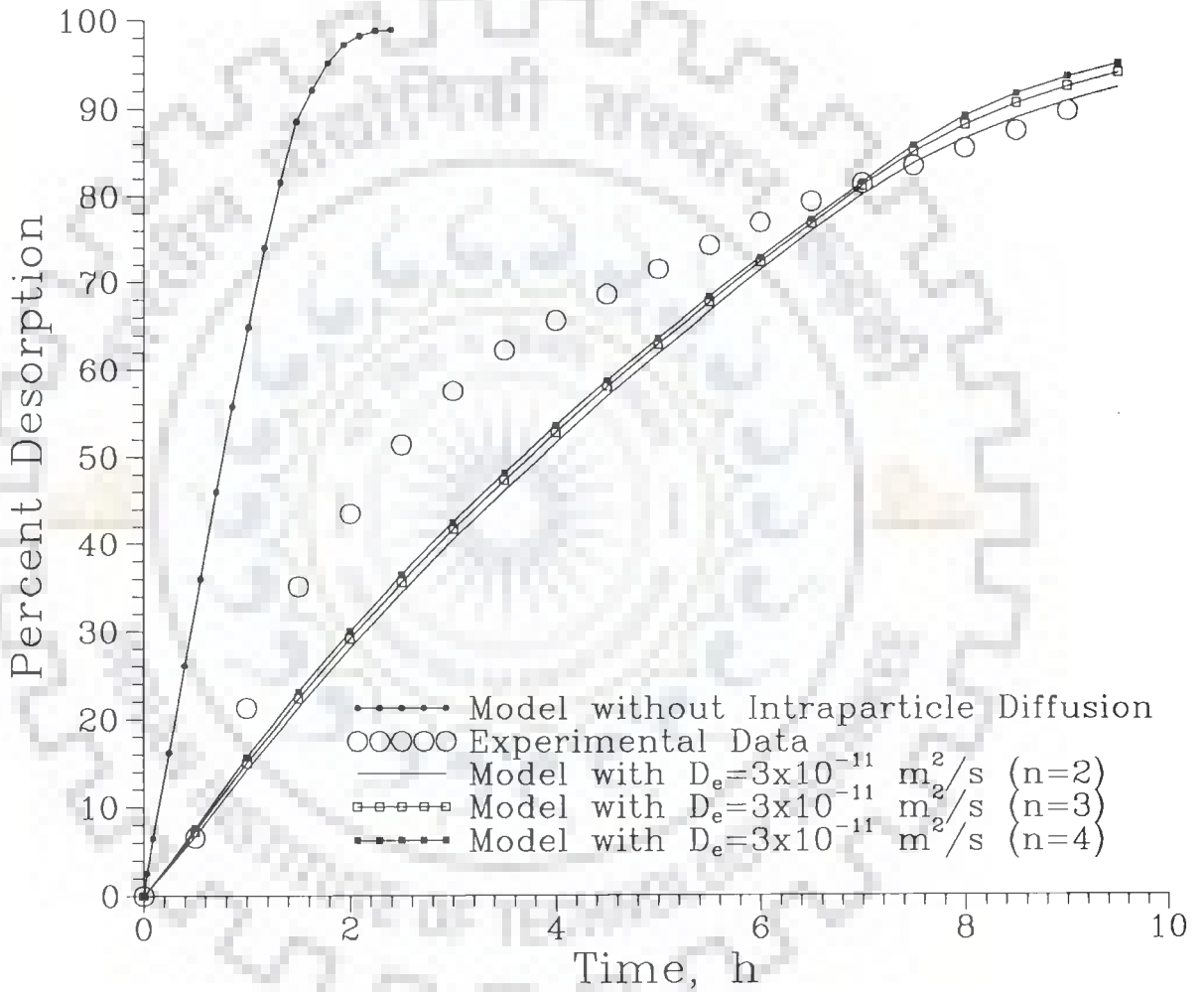


Figure 6.4-3 Comparison of Model Predictions by Equation (6.1-29) for Different Profiles using Constant Diffusivity for Experiment-A

experimental observations. Therefore, it is appropriate to do computations with the accepted parabolic profile ( $n = 2$ ) as assumed in the simplified model. However, no attempt has been made by us to check its validity by solving the mathematical model [Table 6.1-1] without this assumption as it requires prohibitively large computer time.

#### 6.4.1.1 Transient Profiles

Transient profiles describe the progress of desorption in packed bed with time. These also provide sufficient insight about the process occurring there. For the conditions of experiment-A, radial profiles of adsorbate concentration and temperature have been computed by using the model for  $D_e = 3 \times 10^{-11} \text{ m}^2/\text{s}$ , which are depicted in Figures 6.4-4 and 6.4-5 respectively. These Figures indicate that during first one hour period, desorption takes place upto a radial distance of 34 mm (approx.) only. Temperatures in this section of bed are now sufficiently high and can sustain further desorption. Therefore, after one hour, heat also gets transmitted radially by conduction beyond 34 mm. Consequently, the desorption progresses upto 36, 40, 42, and 45 mm at the end of two, three, four, and five hour time respectively. After this time, desorption is more pronounced in the portion of bed which is towards the wall of desorber (between 40-47 mm). After 8 hour, approximately 86 percent of adsorbate is recovered.

Alternate method of representation is to draw the transient profiles at selected radial locations. Accordingly, Figures 6.4-6 and 6.4-7 have been prepared for the adsorbate concentration and temperature in the bed respectively; selected radial locations are 6.5, 10, 15, 20, 25, 30, 40, 45, and 47 mm. It may be noted that the radial location 6.5 mm has not been used in the Figure 6.4-6 as it is on the heater surface. During desorption, Figure 6.4-6 illustrates the movement of adsorbate concentration front in radial direction, while Figure 6.4-7 provides the movement of temperature front.

Similar behaviour has also been observed from the transient



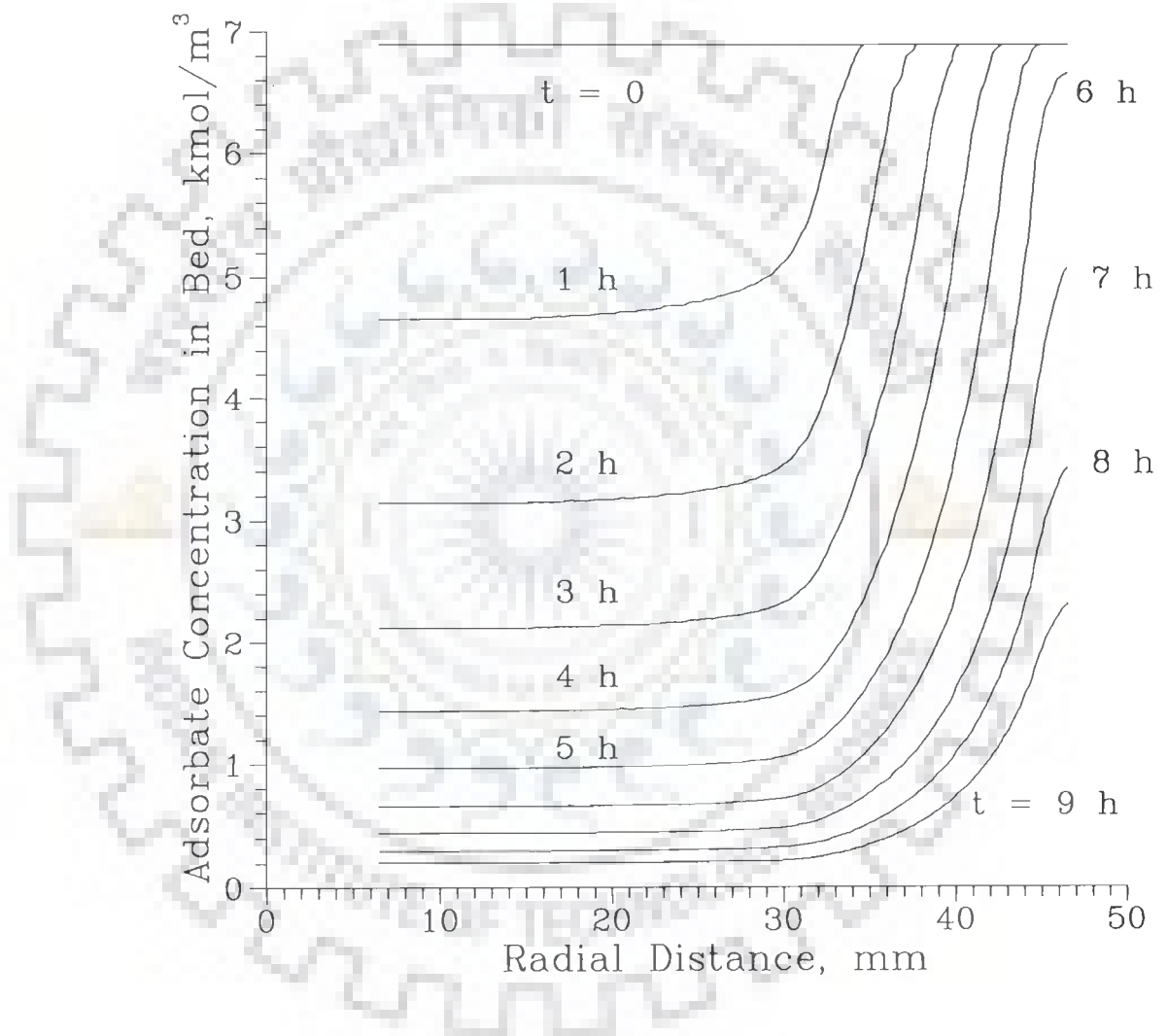


Figure 6.4-4 Radial Adsorbate Concentration Profiles Developed in Bed during Desorption [Predicted by Model with  $D_e = 3 \times 10^{-11}$  m<sup>2</sup>/s for Experiment-A]

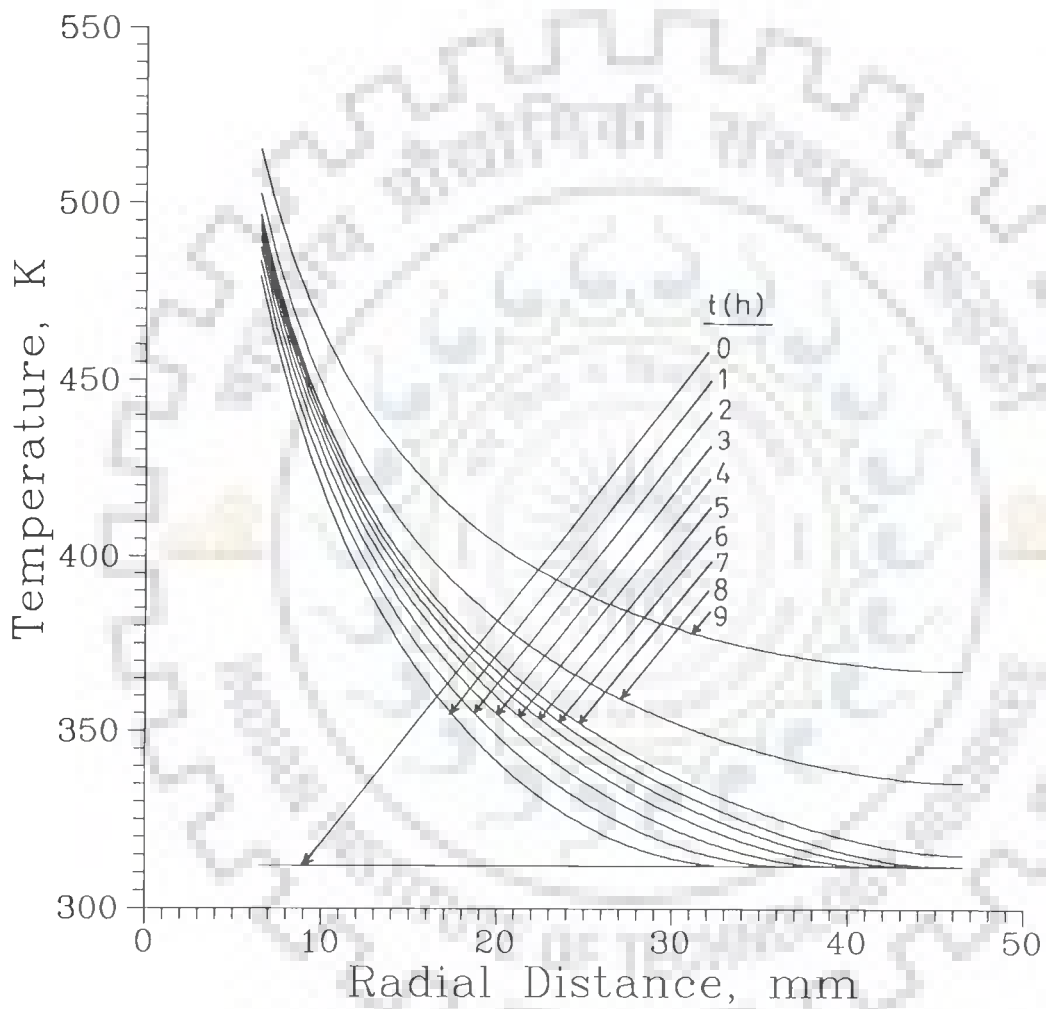


Figure 6.4-5 Radial Temperature Profiles developed in Bed during Desorption, [Predicted by Model with  $D_e = 3 \times 10^{-11} \text{ m}^2/\text{s}$  for Experiment-A]

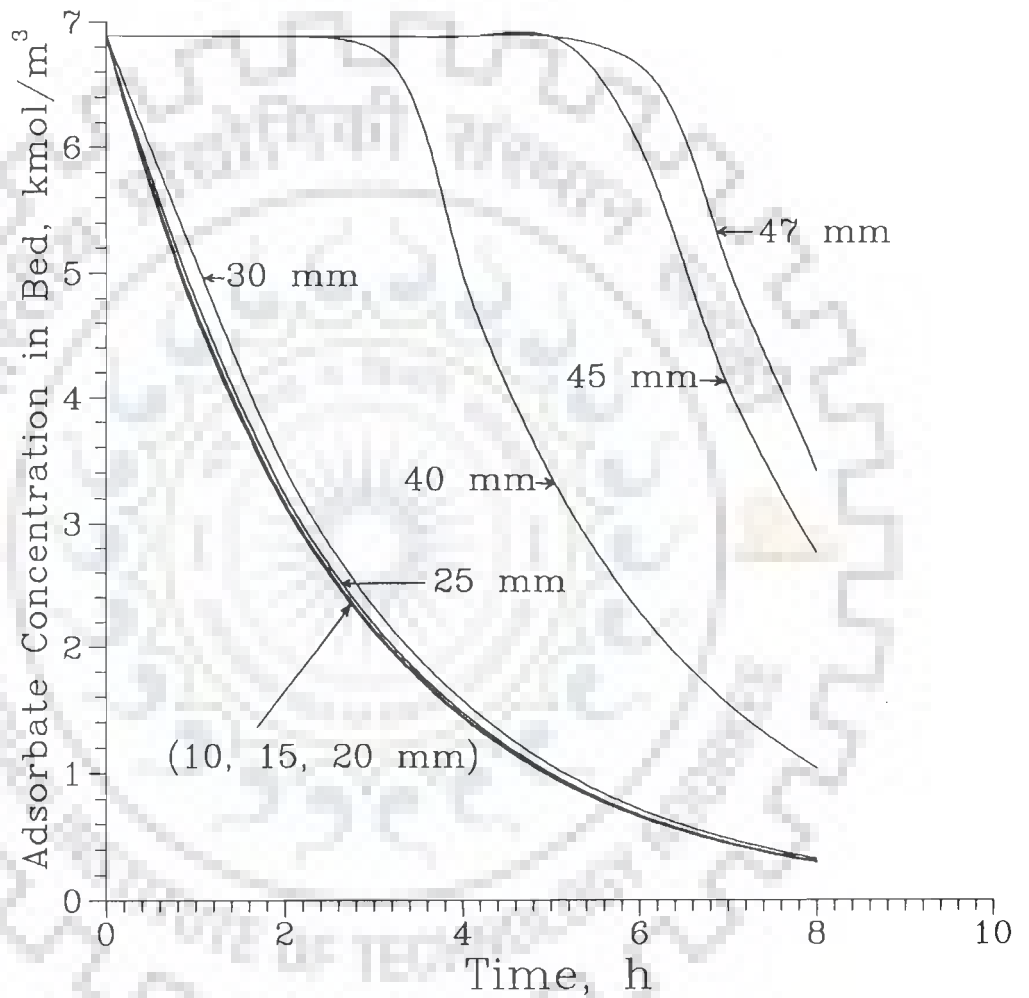


Figure 6.4-6 Variation of Adsorbate Concentration with Time at Selected Radial Locations during Desorption [Predicted by Model with  $D_e=3 \times 10^{-11}$  m<sup>2</sup>/s for Experiment-A]

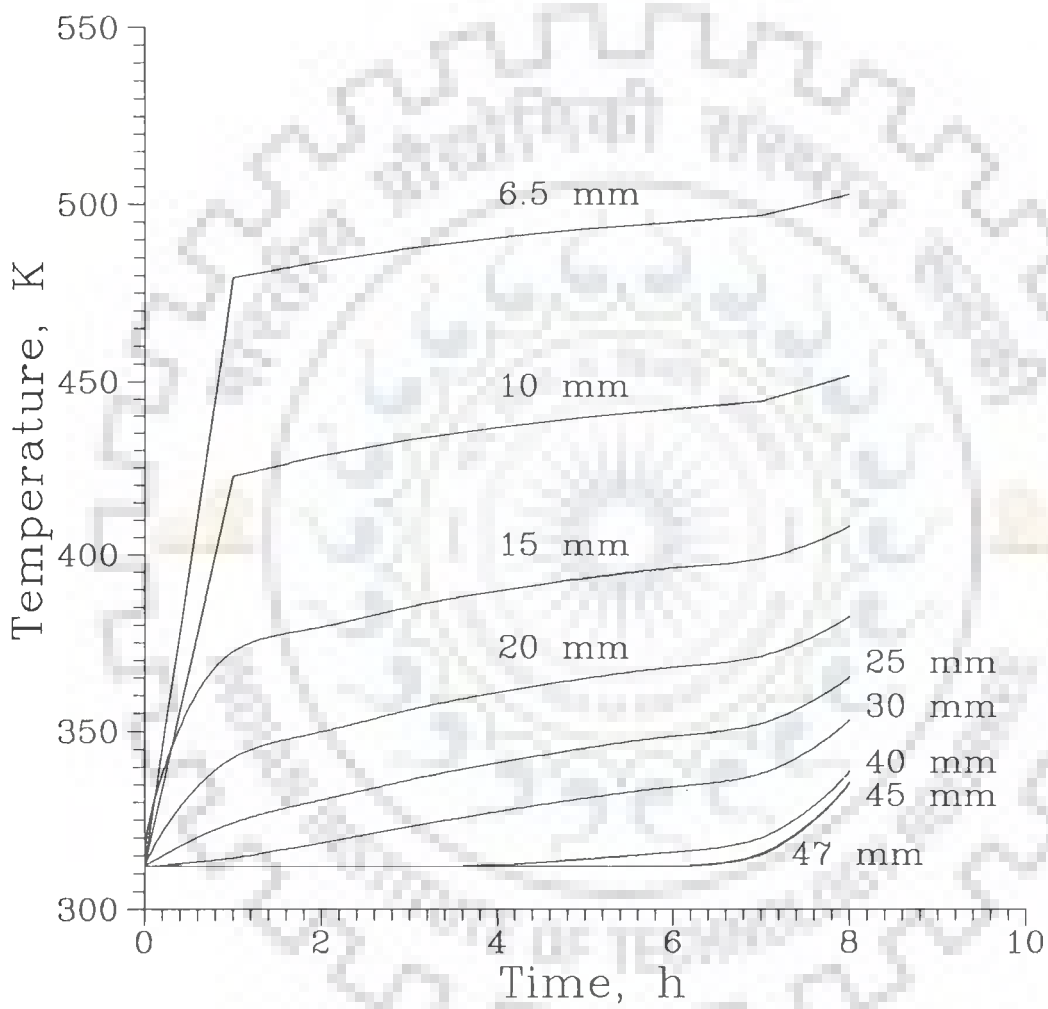


Figure 6.4-7 Variation of Temperature with Time at Selected Radial Locations during Desorption [Predicted by Model with  $D_e=3 \times 10^{-11}$  m<sup>2</sup>/s for Experiment-A]

profiles, computed for the experiment-B. So, these have not been included here.

#### 6.4.2 Model Predictions with Variable Diffusivity

---

It may be noted from the Figure 6.4-1 that the predictions of percent desorption become nearer to experimental ones during first half period of desorption as the diffusivity  $D_e$  is increased from  $2 \times 10^{-11}$  to  $5 \times 10^{-11} \text{ m}^2/\text{s}$ . It advocates the use of higher value of diffusivity whenever adsorbate concentration is high. Consequently, this suggests that the model of desorption process should be solved with variable diffusivity for improving the predictions; the diffusivity would vary as per the adsorbate concentration in the bed.

As a matter of fact, diverse dependences of diffusivity on adsorbate concentration have been reported in literature [Yang (1987)]. In the present study, two types of diffusivity correlations [Garg and Ruthven (1972)] have been examined, which are given below :

$$D(q) = \frac{D_o}{1 - q/q_s} \quad (6.4-1)$$

$$D(q) = \frac{D_o}{(1 - q/q_s)^2} \quad (6.4-2)$$

In both the above correlations, we note that  $D(q)$  becomes infinite as  $q$  approaches  $q_s$ . Such a situation is not desirable in numerical computation. To avoid this, these correlations are modified as follows :

$$D(q) = \frac{D_o}{1 - \alpha_1 q/q_s} \quad (6.4-3)$$

$$D(q) = \frac{D_o}{(1 - \alpha_2 q/q_s)^2} \quad (6.4-4)$$

Where  $\alpha_1$  and  $\alpha_2$  are constants. Their values may be computed by minimum and maximum values of diffusivity, which are likely to be experienced in a particular adsorbate - adsorbent system.

In the present study, several numerical tests have been conducted with the model and experimental data to obtain likely minimum and maximum values of diffusivity; the obtained values are  $1.5 \times 10^{-11}$  and  $1.0 \times 10^{-9} \text{ m}^2/\text{s}$ . Accordingly, values of constants  $\alpha_1$  and  $\alpha_2$  in equations (6.4-3) and (6.4-4) are 0.98500 and 0.87753 respectively.

Figure 6.4-8 shows the variation of diffusivity with fractional uptake for these two correlations. As the improvement in model predictions during first half period of desorption is desired, therefore, the shape of curves suggests that the equation (6.4-4) appears to be the correct choice. This has also been verified by doing extensive computations with the model for two correlations.

At this juncture one remark is in order. In the development of simplified model in section 6.1.2, diffusivity has been considered to be constant. Thus, in order to use diffusivity correlation in the simplified model, it is assumed that the diffusivity remains constant during numerical solution of model over a small time interval,  $\Delta t$ , but its value depends upon the adsorbate concentration prevailing at the grid point and computed at the previous time step. This assumption is reasonable because the extent of desorption shall be very small in a small time interval (1 - 15 s). And thus, the diffusivity may be calculated by using the equation (6.4-4) at each grid point prior to making computation for every time interval.

#### 6.4.2.1 Comparison of Model Predictions with Experimental Data

Simplified model has been solved numerically with the diffusivity correlation (equation 6.4-4) for conditions of both the experiments. Figures 6.4-9 and 6.4-10 present the curves of percent desorption with time, observed experimentally as well as predicted by the model for experiments A and B respectively. Besides, model

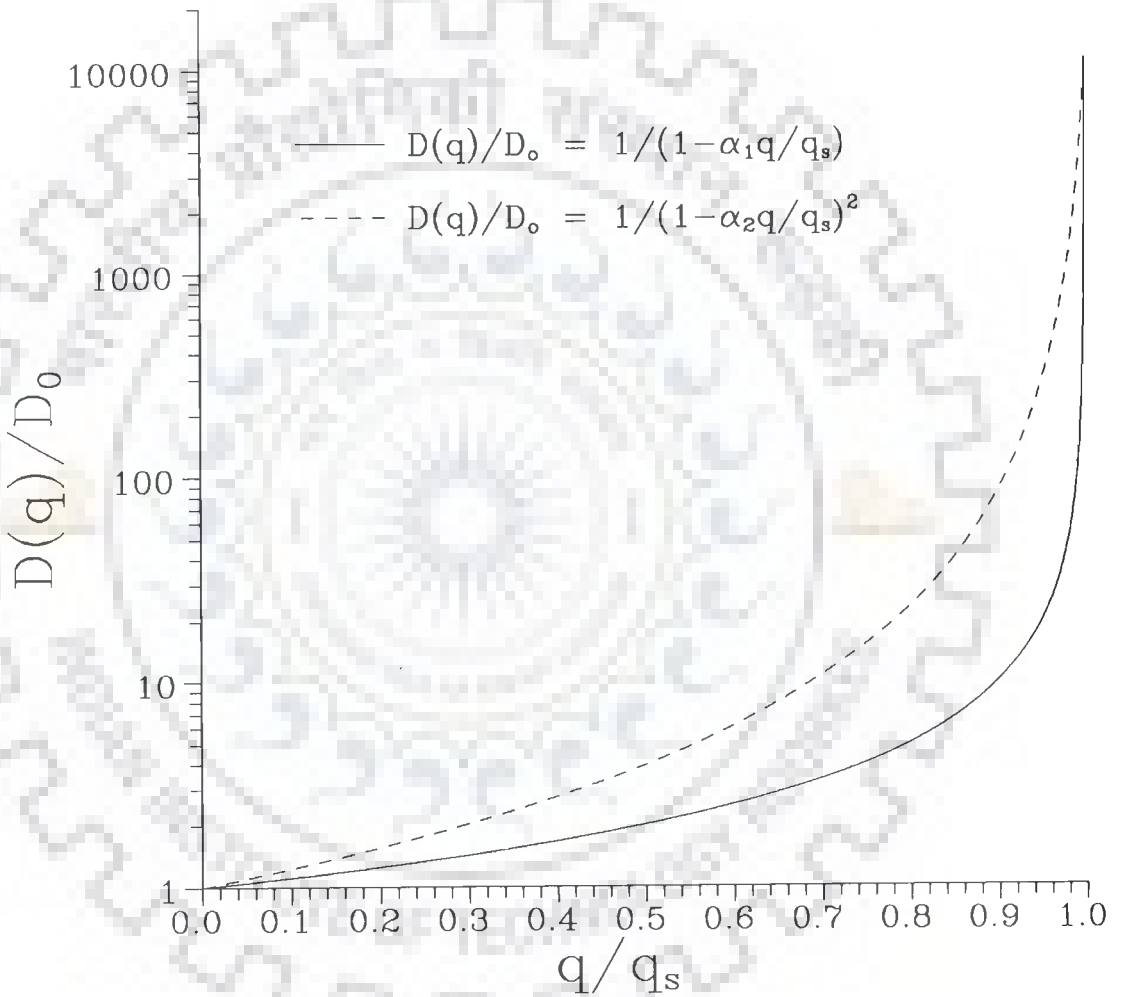


Figure 6.4-8 Variation of Diffusivity with Fractional Uptake for Two Types of Concentration-Dependent Diffusivity Correlations

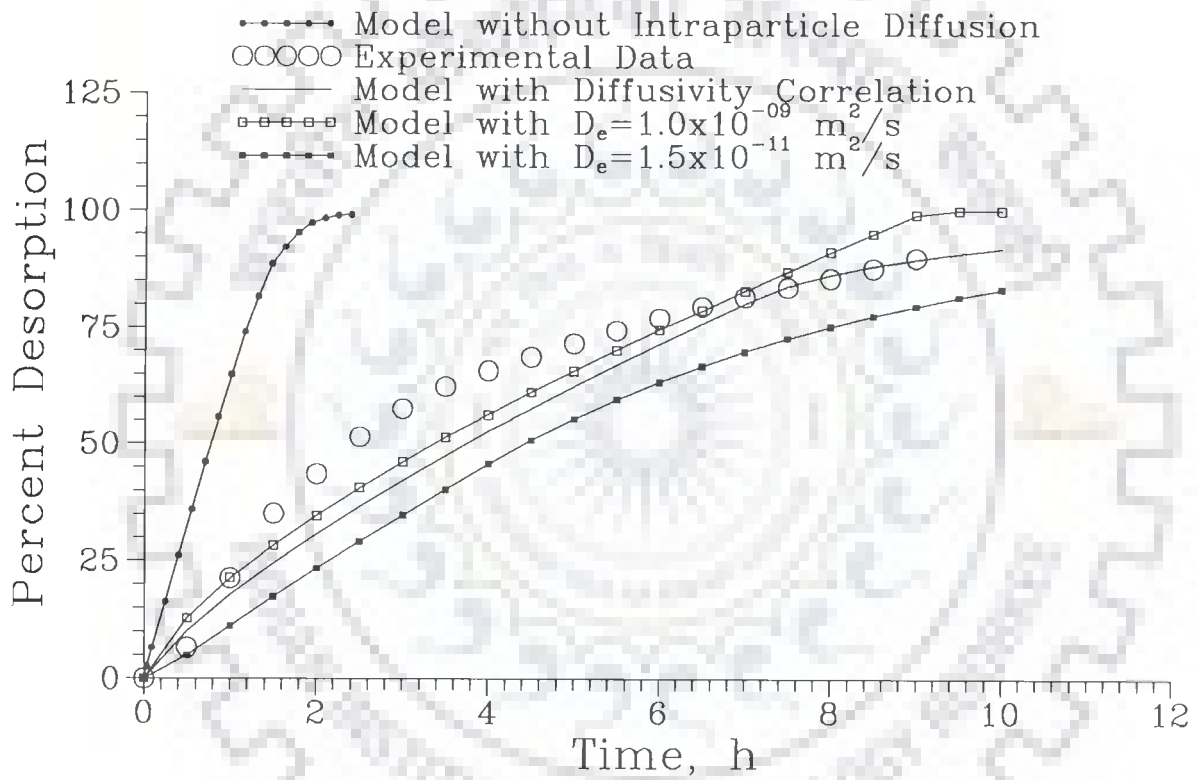


Figure 6.4-9 Comparison of Model Predictions with Experimental Results (Experiment-A)



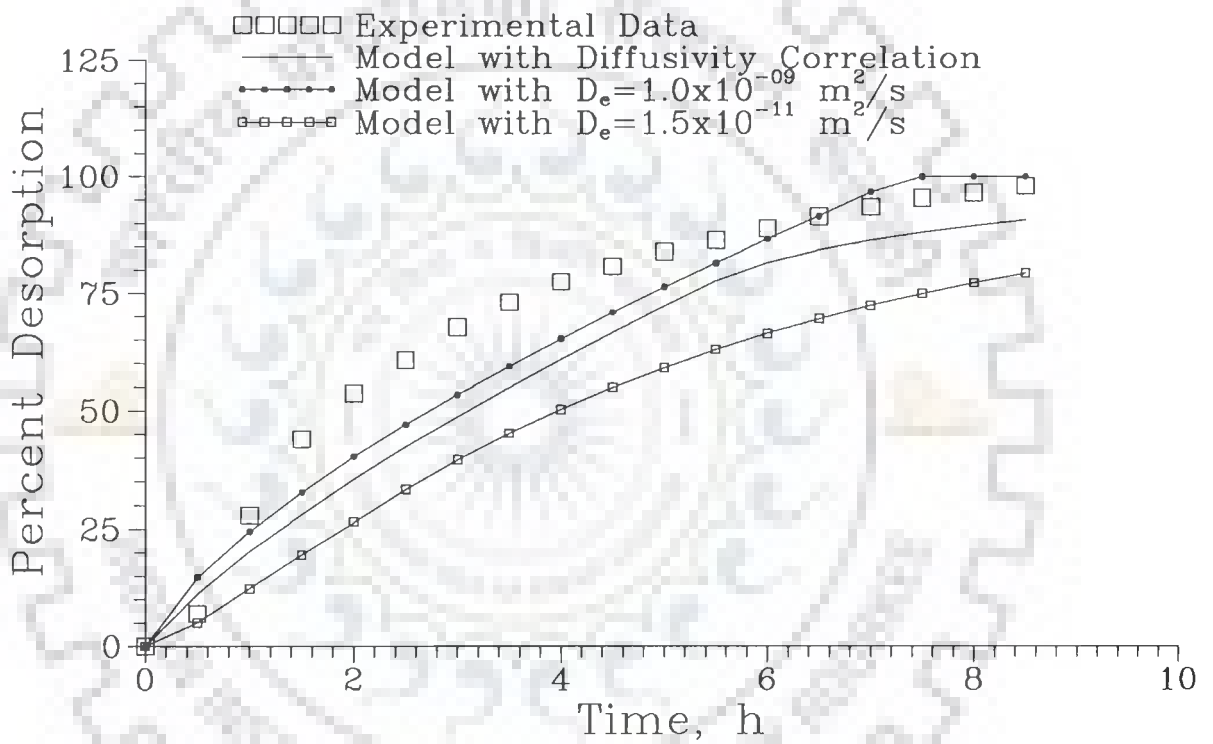


Figure 6.4-10 Comparison of Model Predictions with Experimental Results (Experiment-B)

predictions in these Figures with constant diffusivity,  $1.5 \times 10^{-11}$  and  $1.0 \times 10^{-9} \text{ m}^2/\text{s}$ , provide lower and upper bounds for the predictions of model with the diffusivity correlation. It is observed from both these Figures that the model predictions have been improved by the use of diffusivity correlation, atleast in the first half period of desorption in which the improvement was most desired. This aspect is more clearly illustrated in Tables 6.4-1 and 6.4-2. In these Tables, percent deviation in the model prediction has been calculated with respect to the corresponding experimental observation. It may be noted that the percent deviation has been considerably reduced by the use of diffusivity correlation vis-a-vis constant diffusivity during the period 0.5-4.5 hr. Although, the predictions are still lower than the experimental ones, but the deviation is acceptable. Similar observations can also be made from Figures 6.4-11 and 6.4-12, which compare the predicted and observed percent desorption for the experiments A and B respectively.

It is our view that the further improvement in the model predictions of percent desorption could be possible only if nonlinearity of adsorption isotherm is considered. This conclusion is also in agreement with the remarks made by Yang (1987) about the use of linear isotherm in simplifying the model, that the Linear Driving Force (LDF) approximation as well as other approximations fail during early stage of uptake. Also that the LDF is not a good approximation for highly nonlinear isotherms.

#### 6.4.2.2 Transient Profiles

Transient profiles at selected radial locations have also been computed for experiment A by the model with diffusivity correlation; radial locations are kept same as used earlier in the section 6.4.1.1. These are shown in Figures 6.4-13 and 6.4-14 for the adsorbate concentration and temperature respectively. Comparison of adsorbate concentration fronts in the Figures 6.4-13, and 6.4-6 (for constant diffusivity) indicates that the use of diffusivity correlation has made the fronts quite distinct with each other at the radial

**Table 6.4-1 Comparison of Percent Deviation in Predicted Percent Desorption using proposed Constant and Variable Diffusivities for Experiment-A**

Time (h)	Percent Desorption			Percent Deviation, calculated with respect to Experimental Values	
	Experimental Data	Computed from the Model with		Constant Diffusivity	Variable Diffusivity
		Constant Diffusivity $D_e = 3 \times 10^{-11}$ $m^2/s$	Variable Diffusivity equation (6.4-4)	Constant Diffusivity $D_e = 3 \times 10^{-11}$ $m^2/s$	Variable Diffusivity equation (6.4-4)
0.5	6.57	6.72	9.93	2.28	51.14
1.0	21.29	14.25	17.73	-33.07	-16.72
1.5	35.12	21.35	24.46	-39.21	-30.35
2.0	43.50	28.06	30.73	-35.50	-29.36
2.5	51.43	34.40	36.62	-33.11	-28.80
3.0	57.54	40.44	42.17	-29.72	-26.71
3.5	62.30	46.17	47.45	-25.90	-23.84
4.0	65.70	51.65	52.60	-21.39	-19.94
4.5	68.65	56.91	57.48	-17.10	-16.27
5.0	71.59	61.95	62.32	-13.46	-12.95
5.5	74.36	66.81	66.95	-10.15	-9.96
6.0	77.03	71.51	71.42	-7.17	-7.28
6.5	79.52	76.09	75.82	-4.31	-4.65
7.0	81.56	80.34	80.15	-1.50	-1.73
7.5	83.60	83.85	83.86	0.30	0.31
8.0	85.64	86.73	86.30	1.27	0.77
8.5	87.68	89.10	88.15	1.62	0.54
9.0	89.94	91.04	89.65	1.22	-0.32

**Table 6.4-2 Comparison of Percent Deviation in Predicted Percent Desorption using proposed Constant and Variable Diffusivities for Experiment-B**

Time (h)	Percent Desorption			Percent Deviation, calculated with respect to Experimental Values	
	Experimental Data	Computed from the Model with		Constant Diffusivity	Variable Diffusivity
		Constant Diffusivity $D_e = 3 \times 10^{-11}$ $m^2/s$	Variable Diffusivity equation (6.4-4)	Constant Diffusivity $D_e = 3 \times 10^{-11}$ $m^2/s$	Variable Diffusivity equation (6.4-4)
0.5	7.00	7.34	11.25	4.86	60.71
1.0	28.01	16.12	20.29	-42.45	-27.56
1.5	43.98	24.44	28.16	-44.43	-35.97
2.0	53.78	32.29	35.51	-39.96	-33.97
2.5	60.78	39.73	42.33	-34.63	-30.35
3.0	67.79	46.78	48.80	-30.99	-28.01
3.5	73.11	53.49	55.04	-26.84	-24.72
4.0	77.59	59.90	60.99	-22.80	-21.39
4.5	80.95	66.06	66.68	-18.39	-17.63
5.0	84.03	71.94	72.34	-14.39	-13.91
5.5	86.55	76.95	77.80	-11.09	-10.11
6.0	89.08	81.06	81.76	-9.00	-8.22
6.5	91.59	84.44	84.45	-7.81	-7.80
7.0	93.56	87.22	86.53	-6.78	-7.51
7.5	95.40	89.50	88.23	-6.18	-7.52
8.0	96.60	91.37	89.64	-5.41	-7.20
8.5	98.00	92.91	90.84	-5.19	-7.31

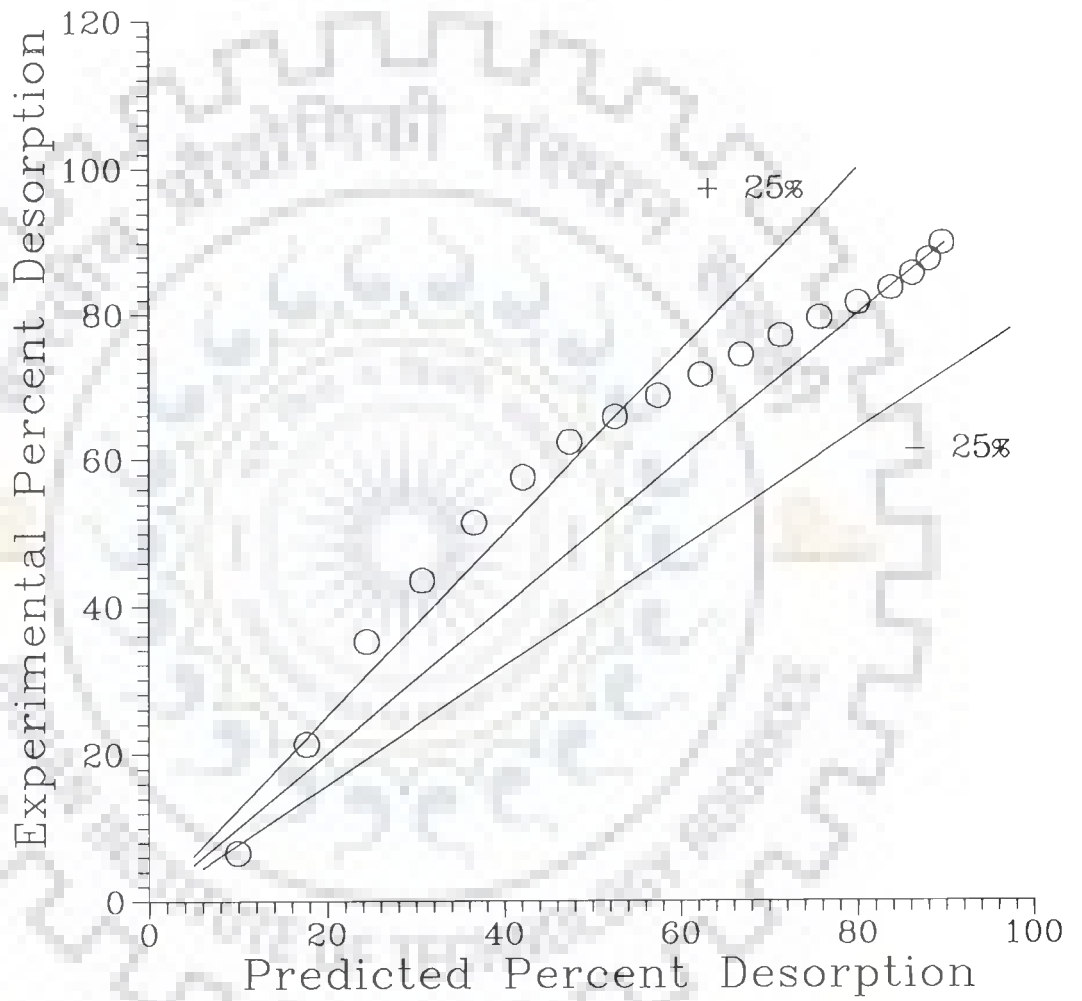


Figure 6.4-11 Comparison of Experimental and Predicted values of Percent Desorption using Diffusivity Correlation for Experiment-A

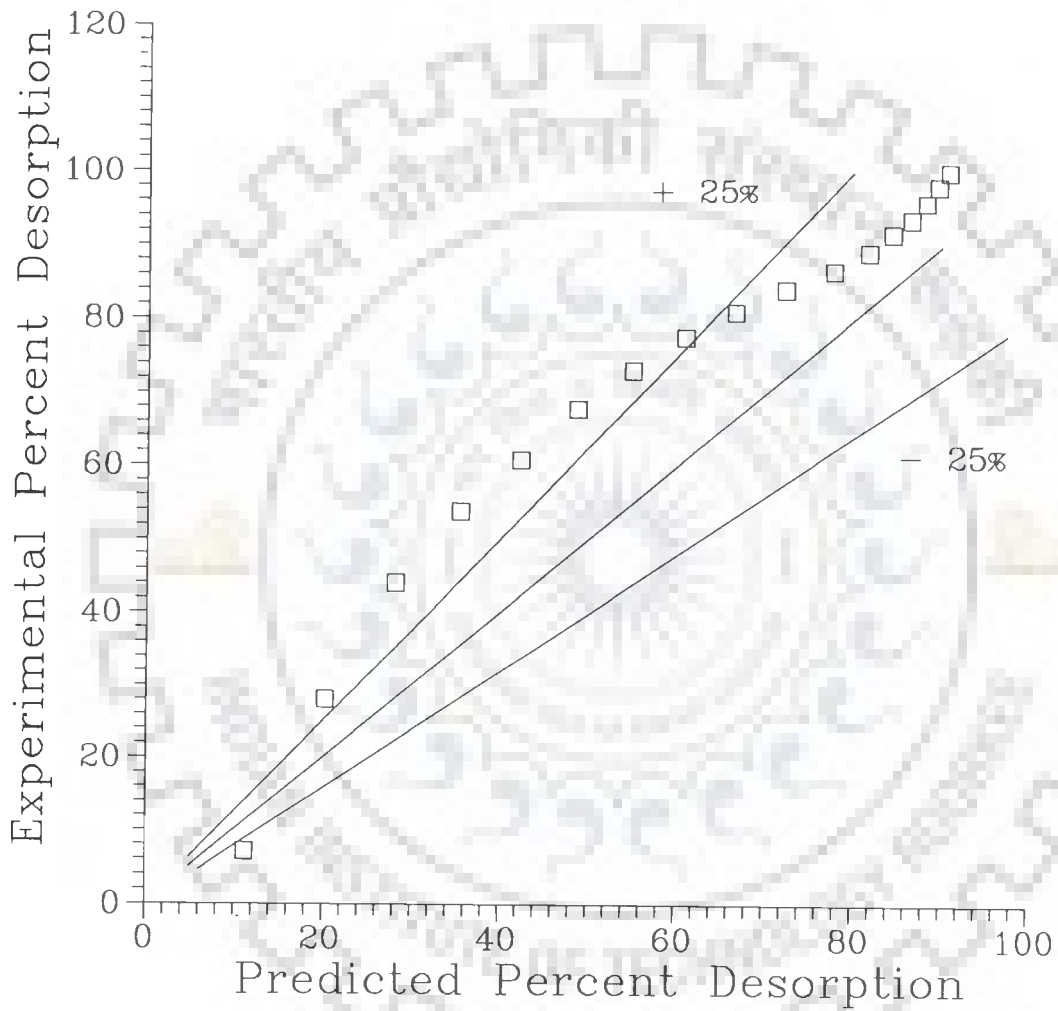


Figure 6.4-12 Comparison of Experimental and Predicted values of Percent Desorption using Diffusivity Correlation for Experiment-B

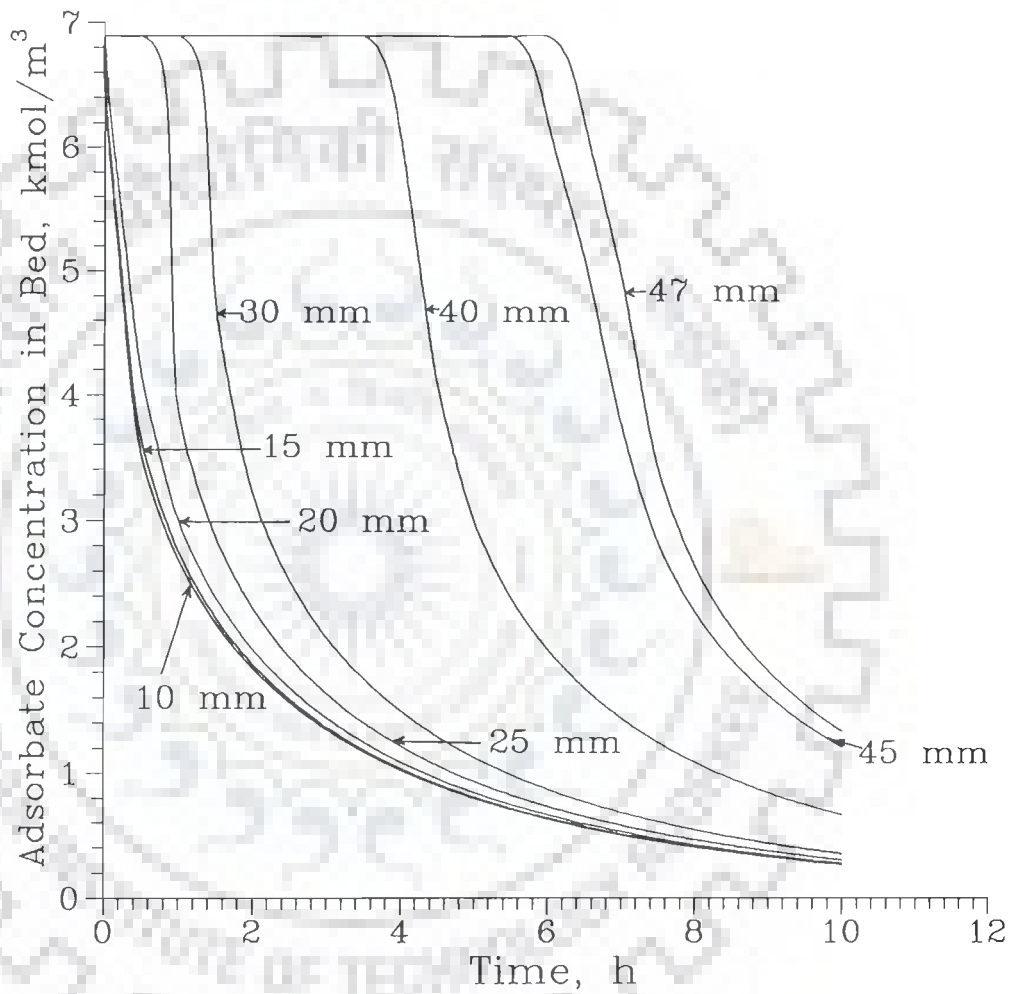


Figure 6.4-13 Variation of Adsorbate Concentration with Time at Selected Radial Locations during Desorption [Predicted by Model with Diffusivity Correlation for Experiment-A]

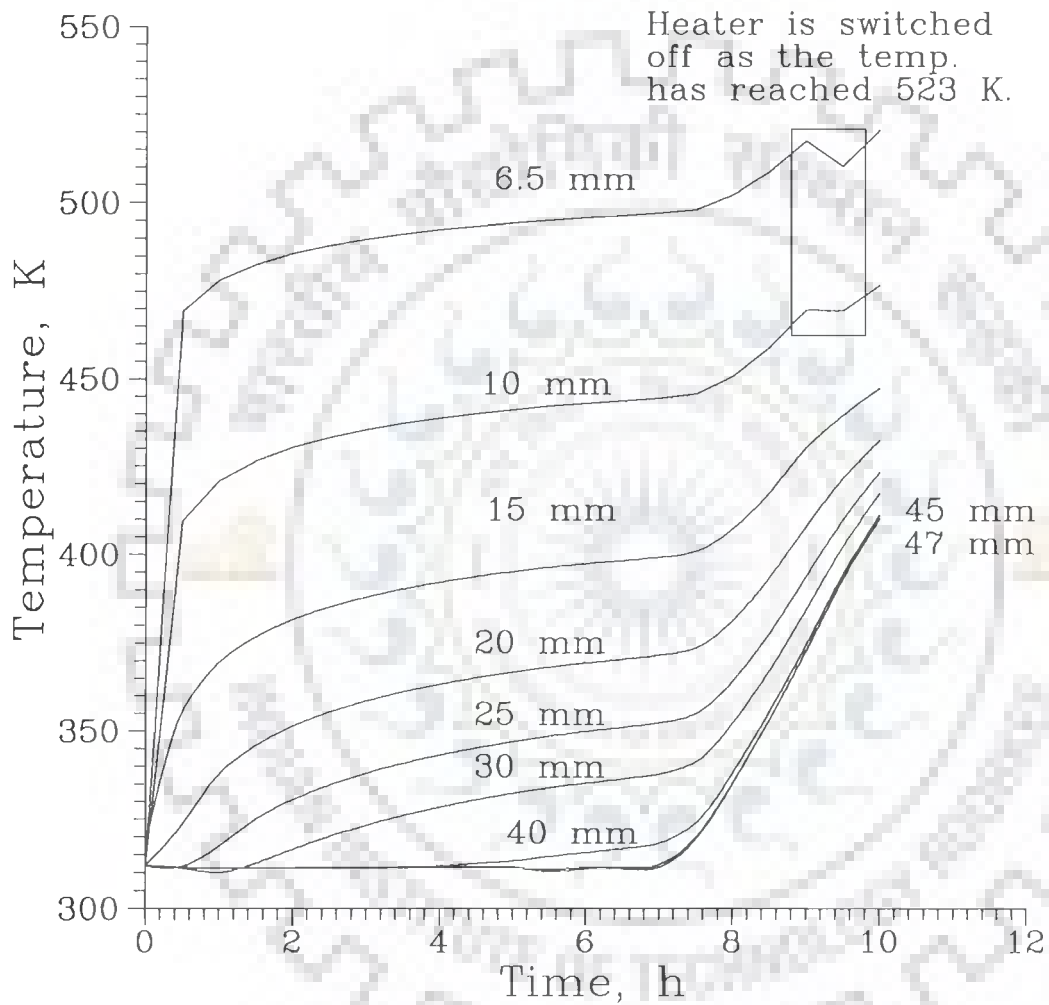


Figure 6.4-14 Variation of Temperature with Time at Selected Radial Locations during Desorption [Predicted by Model with Diffusivity Correlation for Experiment-A]



locations, which are nearer to the heater surface.

Figure 6.4-14 illustrates the movement of temperature fronts during desorption. It is observed that the temperature more than 523 K is attained at the radial location 6.5 mm, which is nearest to the heater surface. As soon as this occurs, electrical heater is purposely switched off during numerical simulation to avoid adverse effect on the adsorption capacity of molecular sieves. Such a practice is always followed during experimentation as well as in industrial applications by using suitable temperature controllers. The profiles during this period are enclosed within a rectangle. Though temperature more than 523 K is attained at 6.5 mm radial location, but the overall effect has also been, expectedly, propagated to other locations and is visible atleast at 10 mm radial location. Further, it is mentioned that the temperature more than 523 K has never been attained during numerical solution of the model with constant diffusivity.

#### 6.4.2.3 Effect of Increase in Heater Wattage on Desorption

Percent desorption versus time profiles have also been computed by the model with diffusivity correlation for electrical heaters having different heater wattages ( $Q_L$ ), viz. 0.2667, 0.3333 and 0.4000 kW/m. These profiles are for experiment-A and shown in Figure 6.4-15. From the Figure, following points may be noted.

- (i) Percent desorption profiles for  $Q_L = 0.3333$  and  $0.4000$  kW/m are quite close to each other. This may be attributed to the fact that the heater with  $Q_L = 0.4$  kW/m starts switching-off and -on from 0.5 hour onwards as the temperature in the bed rises beyond 523 K. While this situation arises only after 5.5 and 9 hour for heaters with  $Q_L = 0.3333$  and  $0.2667$  kW/m respectively.
- (ii) After about 8 hour period, percent desorptions for heaters with  $Q_L = 0.3333$  and  $0.4000$  kW/m are equal, and 90%. During this period, recovery of adsorbate for heater with  $Q_L = 0.2667$  kW/m reduces marginally to 87%. Furthermore, recovery of adsorbate

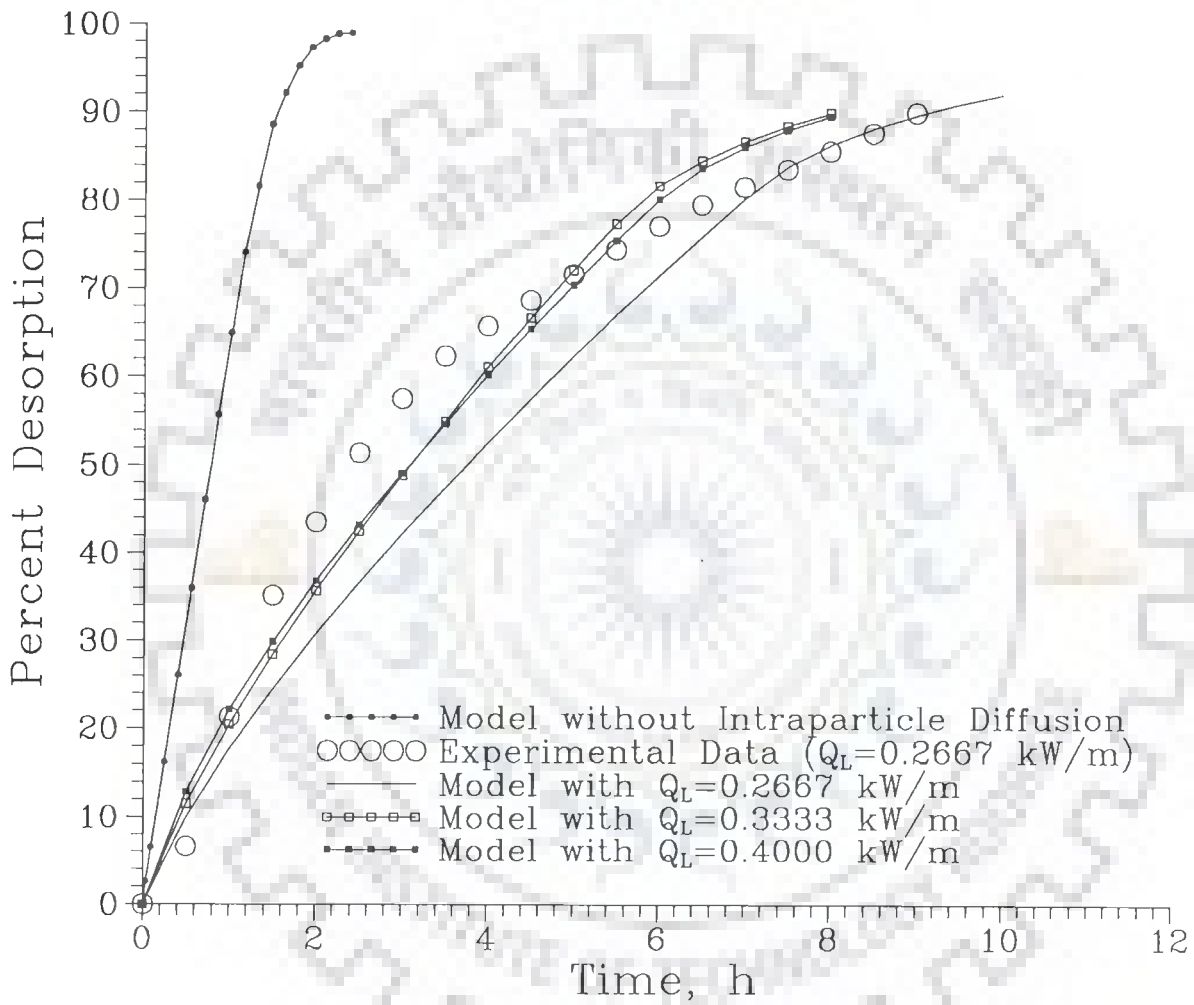


Figure 6.4-15 Percent Desorption vs. Time Profiles for Different Heater Wattages (Experiment-A)

after 7 hour time is about 86% for the heater with  $Q_L = 0.3333$  or  $0.4000$  kW/m, while it is less than 80% for heater with  $Q_L = 0.2667$  kW/m .

From the experiment, it has been observed that the adsorption time for experiment-A is more than 9.5 hour. It is desired that the desorption/regeneration time should be normally less than the adsorption time. In view of this, optimal heater wattage for the bed of experiment-A is  $0.3333$  kW/m. This would permit 86% recovery of adsorbate within about 7 hour period. Thereafter, it is not economical (from the energy consumption point of view) to operate the desorber as diffusivity would be low due to low adsorbate concentration existing everywhere in the bed and it would require significantly large time for the complete desorption of the bed.

#### 6.4.3 Computational Aspects

As described in the section 6.2, simplified model has been solved by using the computational algorithm, developed on the basis of control volume finite difference method (Chapter V). The algorithm is programmed in FORTRAN 77 and executed on a PC-AT 486 (DX2, 66 MHz) Personal Computer.

After conducting several numerical experiments, it has been found that a step size ( $\Delta t$ ) of 15 s in time is appropriate for solving the model with constant diffusivity, i.e.  $D_e = 3 \times 10^{-11}$  m<sup>2</sup>/s. As the value of diffusivity is increased,  $\Delta t$  is to be reduced accordingly for obtaining the convergence. It is interesting to note that for  $D_e = 1 \times 10^{-9}$  m<sup>2</sup>/s, appropriate value of  $\Delta t$  is 0.5 s. When the diffusivity correlation is used in the model, then the diffusivity varies from very large to smaller values during desorption. Due to this reason, computer times required for solving the model with constant diffusivity ( $D_e = 3 \times 10^{-11}$  m<sup>2</sup>/s) and variable diffusivity correlation are 3 1/2 and 9 hour respectively. With such a large requirement of computer time, it is not possible to estimate the parameter(s) of model by using the

experimental data, and thus, this problem has not been attempted.

## 6.5 CONCLUDING REMARKS

In this chapter a mathematical model has been developed for the modified thermal desorption process in which energy required for the desorption is provided by the coaxial electrical heater, imbedded into the bed of molecular sieves. The present model takes into account intraparticle diffusion, which was not considered in the earlier studies [Prasad (1988)]. Based on this, a simplified model has also been obtained, which assumes parabolic concentration profile within the zeolite crystal.

Numerical solution of the simplified model has been obtained by modifying the algorithm, already developed in the Chapter V. The model predictions with constant diffusivity have been compared with those observed in two experiments for water vapour - 13X MS adsorbate-adsorbent system. It is found that the percent desorption profile with time is close to the experimental one in last quarter of the desorption period for both the experiments. In order to improve the predictions during first half period of desorption, a correlation for the diffusivity of adsorbate within zeolite crystal has been proposed. Most of the experimental observations are within  $\pm 25\%$  deviation with respect to the model predictions using diffusivity correlation. The deviation is attributed to the fact that the model assumes linear isotherm. It is our view that the simplified model, developed in the present study, represents the behaviour of this desorption process reasonably well and therefore, it may be used for the simulation and design of units employing it.

---

## CONCLUSIONS AND RECOMMENDATIONS

---

### 7.1 CONCLUSIONS

In the present thesis, a packed bed thermal desorption process has been studied. This process utilizes heat supplied by the electrical heater, which is imbedded into the bed. Advantage of the process is that it is energy efficient and also allows the recovery of adsorbate in pure form. Adsorbate - adsorbent system considered in the studies is water vapour - 13X molecular sieves. Main emphasis in the research work has been given on three aspects, namely Characterization of 13X molecular sieves, Estimation of temperature dependency of effective thermal conductivity of a bed of 13X molecular sieves, and Mathematical modelling of thermal desorption process. Accordingly, the conclusions have been described section-wise as given below.

#### Characterization of 13X Molecular Sieves

13X molecular sieves, manufactured by M/s Indian Petrochemicals Corporation Ltd., CATAD Division, Thane, India, have been used in the present study. Characterization of these molecular sieves has been done by determining various properties, e.g. surface area and total micropore volume, by using adsorption measurements. For this purpose, various available methods, viz. BET, Langmuir, t-Plot, Dubinin-Radushkevich (DR) equation and Dubinin-Astakhov (DA) equation, have been used. Adsorption measurements have been done using two gaseous adsorbates - nitrogen and argon, which are having a symmetric molecule and are nonpolar in nature.

Computational algorithm and software have been developed to use adsorption measurement data in DR and DA equations. A software for

estimation of two parameters in DA equation has also been developed; one of them, i.e. exponent  $n$ , is of direct use. Besides, statistical analysis of estimated parameters has been carried out by plotting 99.95% confidence limits of predicted values and a contour for 95% joint confidence region. The analysis shows that the estimated parameters are correlated, and their values are correct. Value of exponent,  $n$ , in DA equation has been found to be 1.95 and 1.78 for nitrogen and argon adsorption on 13X molecular sieves, respectively.

Critical analyses of the methods used and the results obtained have been carried out. It is concluded from the analysis that

- the exponent, 2, used in DR equation can be safely used for the determination of micropore volume and surface area of 13X molecular sieves. This enables one to avoid the use of DA equation which is relatively cumbersome and time consuming as it requires estimation of the value of exponent,  $n$ .
- the surface area obtained from BET method is approximately 17-25% less than that of Langmuir's method, DR equation, and DA equation with the two adsorbates used in the present study. This observation is also in agreement with the observations made in literature. The values of surface area and micropore volume of 13X molecular sieves have been found to be  $755.8 \text{ m}^2/\text{g}$  and  $0.2686 \text{ cm}^3/\text{g}$  respectively. The results obtained are closely in agreement with the values reported in literature.

#### Estimation of Temperature Dependency of Effective Thermal Conductivity of a Bed of 13X Molecular Sieves

First, an experimental unit has been designed and fabricated to obtain transient radial temperature profiles in a bed of molecular sieves. The unit consists mainly of a cylindrical column

(I.D. = 94 mm, Height = 600 mm) packed with 13X molecular sieves. An electrical heater was imbedded into the bed coaxially to provide thermal energy. In order to measure transient radial temperature profiles, the bed was heated under dry conditions using two heater wattages, e.g. 0.1 and 0.13333 kW/m.

A PC based on-line data acquisition system has been developed on an existing data logger. A software has been developed in C language to acquire, display and store the measured temperatures at desired locations. The software is of 6400 lines code. It is interactive, user friendly, and possesses several advanced features such as context sensitive help and security of data against power failure. The data acquisition software is general in application as it can also be used to acquire three types of other commonly measured variables, viz. DC voltage, AC voltage, and resistance.

Furthermore, dependency of effective thermal conductivity of a bed of 13X molecular sieves on temperature has been estimated by using transient radial temperature profiles obtained in the dry bed. Effective thermal conductivity,  $k$ , has been estimated to vary linearly with temperature  $T$ . The correlation obtained for  $k$  is as follows :

$$k(T) = 8.17635 \times 10^{-5} + 10.915427 \times 10^{-7}(T - T_0) \quad (5.4-4)$$

where  $T_0 = 303 \text{ K}$ .

The values predicted by above correlation are in agreement with the values reported in literature for catalytic and other similar materials.

According to the correlation, effective thermal conductivity of a packed bed of 13X molecular sieves varies from  $8.18 \times 10^{-5}$  to  $22.15 \times 10^{-5}$  kW/m K for a temperature range of 303-431 K. It is interesting to note that the variation in  $k(T)$  is almost three times for a temperature increase of about 130 °C. Thus, an important conclusion of this study is that this variation in  $k$  due to temperature

should be properly accounted for in the modelling and simulation studies.

Statistical analysis of the estimated parameters of correlation has been carried out by plotting the joint confidence contour for an approximate 95% confidence level. Although, the dependence of  $k$  on  $T$  is linear but its use in the model partial differential equations meant for estimation of parameters results into a nonlinear estimation problem. Therefore, the joint confidence contour plotted is of deflated banana shape in a two parameter space. The elongated shape of the contour indicates that the estimated parameters are highly correlated.

During the estimation of  $k(T)$ , temperatures at selected radial locations are to be predicted by numerically solving the model equations [5.2-1a & b, 5.2-2a, b & c]. A computational algorithm has been developed for this purpose, which utilizes the control volume finite difference method. This method has the advantage of satisfying the conservation equations in the discretized form even if the discretization grid is coarse. The algorithm is general in nature, and may be employed to estimate linear as well as nonlinear dependence of  $k$  on temperature.

#### Mathematical Modelling of Thermal Desorption Process

A mathematical model has been developed for the thermal desorption process, which also includes the diffusion of adsorbate in the MS pellet. The model consists of partial differential equations for the bed as well as for the pellet. These are given in Table 6.1-1 alongwith appropriate initial and boundary conditions, and constitutive relationships.

The numerical solution of model equations is complex and requires large computer time. Due to this reason, model has been simplified by assuming that the adsorbate concentration profile within the MS pellet is parabolic in shape with respect to radius. This



assumption is true in almost all of the cases and all the times [Yang (1987)]. The simplified model is summarized in Table 6.1-2.

The computational algorithm, developed in Chapter V, has been modified to make it applicable for the solution of simplified model. Comparison of model predictions with constant diffusivity have been made with the available data for two experiments. It is observed that the percent desorption profile with time is close to the experimental one in the last quarter of the desorption period. The deviation between predicted and experimental values in earlier period may be attributed to the linearity of adsorption isotherm and the constancy of diffusivity, considered in the model. Later, dependence of diffusivity on concentration has also been considered to improve the model predictions.

From the numerical simulation of this process, it has been concluded that

- the thermal desorption of water vapour from 13X molecular sieves is mainly controlled by intraparticle diffusion of adsorbate, which was not considered in the earlier model [Prasad (1988)].
- the effective diffusivity of water vapour in molecular sieves depends strongly on concentration. Following relationship adequately represents the concentration dependence of diffusivity in 13X molecular sieves.

$$D(q) = \frac{D_o}{\left(1 - \alpha_2 \frac{q}{q_s}\right)^2}, \quad (6.4-4)$$

where  $\alpha_2 = 0.87753$  and  $D_o = 1.5 \times 10^{-11} \text{ m}^2/\text{s}$ .

Furthermore, the increase in heat flux to the bed by increasing the heater wattage is expected to make the desorption process faster. But, increase in heater wattage beyond 0.3333 kW/m does

not affect the desorption process significantly, because the heater surface attains the maximum temperature of 523 K within half an hour only, and thereafter, it starts switching -off and -on. Thus, a heater wattage of 0.3333 kW/m is most suitable for the system, studied in the thesis.

### 7.1.1 Final Remarks

---

It is our view that the research work carried out in the thesis has a wide scope for applications in industry. The technique of desorption and the proposed model will be useful in the applications where recovery of adsorbate is a must to improve the economics of the process. This type of system is particularly suitable for smaller units which are used for mobile purposes/vehicles.

The developed model can also be used for modelling the desorption from a large size adsorption column used in the process industries. In such a case, multiple heaters imbedded into the bed on a specific pattern, e.g. triangular, shall be used as a source of thermal energy. The computational algorithm developed for a single heater can also be used for this system with little modification, but it may require a large computer time. Fortunately, with the development of fast computing machines, solution of model equations for desorption with diffusional transport considerations for a large grid size is now feasible.

## 7.2 RECOMMENDATIONS FOR FUTURE WORK

- (i) In the thesis, a correlation has been developed for the effective thermal conductivity of a bed of 13X molecular sieves (equation 5.4-4). In order to examine its validity for other types of molecular sieves, it is desirable to conduct experiments with them, related to dry bed conduction studies.
- (ii) Constitutive relationships play an important role in modelling

and simulation studies. Therefore, efforts may be devoted to determine experimentally the concentration dependence of diffusivity of water vapour within 13X molecular sieves. This would improve the predictions of proposed model during the entire period of desorption.

- (iii) As the solution of model equations requires large computer time, therefore, it would be advantageous to develop efficient computational algorithms to solve the mathematical model of desorption process with linear and nonlinear isotherms.
- (iv) In order to widen the scope of application of this thermal desorption process, it is recommended that both the modelling and experimental studies may be carried out on the desorption of multicomponent mixtures.



## LIST OF RESEARCH PUBLICATIONS

### [A] Published

1. Estimation of Temperature - Dependent Thermal Conductivity of a Packed Bed of 13X Molecular Sieves, *Ind. Eng. Chem. Res.*, **34** (11), pp. 4058-4062, **1995**.
2. Characterization of Zeolite Molecular Sieves by Dubinin-Radushkevich Equation, in **Abstracts and Invited Lectures**, *Indian Chemical Engineering Congress 1995, 48th Annual Session of Indian Institute of Chemical Engineers, December 27-30, 1995, Kalpakkam (T.N.), India*, pp. 138-139.

### [B] Communicated

3. Determination of Micropore Volume and Surface Area of Molecular Sieves by Dubinin-Radushkevich and Dubinin-Astakhov Equations: A Comparative Study, to *Ind. Eng. Chem. Res.*
4. Studies on Packed Bed Thermal Desorption Process using Embedded Electrical Heaters - Development of a Mathematical Model, to *Ind. Eng. Chem. Res.*

---

## REFERENCES

---

**Adams, C.R., A.F. Sartor, and J.G. Welch (1974)**

AICHe Symp. Ser., 70(143), pp.49-54

*Some Practical Problems in Achieving Standardization of Catalyst Testing*

**Anderson, J.R. and K.C. Pratt (1985)**

Academic Press, Sydney

*Introduction to Characterization and Testing of Catalysts*

**Antonson, C.R. and J.S. Dranoff (1967)**

Chem. Eng. Prog. Symp. Ser., 63(74), pp.61-67

*The Kinetics of Ethane Adsorption on Molecular Sieves*

**Aziz, A. (1988)**

In "Handbook of Numerical Heat Transfer," W.J. Minkowycz, E.M. Sparrow, G.E. Schneider, and R.H. Pletcher (Eds.), John Wiley & Sons, New York, pp.625-671

*Perturbation Methods*

**Baksh, M.S.A. and R.T. Yang (1991)**

AICHe J., 37(6), pp.923-930

*Model for Spherical Cavity Radii and Potential Functions of Sorbates in Zeolites*

**Barrer, R.M. (1971)**

Adv. Chem. Ser., (102), pp.1-35

*Intracrystalline Diffusion*

**Barrer, R.M. (1978)**

Academic Press, London

*Zeolites and Clay Minerals as Sorbents and Molecular Sieves*

**Barrett, E.P., L.G. Joyner, and P.P. Halenda (1951)**

J. Am. Chem. Soc., 73(1), pp.373-380

*The Determination of Pore Volume and Area Distributions in Porous Substances. I. Computations from Nitrogen Isotherms*

**Beaver, E.R. (1974)**

AIChE Symp. Ser., 70(143), pp.1-4

*Mechanical Testing of Extruded, Tableted, and Ring-Formed Catalysts*

**Bering, B.P., M.M. Dubinin, and V.V. Serpinsky (1966)**

J. Colloid Interface Sci., 21(2), pp.378-393

*Theory of Volume Filling for Vapor Adsorption*

**Bhambhani, M.R., P.A. Cutting, K.S.W. Sing, and D.H. Turk (1972)**

J. Colloid Interface Sci., 38(1), pp.109-117

*Analysis of Nitrogen Adsorption Isotherms on Porous and Nonporous Silicas by the BET and  $\alpha_s$  Methods*

**Bird, R.B., W.E. Stewart, and E.N. Lightfoot (1960)**

John Wiley & Sons, New York

*Transport Phenomena*

**Breck, D.W. (1974)**

John Wiley & Sons, New York

*Zeolite Molecular Sieves : Structure, Chemistry, and Use*

**Breck, D.W. (1980)**

In "The Properties and Applications of Zeolites," R.P. Townsend (Ed.), Special Publication No. 33, The Chemical Society, London, pp.391-422

*Potential Uses of Natural and Synthetic Zeolites in Industry*

**Broekhoff, J.C.P. and B.G. Linsen (1970)**

In "Physical and Chemical Aspects of Adsorbents and Catalysts," B.G. Linsen (ed.), Academic Press, London, pp.1-62

*Studies on Pore Systems in Adsorbents and Catalysts*

**Broekhoff, J.C.P. and R.H. van Dongen (1970)**

In "Physical and Chemical Aspects of Adsorbents and Catalysts," B.G. Linsen (ed.), Academic Press, London, pp.63-146

*Mobility and Adsorption on Homogeneous Surfaces : A Theoretical and Experimental Study*

**Broussard, L. and D.P. Shoemaker (1960)**

J. Am. Chem. Soc. **82**(5), pp.1041-1051

*The Structures of Synthetic Molecular Sieves*

**Brown, M.G. and D.A. Cadenhead (1979)**

J. Colloid Interface Sci., **70**(1), pp.139-146

*A Comparative Porosity Study of Active Carbons*

**Brunauer, S., J. Skalny, and E.E. Bodor (1969)**

J. Colloid Interface Sci., **30**(4), pp.546-552

*Adsorption on Nonporous Solids*

**Brunauer, S., J. Skalny, and I. Odler (1973)**

Pore Structure and Properties of Materials, (S. Modry, Ed.), vol.1, p. C-3, Academia, Prague

—————[Cited in Dubinin (1974)]

**Brunauer, S., L.S. Deming, W.E. Deming, and E. Teller (1940)**

J. Am. Chem. Soc., **62**(7), pp.1723-1732

*On a Theory of the van der Waals Adsorption of Gases*

**Brunauer, S., P.H. Emmett, and E. Teller (1938)**

J. Am. Chem. Soc., **60**(2), pp.309-319

*Adsorption of Gases in Multimolecular Layers*

**Cahen, R.M. and J. Marechal (1963)**

Anal. Chem., **35**(2), pp.259-260

*Surface Area Determination by the Continuous Flow Method*

**Carslaw, H.S. and J.C. Jaeger (1959)**

Clarendon Press, Oxford

*Conduction of Heat in Solids*

**Carter, J.W. (1966)**

Trans. Instn. Chem. Engrs., **44**(7), pp.T253-T259

*A Numerical Method for Prediction of Adiabatic Adsorption in Fixed Beds*

**Carter, J.W. (1968a)**

Trans. Instn. Chem. Engrs., **46**(7), pp.T213-T222

*Isothermal and Adiabatic Adsorption in Fixed Beds*

**Carter, J.W. (1968b)**

Trans. Instn. Chem. Engrs., **46**(7), pp.T222-T224

*Some Aspects of the Prediction of Performance of a Large Air-Dryer*

**Carter, J.W. (1969)**

Brit. Chem. Eng., **14**(3), 303-306

*Scale-up in the Design of Fixed Bed Adsorption Plant*

**Carter, J.W. (1980)**

In "The Properties and Applications of Zeolites," R.P. Townsend (Ed.),  
Special Publication No. 33, The Chemical Society, London, pp.76-91

*The Adsorption Separation Process*

**Carter, J.W. and D.J. Barrett (1973)**

Trans. Instn. Chem. Engrs., **51**(2), pp.75-81

*Comparative Study for Fixed Bed Adsorption of Water Vapour by Activated Alumina, Silica Gel, and Molecular Sieve Adsorbents*

**Chihara, K. and M. Suzuki (1983)**

J. Chem. Eng. Japan, **16**(4), pp.293-299

*Air Drying by Pressure Swing Adsorption*



**Coberly, C.A. and W.R. Marshall, Jr. (1951)**

Chem. Eng. Prog., **47**(3), pp.141-150

*Temperature Gradients in Gas Streams Flowing through Fixed Granular Beds*

**Collins, J.J. (1967)**

Chem. Eng. Prog. Symp. Ser., **63**(74), pp.31-35

*The LUB/Equilibrium Section Concept for Fixed-Bed Adsorption*

**Collins, J.J. (1968)**

Chem. Eng. Prog., **64**(8), pp.66-71

*Where to Use Molecular Sieves*

**Danner, R.P. and E.C.P. Chol (1978)**

Ind. Eng. Chem. Fundam., **17**(4), pp.248-253

*Mixture Adsorption Equilibria of Ethane and Ethylene on 13X Molecular Sieves*

**Dart, J.C. (1974)**

AIChE Symp. Ser., **70**(143), pp.5-8

*Mechanical Tests to Determine Strength and Abrasion Resistance of Catalysts*

**Davis, M.E. (1991)**

Ind. Eng. Chem. Res. **30**(8), pp.1675-1683

*Zeolites and Molecular Sieves : Not Just Ordinary Catalysts*

**De Boer, J.H., B.G. Linsen, Th. van der Plas, and G.J. Zondervan (1965)**

J. Catal., **4**(6), pp.649-653

*Studies on Pore Systems in Catalysts : VII. Description of the Pore Dimensions of Carbon Blacks by the t Method*

**De Wasch, A.P. and G.F. Froment (1972)**

Chem. Eng. Sci., **27**(3), pp.567-576

*Heat Transfer in Packed Beds*

**Do, D.D. and P.L.J. Mayfield (1987)**

AICHE J., **33**(8), pp.1397-1400

*A New Simplified Model for Adsorption in a Single Particle*

**Dollimore, D. and G.R. Heal (1964)**

J. Appl. Chem., **14**(3), pp.109-114

*An Improved Method for the Calculation of Pore Size Distribution from Adsorption Data*

**Doraiswamy, L.K. and M.M. Sharma (1984)**

John Wiley & Sons, New York

*Heterogeneous Reactions : Analysis, Examples, and Reactor Design; vol.1; Gas-Solid and Solid-Solid Reactions*

**Draper, N.R. and H. Smith (1966)**

John Wiley & Sons, New York, First edition

*Applied Regression Analysis*

**Dubinin, M.M. (1967)**

J. Colloid Interface Sci., **23**(4), pp.487-499

*Adsorption in Micropores*

**Dubinin, M.M. (1974)**

J. Colloid Interface Sci., **46**(3), pp.351-356

*On Physical Feasibility of Brunauer's Micropore Analysis Method*

**Dubinin, M.M. and H.F. Stoeckli (1980)**

J. Colloid Interface Sci., **75**(1), pp.34-42

*Homogeneous and Heterogeneous Micropore Structures in Carbonaceous Adsorbents*

**Dubinin, M.M., V.A. Astakhov (1971)**

Adv. Chem. Ser., (102), pp.69-85

*Description of Adsorption Equilibria of Vapors on Zeolites Over Wide Ranges of Temperature and Pressure*

**Eberly, P.E. Jr., (1961)**

J. Phys. Chem., 65(7), pp.1261-1265

*Measurement of Adsorption Isotherms and Surface Areas by Continuous Flow Method*

**Finlayson, B.A. (1972)**

Academic Press, New York, U.S.A.

*The Method of Weighted Residuals and Variational Principles*

**Friday, D.K. and M.D. Levan (1982)**

AIChE J., 28(1), pp.86-91

*Solute Condensation in Adsorption Beds During Thermal Regeneration*

**Garg, D.R. and D.M. Ruthven (1972)**

Chem. Eng. Sci., 27(2), pp.417-423

*The Effect of the Concentration Dependence of Diffusivity on Zeolite Sorption Curves*

**Garg, D.R. and D.M. Ruthven (1973a)**

Chem. Eng. Sci., 28(3), pp.791-798

*Theoretical Prediction of Breakthrough Curves for Molecular Sieve Adsorption Columns-I : Asymptotic Solutions*

**Garg, D.R. and D.M. Ruthven (1973b)**

Chem. Eng. Sci., 28(3), pp.799-805

*Theoretical Prediction of Breakthrough Curves for Molecular Sieve Adsorption Columns-II : General Isothermal Solution for Micropore Diffusion Control*

**Garg, D.R. and D.M. Ruthven (1974a)**

Chem. Eng. Sci., 29(2), pp.571-581

*The Performance of Molecular Sieve Adsorption Columns : Systems with Micropore Diffusion Control*

**Garg, D.R. and D.M. Ruthven (1974b)**

Chem. Eng. Sci., 29(9), pp.1961-1967

*The Performance of Molecular Sieve Adsorption Columns : Systems with Macropore Diffusion Control*

**Garg, D.R. and D.M. Ruthven (1975a)**

AIChE J., 21(1), pp.200-202

*Linear Driving Force Approximations for Diffusion Controlled Adsorption in Molecular Sieve Columns*

**Garg, D.R. and D.M. Ruthven (1975b)**

Chem. Eng. Sci., 30(9), pp.1192-1194

*Performance of Molecular Sieve Adsorption Columns: Combined Effects of Mass Transfer and Longitudinal Diffusion*

**Haefner, D.R. and G. Thodos (1986)**

Ind. Eng. Chem. Fundam., 25(4), pp.498-503

*Transient Sorption of Water Vapour from Air Flowing Through Beds of Zeolite 13X*

**Harkins, W.D. and G. Jura (1944)**

J. Am. Chem. Soc., 66(6), pp.919-927

*Surface of Solids. X. Extension of the Attractive Energy of a Solid into an Adjacent Liquid or Film, the Decrease of Energy with Distance, and the Thickness of Films*

**Harriott, P. (1975)**

Chem. Eng. J. 10(1), pp.65-71

*Thermal Conductivity of Catalyst Pellets and Other Porous Particles. Part I : Review of Models and Published Results*

**Hersh, C.K. (1961)**

Reinhold Publishing Corporation, New York

*Molecular Sieves*

**Hills, J.H. (1991)**

Chem. Eng. Sci., **46**(1), pp.69-74

*Non-Isothermal Adsorption in a Pellet*

**Himmelblau, D.M. (1970)**

John Wiley & Sons, New York

*Process Analysis by Statistical Methods*

**Himmelblau, D.M. (1972)**

McGraw-Hill Book Co., New York

*Applied Nonlinear Programming*

**Holman, J.P. (1976)**

McGraw-Hill Kogakusha Ltd., Tokyo

*Heat Transfer*

**Hong, A., R.K. Mariwala, M.S. Kane, and H.C. Foley (1995)**

Ind. Eng. Chem. Res., **34**(3), pp.992-996

*Adsorbate Shape Selectivity: Separation of the HF/134a Azeotrope over Carbogenic Molecular Sieve*

**Horváth, G. and K. Kawazoe (1983)**

J. Chem. Eng. Japan, **16**(6), pp.470-475

*Method for Calculation of Effective Pore Size Distribution in Molecular Sieve Carbon*

**Hougen, O.A. and W.R. Marshall, Jr. (1947)**

Chem. Eng. Prog., **43**(4), pp.197-208

*Adsorption from a Fluid Stream Flowing through a Stationary Granular Bed*

**Huang, C.C. and J.R. Fair (1988)**

AIChE J., **34**(11), pp.1861-1877

*Study of the Adsorption and Desorption of Multiple Adsorbates in a Fixed Bed*

- Hyun, S.H. and R.P. Danner (1985)**  
AIChE J., 31(7), pp.1077-1085  
*Adsorption Equilibrium Constants and Intraparticle Diffusivities in Molecular Sieves by Tracer-Pulse Chromatography*
- Innes, W.B. (1968)**  
In "Experimental Methods in Catalytic Research," vol. I, Edited by B. Anderson, Academic Press Inc., New York, pp.44-99  
*Surface Area and Pore Structure Determination*
- Inui, T., Y. Okugawa, and M. Yasuda (1988)**  
Ind. Eng. Chem. Res., 27(7), pp.1103-1109  
*Relationship between Properties of Various Zeolites and Their CO<sub>2</sub>-Adsorption Behaviors in Pressure Swing Adsorption Operation*
- James, M.L., G.M. Smith, and J.C. Wolford (1977)**  
IEC - A Dun - Donnelley Publisher, New York  
*Applied Numerical Methods for Digital Computation with FORTRAN and CSMP*
- Jury, S.H. and J.S. Horng (1973)**  
AIChE J., 19(2), pp.371-372  
*The Molecular Sieve 4-A Water Vapor Sorption Therm*
- Kärger, J. and D.M. Ruthven (1992)**  
John Wiley & Sons, Inc., New York  
*Diffusion in Zeolites: and other Microporous Solids*
- Kumar, R. and G.R. Dissinger (1986)**  
Ind. Eng. Chem. Process Des. Dev., 25(2), pp.456-464  
*Nonequilibrium, Nonisothermal Desorption of Single Adsorbate by Purge*
- Kumar, S., Shashi and A. Pethö (1993)**  
Commun. Numer. Methods Eng., 9(4), pp.353-359  
*An Algorithm for the Numerical Inversion of a Tridiagonal Matrix*

**Lee, H.H. (1985)**

Butterworth Publishers, Boston

*Heterogeneous Reactor Design*

**Lamond, T.G. and C.R. Price (1969)**

J. Colloid Interface Sci., **31**(1), pp.104-110

*Size of Carbon Black Micropores Deduced from Nitrogen and Dye Adsorption*

**Lee, H. and W.P. Cummings (1967)**

Chem. Eng. Prog. Symp. Ser., **63**(74), pp.42-49

*A New Design Method for Silica Gel Air Driers Under Nonisothermal Conditions*

**Lerou, J.J. and G.F. Froment (1978)**

Chem. Eng. J., **15**(3), pp.233-237

*Estimation of Heat Transfer Parameters in Packed Beds from Radial Temperature Profiles*

**Li, C.H. and B.A. Finlayson (1977)**

Chem. Eng. Sci., **32**(9), pp.1055-1066

*Heat Transfer in Packed Beds - A Reevaluation*

**Liaw, C.H., J.S.P. Wang, R.A. Greenkorn, and K.C. Chao (1979)**

AIChE J., **25**(2), pp.376-381

*Kinetics of Fixed-Bed Adsorption : A New Solution*

**Lippens, B.C., B.G. Linsen, and J.H. de Boer (1964)**

J. Catal., **3**(1), pp.32-37

*Studies on Pore Systems in Catalysts I. The Adsorption of Nitrogen; Apparatus and Calculation*

**Lippens, B.C. and J.H. de Boer (1965)**

J. Catal., **4**(3), pp.319-323

*Studies on Pore Systems in Catalysts V. The  $t$  Method*

**Malecký, M., M. Marek, K. Kubiček, and J. Schöngut (1991)**

Int. Chem. Eng., 31(4), pp.708-714

*Mathematical Modeling of an Adsorption Column with Thermal Regeneration*

**Mantell, C.L. (1951)**

McGraw-Hill Book Co., New York

*Adsorption*

**Marcussen, L. (1970)**

Chem. Eng. Sci., 25(9), pp.1487-1499

*The Kinetics of Water Adsorption on Porous Alumina*

**Marcussen, L. (1982)**

Chem. Eng. Sci., 37(2), pp.299-309

*Comparison of Experimental and Predicted Breakthrough Curves for Adiabatic Adsorption in Fixed Bed*

**Marcussen, L. and C. Vinding (1982)**

Chem. Eng. Sci., 37(2), pp.311-317

*Experimental Breakthrough Curves Determined Under Carefully Controlled Conditions for the Adsorption of Water Vapour on Alumina in Adiabatic Fixed Beds*

**Marsh, H. and B. Rand (1970)**

J. Colloid Interface Sci., 33(1), pp.101-116

*The Characterization of Microporous Carbons by Means of the Dubinin-Radushkevich Equation*

**Mathews, J.H. (1994)**

Prentice-Hall of India, New Delhi

*Numerical Methods for Mathematics, Science, and Engineering*

**Meier, W.M. and D.H. Olson (1971)**

Adv. Chem. Ser., (101), pp.155-170

*Zeolite Frameworks*



**Michelsen, M.L. (1979)**

Chem. Eng. J., 18(1), pp.67-72

*Estimation of Heat Transfer Parameters in Packed Beds from Radial Temperature Measurements*

**Micromeritics Corporation (1993)**

Micromeritics Multipoint Surface Area and Pore Volume Analyser ASAP 2000 M V 3.00

*Operator's Manual*

**Mikhail, R.Sh., S. Brunauer, and E.E. Bodor (1968a)**

J. Colloid Interface Sci., 26(1), pp.45-53

*Investigations of a Complete Pore Structure Analysis : I. Analysis of Micropores*

**Mikhail, R.Sh., S. Brunauer, and E.E. Bodor (1968b)**

J. Colloid Interface Sci., 26(1), pp.54-61

*Investigations of a Complete Pore Structure Analysis : II. Analysis of Four Silica Gels*

**Nelsen, F.M. F.T. Eggertsen (1958)**

Anal. Chem., 30(8), pp.1387-1390

*Determination of Surface Area: Adsorption Measurements by a Continuous Flow Method*

**Nutter, J.I. and G. Burnet, Jr. (1966)**

Ind. Eng. Chem. Process Des. Dev., 5(1), pp.1-5

*Fixed Bed Drying of Air Using Molecular Sieves*

**Özisik, M.N. (1981)**

McGraw-Hill International Book Co., Tokyo

*Basic Heat Transfer*

**Parfitt, G.D., K.S.W. Sing, and D. Urwin (1975)**

J. Colloid Interface Sci., 53(2), pp.187-193

*The Analysis of the Nitrogen Adsorption Isotherms of Microporous Materials*

**Patankar, S.V. (1980)**

Hemisphere Publishing Corporation, Washington

*Numerical Heat Transfer and Fluid Flow*

**Ponec, V., Z. Knor, and S. Černý (1974)**

In "Adsorption on Solids," English Translation edited by D. Smith, and N.G. Adams, Butterworths, London, pp.540-595

*Practical Applications of Adsorption*

**Prasad, R. (1988)**

Ph.D. Dissertation, Deptt. of Chemistry, University of Roorkee, Roorkee, India

*Studies of Adsorption/Desorption in Packed Bed of Molecular Sieves*

**Punwani, D., C.W. Chi, and D.T. Wasan (1968)**

Ind. Eng. Chem. Process Des. Dev., 7(3), pp.410-415

*Dynamic Sorption by Hygroscopic Salts*

**Rand, B. (1976)**

J. Colloid Interface Sci., 56(2), 337-346

*On the Empirical Nature of the Dubinin-Radushkevich Equation of Adsorption*

**Rao, S.S. (1978)**

Wiley Eastern Ltd., New Delhi

*Optimization Theory and Applications*

**Rice, R.G. (1982)**

Chem. Eng. Sci., 37(1), pp.83-91

*Approximate Solutions for Batch, Packed Tube and Radial Flow Adsorbers-Comparison with Experiment*

**Rosen, J.B. (1952)**

J. Chem. Phys., 20(3), pp.387-394

*Kinetics of a Fixed Bed System for Solid Diffusion into Spherical Particles*

**Ruthven, D.M. (1980)**

In "The Properties and Applications of Zeolites," R.P. Townsend (Ed.),  
Special Publication No. 33, The Chemical Society, London, pp.43-57  
*Diffusion in Zeolites: A Review of Recent Progress*

**Ruthven, D.M. (1984)**

John Wiley & Sons, New York

*Principles of Adsorption and Adsorption Processes*

**Ruthven, D.M. and K.F. Loughlin (1971)**

AICHE Symp. Ser., 67(117), pp.35-42

*Diffusion in Molecular Sieves*

**Saito, A. and H.C. Foley (1991)**

AICHE J., 37(3), pp.429-436

*Curvature and Parametric Sensitivity in Models for Adsorption in Micropores*

**Sastry, S.S. (1990)**

Prentice-Hall of India, New Delhi

*Introductory Methods of Numerical Analysis*

**Satterfield, C.N. (1980)**

McGraw-Hill Book Co., New York

*Heterogeneous Catalysis in Practice*

**Schoofs, G.R. (1992)**

AICHE J., 38(9), pp.1385-1394

*Fire and Explosion Hazards Induced by Re-pressurization of Air Driers*

**Seifert, J. and G. Emig (1991)**

Int. Chem. Eng., 31(1), pp.29-41

*Studies of the Microstructures of Porous Solids by Physisorption Measurements*

**Shibuya, H. and K. Kawazoe (1978)**

J. Chem. Eng. Japan, 11(3), pp.239-241

*Diffusion of Heavy Water in Commercial Adsorbent Particles*

**Towler, B.F. and R.G. Rice (1974)**

Chem. Eng. Sci., 29(8), pp.1828-1832

*A Note on the Response of a CSTR to a Spherical Catalyst Pellet*

**Tsang, T.H., T.F. Edgar, and J.O. Hougen (1976)**

Chem. Eng. J., 11(1), pp.57-66

*Estimation of Heat Transfer Parameters in a Packed Bed*

**Vermeulen, T. (1978)**

In "Kirk-othmer Encyclopedia of Chemical Technology," 3rd ed., vol.1,  
John Wiley & Sons, New York, pp.531-544

*Adsorptive Separation*

**Villadsen, J. and M.L. Michelsen (1978)**

Prentice-Hall, Inc., Englewood Cliffs, N.J. 07632

*Solution of Differential Models by Polynomial Approximation*

**Weiner, A.L. (1974)**

Chem. Eng., 81(19), Sept. 16, pp.92-101

*Drying Gases and Liquids : Dynamic Fluid Drying*

**Weisz, P.B. (1995)**

Ind. Eng. Chem. Res., 34(8), pp.2692-2699

*Molecular Diffusion in Microporous Materials: Formalisms and Mechanisms*

**Xiu, G.H. and N. Wakao (1993)**

AIChE J., 39(12), pp.2042-2044

*Batch Adsorption : Intraparticle Adsorbate Concentration Profile Models*

**Yang, R.T. (1987)**

Butterworths, Boston

*Gas Separation by Adsorption Processes*

**Yang, R.T. and S.J. Doong (1985)**

AIChE J., **31**(11), pp.1829-1842

*Gas Separation by Pressure Swing Adsorption: A Pore Diffusion Model for Bulk Separation*

**Zwiebel, I. R.L. Gariepy, and J.J. Schnitzer (1972)**

AIChE J., **18**(6), pp.1139-1148

*Fixed Bed Desorption Behaviour of Gases with Non-Linear Equilibria : Part I. Dilute, One Component, Isothermal Systems*



**COMPARISON OF EXPERIMENTALLY OBSERVED TEMPERATURES  
WITH THOSE PREDICTED BY USING  $\bar{k}$  AND  $k(T)$  CORRELATION**

The comparison in this appendix pertains to section 5.4.1 of Chapter V. Correlation and value of parameter used are given below.

$$(i) \quad k(T) = 8.1722 \times 10^{-5} + 9.80664 \times 10^{-7} (T - T_o) \quad (5.4-1)$$

$$(ii) \quad \bar{k} = 1.444845 \times 10^{-4} \text{ kW/m K (Range of Temp. 303 - 431 K)}$$

**Table A.1 Experimentally Observed Temperatures and Temperatures Predicted Using  $\bar{k}$  and  $k(T)$  relationship alongwith their Percent Deviations for  $Q_L=0.1$  kW/m at 300 s**

S.No.	Experimental Temperature K	$\bar{k}$		$k(T)$	
		Pred. Temp., K	% Dev.	Pred. Temp., K	% Dev.
1	327.2	378.91	-13.65	382.04	-14.36
2	313.8	340.28	-7.78	346.10	-9.33
3	308.1	316.67	-2.71	318.51	-3.27
4	305.8	307.90	-0.68	307.49	-0.55
5	304.9	304.61	0.09	304.02	0.29
6	304.7	303.47	0.41	303.18	0.50
7	304.5	303.02	0.49	303.0	0.50
8	304.2	303.00	0.40	303.0	0.40
9	304.2	303.00	0.40	303.0	0.40

Table A.2 Experimentally Observed Temperatures and Temperatures Predicted Using  $\bar{k}$  and  $k(T)$  relationship alongwith their Percent Deviations for  $Q_L=0.1$  kW/m at 600 s

S.No.	Experimental Temperature K	$\bar{k}$		k(T)	
		Pred. Temp., K	% Dev.	Pred. Temp., K	% Dev.
1	348.6	389.30	-10.45	390.63	-10.76
2	329.0	350.08	-6.02	356.43	-7.70
3	318.7	324.42	-1.76	328.56	-3.00
4	313.5	313.23	0.09	314.45	-0.30
5	310.2	307.84	0.77	307.61	0.84
6	309.5	305.21	1.41	304.65	1.59
7	308.9	303.42	1.81	303.14	1.90
8	307.1	303.23	1.28	303.04	1.34
9	307.1	303.21	1.28	303.03	1.34

**Table A.3 Experimentally Observed Temperatures and Temperatures Predicted Using  $\bar{k}$  and  $k(T)$  relationship alongwith their Percent Deviations for  $Q_L=0.1$  kW/m at 900 s**

S.No.	Experimental Temperature K	$\bar{k}$		$k(T)$	
		Pred. Temp., K	% Dev.	Pred. Temp., K	% Dev.
1	363.1	394.53	-7.97	394.81	-8.03
2	340.6	355.13	-4.09	361.49	-5.78
3	328.0	328.80	-0.24	334.00	-1.80
4	321.4	316.71	1.48	319.18	0.70
5	316.3	310.41	1.90	310.98	1.71
6	313.6	306.99	2.15	306.67	2.26
7	313.1	304.24	2.91	303.65	3.11
8	309.7	303.89	1.91	303.34	2.10
9	309.7	303.86	1.92	303.32	2.10



Table A.4 Experimentally Observed Temperatures and Temperatures Predicted Using  $\bar{k}$  and  $k(T)$  relationship alongwith their Percent Deviations for  $Q_L=0.1$  kW/m at 1200 s

S.No.	Experimental Temperature K	$\bar{k}$		$k(T)$	
		Pred. Temp., K	% Dev.	Pred. Temp., K	% Dev.
1	373.5	397.89	-6.13	397.41	-6.02
2	349.6	358.41	-2.46	364.63	-4.12
3	335.5	331.76	1.13	337.49	-0.59
4	328.0	319.23	2.75	322.48	1.71
5	322.1	312.46	3.08	313.67	2.69
6	318.9	308.62	3.33	308.60	3.34
7	317.2	305.31	3.90	304.46	4.18
8	312.0	304.85	2.34	303.95	2.65
9	312.0	304.82	2.35	303.92	2.66

**Table A.5 Experimentally Observed Temperatures and Temperatures Predicted Using  $\bar{k}$  and  $k(T)$  relationship alongwith their Percent Deviations for  $Q_L=0.1$  kW/m at 1500 s**

S.No.	Experimental Temperature K	$\bar{k}$		$k(T)$	
		Pred. Temp., K	% Dev.	Pred. Temp., K	% Dev.
1	382.1	400.22	-4.53	399.23	-4.29
2	357.1	360.70	-1.00	366.82	-2.65
3	341.9	333.88	2.40	339.97	0.57
4	333.6	321.13	3.88	324.93	2.67
5	327.1	314.12	4.13	315.83	3.57
6	323.9	310.05	4.47	310.33	4.37
7	321.0	306.43	4.76	305.47	5.08
8	314.2	305.92	2.71	304.81	3.08
9	314.2	305.88	2.72	304.76	3.10

**Table A.6 Experimentally Observed Temperatures and Temperatures Predicted Using  $\bar{k}$  and  $k(T)$  relationship alongwith their Percent Deviations for  $Q_L=0.1$  kW/m at 1800 s**

S.No.	Experimental Temperature K	$\bar{k}$		k(T)	
		Pred. Temp., K	% Dev.	Pred. Temp., K	% Dev.
1	389.7	402.01	-3.06	400.51	-2.70
2	363.7	362.46	0.34	368.36	-1.26
3	347.6	335.56	3.59	341.74	1.72
4	338.5	322.68	4.90	326.72	3.60
5	331.6	315.54	5.09	317.51	4.44
6	328.6	311.34	5.54	311.78	5.40
7	324.5	307.54	5.51	306.49	5.88
8	316.4	307.01	3.06	305.75	3.48
9	316.3	306.97	3.04	305.69	3.47

Table A.7 Experimentally Observed Temperatures and Temperatures Predicted Using  $\bar{k}$  and  $k(T)$  relationship alongwith their Percent Deviations for  $Q_L=0.1$  kW/m at 2100 s

S.No.	Experimental Temperature K	$\bar{k}$		k(T)	
		Pred. Temp., K	% Dev.	Pred. Temp., K	% Dev.
1	396.2	403.59	-1.83	401.57	-1.34
2	369.5	364.02	1.50	369.64	-0.04
3	352.7	337.06	4.64	343.23	2.76
4	342.8	324.11	5.77	328.28	4.42
5	335.4	316.88	5.84	319.01	5.14
6	332.9	312.60	6.49	313.15	6.31
7	327.6	308.70	6.12	307.60	6.50
8	318.4	308.14	3.33	306.80	3.78
9	318.2	308.09	3.28	306.74	3.74

Table A.8 Experimentally Observed Temperatures and Temperatures Predicted Using  $\bar{k}$  and  $k(T)$  relationship alongwith their Percent Deviations for  $Q_L=0.1$  kW/m at 2400 s

S.No.	Experimental Temperature K	$\bar{k}$		$k(T)$	
		Pred. Temp., K	% Dev.	Pred. Temp., K	% Dev.
1	401.7	405.02	-0.82	402.50	-0.20
2	374.6	365.45	2.50	370.76	1.04
3	357.3	338.45	5.57	344.53	3.71
4	346.8	325.46	6.56	329.67	5.20
5	339.0	318.18	6.54	320.39	5.81
6	336.5	313.85	7.22	314.47	7.01
7	330.8	309.88	6.75	308.76	7.14
8	320.5	309.31	3.62	307.92	4.09
9	320.3	309.27	3.57	307.86	4.04